Graphene-Based Polymer Nanocomposites

STRUCTURE- PROPERTIES RELATIONSHIPES IN GRAPHENE-REINFORCED POLYMER NANOCOMPOSITES

By

Haia Aldosari

Supervisors: Prof Nigel Clarke & Prof Patrick Fairclough

A thesis submitted in partial fulfilment for the degree of Doctor of Philosophy in Physics

Department of Physics and Astronomy

The University of Sheffield

2018

Declaration

This project described in this thesis was undertaken at The University of Sheffield between September 2015 and December 2018 under the supervision of Professors Nigel Clarke & Patrick Fairclough. Unless stated, it is the work of the author and has not been submitted in whole or in part for any other degree at this or any other institution.

Haia Aldosari
2018

STRUCTURE- PROPERTIES RELATIONSHIPES IN GRAPHENE-REINFORCED POLYMER NANOCMPOSITES

Haia Aldosari

Publicly Presented Work

1- The Sheffield Composites Conference. The University of Sheffield, Sheffield, UK, 2016. Poster entitled “STRUCTURE –PROPERTIES RELATION IN METALLOCENE LINEAR LOW DENSITY POLYETHYLENE/POLYPROPYLENE BLENDS.

2- “GRAPOL” 1- day conference on polymer nanocomposites, London, UK, 2017. Presented poster entitled “STRUCTURE-PROPERTY RELATIONS IN GRAPHENE OXIDE REINFORCED POLYMER NANOCOMPOSITES”

3- Nanomaterials: from theory to application Conference, Manchester University, UK, 2017. presented poster entitled “PROCESSING, MORPHOLOGY AND PROPERTIES OF GRAPHENE OXIDE REINFORCED POLYMER NANOCOMPOSITES”

4- Physical Aspects of Polymer Science Conference. Swansea University, Swansea, UK, 2017. Presented poster entitled “THE EFFECT OF THE GRAPHENE OXIDE DISPRATION ON STRUCTURE RELATIONSHIPS IN POLYMER/GRAPHENE NANOCOMPOSITES”

Acknowledgements

I deeply need to thank God for giving me the strength and blessings to finish this stage of life. Next, I would like to express my great gratitude to all those who have supported and accompanied me during my PhD work.

First of all, my deepest appreciation goes to my supervising guide, **Prof. Nigel Clarke**, Professor of Condensed Matter Physics Theory at The University of Sheffield. I thank him for his constant supervisions, recommendations and suggestions during all years involved in my research work. I could not have imagined having a better advisor and mentor for my Ph.D., and without his excellent guidance and continuous support, knowledge and perceptiveness I would never have finished. I would like to thank him for providing me with a lot of opportunities and independence by giving me the freedom to develop myself as a truly independent researcher with creativity, by developing my ideas. His professional and personnel attitude has made my stay in the University a very rewarding and memorable experience. It is my great pleasure and honor to be his student.

I would like to express with great pleasure, my deep sense of obligation and gratitude to **Prof. Patrick Fairclough**, Professor of Composite Engineering, at The University of Sheffield and to his group for their invaluable guidance, constant support and encouragement during the entire course of my research work.

My heartfelt thanks and grateful are due to **Dr. Michael P Weir**, research follow at physics department in The University of Sheffield for their moral support and encouragement.

I would like to acknowledge my earnest thanks to my colleagues **Stephanie Burg**, **Liyana Valiya Peedikakkal**, **Ying Lan Ang** and **Stephen Knox**.

To **Dr. Andrew Parnell** and all of the other research and support staff at the university along with the administrative staff without whom this thesis could not have been completed.

I am very much thankful to head of the department and all teaching staff of The University of Sheffield for giving me space, encouragement and all possible help to complete my research. I specially acknowledge my University for giving me an opportunity to work over here, and also my unbound gratitude goes to my beloved parents **Hamad** and **Noura** who took a lot of pain to help me and blessed me with their prayers.

I am deeply indebted to my husband **Khalid** and my children **Nwaf**, **Juri**, **Basil** and **Meral** for their understanding, tolerance, support and unlimited patience without which I would not have completed this study.

Dedication

To my family and friends.

Abstract

Graphene's unique combination of excellent electrical, thermal and mechanical properties can provide multi-functional reinforcement for polymer nanocomposites. However, poor dispersion of graphene in non-polar polyolefins (polyethylene, polypropylene) limits its applications as a universal filler. Hence, the overall objective of this thesis was to develop processing-structure-property relationships by improving graphene's dispersion in graphene/polyolefin nanocomposites by altering the C/O ratio of the graphene of the graphene/polymer nanocomposites. Translating graphene's unique properties to nanocomposites is difficult, since graphene is known to poorly disperse in polyolefins, including polyethylene and polypropylene, owing to the nonpolar nature of polyolefins. A higher concentration required for percolation is directly correlated with poor dispersion, which leads to larger graphene aggregates in polyolefins. As a consequence we used 4wt% as the highest concentration. Improved dispersion of graphene in polyolefins was reported using the solution method to prepare samples. Introducing functional groups onto the polymer could improve dispersion of the nano-fillers in polyolefins. Ethylene- co -glycidyl methacrylate (PE-co-GMA) as a compatibilizer was used for graphene/polyolefins nanocomposites. Furthermore, it may improve adhesion between polymers and nano particles.

Three types of graphene (GO, rGO and G) were incorporated into a range of model polymers (PE, PP, PB and PBC). The process of solvent method resulted in better dispersion of graphene in the thermoplastic polymers. Using solvent mixing, the polyolefins lead to higher thermal stability at even less than 0.5wt% of graphene. Just 0.25wt% of graphene is enough to improve the thermal stability of the thermoplastic by increasing the degradation temperature to $165 \pm 3\ ^{o}C$, greater than that of the pure polymer. The morphology of the graphene in the polyolefins was characterized with WAXD and SAXS. All types of graphene have a similar level of dispersion in the thermoplastic polymer. FTIR and Raman spectroscopy showed no chemical reaction throughout the solvent mixing method. XPS was used to characterize the C/O ratio of all types of graphene, and to study the impact of the C/O ratio on the structure and properties of the polymer/ graphene nanocomposites. The crystallization and melting behaviour of the nanocomposites was obtained using DSC. An increase in the crystallization temperature of PE and PP in the presence of graphene has technological importance, resulting in a shorter processing cycle, thereby increasing the production rate.

Graphene-based polymer nanocomposites can be a new versatile, soft material with numerous advantages. For maximum benefits, composite morphology must be tailored appropriately with an understanding of its structure-property relationships.

Table of Contents

List of Tables XI
List of Figures XIV
List of Abbreviations 1
Chapter 1. Introduction and Objectives of the Project……5
1.1. Introduction……5
1.2. Aims of the Project……7
1.3. Overview of Thesis 8
References..... 9
Chapter 2. Literature Review.....10
2.1. Introduction to Graphene Reinforced Polymer Nanocomposites ……10
2.2. Nanotechnology……10
2.3. Nanoparticles ……11
2.4. Nanomaterials……11
2.4.1. Nanomaterials Classification ……11
2.5. Graphene ……12
2.5.1. Synthesis of Graphene……13
2.5.2. Graphene Properties and Applications……14
2.6. Nanocomposites……15
2.7. Graphene-based Polymer Nanocomposites……15
2.7.1. Preparation Methods of Polymer Nanocomposites……17
2.7.1.1.In-situ Polymerization……18
2.7.1.2. Solvent blending……18
2.7.1.3. Melt Blending ……18
2.8. The Importance of Blending Polymers ……19
2.9. Polymer blend methods ……19
2.9.1. Mechanical-melt mixing ……20
2.9.2. Solution cast techniques ……20
2.9.3. Latex blending ……20
2.9.4. Spray or freeze drying …… 20
2.9.5 Fine powder mixing …… 20
2.9.6. In-situ polymerization …… 20
2.10. Properties of Polymer Blends Polymer…… 21
2.11. Theory of Miscibility …… 21
2.12. The classification of the polymer blend …… 24
2.12.1. Miscible Polymer Blends …… 24

2.12.2. Partially Miscible Polymer Blends …… 24
2.12.3. Immiscible Polymer Blends…….. 25
2.13 Compatibilization of Immiscible Blends ……... 25
2.13.1. Ziegler-Natta Catalysts Compatibilization ……... 25
2.13.2. Graphene Compatibilization ……... 26
2.14. Properties of Graphene/Based Polymer Nanocomposites ……... 27
2.14.1. The Mechanical Properties ……... 27
2.14.2. Electrical Properties ……... 27
2.14.3. Thermal Properties ……... 28
References..... 29
Chapter 3. Characterisation and Experimental Techniques ……..……38
3.1. Scanning Electron Microscope (SEM) ……..…….38
3. 2. Wide Angle X-ray Diffraction (WAXD)…….. 39
3.3. Small Angle X-ray Scattering Measurements (SAXS)…….. 40
3.4. X-ray photoelectron spectroscopy (XPS) ……... 41
3.5. Fourier transformed infrared spectroscopy (FTIR)……... 42
3.6. Ultraviolet Visible Spectroscopy (UV-Vis) ……... 43
3.7. Raman Spectroscopy ……... 45
3.8. Deferential Scanning Calorimetry (DSC) ……..…….....45
3.9. Thermal gravimetric analysis (TGA) ……... 46
3.10. Conductivity measurement ……... 48
3.11. Mechanical Properties ……... 48
3.12. Dynamic Mechanical Analysis (DMA) ……... 49
References ……... 50
Chapter 4. Understanding the Structure, Phase Transition and Properties Behaviour of the Polymer Host Matrix of Graphene Nanoparticles…….……...53
4.1. Materials ……...……...53
4.2. GPC/SEC Analysis ……... 54
4. 3. Preparation …….……...54
4.4. Results and Discussion ……... 56
4.4.1. WAXD results ……... 56
4.4.2. SAXS study ……...60
4.4.3. Crystallization and Melting Behaviour ……..…65
4.4.4. Thermal Behaviour …….……..……..67
4.4.5. Mechanical Properties …….……68
4.4.6. Dynamic Mechanical Analysis (DMA) ……..…….70
4.5. Summary and Conclusion …….……..……71

References ……72
Chapter 5. The Effect of Graphene Oxide Dispersion on Structure-Property Relationships in Polymer/Graphene nanocomposites ……76
5.1. Materials ……76
5.2. Solubility Tests ……78
5. 3. Polymer Nanocomposite Processing ……80
5.3.1 Solvent method ……80
5.3.2. Sonication mixing ……..81
5.3.3. Mixing polymer with graphene ……81
5.3.4 Recovering and pelletizing the nanocomposites ……...81
5.4. Results and Discussion ……....85
5.4.1. WAXD results …….. 85
5.4.2. SAXS study …….. 88
5.4.3. FTIR analysis ……... 90
5.4.4 Raman Spectra …….. 91
5.4.5. Crystallization and Melting Behaviour …… 96
5.4.6. Thermal Stability ……. 98
5.4.7. Conductivity measurement …….. 102
5.4.8. Mechanical Properties ……... 104
5.5. Summary and Conclusion ……... 108
References ……... 109
Chapter 6. The Effect of Carbon/Oxygen Ratio upon Structure-Property Relationships in Polymer/Graphene Nanocomposites ……... 113
6.1. Materials ……...113
6. 2. Polymer nanocomposite preparation ……...115
6.3. Results and Discussion ……..…….....118
6. 3. 1. XPS results ……...……118
6.3.2. WAXD study ……...122
6.3.3. Raman spectroscopy ……...127
6.3.4. FTIR analysis ……...130
6.3.5. UV–vis spectroscopy ……..…….....134
6.3.6. Crystallization and Melting Behaviour ……136
6.3.7. Thermal stability ……...138
6.4. Summary and Conclusion……...…….....142
References ……...143
Chapter 7. Conclusion and Future Recommendation ……148
7.1 Summary and Conclusions.....148

7.2 Future Research Directions ……...150
Appendix 151
Bibliography.....152

List of Tables

Table.4.1. Polymer materials information, the melt flow index and the density from supplier, the melting temperature from DSC and molecular weight details from PSS……..…….…….53

Table 4.2. The GPC/SEC results of the samples with broad molar mass distribution……..…… 54

Table 4. 3. Weight percent of each component in the different samples …….…… 55

Table 4. 4. The crystallite size values of PE, PB and PP in the reflection peaks in WAXD data …….. 58

Table 4.5. The interlayer spacing of PE, PB and PP…….…… 58

Table 4.6. The FWHM values of PB and PBC reflection peaks in WAXD data and crystallite size …….…….. 59

Table 4.7. The interlayer spacing of the PB and PBC…….. 59

Table 4.8. The thickness of the crystalline lamellae and amorphous lamellae, long period and linear crystallinity of the PE, PB, PP, PB and PBC samples …….…… 64

Table 4.9. Crystallization, melting and melting enthalpy temperature of PE and PP in the blend …….…….. 67

Table 4.10. Decomposition temperatures of the samples at different remaining weights percentages …….……..... 68

Table 4.11. The tensile properties of the polymer blends…….…… 69

Table 5.1. The polarity Index and the boiling point of some solvents ……. 79

Table 5.2. Weight percent of polymers pellets, graphene and compatibilizer used in the nanocomposites preparation …….…… 81

Table 5. 3. Weight of polymers pellets, graphene and compatibilizer used in the nanocomposites preparation……... 82

Table 5.4. The interlayer spacing of pure PE, PP, PB, PBC and PNCs of 4wt% of GO ……. 86

Table 5.5. The FWHM values of pure PE, PP, PB, PBC and PNCs of 4wt% of GO reflection

peaks in WAXD data and crystallite size…… 87

Table 5.6. The long period, the thickness of the crystalline and amorphous layers and the linear crystallinity of pure PE, PP, PB and PBC and PNCs of 4wt% of GO……..…..……88

Table 5.7. Wavenumber (cm^{-1}) and assignments of the Raman bands of both PB and PBC ……..…….. 92

Table 5.8. The DSC parameters of PE/GO nanocomposites. ……..……. 95

Table 5.9. The DSC parameters of PP/G nanocomposites……..…….. 96

Table 5.10. The DSC parameters of PB/G nanocomposites ……..……..... 97

Table 5.11. The DSC parameters of PBC/G nanocomposites ……..…… 98

Table 5.12. Thermal degradation temperatures of the PE/GO nanocomposites……... 98

Table 5. 13. Thermal degradation temperatures of PP /GO nanocomposites …….……..…99

Table 5.14. Thermal degradation temperatures of PB /GO nanocomposites ……..…100

Table 5.15. Thermal degradation temperatures of PBC /GO nanocomposites ……..……..…...101

Table 5.16. The elastic modulus and the tensile strength at break of PE nanocomposites…….....… 103

Table 5.17. The elastic modulus and the tensile strength at break of PP nanocomposites…….….104

Table 5.18. The elastic modulus and the tensile strength at break of PB nanocomposites….....…105

Table 5.19. The elastic modulus and the tensile strength at break of PBC nanocomposites…….....106

Table 6.1. Graphene materials details from supplier …….….112

Table 6.2. Weight percent of polymers pellets, graphene and compatibilizer used in preparation of polymer /graphene nanocomposites ……..…..116

Table 6.3. Weight of polymers pellets, graphene and compatibilizer used in preparation of polymer/graphene nanocomposites.……..……116

Table 6.4. Surface compositions (atomic %) determined by quantifying XPS survey scans…...…...117

Table 6.5. Atomic composition of carbon and oxygen, as well as the C/O ratios obtained from XPS analysis of G, rGO and GO…….....118

Table 6.6. The FWHM values of the PE /graphene of reflection peaks in WAXD data and crystallite size ……..... 123

Table 6.7. The interlayer spacing of the PE /graphene nanocomposites …….....….. 123

Table 6.8. The FWHM values of the PP /graphene of reflection peaks in WAXD data and crystallite size.…….……124

Table 6.9. The interlayer spacing of the PP /graphene nanocomposites……...……..…… 124

Table 6.10. The FWHM values of the PB /graphene of reflection peaks in WAXD data and crystallite size……..……...……. 125

Table 6.11. The interlayer spacing of the PB /graphene nanocomposites. ……..……...……125

Table 6.12. The FWHM values of the PBC /graphene of reflection peaks in WAXD data and crystallite size. ……...……..……126

Table 6.13. The interlayer spacing of the PBC /graphene nanocomposites……...…….. 126

Table 6.14. The ID/IG ratio of GO, rGO and G……...…..……. 129

Table 6.15. Characteristic infrared transmission of PE nanocomposites ……..…...….. 130

Table 6.16. Characteristic infrared transmission of PP nanocomposites ……..……...….. 131

Table 6.17. Characteristic infrared transmission of PB nanocomposites ……..……..…. 132

Table 6.18. Characteristic infrared transmission of PBC nanocomposites ……..……..133

Table 6.19. The DSC parameters of the polymer/ GO, rGO and G nanocomposites ……..…...….. 136

Table 6.20. The lost weight percent of G, rGO and GO in different temperatures.…….....….. 137

Table 6.21. Thermal stability behaviour of the PE nanocomposites ……..…...… 139

Table 6.22. Thermal stability behaviour of the PP nanocomposites ……...…...… 139

Table 6.23. Thermal stability behaviour of the PB nanocomposites ……..……140

Table 6.24. Thermal stability behaviour of the PBC nanocomposites……...…...….. 141

Table A.1. Surface compositions (atomic %) determined by quantifying XPS survey scans…….....151

List of Figures

Figure1.1. Source of all graphitic forms. Graphene is a 2D building material for carbon materials of all other dimensionalities. It can be made into 0D buckyballs, 1D nanotubes or to3D graphite ……...6

Figure1. 2. Polyethylene (PE) structure…….....7

Figure 1.3. Polypropylene (PP) structure ……...…….7

Figure 2.1. Layered structure of graphite showing the sp^2 hybridized carbon atoms bonded in hexagonal rings …….13

Figure 2.2. Filler dispersion in graphene-based nanocomposites: (a) separated, (b) intercalated and (c) exfoliated phases. ……. 17

Figure 2.3. Phase diagram showing LCST and UCST behavior for polymer blends …….……..23

Figure 3.1. Scheme to explain the Bragg law …….. 39

Figure 3.2. The working principle difference in the WAXD and SAXS ……..40

Figure 3.3. Simplified working diagram of scattering instrument ……... 41

Figure 3.4. Different molecular orbital transitions ……..... 44

Figure 3.5. A typical DSC curve for polymer ……...……... 46

Figure 3.6. A typical thermal degradation TGA curve ……..…….. 47

Figure 3.7. Dimensions of tensile composite specimen (mm) ……..……... 48

Figure 3.8. The typical Stress-Strain curve ……...49

Figure 4.1. The Preparation of polymers matrices.……...……... 55

Figure 4. 2. The curves of WAXD patterns of PP……..…….. 56

Figure 4. 3. The curves of WAXD patterns of PE ……...……..…….. 56

Figure 4. 4. The curves of WAXD patterns of PB……..…57

Figure 4. 5. The curves of WAXD patterns of PE, PB and PP……...……..… 57

Figure 4.6. Schematic of the interlayer spacing of semi-crystalline polymers ……..…….. 58

Figure 4.7. The curves of WAXD patterns of PBC…….. 59

Figure 4.8. The curves of WAXD patterns of PB and PBC ……. 59

Figure 4.9. SAXS profiles for the PE sample ……...61

Figure 4.10. SAXS profiles for the PB sample……..……61

Figure 4.11. SAXS profiles for the PP sample …….……62

Figure 4.12. SAXS profiles for the PBC sample.……...……..……. 62

Figure 4.13. Lorentz-corrected SAXS curves for the PE, PB, PP samples ……...……..62

Figure 4.14. Lorentz-corrected SAXS curves for the PB and PBC samples ……...…… 63

Figure 4.15. Display the long period distance of lamellar……...……. 63

Figure 4.16. γ(r) Function of the PE at room temperature…….……...……. 63

Figure 4.17. γ(r) Function of the PP at room temperature……..…..……. 64

Figure 4.18. γ(r) Function of the PB at room temperature……..…..……. 64

Figure 4.19. γ(r) Function of the PBC at room temperature……..……..…….. 64

Figure 4.20. The DSC curve of a blend of PE ……..…… 65

Figure 4.21. The DSC curve of a blend of PP ……..…… 66

Figure 4.22. The DSC curve of a blend of PB ……...……...……...… 66

Figure 4.23. The DSC curve of a blend of PBC……..……. 66

Figure 4.24. The TGA decomposition curves of the sample……...…...……... 68

Figure 4.25. Mechanical properties of polymer blends …….…….. 69

Figure 4.26. Mechanical loss factor spectra of blends polymer ……..…… 70

Figure 5. 1. SEM images of pure GO with different magnifications ……..…… 76

Figure 5.2. AFM image and thickness height profile of the GO deposited onto Functionalized mica.77

Figure 5.3. The dispersion of GO in four different polar and non-polar solvents ……...……... 78

Figure 5.4. The preparation steps of nanocomposites ……...83

Figure 5. 5. The curves of WAXD patterns of GO pure……..……85

Figure 5. 6. The curves of WAXD patterns of PE and PE/ GO4…….....…..85

Figure 5. 7. The curves of WAXD patterns of PP and PP/ GO4…….……..85

Figure 5. 8. The curves of WAXD patterns of PB and PB/ GO4…….……..…….…..... 86

Figure 5. 9. The curves of WAXD patterns of PBC and PBC/GO4……..……..……..……. 86

Figure 5. 10. Figure 5. 10. Lorentz-corrected SAXS curves for the pure PE, PP, PB and PBC samples and their PNCs. ……..……..... 88

Figure 5.11. Long period of lamellar of pure PE, PP, PB and PBC and PNCs of 4wt% of GO……. 89

Figure 5.12. FTIR spectra of pure PE, PP, PB and PBC and PNCs of 4wt% of GO ……..… 90

Figure 5.13. Raman spectra of PE, PE/GO4……..……... 93

Figure 5.14. Raman spectra of PP and PP/GO4 ……...……..... 93

Figure 5.15. Raman spectra of PB and PB/GO4 ……...……... 94

Figure 5.16. Raman spectra of PBC and PBC/GO4 ……..…….. 94

Figure 5.17. Raman spectra of pure graphene oxide GO ……..…..... 94

Figure 5.18. The optical phonon vibrations of graphene, with the sp^2 C-C stretching modes which correspond to (a) the G band, and (b) the D and G' bands in Raman ……..…… 94

Figure 5.19. The a) crystallization temperature b) melting temperature of PE, PP and

their GO nanocomposites ……..……... 96

Figure 5. 20. TGA curves of PE nanocomposites …….....98

Figure 5. 21. TGA curves of PP nanocomposites …….....99

Figure 5.22. TGA curves of PB nanocomposites ……..…..100

Figure 5.23. TGA curves of PBC nanocomposites …….....101

Figure 5.24. The I-V characteristic curves, defines the resistive the graphene/polymer

Nanocomposites ……..……102

Figure 5.25. Molecular structure of graphene and graphene oxide ……103

Figure 5.26. The elastic modulus and the tensile strength at break of PE nanocomposites ……...104

Figure 5.27. The elastic modulus and the tensile strength at break of PP nanocomposites ……...….104

Figure 5.28. The elastic modulus and the tensile strength at break of PB nanocomposites ……...105

Figure 5.29. The elastic modulus and the tensile strength at break of PBC nanocomposite.……..…106

Figure 6.1. SEM image of GO at various level of magnification ……..…..113

Figure 6.2. SEM image of rGO at various level of magnification …….……113

Figure 6.3. SEM image of G at various level of magnification …….……114

Figure 6.4. 10 mg of the GO, rGO and G…….……...114

Figure 6.5. The preparation steps of polymer/graphene nanocomposites ……..…….115

Figure 6.6. XPS survey scan of graphene …….……..118

Figure 6.7. XPS survey scan of graphene oxide…….…….118

Figure 6.8. XPS Survey scan of reduced graphene oxide ……..…….118

Figure 6.9. Deconvolution of C 1s scan core-level XPS spectra of the Graphene ……..……...119

Figure 6.10. Deconvolution of C 1s scan core-level XPS spectra of the graphene oxide ……..……119

Figure 6.11. Deconvolution of C 1s scan core-level XPS spectra of the reduced

graphene oxide …….……...119

Figure 6.12. Deconvolution of O1s scan core-level XPS spectra of the graphene ……..…...120

Figure 6.13. Deconvolution of O1s scan core-level XPS spectra of the graphene oxide ……..…….120

Figure 6.14. Deconvolution of O1s scan core-level XPS spectra of the reduced graphene oxide 120

Figure 6.15. The WAXD pattern of the pure GO, rGO and G ……....122

Figure 6.16. The WAXD curves patterns of the PE/graphene nanocomposites ……..…123

Figure 6.17. The WAXD curves patterns of the PP/graphene nanocomposites……..…124

Figure 6.18. The WAXD curves patterns of the PB/graphene nanocomposites ……....124

Figure 6.19. The WAXD curves patterns of the PBC/graphene nanocomposites……...125

Figure 6.20 The Raman spectra of graphene oxide ……..……...127

Figure 6.21. E_{2g} vibrational mode of carbon atoms in one graphite layer…….…..127

Figure 6.22. The Raman spectra of reduced graphene oxide. ……..…128

Figure 6.23. The Raman spectra of pristine graphene …….…...128

Figure 6.24. FTIR spectra of pure PE and PEs graphene nanocomposites ……..……...130

Figure 6.25. FTIR spectra of pure PP and PPs graphene nanocomposites …….……131

Figure 6.26. FTIR spectra of pure PB and PBs graphene nanocomposites ……..……..132

Figure 6.27. FTIR spectra of pure PBC and PBCs graphene nanocomposites ……..…….133

Figure 6.28. UV-visible spectra of GO and rGO …….……...134

Figure 6.39. UV-visible spectra of GO, rGO and G …….……..134

Figure 6.30. The melting temperature (T_m) of PE and PP nanocomposites …….…….…136

Figure 6.31. The crystallization temperature (T_c) of PE and PP nanocomposites ……..……137

Figure 6.32. The TGA curves of the G, rGO, GO from room temperature to 700 ^{o}C ……..……..138

Figure 6.33. The TGA decomposition curves of the PE and its nanocomposites ……...….... 138

Figure 6.34. The TGA decomposition curves of the PP and its nanocomposites ……..…… 139

Figure 6.35. The TGA decomposition curves of the PB and its nanocomposites……..…….140

Figure 6.36. The TGA decomposition curves of the PBC and its nanocomposites……..……...141

Figure A.1. The molar mass distribution curves of PE and PP …….……..151

Symbols and Abbreviations

l_a	Amorphous layers thickness
l_c	Crystalline layers thickness
L_p	Long period
χ_l	Linear degree of crystallinity
ΔH_o	Melt enthalpy of a 100% crystalline sample
0 D	0 Dimensions
1D	1 Dimension
2D	2D Dimensions
Å	Angstrom
a	Area
AFM	Atomic force microscopy
au	Arbitrary unit
BE	Binding energy
C	Carbon
C-O-C	Epoxide
C-O-OH	Carboxyl
C-OH	Hydroxyl
C=O	Carbonyl
cm^{-1}	Wavenumber
CNT	Carbon nanotube
CONH	Amide
cps	Counts per second
d spacing	Interplanar distance between atomic planes
DI	Deionised
DMA	Dynamic mechanical analysis
DMF	Dimethylformamide
DMF	N, N-dimethylformamide
DSC	Deferential Scanning Calorimetry
DUHMWPE	Disentangled ultrahigh molecular weight polyethylene
E	Young's modulus
E'	Tensile storage modulus
E"	Tensile loss modulus
FTIR	Fourier transformed infrared spectroscopy
FWHM	Full width half maximum intensity

g	Gram
G	Pristine graphene
g\L	Gram per litre
GNP	Graphite nanoplatelets
GO	Graphene oxide
GPa	Giga pascal
GPC	Gel permeation chromatography
h	Hour
HCl	Hydrochloric acid
HDPE	High density polyethylene
Hz	Hertz
I	Intensity
I	Current
ID/IG	Intensity of disorder peak to graphitic peak
J/g	Joule per gram
K	Dimensionless shape factor
kHz	Kilohertz
kV	Kilovolt
l	Thickness
lcst	Lower critical solution temperatures
LDPE	Low density polyethylene
LLDPE	Linear low density polyethylene
mA	Milliamp
mg	Milligram
min	Minutes
ml	Millilitre
mm	Millimetre
MMD	Molar mass distribution
MPa	Mega pascal
MPa	Megapascal
mW	Milli Watts
mW	Milliwatt
Mw	Molar mass averages
Mw	Weight-average molecular weight
MWCNT	Multi walled carbon nanotube
N/m^2	Newton per square metre
nm	Nanometer.

NPL	The National Physical Laboratory
O	Oxygen
PB	Polymer blend
PBC	Polymer blend with compatibilizer
PDI	Polydispersity index
PE	Polyethylene
PE-co-GMA	Poly (ethylene- co -glycidyl methacrylate)
PNCs	Polymer nanocomposites
POs	Polyolefins
PP	Polypropylene
q	Scattering vector
R	Resistance
rGO	Reduce graphene oxide
S/cm	Siemens per centimetre
SAXS	Small Angle X-ray Scattering
SEC	Size Exclusion Chromatography
SEM	Scanning electron microscope
sp^2	Electron orbital arrangement of 2 dimensional graphene
sp^3	Electron orbital arrangement of 3 dimensional carbon
SWCNT	Single walled carbon nanotube
t	Time
T	Temperature
T_c	Crystallization temperature
TEM	Transmission electron microscopy
T_g	Glass transition temperature
TGA	Thermogravimetric analysis
THF	Tetrahydrofuran
T_m	Melting temperature
TPa	Tera pascal
ucst	Upper critical solution temperatures
UHMWPE	Ultrahigh molecular weight polyethylene
UV-Vis	Ultraviolet Visible Spectroscopy
V	Electron volt
V	Voltage
WAXD	Wide Angle X-ray Diffraction
wt%	Reinforced weight percentage

X_c	Crystallinity degree
XPS	X-ray photoelectron spectroscopy
β	Line broadening at half the maximum intensity
$\gamma(r)$ (LCF)	Dimensional linear correlation function
δ	Phase angle between *E*' and *E*''
ΔH_m	Melt enthalpy
2θ	X-ray scattering angle
λ	Wavelength
μL	Microlitre
μm	Micrometer
σ	Electrical conductivity
τ	Crystallite size

Chapter 1

Introduction and Objectives of the Project

1.1. Introduction

Graphene reinforced polymer is classified as a multiphase material containing a single type of polymer, copolymer or a blend of polymers with nanofillers or nanoparticles (with dimensions of 1–50 nm) incorporated into the polymer matrix. This considerably affects the different physical, chemical and mechanical properties.

The plurality of the study has concentrated on polymer nanocomposites based on nanofillers: pristine graphene (G), reduce graphene oxide (rGO) and graphene oxide (GO), with view of improving the polymer's electrical, mechanical, thermal, and gas barrier properties [1][2]. Recently, graphene has shown the greatest promise as nanofiller due to its superior exceptional physical properties. This has created a novel category of polymeric nanocomposites. Graphene, a novel type of carbon, is a one atom thick plane in a two dimensional sheet formed of sp^2 hybridised carbon atoms arranged in a hexagonal crystalline structure. It is the thinnest recognized material until at present [3] [4]. In addition, it is one of the distinct allotropes of carbon that is the basic block to build of all graphitic derivatives forms shown in Figure 1.1. Graphene can be arranged and stacked in each layer into graphite with three dimensions (3D), rolled into carbon nanotubes with one dimension (1D) and wrapped into fullerene with zero dimensions (0D). Graphene with two dimensions (2D) has distinct physical, chemical and engineering properties, with a large surface area, high thermal stability, electrical and thermal conductivity and high stiffness. These unique features make graphene promising nanofiller in the field of polymer nanocomposites. As well it exhibitits great potential for many applications in different fields like electronic, medical and engineering fields [5] [6] [7] [8] [9].

Polyolefin (PO) nanocomposites based on nanofillers offer many opportunities to improve and develop the POs, with just small loud amounts of nanofillers. POs like polyethylene and polypropylene are the most readily available synthetic polymers and have the highest production demand levels in the world. More than 60% of PE and PP inserted into the industrial world have been used for compounding objective with high mechanical properties and thermal properties. Only 23% of other thermoplastic POs are synthesis by the polymerisation of ethylene, propylene or other olefin monomers such as butene-1 and hexene-1 using Ziegler–Natta and other catalysts (see Figures 1.2 and 1.3). Depending on two key variables, which are branching and density, polyethylenes (PEs) are categorized to different categories. Low density polyethylene (LDPE), linear low density polyethylene

(LLDPE), high density polyethylene (HDPE), ultrahigh molecular weight polyethylene (UHMWPE). Polypropylenes (PPs) are categorized as isotactic, syndiotactic and atactic, based on their geometrical shape. Polyolefins are widespread due to their low cost, light weight, recyclability, availability and easy processability. POs have a wide variety of applications in different industrial fields. However, for use in innovative products, it is necessary to improve the properties of polyolefins by introducing new functional groups, by adding nano fillers to the polymer host matrix, and amending the polymer matrix by using a new kind of polymer like disentangled ultrahigh molecular weight polyethylene (DUHMWPE). Recently, graphene has been explored for use as promising nanofiller for POs. Many published articles demonstrate that graphene can be used for the reinforcement of polyolefins due to its exceptional physical and mechanical characteristics [10] [11]. The polyolefin/graphene nanocomposite is still in the early steps of development and improvement. However, the enormous possibilities of this material has become obvious in different research fields including automotive, electronics and recently, in gas and water barrier applications. The main challenge to completely exploit graphene/polyolefin composites is to achieve a high level of homogeneous dispersion of graphene for maximum benefit [12].

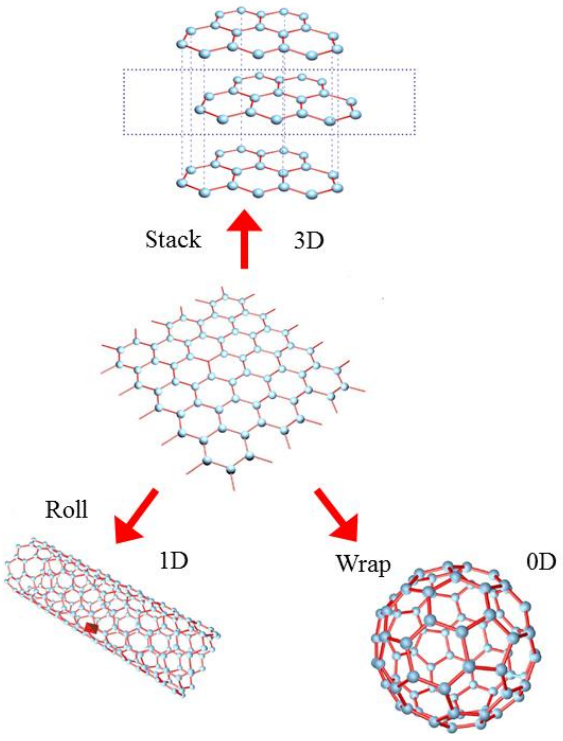

Figure1.1. Source of all graphitic forms. Graphene is a 2D building material for carbon materials of all other dimensionalities. It can be made into 0D buckyballs, 1D nanotubes or to3D graphite[13].

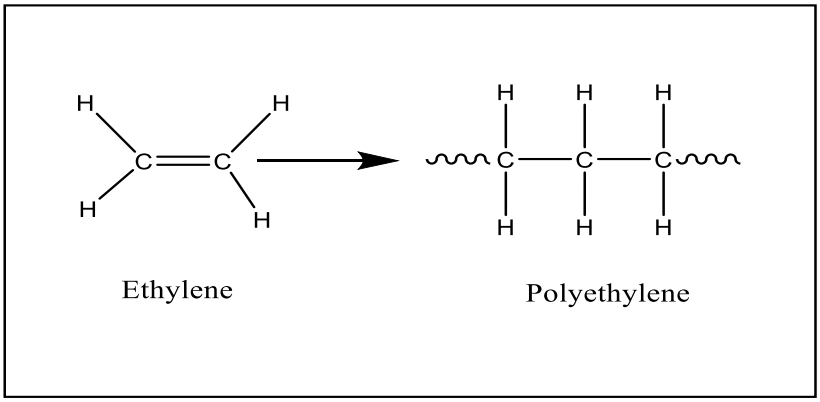

Figure1. 2. Polyethylene (PE) structure.

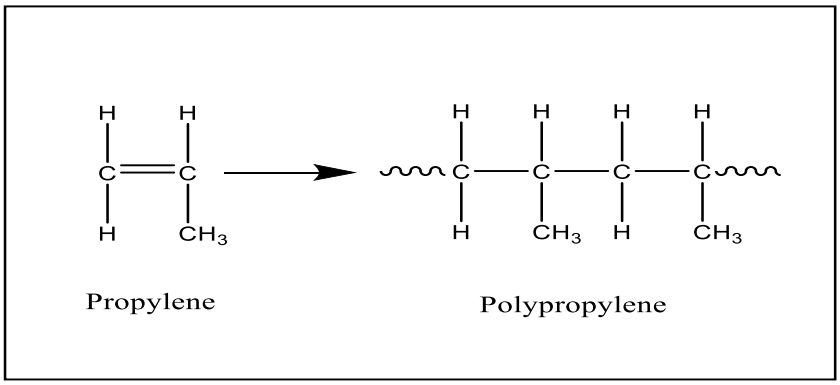

Figure 1.3. Polypropylene (PP) structure.

1.2. Aims of the Project

The main objective of this research was to achieve a fundamental understanding of the reinforcing behaviour of graphene in polymer nanocomposites by correlating them with the structure of the nanocomposites. The project also aimed to develop and improve the performance graphene based polyolefins nanocomposites. In order to achieve this target, the following aspects were explored:

- Preparation of the polymer host matrix, followed by study of the structure and properties behaviour of the polymers.
- Study the miscibility and phase transition of blend polymer in the polymer host matrix.
- Fabrication of a series samples of GO/ polymer nanocomposites with 0.25wt% and 4wt% as the least and highest content respectively.
- Study the GO dispersion effect on the nanocomposites morphology, physical and mechanical properties, and then determine the best percent of GO load for use in industrial applications.
- Reduce the O/C ratio in the graphene/ polymer nanocomposites through the use of reduced graphene oxide and pristine graphene.

- Process the polymer matrix nanocomposites by incorporating three sources of the graphene with one optimal weight percent (2wt %).
- Characterize the chemical structure of the three graphene types by determining the chemical bonds, chemical elements and functional groups.
- Study the C/O ratio impact on the physical properties to determine the optimal C/O ratio for use in industrial applications.

From a technical perspective, the ambition is to develop polyolefins nanocomposites with improved physical properties and performance for practical uses and industrials applications. The scientific aim of this research is to attain fundamental understanding of why and how graphene nanoparticles impact the structure, mechanical, electrical and thermal properties of the polymers.

1.3. Overview of Thesis

This thesis addresses the processing, characterisation and properties test of graphene-reinforced polymer nanocomposites. The structure of the thesis follows the chronological order of work conducted in order to achieve the stated aims and objectives. As such, the thesis content is organised into seven chapters, including this introductory chapter.

Chapter 2 provides a brief literature review of previous research on graphene and graphene-based nanofillers and their polymer nanocomposites. It outlines an introduction to graphene nanoparticles, graphene synthesise, nanocomposites preparation and properties, establishes the background knowledge to understand the mechanism of nanofillers and their impact on the structure, physical and mechanical properties of different polymers.

Chapter 3 discusses the background to the characterization methods applied in this project, and description of the experimental process of characterization and test specimens.

Chapter 4 mainly focuses on a fundamental understanding of the structure and properties behaviour of the polymer host matrix prior to the addition of the graphene nanoparticles.

Chapter 5 explores the effect of graphene oxide on structure-property relationships in graphene/polymer nanocomposites.

Chapter 6 presents the results of the impact of C/O ratio on structure-property relationships in polymer/graphene nanocomposites.

Chapter 7 summarizes all of the key results of this graphene/polymer nanocomposite study and provides suggestions for future research.

The references to all published works utilized in creating this thesis are listed at the end of the study.

References

[1] Huang, J. C. (2002). Carbon black filled conducting polymers and polymer blends. Advances in Polymer Technology, 21(4), 299–313.
[2] Moniruzzaman, M., & Winey, K. I. (2006). Polymer nanocomposites containing carbon nanotubes. Macromolecules, 39(16), 5194–5205.
[3] Suk, J. W., Piner, R. D., An, J., & Ruoff, R. S. (2010). Mechanical Properties of Monolayer Graphene Oxide, 4(11), 6557–6564.
[4] Snook, G. A., Kao, P., & Best, A. S. (2011). Conducting-polymer-based supercapacitor devices and electrodes. Journal of Power Sources, 196(1), 1–12.
[5] Yin, Z., Wu, S., Zhou, X., Huang, X., Zhang, Q., Boey, F., & Zhang, H. (2010). Electrochemical deposition of ZnO nanorods on transparent reduced graphene oxide electrodes for hybrid solar cells. Small, 6(2), 307–312.
[6] Yin, Z. Y., Sun, S. Y., Salim, T., Wu, S. X., Huang, X. A., He, Q. Y., Zhang, H. (2010). Organic Photovoltaic Devices Using Highly Flexible Reduced Graphene Oxide Films as Transparent Electrodes. Acs Nano, 4(9), 5263–5268.
[7] Yavari, F., & Koratkar, N. (2012). Graphene-based chemical sensors. Journal of Physical Chemistry Letters, 3(13), 1746–1753.
[8] Mishra, S. K., Tripathi, S. N., Choudhary, V., & Gupta, B. D. (2014). SPR based fibre optic ammonia gas sensor utilizing nanocomposite film of PMMA/reduced graphene oxide prepared by in situ polymerization. Sensors and Actuators, B: Chemical, 199, 190–200.
[9] Cromer, B. M., Scheel, S., Luinstra, G. A., Coughlin, E. B., & Lesser, A. J. (2015). In-situ polymerization of isotactic polypropylene-nanographite nanocomposites. Polymer (United Kingdom), 80, 275–281.
[10] Chee, W. K., Lim, H. N., Huang, N. M., & Harrison, I. (2015). Nanocomposites of graphene/polymers: a review. RSC Adv., 5(83), 68014–68051
[11] Park, S., An, J., Potts, J. R., Velamakanni, A., Murali, S., & Ruoff, R. S. (2011). Hydrazine-reduction of graphite- and graphene oxide. Carbon, 49(9), 3019–3023.
[12] Tripathi, S. N., Rao, G. S. S., Mathur, A. B., & Jasra, R. (2017). Polyolefin/graphene nanocomposites: a review. RSC Adv., 7(38), 23615–23632.
[13] Wan, X., Huang, Y., & Chen, Y. (2012). Focusing on energy and optoelectronic applications: A journey for graphene and graphene oxide at large scale. Accounts of Chemical Research, 45(4), 598–607.

Chapter 2

Literature Review

2.1. Introduction to Graphene Reinforced Polymer Nanocomposites

Nanotechnology is used in many fields with applications ranging widely from medical to construction. The unique feature of this technology is the size. Materials with nano size have distinct characteristics such as high surface area with low surface defects, which impacts significantly upon the consequent materials characteristics. To illustrate, in nanotechnology, composites can be use as materials filler to decrease the weight of composite and increase the composite stiffness and fire resistance.

Nanocomposites are extensively used in different applications, e.g. solar cells, transport, construction, and several other new implementations because of their unusual properties. They present superior mechanical and thermal properties, whilst being lightweight, characteristics which are complicated to obtain separately from the parent components. Nanocomposites, compared to classic composites, have a nano size dimension and an exclusive set of characteristics because of their nano size. Consequently this modern type of material presents progressive technological opportunities. Recently, a significant research body has focused on polymer nanocomposites both in the engineering and scientific fields to explore the distinctive properties of the nanosize system. It offers a sustainable alternative to classical loaded polymers, by adding nanofillers which have high surface area to a polymer host matrices substance. The poor performance of most polymers can be enhanced to meet the needs and requirements of a wide range of scientific and engineering applications. In polymer nanocomposites, various categories of polymers, like thermoplastics, thermosets and elastomers can be used as materials matrices. However, the thermoplastic-based nanocomposites are attracting the most attention from both academic and industrial sources, due to their potential to be recyclable. The thermomechanical recycling procedure is the most cost effective process for large scales of polymers. Throughout the thermomechanical recycling process, polymers undergo several kinds of thermal and mechanical process that could change the polymer molecular structure, consequently changing the polymer performance. Recycled polymers usually have lower performance compared to original polymers especially in applications which require low strength polymers. The added nanofillers such as graphene have the potential to improve the properties of the polymer even after recycling [1].

2.2. Nanotechnology

Nanotechnology refers to materials and devices with design, characterization, production and application at nanometer scale. Nano is a Greek word which meaning dwarf, indicating a decrease of size, or time, 10^{-9} fold, that is smaller than a micron by one thousand times. One cubic nanometer (nm^3)

is approximately 20 times the volume of an individual atom. A nanoelement's size relative to a basketball is the same as a basketball's size compared to the earth. These nanoscale materials display at least one unique feature because their nanoscale size. A high surface area and quantum effects from the nanosize material contribute to improving the materials by reinforcing their reactivity, thermal, electrical and mechanical properties. Nanoscience studies the structure and properties of materials at atomic and molecular levels, based on the dimensions of the materials [2].

2.3. Nanoparticles

Particles with one dimension at least, that is around 1000nm (1 micron) and less, and possibly as atomic size and molecular length scales (~0.2 nm), are termed as nanoparticles. Nanoparticles can take both crystalline and amorphous form and have high surface area per the unit of volume. That unique property offers greater chemical reactivity than any other particles with a larger size, even with the same surface. To a certain degree, nanoparticulate material should be considered a featured state of material, in addition to solid, liquid, gas and plasma states, because of its unique features with a large surface area. Typical nanoparticle crystalline forms are fullerenes and carbon nanotubes, while conventional crystalline forms are graphite and diamond. The materials formed from nanoparticles offer unfamiliar characteristics compared to conventional bulk materials. Many researchers limit the size of nanomaterials to around 50 nm [3] or 100 nm [4]. This maximum limit is justified by the actuality that some physical properties of nanoparticles equal those of bulk particles when their size reaches these values. However, a fair definition extends this upper limit, so that many particles up to 1 micron are classified as nanoparticles [5].

2.4. Nanomaterials

Materials that contain structural building blocks of less than 1 μm and at least zero dimensions are known as nanomaterials. However bulk crystals with nanometer lattice spacing but macroscopic dimensions overall, are generally eliminated.

2.4.1. Nanomaterials Classification

Nanomaterials are categorized based on many features such as nanoparticle geometry, morphology, composition, uniformity and agglomeration. This research uses a rating based on nanoparticle dimensions, whereby nanomaterials are classified as 0D, 1D, 2D and 3D [6].

- Zero dimensional (0D): this type of nanomaterial has nano size in all three dimensions. Metal nanoparticles like gold and silver nanoparticles are a good example of this type of 0D nanoparticles. The majority of these nanoparticles type are spherical and the particle diameters are in the 1-50 nm range.

- One dimensional (1D): this type of nanostructures has one dimension not at the nanometer range. These include nanowires and nanotubes. These materials are long (few micrometres in length), while the diameter just a few nanometers. Nanotubes materials are good example of this type of nanomaterial.
- Two dimensional (2D): this type of nanomaterial has two dimensions that are not in the nanometre range. These include many different types of nanomaterials and the best example is the graphene. The area of this type of nanomaterials may be in the range of a square micrometre, but the thickness remains in the nano scale size.
- Three dimensional (3D): in this type of nanomaterials all the dimensions are not in the nano meter range. These include bulk materials such as graphite [7][8].

This project is interested in the most recent type of nanomaterial, which is graphene.

2.5. Graphene

The study of graphene is one of the most interesting areas in condensed matter and materials science physics [9]. Moreover, graphene has potential for many applications in several fields [10][11]. The plurality of the original research into graphene has focused on its thermal and mechanical properties, and analysed its use in manufacturing applications [12] [13]. Graphene consists of a single atomic layer of sp^2 hybridized carbon atoms arranged in hexagonal honey comb structures which are covalently bonded to three others with a carbon–carbon bond length of 0.142 nm to create a hexagonal ring structure. Graphite, a 3D layered crystal lattice structure, is formed by stacking parallel 2D graphene sheets. The neighbouring graphene sheets in graphite are held together by weak van der Waals forces, with a separation distance of 0.335 nm as shown in Figure 2.1. Research on graphene has now extended significantly, amidst growing recognition that graphene could have exciting and interesting physical behaviour and features like a high stiffness and strength, thermal and electrical conductivity and impermeability to gases (Helium, Oxygen, Nitrogen etc.). For applications in the nanocomposites field [14] [15] researchers looking at other nanocomposites forms have recently refocused their efforts to graphene nanocomposites. Furthermore, there was pre-existing expertise in graphite exfoliation and the preparation of graphene oxide from graphite oxide. Graphene oxide is related to reduced graphene oxide and pristine graphene by chemical modification[16].

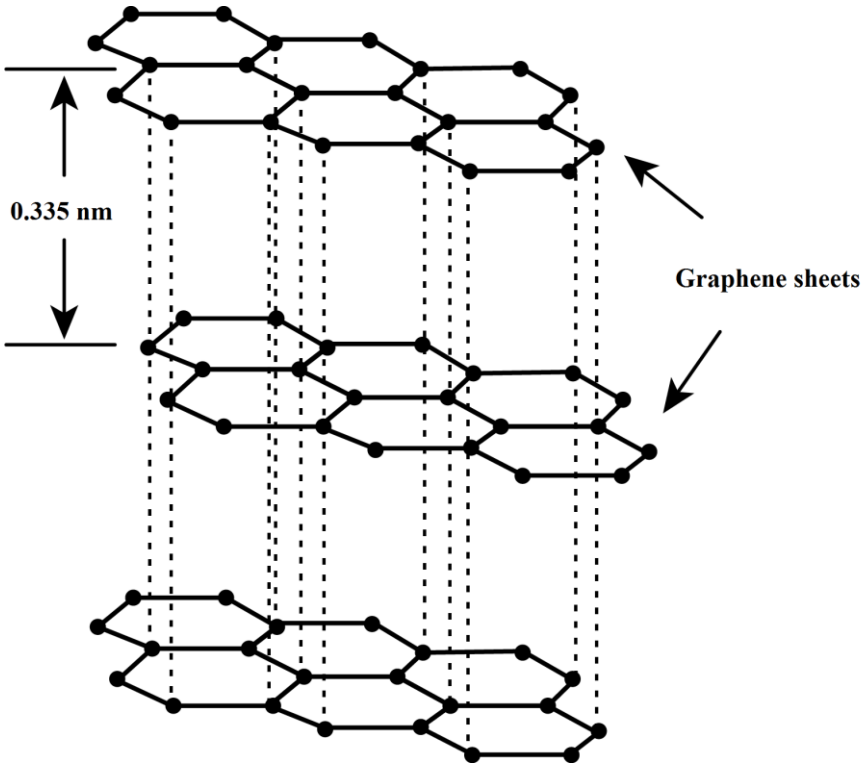

Figure 2.1. Layered structure of graphite showing the sp^2 hybridized carbon atoms bonded in hexagonal rings [17].

2.5.1. Synthesis of Graphene

The first successful attempts to create a single sheet of graphene using mechanical exfoliation are referred to as the "scotch tape method". However, the scotch tape method produces quantities suitable for laboratory research but insufficient volumes for applications as nanocomposites. Much effort is necessary to produce single sheets of graphene. It is necessary to synthesise the monolayer graphene by using procedures like chemical vapour deposition (CVD), epitaxial growth on silicon carbide, molecular beam epitaxy, etc. This approach is known as ''bottom-up'' and is not relevant to the current project. The other method involves breaking graphite down into graphene sheets using the mechanical cleavage or liquid phase exfoliation known as ''top-down'' [18]. In top-down processes, graphene is synthesised in several ways, such as:

- Micromechanical exfoliation of graphite
- Direct sonication of graphite
- Chemical reduction of organically treated Graphite Oxide (GO)
- Thermal exfoliation/reduction of GO

The graphene used in this project is synthesised using thermal exfoliation and reduction. GO is synthesized by oxidizing the graphite nanoparticles with a mixture of sulfuric acid, sodium nitrate,

potassium permanganate and flake graphite. Flake graphite is the most common source of graphite used for oxidation. This naturally occurring form of graphite is purified to remove heteroatom contamination and contains numerous localized defects to aid the oxidation process. However, the elucidation of the precise oxidation mechanism remains an ongoing challenge due to the chemical complexity of flake graphite and the defects that are inherent as a consequence of its natural source. GO reduction can be performed either through a chemical or thermal reduction approach. Chemical reduction of GO sheets is performed using several reducing agents like hydrazine and sodium borohydride. Thermal reduction uses a heat process to remove the oxygen functional groups from GO surfaces, this is known as "the Hummers method" [19][20].

2.5.2. Graphene Properties and Applications

Graphene is known as one of the most favourable nanomaterials because of its unparalleled group of excellent properties. This provides opportunities for its utilization in a wide variety of applications that can benefit from superior electrical, optical, chemical, thermal and mechanical properties. Graphene can be utilized for applications in electronics, semiconductors, gas absorbers, sensors, solar cells, fuel cells, optic devices and composites. The most promising applications of graphene rely on the material's transparency and very high conductivity. Single layer graphene has a unique electronic structure and properties with zero band gap and a resultant high mobility of charge carriers. The material displays transport and conductivity at room temperature. Single layer graphene also displays room temperature ambipolar characteristics, or the quantum Hall effect [21]. These unusual properties make graphene suitable for applications in electronics. Graphene's exceptional electrical properties, combined with its 2D structure and high specific surface area (calculated value ~ 2630 m^2g^{-1}), make it an efficient gas absorber with which to fabricate next-generation sensors. However, GO sheets are naturally insulating, displaying electrical resistance values of around 1012 Ω/sq or higher due to the presence of sp^3 hybridized carbon clusters, the high density of electronegative oxygen atoms bonded to carbon and other defects. Chemical or thermal reduction can make GO electrically conductive. Heat treatment of GO reduces its oxygen functionalities and restores the sp^2 carbon clusters. This leads to higher electrical conductivity and decreases the electrical resistance [22]. The fully reduced GO has sp^3 and sp^2 concentration of ~8% and 80%, respectively. It has been observed that the presence of residual oxygen considerably impedes carrier charge (electrons or holes) transport. Further, studies have shown that transport is dominated by hopping and tunnelling among the sp^2 clusters at the initial stages of reduction, at the later stages of reduction and by percolation as original sp^2 clusters are connected by newly formed small domains, at the later stages of reduction [23]. The Young's modulus and the tensile strength of free standing monolayer graphene were measured as 1.0 TPa and 130 GPa, respectively, using nanoindentation in AFM. In another study [24], the mechanical properties of GO sheets were measured using AFM and established that the effective elastic modulus

of monolayer GO (thickness of 0.7 nm) was 207±23 GPa. The attachment of oxygen functional groups alters the perfect 2D structure of graphene, leading to a much lower strength GO sheet compared to pristine graphene. Molecular simulation studies [25] showed that the elastic modulus of GO is strongly dependent on the degree of functionalization and the molecular structure of the functional groups. Changes in molecular structure and binding energy with the presence of functional groups cause the graphene sheets to become unstable and leads to a reduction in their elastic properties, as discussed later in chapter 5. Comparable to its mechanical and electrical behaviour, the thermal conductivity of GO is much lower than that of pristine graphene, owing to the presence of defects and disorders [26] [27]. However, graphene exhibits high thermal stability up to 2600 K, dependent on the C/O ratio, as discussed in chapter 6 [28]. A unique combination of high electrical, thermal and mechanical properties has made graphene a multi-functional reinforcement for polymers and opened new possibilities for developing and improving high strength and lightweight polymer composites for vehicle and aerospace applications and gas barriers for food packaging. To exploit graphene's superior properties in such applications it is necessary to mix it with other materials (such as polymer) to make stronger and tougher composites known as nanocomposites.

2.6. Nanocomposites

Nanocomposites are a combination of two or more distinct materials, in which one is known as the reinforcing phase, which may be in the form of fibres, sheets or particles dispersed in the other material known as the matrix phase. The materials are expected to display features, as a result of the combined features of each parent components, that are greater than those of single components. Typically, the host matrix material is improved with just small concentrations of reinforcing materials. For example, if the nanocomposite is designed and fabricated correctly, it may gain reinforcement strength whilst retaining the matrix toughness, thereby exhibiting a combination of desirable properties which are not available in single components [29]. An advantage of nanocomposites, compared to traditional composites, is that such reinforcement should be achieved with the addition of a small percentage of nano particulate to the host matrix material. Consequently, the nanocomposites are much lighter weight than traditional composites, but only if the density of the nanoparticle is greater than that of the matrix. Due to that, nanocomposites are a potentially revolutionary alternative to classical composites for many possible applications [30].

2.7. Graphene-Based Polymer Nanocomposites

In general nanocomposites are classified based on the host matrix materials type and type of reinforcement nanoparticles. According to the matrix material type, nanocomposites are classified into three types:

1. Polymer matrix based nanocomposites

2. Ceramic matrix based nanocomposites

3. Metal Matrix Based nanocomposites [31]

The most common is polymer matrix based nanocomposites due to the fact that most polymers display light weight and high toughness, are easy to process, have high chemical resistance, flexibility and low charge. However, compared to other materials like metals and ceramics, the polymers have comparatively poor mechanical behaviour, thermal stability and electrical conductivity. Polymers have as well poor gas barrier and heat resistance properties. The most obvious differentiator of polymers compared with ceramic and metal is weight, due to their lower density. They have low mass atoms of carbon and hydrogen as a backbone, making them suitable for use as light weight structural components and construction materials. Polymer nanocomposites (PNCs) have been widely studied in industrial and academic fields to identify the unique features of nanosized particles. PNCs have different structures, which can impact the interactions between the polymer and the nanoparticles as filler. Furthermore, composite structures are governed by the type of nanoparticles and the polymer used. The polymers are classified into three different categories: thermoplastic, elastomers and thermosets. These classifications are based on the molecular structure of the polymer. Thermoplastics are often referred to just as plastics, which are linear or branched polymers. They can be moulded and remoulded many times into different shapes. However, this type of polymer do not easily crystallize on cooling to a solid state, a process that requires huge organisation of the highly coiled and entangled macromolecules present in the liquid state. Thermoplastic polymers cannot fully crystallize because of their inherent structure. The chemical structure of PE and PP polymers support some degree of crystallization. In such cases, crystallisation depends on experimental conditions, such as the cooling rate and time (in case of isothermal experiments). These polymers however cannot undergo complete crystallization to achieve 100% crystallinity when cooled from the melt. Hence, one part is amorphous, which starts flowing at T_g (glass transition temperature), while the crystalline part melts at T_m (melting temperature), creating a semi-crystalline polymers. Accordingly, the crystalline phases are characterized by their T_m. When a polymer reaches the melting temperature T_m, the polymer chains lose their ordered arrangement and move around freely. However, many thermoplastics are completely amorphous, even upon annealing. Amorphous polymers are characterized by the T_g, above that the materials are rubbery or fluid, and below it they are rigid. Semi-crystallinity is a desirable characteristic due to imparting the strength and flexibility of crystalline and amorphous areas respectively. Consequently, these types polymers can be rigid with the ability to twist or bend without fracturing. Crystal lamellar are obtained through crystallization from dilute solution. When crystals are formed from the melt, chain entanglements are quite important. In this case, the solid is more irregular, with polymer chains weaving in and out of crystalline portions. The lamellae are the

crystalline part while the amorphous part is that part outside the lamellae. The crystals regions are linked to the amorphous regions by polymer chains. There may be no clear edges limits between those two regions. However, in some polymers, like polyvinyl alcohol, there is a notable separation between the crystalline and amorphous regions, though in other polymers, like PE, the structure basically is crystalline with imperfections that is the amorphous regions. The short branches in LDPE interfere with the packing of molecules, so they cannot form a fully ordered structure. The lower density and stiffness make it appropriate for use as films in food packaging and carrier bags [32].

Regarding the structure and properties of the polymer, the nanoparticles and preparation method, there are three major structural types of composites based on how the filler is dispersed in the polymer. Figure 2.2 shows (a) phase-separated microcomposites, where the polymer interacts only with the exterior surface of the layered filler, (b) intercalated nanocomposites, in which the layers of filler are sufficiently separated to allow for the polymer to cover each layer, and (c) exfoliated nanocomposites, where the layers are separated entirely and dispersed throughout the polymer phase. Moreover the PNCs' properties can be enhanced by blending more than one polymer [33].

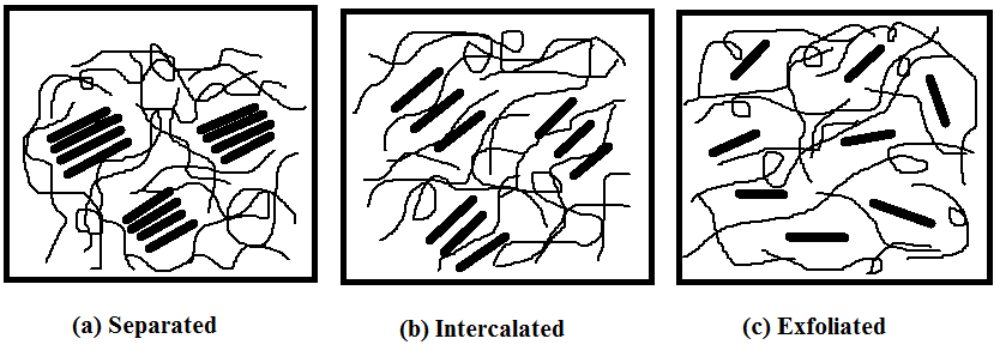

Figure 2.2. Filler dispersion in graphene-based nanocomposites: (a) separated, (b) intercalated and (c) exfoliated phases.

2.7.1. Preparation Methods of Polymer Nanocomposites

Polymer nanocomposites can be made using chemical, physical and mechanical procedures. One of the major difficulties in the polymer nanocomposites fabrication is good dispersion and distribution of nanofiller into the polymer matrix. Due to the high surface energy of the nanoparticles, they tend to aggregate into micron sized clusters of filler, which restricts the dispersion and distribution of nanoparticles. Considerable effort has been made to disperse and distribute nanofillers equally into the matrix, regularly assisted by modification of nanofiller surface, chemical reactions or polymerization reactions which makes them unsuitable for large-scale production [34]. Many preparation methods

have been used to prepare graphene nano filler reinforced polymer nanocomposites. However, there are three main methods for incorporating the filler into the host polymer matrix [35] [36].

2.7.1.1. In-situ Polymerization

In-situ polymerization methods for polymer nanocomposites fabrication usually include blending the filler in pure monomer, or monomer solution [37], and then the resulting blend is polymerized using polymerization methods like radiation, heat, initiator diffusion or an organic initiator. The monomer polymerizes between interlayers, creating either exfoliated or intercalated nanocomposites to improve and develop the dispersion between that two phases. The drawback to this method is that the high temperature synthesis causes decomposition of the polymer. Moreover, this process requires the organic modification of the particle surface and employs complex chemical reactions and polymerization reactions [38].

2.7.1.2. Solvent blending

Solvent blending or solution method is the most commonly used technique for fabricating the PNCs, specifically with higher molecular weight polymers. It involves blending nanoparticles and polymer solution in a suitable temperature and solvent. Typically, the solution method incorporates three preparation stages: sonicate the nanoparticles in a suitable solvent for dispersion process, blending it with the polymer solution through simple stirring or shear mixing (at room temperature or higher temperature) and recover the nanocomposite by precipitating or casting the solution mixture as a film. The solution method considerably improves the distribution and dispersion of nanoparticles in the polymer matrix. It offers the advantage of lower viscosity, facilitating regular mixing and good dispersion of the nanoparticles. One of the main drawbacks of this preparation method is the use of large solvents volumes, whose evaporation can impact negatively on the environment [39].

2.7.1.3. Melt Blending

Melt compounding is most common and favourable method used in industry. This method includes blending the nanofillers into the polymer host matrix at a high melting temperature. During the process, the internal shear stress is dissipated in the matrix by viscous drag. That shear stress is applied to break down the nanofiller aggregation and enhance regular and good dispersion of nanofiller in the polymer host matrix. This method is appropriate with present industrial procedures, like extrusion and injection moulding. Melt compounding includes melting the polymer powder or pellets to create a viscous solution and the nanofillers are added to the polymer solution by high temperature and high shear. The final form of the components can be produced using compression moulding or injection moulding. Compared with solution mixing, melt mixing is considered to be

more economical and environmentally friendly with no solvent waste and is more effective in industry due to large production volumes [40][41].

The polymer matrix nanocomposites can include more than one polymer, which provides opportunities to improve the polymer matrix nanocomposite properties.

2.8. The Importance of Blending Polymers

A polymer blend (PB) is a mixture of two or more of polymers or copolymers. Blending is a method of obtaining new polymer materials. A mixture of two polymers is referred to as a "polymer blend", "polyblends", or simply "blends". The polymer blend is produced by physical mixing with or without new chemical bonding between the parent components. They are prepared in order to produce a new material with different physical behaviour from the parent polymers. The objective of polymer blending is to achieve sustainable products that either have exclusive properties or lower cost than single polymers. Homogeneous blends are molecular mixed. Heterogeneous blends are thermodynamically immiscible in some concentration range. Some blends are prepared for economic reasons, while others are created to improve some property in the blend. Approximately 10% of all thermoplastics and 75% of all elastomers are polyblends. Only a few commercial blends of two thermoplastics are single-phase blends. All single-phase blends possess negative or slightly positive interaction parameters. They are amorphous blends; their glass temperature varies monotonically with composition. Blends can be compatible but not thermodynamically miscible. Many blends are created from amorphous and (or) semicrystalline polymers. The majority of these blends are compatible. Blends of two semicrystalline polymers are rarely used. The components of these blends are usually of a very similar structure. Blending also offers many possibilities for recycling of polymer for reuse [42].

2.9. Polymer blend methods

The properties of polymer blends depend on the preparation technique. There are many methods used to prepare the polymer blends. The following are the most important and commonly used.

2.9.1. Mechanical-melt mixing

This is the most important and cheapest method by which to prepare industrial polymer blends. The simplest process for making a polymer blend from thermoplastic is to blend the polymers in a melted condition in suitable devices such as rollers, extruders, etc. Under appropriate conditions, chemical reactions such as chain scissions and cross linking can take place in the polymer melt. A grafting reaction can also be caused by adding appropriate monomers to polymer melts in extruders [43] [44].

2.9.2. Solution cast techniques

Solution casting is an important method employed to make thin layered films. The solution cast process involves placing the solution of the film component in a suitable common solvent, which is subsequently dried so that the solvent evaporates. The resultant film is then removed from the substrate. A solution casting method is more advantageous than the melt process, as it results in higher quality film with uniform thickness, high clarity and pure films without residuals and pinholes. It is also possible to produce patterned films [45].

2.9.3. Latex blending

A latex is a colloidal dispersion of a polymer substance in an aqueous medium. Latex blends are prepared by blending two polymers where each polymer is present in the form of polymeric microspheres dispersed in a fluid medium [46]. Blends prepared with this method are expected to have a very high interfacial area. The early emulsion polymerization of rubbers and thermoplastic acrylates provided raw components for latex blending. Latex blends were used either directly as paints, adhesive and sealants or they were pelletized or spray dried [47].

2.9.4. Spray or freeze drying

During spray drying, the fluid of blend materials is transformed into dried particulate form by spraying the fluid into a hot substrate. This is an ideal process used when the end products require precise quality, no remaining moisture content. In freeze drying, the polymers are first heated above the glass transition to form a solution, then the polymer solution is frozen to achieve solid polymer [48][49].

2.9.5 Fine powder mixing

In this technique, mixtures of polymer powders are mixed at higher temperatures using ball milling. The temperatures used are above glass transition temperature (T_g) of constituent polymers [50].

2.9.6. In-situ polymerization

The polymerization of one polymer is conducted in the presence of another polymer resulting in interpenetrating polymer networks. Polymer electrolytes are prepared using this technique [51]. The preparation method of the blend polymer can impact the miscibility between two or more polymers then their properties.

2.10. Properties of Polymer Blends

Generally, a PB has been prepared in order to create polymeric materials that can perform under demanding mechanical, chemical, thermal and electrical conditions. They must also be capable of performing in complex atmospheric conditions. All of these factors highlight the necessity of studying the structure, behaviour and performance of the PB. The main study for assessing a polymer blend performance is to assess the structure of the blend first, since this impacts upon the material's mechanical, chemical, thermal, flame inhibition, electrical and optical properties. Polymer blends offer excellent advantages such as better processing, superior mechanical (creep, impact, stiffness, strength, modulus and hardness) performance, better heat resistance, lighter weight, gas and water barrier, chemical resistance, optical and electrical properties and low-cost production. PB enable the development and improvement of modified polymers without new polymerization steps [52].

Due to their high molar mass, the mixing entropy of polymers is relatively low and consequently, particular favourable interactions are necessary to obtain miscible or homogeneous blends on a molecular scale [53]. The overall physical and mechanical behaviour depends on the miscibility of the blends, which can be determined by studying the structure of the blend, such as its crystallinity degree, melting and crystallisation behaviour and phase separation [54][55][56][57].

2.11. Theory of Miscibility

Polymer blends are created when two or more polymers are physically mixed, either in a molten or dissolved state in a suitable solvent. Polymer blends created by the mixing of polymers can be miscible, partially miscible and immiscible. Blends can be also considered as compatible or incompatible.

Immiscible blends with separate phases commonly have poor mechanical behaviour. Miscible blends with a single phase have various components that are not in separate phase. That type of polymer blends display greater mechanical behaviour than the parent polymers. However, incompatible (immiscible) blends are more common than compatible (miscible) polymer blends [58][59].

The most influential factor for obtaining a miscible polymer blend is the low molecular weight polymers which has a large combinatorial entropy contribution comparing with high molecular weight polymers [60].

Whether a polymer blend is miscible, partially miscible or immiscible is determined by the thermodynamics of interaction between the blend components. In order to obtain spontaneous single-phase blending, the most important factor controlling mixtures of dissimilar components is the Gibbs free energy of mixing (ΔG_m), which should be negative:

$$\Delta G_m = \Delta H_m - T\,\Delta S_m \leq 0 \qquad 2.1$$

where ΔH_m and ΔS_m are the enthalpy and entropy of mixing, respectively, and T is temperature. This is, however, a necessity but not a sufficient condition. Furthermore, a second condition should also be fulfilled for each blend compositions to attain a single phase binary polymer mixture:

$$\left(\frac{\partial^2 G_m}{\partial \varphi_i{}^2}\right) > 0 \qquad 2.2$$

where φ_i is a volume fraction of the component. If ΔG_m is negative and equation 2.2 is not fulfilled, the polymer blend will separate into two phases. Figure 2.3 shows a generic phase diagram for polymer blend systems. The spinodal curve is related to the condition

$$\left(\frac{\partial^2 G_m}{\partial \varphi_i{}^2}\right)_{T,P} = 0 \qquad 2.3$$

Within these curves, the polymer mixture is unstable and will undergo spinodal decomposition. External to the spinodal curve lies the stable and metastable regions. The transition between these two regions is the binodal curve, which is where ΔG_m = 0. Blends in the metastable region will spontaneously nucleate due to composition fluctuations and separate into continuous and dispersed phases. Blends in the stable region will undergo spontaneous mixing and exhibit a single, homogenous phase [61][62].

For low molecular weight materials, an increased temperature mostly leads to greater miscibility as the $T\,\Delta S_m$ term increases, thus driving $\Delta G_m$to more negative values. For higher molecular weight components, the $T\,\Delta S_m$ term is small and other factors (such as non-combinatorial entropy contributions and temperature dependant ΔH_m values) can dominate and lead to the reverse behaviour, namely, decreasing miscibility with increasing temperature.

Solvent blends that are borderline in miscibility normally show upper critical solution temperatures (UCST) and polymer-polymer mixtures normally show lower critical solution temperatures (LCST). This behaviour is shown in Figure 2.3 [63] [64].

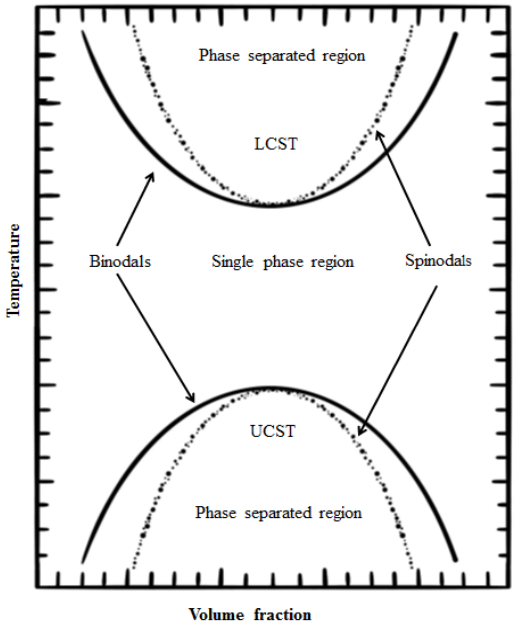

Figure 2.3. Phase diagram showing LCST and UCST behavior for polymer blends [65].

The simplest theory to calculate ΔGm for component of two polymers blends is the Flory-Huggins expression. That theory for the free energy of mixing of polymer-solvent systems has been extended to include polymer-polymer mixtures:

$$\frac{\Delta G_m}{VRT} = \frac{\varphi_1}{\upsilon_1 N_1} ln\varphi_1 + \frac{\varphi_2}{\upsilon_2 N_2} ln\varphi_2 + \varphi_1\varphi_2 \frac{\chi}{\upsilon} \qquad 2.4$$

where V is the total volume of specimen, T is absolute temperature, υ_i is the molar component volume of component i, N_i is the degree of component i polymerization , φ_i is the component i volume fraction, $\boldsymbol{\upsilon}$ is a reference volume, and χ is the Flory-Huggins interaction parameter. The first two terms on the right hand side of equation 2.4 account for the $T\Delta S_m$ term in equation 2.1 and are the entropic contribution of each component to mixing. The final term on the right describes the enthalpic mixing contribution to ΔG_m.

For large size components ($N_i > 1000$) the respective entropic term becomes negligible. A critical spontaneous mixing interaction parameter χ_c can be defined when $\Delta G_m = 0$ and $\frac{\partial^2 G_m}{\partial \varphi_i^2} = 0$ which leads to:

$$\chi_c = \frac{\upsilon}{2}\left(\frac{1}{\sqrt{\upsilon_1 N_1}} + \frac{1}{\sqrt{\upsilon_2 N_2}}\right)^2 \qquad 2.5$$

Equation 2.5 can be simplified further when both components have equal degrees of polymerisation ($N_1 = N_2$) and molecular volumes ($\upsilon_1 = \upsilon_2$), yielding:

$$\chi_c N = 2 \qquad 2.6$$

Comparing the χN values for different blend systems to this critical $\chi_c N$ value allowing for a first-order determination of whether a polymer blend is miscible, partially miscible or immiscible leading to a more complex two-phase system [65].

2.12. The classification of the polymer blend

Polymer blends are classified into the following types: miscible polymer blends, partial miscible polymer blends and immiscible polymer blends [66].

2.12.1. Miscible Polymer Blends

Compatible blends are characterised by a $\chi N < 2$ and can create a single phase or homogeneous phase due to short chain lengths or suitable enthalpies ΔH_m of blending. Frequently, negative ΔH_m values are caused by complimentary intermolecular forces between side groups such as acid-base interaction, hydrogen bonds, dipoles, ionic groups and π-orbital complexes. For instance, the interaction of styrene groups allows polystyrene and poly (2,6-dimethylphenylene oxide) (PS/PPO) to be miscible with each other. These type of blends show enhanced physical properties and a single glass transition temperature, highlighting the existence of only one phase [67].

2.12.2 . Partially Miscible Polymer Blends

Binary blends of polymer that have a χN value of ≈ 2 can be classified as partially miscible. These blends show two distinct phases with a quite broad interface region separating them. Moreover, there are sufficient concentrations of minority components in both phases to modify the bulk properties. Mixture of polystyrene and acrylonitrile butadiene styrene (PS/ABS) belongs to this type. Blends show two glass transition temperatures (T_g), with the T_g of each component shifting slightly toward the other compared to pure polymer transitions. The separated phases limit the deformation mechanisms of the blend, which promotes irreversible micro crazing [68]. This blending regime can be referred to as “compatible blends”.

2.12.3. Immiscible Polymer Blends

Polymer blends with $\chi N > 2$ are referred as immiscible (incompatible) polymer blends. The notable feature of this blend is two distinct phases separated by a sharp interface. The interfaces have minor interaction between the two phases and as a result show very poor cohesion. Therefore, the physical properties of immiscible blends are almost poorer than either of the parent polymers alone. When a blend solidifies, the minor, dispersed phase, thermodynamically favours specific geometries depending on the blend composition [69].

2.13 Compatibilization of Immiscible Blends

Most polymers blend are immiscible due to the positive Gibbs energy of mixing, that results in strong phase separation, poor adhesion at interfaces and deteriorated ultimate properties. Recently, many methods have been used to develop and improve interactions across the interfacial region of immiscible polymer blends. The most simple and effective method to compatibilize immiscible polymers is to use appropriate compatibilizers. Compatibilization involves the incorporation of suitable copolymers to an immiscible polymers blend that will raise their stability. Polymer blends typically possess unstable phase morphologies, resulting in poor mechanical properties. Compatibilizing the system leads to a stable and better mixed phase morphology by generating interaction between the two immiscible polymers [70]. There are many different types of compatibilizers such as graft or block copolymers [71] and nanofillers such as clay or layered silicates [72], carbon nanotubes [73], and graphene oxide (GO) or its derivatives [74][75].

2.13.1. Compatibilization Using Ziegler-Natta Catalysed Copolymers

Ziegler-Natta catalysts are the most commonly catalysts used in polymerization manufacturing for the production of PE and PP [76]. On the basis of solubility, the Ziegler-Natta catalyst can categorized as either:

- Heterogeneous catalysts: These catalysts are usually in combination compounds, such as poly (ethylene- co -glycidyl methacrylate) (PE-co-GMA) for PE and PP blend co-catalyst [77][78].

- Homogeneous catalysts: random copolymers of ethylene-α-olefin and metallocene linear low density polyethylene (PE) are obtained using metallocene catalyst [79][80].

Graft or block copolymers are commonly used as compatibilizing agents. The copolymers employed for that purpose is comprised of two polymers in the immiscible blend. The relevant parts of the copolymer can interact with the two phases of the blend to support the stability of the phase morphology [81] [82]. That stability improvement is achieved due to a decrease in the phase separation size of the polymers in the blend. The decreased size results from the lower interfacial tension, due to the accrual of block copolymers at the interfaces between the two polymers. This enables the immiscible blends to break up into smaller particles in the melt phase. These phase separated particles will not be as likely to grow because the interfacial tension is now considerably lower. This stabilizes the polymer blend to enable usage in an applicable product [83]. An example of this is ethylene/propylene copolymers. Such polymers act as good compatibilizing agents for blends of polypropylene and low density polyethylene. In this particular case, longer ethylene series are preferred in the copolymer. This is because co-crystallization is also a factor into this case, and the longer ethylene series will keep some remaining crystallinity [84] [85]. However, copolymers generally add few benefits relative to the polymer blends strength and stiffness, due to their low molecular weights compared with that of the bulk polymer. Furthermore, copolymers with specific structures are often not easily synthesised, making them relatively costly to engineer. Therefore, it is necessary to search for another efficient compatibilization strategy at low cost [86] [87] [88].

2.13.2. Graphene Compatibilization

The high performance and low cost of inorganic nanofillers are quite attractive to compatibilize immiscible polymer blends. GO as a product of the oxidative exfoliation of natural graphite and consist of multilayers of sp^2-hybridized carbon atoms with a mixture of carboxyl, hydroxyl, and epoxy functional groups on the basal plane and the edges [89][90][91][92]. The polar groups of GO layers can create hydrogen bonds with polar polymers [93]. The π-π stacking effects between GO and aromatic rings of some polymers could be used to improve interfacial interactions, leading to improved compatibility, resulting in improved mechanical strength [94]. Thus, GO in polymer blends may not simply assist as compatibilizer, but also act as reinforcing fillers due to their high modulus, making GO and its derivatives better than a classical copolymer compatibilizer. In addition to the surface modification of the filler and suitable compatibilizer, the processing technique also presents an opportunity to achieve the required improvement in properties and structure. The efficiency of the processing system in dispersing the fillers becomes critical, particularly with nanofillers that have a strong tendency to aggregate and agglomerate due to their high surface energies[95].

2.14. Properties of Graphene/Based Polymer Nanocomposites

In general, nanocomposites need to be thermally stable for many applications, such as in the aerospace industry. However, most polymer nanocomposites suffer from low temperature degradation, which limits their use in many possible applications. Graphene, which is one sheet of graphite, has unique features such as high conductivity, strength and thermal stability. This exceptional material can be incorporated into the polymer composites as nanofillers in order to enhance properties.

As a result of the fact that graphene/ polymer nanocomposites are a relatively recent development, the literature is still in its early stages but is developing rapidly. Already surprising developments and enhancements in mechanical, electrical and thermal properties and water and gas barriers of these materials have been achieved at very low concentrations of graphene nanoparticles in the polymer host matrix.

2.14.1. The Mechanical Properties

Graphene is considered as a strong material which offer the possibility to make refinements in the mechanical behaviours of polymeric materials at low concentrations, in particular enhancing the tensile strength and Young's modulus. However, the mechanical properties of PNCs depend on the dispersion and distribution of graphene flakes into the polymer matrix and the degree of interfacial bonding between the nanofiller and the matrix. Generally, to develop and improve the mechanical behaviour of graphene/polymer nanocomposites, GO is typically used due to its outstanding mechanical behaviour and the presence of chemical groups to assist strong interfacial interaction [96]. Although pure graphene is incompatible with polymers and will aggregate, through layer-by-layer stacking, GO, which contains hydroxyl and epoxy groups on the plane of the sheet and carbonyl and carboxyl groups at the edges, interacts more strongly with polymers. Its surface is comparatively easy to modify through the presence of amines, esters, aromatics and isocyanate functionalities that stabilize dispersions; thereby facilitating treating the composite [97].

2.14.2. Electrical Properties

Electrical behavior is one of the most interesting features of graphene/polymer nanocomposites, enabling them to be employed in electronics applications because of the low electrical resistance and high electrical conductivity. When used as filler, graphene might raise the material conductivity of an insulator polymer, such as polystyrene and polyethylene terephthalate. To make the nanocomposite conductive, the percentage of the conducting filler should be above the electrical percolation threshold

where a conductive network of nanoparticles filler is formed. However, GO is an insulator and not ideal filler for producing electrically conducting composites. Another method involves GO surface modification, reduction to recover, at least partially, the electrical and thermal conductivity through restoring the graphitic network of the sp^2 hybridized carbon by reducing the carbon oxygen function to have reduced graphene oxide or even pristine graphene [98] [99][100].

2.14.3. Thermal Properties

When graphene/polymer nanocomposites are prepared through the solvent method, a well-dispersed system is created maximising the graphene surface area, which will contribute to superb material thermal stability [101] [102]. Covalent modifications can be used to improve the graphene dispersion and distribution into polymer matrix to attain the most significant effect. The modification could also change the microstructure of graphene, resulting in a graphene with a high carbon-to-oxygen atom ratio (C/O ratio). This may increase thermal stability, through a decrease in the oxygen functional group content and an increase in the C/O ratio [103] [104]. In general, a tiny loaded amount of graphene can notably enhance the thermal stability of polymer materials [105] [106].

References

[1] Barkoula, N. M., Alcock, B., Cabrera, N. O., & Peijs, T. (2008). Fatigue properties of highly oriented polypropylene tapes and all-polypropylene composites. Polymers and Polymer Composites, 16(2), 101–113.

[2] Dowling, a, Clift, R., Grobert, N., Hutton, D., Oliver, R., & O'neill, O. (2004). Nanoscience and nanotechnologies : opportunities and uncertainties. London The Royal Society The Royal Academy of Engineering Report, 46(July), 618–618.

[3] Kittelson D B (2001) Recent measurements of nanoparticle emission from engines Current Research on Diesel Exhaust Particles, Japan Association of Aerosol Science and Technology, 9 January ,Tokyo,Japan.

[4] Borm P J A, Robbins D, Haubold S, Kuhlbusch T, Fissan H, Donaldson K, Schins R P F, Stone V, Kreyling W, Lademann J, Krutmann J, Warheit D, Oberdorster E (2006) The potential risks of nanomaterials: a review carried out for ECETOC (review) Part. Fibre Toxicol, 3–11.

[5] Cristina, B. , Ivan. I., Pacheco, B. & Kevin, R.(2007). Nanomaterials and nanoparticles: Sources and toxicity. Biointerphases , 2(4), 17 –172.

[6] Teo, B. K., & Sun, X. H. (2007). Classification and representations of low-dimensional nanomaterials: Terms and symbols. Journal of Cluster Science, 18(2), 346–357.

[7] Churg, A. (2003). Interactions of exogeneous or evoked agents and particles: the role of reactive oxygen species Free Radical Biol. & Med, 34, 1230–1235

[8] Donaldson, K., Stone, V., Borm, A., Jimenez, A., Gilmour, S., Schins, F., Knaapen, M., Rahman, I., Faux, P., Brown, M., MacNee, W. (2003). Oxidative stress and calcium signaling in the adverse effects of environmental particles PM10 Free Radical Biol. & Med, 34, 1369-1382.

[9]Geim, A.K., Novoselov K.S.(2007). The rise of graphene. Nature Materials,

6(3),183–191.

[10] Geim, A.K. (2011). Nobel Lecture: Random walk to graphene. Reviews of Modern

Physics, 83(3),851–862.

[11] Novoselov, K.S.(2011) Nobel lecture: Graphene: Materials in the flatland. Reviews

of Modern Physics, 83(3):837–849

[12] Avouris, P.(2010) Graphene: Electronic and photonic properties and devices. Nano Letters, 10(11):4285–4294.

[13] Schwierz, F.(2010) Graphene transistors. Nature Nanotechnology, 5(7):487–496.

[14] Kim, H., Abdala, A.A.& Macosko, C.W.(2010) Graphene/polymer nanocomposites. Macromolecules, 43 (16):6515–6530.

[15] Singh V., Joung D., Zhai L., Das S., Khondaker S.I.& Seal S.(2011) Graphene based materials: Past, present and future. Progress in Materials Science,56(8):1178–1271.

[16] Verdejo R., Bernal M.M., Romasanta L.J., Lopez-Manchado M.A.(2011) Graphene filled polymer nanocomposites. Journal of Materials Chemistry, 21(10):3301–3310.

[17] Sengupta, R., Bhattacharya, M., Bandyopadhyay, S., & Bhowmick, A. K. (2011). A review on the mechanical and electrical properties of graphite and modified graphite reinforced polymer composites. Progress in Polymer Science (Oxford), *36*(5), 638–670.

[18] Young, R. J., Kinloch, I. a., Gong, L., & Novoselov, K. S. (2012). The mechanics of graphene nanocomposites: A review. Composites Science and Technology, 72(12), 1459–1476.

[19]Gao, W. (2015). The chemistry of graphene oxide. Graphene Oxide: Reduction Recipes, Spectroscopy, and Applications, 61–95.

[20]Layek, R. K., Samanta, S., & Nandi, A. K. (2012). The physical properties of sulfonated graphene/poly(vinyl alcohol) composites. Carbon, 50(3), 815–827.

[21] Choi, W., Lahiri, I., Seelaboyina, R., & Kang, Y. S. (2010). Synthesis of graphene and its applications: A review. Critical Reviews in Solid State and Materials Sciences, 35(1), 52–71.

[22] Wang, S. J., Geng, Y., Zheng, Q., & Kim, J. K. (2010). Fabrication of highly conducting and transparent graphene films. Carbon, 48(6), 1815–1823.

[23]Mattevi, C., Eda, G., Agnoli, S., Miller, S., Mkhoyan, K. A., Celik, O., & Chhowalla, M. (2009). Evolution of electrical, chemical, and structural properties of transparent and conducting chemically derived graphene thin films. Advanced Functional Materials, 19(16), 2577–2583.

[24] Wang, C., Frogley, M.D. , Cinque, G., Liu, L.-Q. &Barber, A.H. (2013). Deformation and failure mechanisms in graphene oxide paper using in situ nanomechanical tensile testing .Carbon, 63 , 471–477.

[25] Zheng,Q., Li,Z., Jialin,Y. & Kim,J. (2010). Molecular Dynamics Study of the Effect of Chemical Functionalization on the Elastic Properties of Graphene Sheets. Journal of Nanoscience and Nanotechnology ,10(11),7070–7074.

[26] Lee, C., Wei, X., Kysar, J. W., & Hone, J. (2008). Measurement of the Elastic Properties and Intrinsic Strength of Monolayer Graphene. Science, 321(July), 385–388.

[27] Suk, J. W., Piner, R. D., An, J., & Ruoff, R. S. (2010). Mechanical Properties of Monolayer Graphene Oxide, 4(11), 6557–6564.

[28]Kim, K., Regan, W., Geng, B., Alemán, B., Kessler, B. M., Wang, F., Zettl, A. (2010). High-temperature stability of suspended single-layer graphene. Physica Status Solidi - Rapid Research Letters, 4(11), 302–304.

[29] Henrique, P., Camargo, C., Satyanarayana, K. G., & Wypych, F. (2009). Nanocomposites : Synthesis , Structure , Properties and New Application Opportunities. Materials Research, 12(1), 1–39.

[30] Kerstin, M., Elodie B., Marcos L., Maria J., Yolanda, E., José, L., Oliver, M., Alvise ,B., Steve, H., Uwe, B., Germán, P., Marius, J., Martina, L., Zuzana, S., Sara ,C.& Markus, S.(2017). Review on the Processing and Properties of Polymer Nanocomposites and Nanocoatings and Their Applications in the Packaging, Automotive and Solar Energy Fields. nanomaterials Review.7–47.

[31] Young, R.J &Lovell, P.A (2011).Introduction to polymers ,3 edition ,CRC press, London, United Kingdom.

[32] In-Yup, J.,& Jong-Beom, B.(2010). Nanocomposites Derived from Polymers and Inorganic Nanoparticles. Materials. 3, 3654–3674.

[33] Pedro ,C., Kestur, S. & Fernando, W.(2009) Nanocomposites: Synthesis, Structure,

Properties and New Application Opportunities. Materials Research, 12(1), 1-39.

[34] Deng, H., Lin, L., Ji, M., Zhang, S., Yang, M., & Fu, Q. (2014). Progress on the morphological control of conductive network in conductive polymer composites and the use as electroactive multifunctional materials. Progress in Polymer Science, 39(4), 627–655.

[35] Kuilla, T., Bhadra, S., Yao, D., Kim, N. H., Bose, S., & Lee, J. H. (2010). Recent advances in graphene based polymer composites. Progress in Polymer Science Volume, 35(11), 1350–1375.

[36] Sadasivuni, K. K., Ponnamma, D., Kim, J., & Thomas, S. (2015). Graphene-based polymer nanocomposites in electronics. Graphene-Based Polymer Nanocomposites in Electronics, 1–382.

[37] Potts, J. R., Dreyer, D. R., Bielawski, C. W., & Ruoff, R. S. (2011). Graphene-based polymer nanocomposites. Polymer, 52(1), 5–25.

[38] Tripathi, S. N., Rao, G. S. S., Mathur, A. B., & Jasra, R. (2017). Polyolefin/graphene nanocomposites: a review. RSC Adv., 7(38), 23615–23632.

[39] Chee, W. K., Lim, H. N., Huang, N. M., & Harrison, I. (2015). Nanocomposites of graphene/polymers: a review. RSC Adv., 5(83), 68014–68051.

[40]Nguyen, Q.T., Baird, D.G., (2006). Preparation of polymer–clay nanocomposites and their properties. Adv. Polymer. Tech. 25, 270-285.

[41] Kalaitzidou, K., Fukushima, H., Drzal, L.T., (2007). A new compounding method for

exfoliated graphite-polypropylene nanocomposites with enhanced flexural properties and lower percolation threshold. Compos. Sci. Technol. 67, 2045-2051.

[42] Shemouratov, Y. V., Prokhorov, K. A., Sagitova, E. A., Nikolaeva, G. Y., Pashinin, P. P., Lebedev, Y. A., & Antipov, E. M. (2009). Raman study of polyethylene-polypropylene blends. Laser Physics, 19(12), 2179–2183.

[43] Braun, D., Cherdron, H., Rehahn, M., Ritter, H. & Voit, B. (2005) Polymer synthesis: Theory and Practice, 4th edition, Springer-Verlag Berlin Heidelberg, 12.

[44] Samperi, F., Battiato, S., Recca, G., Puglisi, C., & Mendichi, R. (2015). Reactive melt mixing of PC/PEN blend. Structural characterization of reaction products. Polymer, 74, 108–123.

[45] Topham, P. D., Howse, J. R., Fernyhough, C. M., & Ryan, A. J. (2007). The performance of poly(styrene)-block-poly(2-vinyl pyridine)-block-poly(styrene) triblock copolymers as pH-driven actuators. Soft Matter, 3(12), 1506–1512.

[46] Feng, J., Winnik, M. A., Shivers, R. R., & Clubb, B. (1995). Polymer Blend Latex Films: Morphology and Transparency. Macromolecules, 28(23), 7671–7682.

[47] Song, P., Cao, Z., Cai, Y., Zhao, L., Fang, Z., & Fu, S. (2011). Fabrication of exfoliated graphene-based polypropylene nanocomposites with enhanced mechanical and thermal properties. Polymer, 52(18), 4001–4010.

[48] Paudel, A., Worku, Z. A., Meeus, J., Guns, S., & Van Den Mooter, G. (2013). Manufacturing of solid dispersions of poorly water soluble drugs by spray drying: Formulation and process considerations. International Journal of Pharmaceutics, 453(1), 253–284.

[49]Tiwari, R., Srivastava, B., Tiwari, G., & Rai, A. (2009). Extended release promethazine HCl using acrylic polymers by freeze-drying and spray-drying techniques: Formulation considerations. Brazilian Journal of Pharmaceutical Sciences, 45(4), 829–840.

[50] Koch, C. C. (2003). Top-Down Synthesis of Nanostructured Materials: Mechanical and Thermal Processing Methods. Rev.Adv.Mater.Sci, 5, 91–99.

[51] Ogawa, T. (1997.). Poly (silmethylene) -Based Polymer Blends . L In Situ Polymerization in Silicon-Based Polymers, 399–405.

[52] Shanks, R. A., Li, J., and Yu, L. (2000). Polypropylene – polyethylene blend morphology controlled by time – temperature – miscibility. Materials Science, 41, 2133–2139.

[53] Walsh, D. J. & Rostami, S.(1984). The miscibility of high polymers: The role of specific interactions. Advances in Polymer Science,120–163.

[54] Scobbo, J.J, Jr and Goettler, L.A. (2003)Applications of polymer alloys and blends,

in Polymer Blends Handbook (ed. L.A. Utracki), Kluwer Academic Publishers, pp. 951–976.

[55]Yu, L., Dean, K., & Li, L. (2006). Polymer blends and composites from renewable resources. Progress in Polymer Science (Oxford), 31(6), 576–602.

[56] Zhang, J., Jiang, D. D., & Wilkie, C. A. (2005). Polyethylene and polypropylene nanocomposites based upon an oligomerically modified clay. Thermochimica Acta, 430(1–2), 107–113.

[57] Deka, B. K., & Maji, T. K. (2011). Study on the properties of nanocomposite based on high density polyethylene, polypropylene, polyvinyl chloride and wood. Composites Part A: Applied Science and Manufacturing, 42(6), 686–693.

[58] Freudenberg K (1932) The relation of cellulose to lignin in wood. J Chem Edu 9(Part II) 1171–1180.

[59] Lee K et al (2014) On the use of nanocellulose as reinforcement in polymer matrix. Compos Sci Technol 105:15–27

[60] Saldivar-Guerra,E. & Vivaldo-Lima. E. (2013). Handbook of Polymer Synthesis, Characterization, and Processing. 3rd edition. New York: John Wiley & Sons, 11–12.

[61] Robeson, L. M., Ed.(2007). Polymer Blends : a Comprehensive Review; Hanser: Munich ; Cincinnati.

[62] Flory,P. (1941). Thermodynamics of High Polymer Solutions. Journal of chemical physics, 9(21), 440-440.

[63] Seuring, J., & Agarwal, S. (2012). Polymers with upper critical solution temperature in aqueous solution. Macromol. Rapid Commun., 33(22), 1898–1920.

[64] Zhang, Q. & Hoogenboom, R (2015). Polymers with upper critical solution temperature behavior in alcohol/water solvent mixtures. Progress in Polymer Science, 48 ,122–142 .

[65] Seuring, J., & Agarwal, S. (2012). Polymers with upper critical solution temperature in aqueous solution. Macromol. Rapid Commun., 33(22), 1898–1920.

[66] Müller, M. (2004). Phase Behavior and Chain Conformations in Polymer Blends: Monte Carlo Simulation vs Mean Field Theory. Computational Soft Matter: From Synthetic Polymers to Proteins, Lecture Notes (Vol. 23).

[67] Fekete, E., Foldes, E., Damsits, F., & Pukanszky, B. (2000). Interaction-structure-property relationships in amorphous polymer blends. Polymer Bulletin, 44(4), 363–370.

[68] Weeks, N. E., Karasz, F. E. & MacKnight, W. J.(1977). Enthalpy of mixing of poly(2,6-dimethyl phenylene oxide) and polystyrene. Journal of Applied Physics, 48, 4068–4071.

[69] Yokouchi, M., Seto, S.& Kobayashi, Y.(1983). Comparison of polystyrene, poly (styrene/acrylonitrile), high-impact polystyrene, and poly(acrylonitrile/butadiene/styrene) with respect to tensile and impact properties. Journal of applied polymer, 28(7), 2209–2216.

[70] Sundararaj, U.& Macosko, C. W.(1995). Drop Breakup and Coalescence in Polymer Blends: The Effects of Concentration and Compatibilization. Macromolecules, 28, 2647–2657.

[71] Utracki, L.(2002). Compatibilization of Polymer Blends. The Canadian Journal of Chemical Engineering, 80, 1008–1016.

[72] Chen, C., & White, J. (1993). Compatibilizing Agents in Polymer Blends: Interfacial Tension, Phase Morphology, and Mechanical Properties. Polymer Science and Engineering, 33(14), 923-930.

[73]Aziz, A. A., Akil, H. M., Jamaludin, S. M. S., & Ramli, N. A. M. (2011). The effect of multiple compatibilizers on the impact properties of polypropylene/polystyrene (PP/PS) blend. Polymer - Plastics Technology and Engineering, 50(8), 768–775.

[74]Singh ,A. K., Rajiv, P. and Dhananjai, P.(2013). A comparative thermal, optical, morphological and mechanical properties studies of pristine and C15A nanoclay-modified PC/PMMA blends: a

critical evaluation of the role of nanoclay particles as compatibilizers. The Royal Society of Chemistry, 3, 15411–15420.

[75]Kasaliwal, G. , Goldel, A. and Potschke, P. (2009).Influence of processing conditions in small-scale melt mixing and compression molding on the resistivity and morphology of polycarbonate-MWNT composites. Journal of Applied Polymer Science, 112(6), 3494–3509.

[76] Pandikumar, A., Soon How, G. T. & See, T. P. (2014) .Graphene and its nanocomposite material based electrochemical sensor platform for dopamine, RSC Advances, 4(108), 63296–63323,.

[77] Upadhyay, R. , Soin, N. and Roy, S.(2014) .Role of graphene/metaloxide composites as photocatalysts, adsorbents and disinfectants in water treatment: a review," RSC Advances,. 4(8) 3823–3851.

[78]Taniike, T., Goto, K., & Terano, M. (2015). Active site nature of magnesium dichloride-supported titanocene catalysts in olefin polymerization, 2(1), 57–63.

[79]Deka, B. K., & Maji, T. K. (2010). Effect of coupling agent and nanoclay on properties of HDPE, LDPE, PP, PVC blend and Phargamites karka nanocomposite. Composites Science and Technology, 70(12), 1755–1761.

[80]Natta, G.; Pino, P.; Mazzanti, P.(1973) Regular linear head-to-tail polymerizates of certain unsaturated hydrocarbons and filaments comprising said polymerizates. U.S. Patent 3,715,344.

[81]Sonnier, R., Massardier, V., & Cassagnau, P. (2008). Compatibilization of hiPP / HDPE blends by a metallocene copolymer. Journal of Materials, 1–4.

[82]Shamiri, A., Chakrabarti, M. H., Jahan, S., Hussain, M. A., Kaminsky, W., Aravind, P. V., & Yehye, W. A. (2014). The influence of Ziegler-Natta and metallocene catalysts on polyolefin structure, properties, and processing ability. Materials, 7(7), 5069–5108.

[83]Wildes, G., Keskkula, H., & Paul, D. R. (1999). Coalescence in PC/SAN blends: Effect of reactive compatibilization and matrix phase viscosity. Polymer, 40(20), 5609–5621.

[84]Robeson, L. (2014). Historical perspective of advances in the science and technology of polymer blends. Polymers, 6(5), 1251–1265.

[85] Roe, R.J. (1993). Use of Block Copolymer as Polymer Blend Compatibilizer. U.S. Army Research Office.

[86] Rudin, A. & Phillip, C. (2013). The Elements of Polymer Science and Engineering. 3rd. Oxford: Academic Press.

[87] Jump up to: a b Tan, N. (1994). Reactive Compatibilization in Immiscible Polymer Blends. Doctor of Philosophy Thesis, University of Maryland.

[88] Pandikumar, A., Soon How, G. T., See, T. P., Omar, F. S., Jayabal, S., Kamali, K. Z., Huang, N. M. (2014). Graphene and its nanocomposite material based electrochemical sensor platform for dopamine. RSC Adv., 4(108), 63296–63323.

[89] Si, M., Araki, T., Ade, H., Kilcoyne, a. L. D., Sokolov, J. C., Rafailovich, M. H., & Fisher, R. (2006). Compatibilizing Bulk Polymer Blends by Using Organoclays Compatibilizing Bulk Polymer Blends by Using Organoclays. Macromolecules, 39(14), 4793–4801.

[90] Li, B., Wan, C., Zhang, Y.& Ji, J.(2010). Blends of Poly(2,6-dimethyl-1,4-phenylene oxide)/ Polyamide 6 Toughened by Maleated Polystyrene-based Copolymers: Mechanical Properties, Morphology, and Rheology. Journal of Applied Polymer Science, 115,3385–3392.

[91] Tong, J., Huang, H.-X., & Wu, M. (2017). Promoting compatibilization effect of graphene oxide on immiscible PS/PVDF blend via water-assisted mixing extrusion. Composites Science and Technology, 149, 286–293.

[92] Yang, J., Feng, C., Dai, J., Zhang, N., Huang, T., Wang, Y. (2013) . Compatibilization of immiscible nylon 6/poly(vinylidene fluoride) blends using graphene oxides .Polymer International, 62 (7), 1085-1093.

[93] Jaemyung, K., Laura, J., Cote, F., Wa, Y., Kenneth, R., Shull, A., & Huang, J. (2010). Graphene Oxide Sheets at Interfaces. J. Am. Chem. Soc., 132(23), 8180–8186.

[94] Dreyer, D., Park, S., Christopher, B. & Ruoff, R.(2009). The chemistry of graphene oxide

Daniel. Chem.Soc.Rev., 39, 228–240.

[95]Cao, Y., Zhang, J., Feng, J., & Wu, P. (2011). Compatibilization of immiscible polymer blends using graphene oxide sheets. ACS Nano, 5(7), 5920–7.

[96] Kar, G. P., Biswas, S., & Bose, S. (2015). Tailoring the interface of an immiscible polymer blend by a mutually miscible homopolymer grafted onto graphene oxide: outstanding mechanical properties. Phys. Chem. Chem. Phys., 17(3), 1811–1821.

[97] Amani, M., Sharif, M., Kashkooli, A., Rahnama, N., & Fazli, A. (2015). Effect of mixing conditions on the selective localization of graphite oxide and the properties of polyethylene/high-impact polystyrene/graphite oxide nanocomposite blends. RSC Advances, 5(95), 77723–77.

[98] Won, J., Richard, S., Piner, D., An, J. & Ruoff. R.(2010) American Chemical Society , 4 (11), 6557–6564 .

[99] Moon, I. K., Lee, J., Ruoff, R. S., & Lee, H. (2010). Reduced graphene oxide by chemical graphitization. Nature Communications, 1(6), 1–6.

[100] Zhanga, H., Zhenga, W., Yana, Q., Yanga, Y., Wang, J., Lu, Z., Ji, G.& Yu, Z.(2010) Electrically conductive polyethylene terephthalate/graphene nanocomposites prepared by melt compounding. Polymer ,51 , 1191–1196.

[101]Stankovich, S., Dikin, D. A., Dommett, G. H. B., Kohlhaas, K. M., Zimney, E. J., Stach, E. A., Ruoff, R. S. (2006). Graphene-based composite materials. Nature, 442(7100), 282–286. http://doi.org/10.1038/nature04969

[102] Singh, R. K., Kumar, R., & Singh, D. P. (2016). Graphene oxide: strategies for synthesis, reduction and frontier applications. RSC Adv., 6(69), 64993–65011.

[103] Park, S. & Ruoff, R.(2009). Chemical methods for the production of graphenes. Naturenanotechnology,4, 217–224.

[104] Dreyer, D., Park, Sungjin., Bielawski, C. & Ruoff, R.(2010). The chemistry of graphene oxide, Chem.Soc.Rev., 39, 228–240.

[105] Liu, J., Tang, J., & Gooding, J. J. (2012). Strategies for chemical modification of graphene and applications of chemically modified graphene. Journal of Materials Chemistry, 22(25), 12435.

[106] Liu, J., Yang, W.& Tao, L. (2010) Thermosensitive graphene nanocomposites formed using pyrene-terminal polymers made by RAFT polymerization. J Polym Sci Part A: Polym Chem;48,425–33.

Chapter 3

Characterisation and Experimental Techniques

The polymer, graphene and graphene/polymer nanocomposites samples were classified according to different characterization techniques to study their physical and chemical structural, optical, thermal, electrical and mechanical properties. The different characterization techniques and their working principles are set out below.

3.1. Scanning Electron Microscope (SEM)

Scanning electron microscopy (SEM) is a most popular characterization method for materials. SEM scans a focused electron beam on a sample to reveal its surface morphology and composition details [1]. The incident electron beam will react with atoms in the test specimen, which then release a range of signals which can be detected, analysed and imaged. SEM uses an electron beam focussed using magnetic lenses to create clear image information of a specimen located inside a vacuum chamber. Detectors inside the chamber capture electrons that scatter off the specimen from either the incident electron beam or secondary electrons that are released from the specimen surface after being excited by the incident electron beam. Non-conductive specimens in SEMs can rapidly develop a charge from the electron beam. This can result in poor images and heat which can damage the specimen. Consequently, the specimen surfaces should be coated with a layer conductive, like silver or gold, before the SEM scan [2]. The most common method and widely used for coating the surface of the specimen is sputter coating, otherwise known as sputter deposition. The specimen is located inside a vacuum chamber and the pressure reduced to <100 mbar. Argon gas is released into the chamber and an electrical field is applied at an anode to excite the argon into plasma and impact a gold foil cathode. The argon collisions discharge gold atoms off the foil surface, creating a deposit on the sample surface. The deposition layer thickness is determined by changing the strength of the plasma-creating electric field and time of sputter. The gold atoms move as a result of the ionic argon momentum and sputtering occurs at ambient temperatures [3].

The morphology of the sample surface was evaluated by JEOL JSM-6010LA analytical scanning electron microscope (SEM). The samples were placed on aluminum pan and attached to the SEM stubs. The pressed specimens were located up the stub by tape of conductive carbon with the fractured surface facing upwards and subsequently coated with conductive material by gold sputtering. A Denton Vacuum Desk IV Coater/Etcher was used to sputter coat the specimen. The specimens were sputter coated using sputter strength of 50% and sputter time of 32 seconds. SEM was performed with an accelerating voltage of 10 kV under a vacuum environment. The magnification image was between 300-5000 × for each sample. For each specimen, at least 30 different sections were randomly selected.

3.2 .Wide Angle X-ray Diffraction (WAXD)

Studying and understanding the structure of nanocomposites on the mesoscopic scale (2-50 nm), for example clusters, aggregates, and nanosized materials, can also be undertaken using X-ray scattering, which depends on differing electron densities of the constituent materials. WAXD is commonly used to study the crystallisation structure on nanometre length scale [4]. WAXD is a non-damaging analytical technique that provides the characterisation of interlayer spacing, orientation, crystallite size and crystalline phases in the specimen. It provides details about the oxidation degree of graphene or graphite and exfoliation of the graphene into the polymer layers, while also presenting useful data about the crystallinity degree and the crystal phases of the materials. WAXD is established on the principle of constructive interference of the scattered X-rays, with an angular dependence that depends on the crystalline nature of the constitutive materials. For crystalline materials, Bragg's law can be used to determine the d-spacing by using the following equation

$$n\lambda = 2dsin\theta \qquad 3.1$$

The X-rays are diffracted from the material and collected by a detector. The 2θ values of x-rays diffraction are plotted in a diffraction pattern. The peaks correlate to a particular interatomic distance. In general, the amorphous peak areas in materials show a range of d-spacing values and consequently show wide peak while crystalline peak areas show sharp and narrow peaks in a diffraction pattern. [5][6].

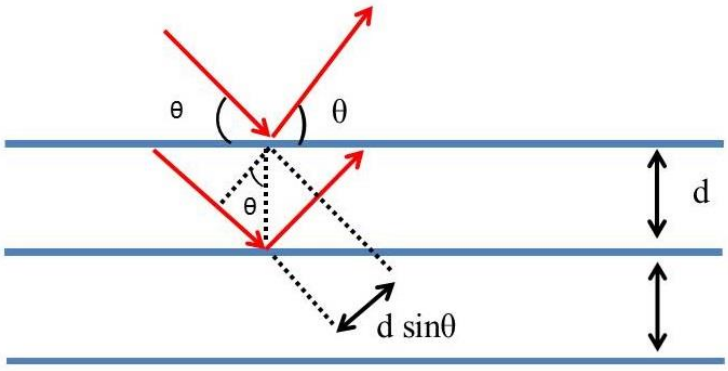

Figure 3.1. Scheme to explain the Bragg law

WAXD experiments were carried out on a Siemens D5000 (Cu, GA- XRD) unit, operating the intensity of the beam at 40kV, and 40mA to carry out the experiments at room temperature. The X-ray

source was CuKα radiation with a wavelength of λ = 1.54178 Å. Scattered intensities were measured over 2θ values between 2° and 40° in steps of 0.050° sec^{-1}, and analysed using the DIFFRAC. EVA software.

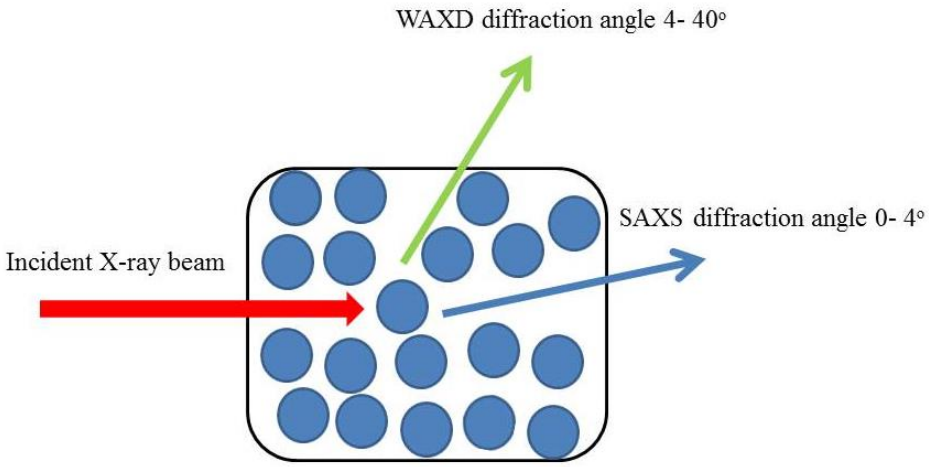

Figure 3.2. The working principle difference in the WAXD and SAXS.

3.3. Small Angle X-ray Scattering Measurements (SAXS)

Since studying ideal lamellae in polymers in the 1960s, SAXS has become one of the most commonly used techniques to study the morphology of solid polymers. SAXS is an investigative technique employed to determine the structure of particle systems' average particle sizes and shapes. The materials may be in a solid, liquid or gaseous state or be a combination of materials. Normally, X-rays are transmitted through the material and all particles that are exposed to the beam will contribute to the scattered signal. The SAXS method is accurate, non-damaging and generally needs only a small piece of the sample with a wide range of application areas such as biological materials, polymers, colloids, chemicals, nanocomposites, metals, minerals, food and medicines[7].

SAXS can be used for many different types of materials that contain two-phase structures, where the electron density of one phase is much higher than other phase. Interpretation of the data often requires that a two-phase approximation can be made. As such, a larger electron density difference results in a higher scattering contribution. In a two-phase approximation, SAXS is used to study precipitation in metal alloys, diamond structural defects, pore structures in fibres, particle growth in solutions, catalyst characterization, glass structure, ceramics void structure and also has biological applications. When the phases number in the specimen increases to three, complexity increases significantly, which limits the possible applications. In multiphase systems, SAXS is rarely used, however some basic work for such applications has recently taken place [8]. SAXS provides crucial information about structural changes in polymers on a molecular scale with dimensions range of 10Å to a few thousands angstrom. A graphic characterization of the SAXS working process and example of a scattering curve,

the intensity versus the scattering vector (q), is displayed in Figure 3.3. The scattering vector is calculated from the diffraction angle as $q = 4\pi/\lambda \sin(\theta/2)$. From the absolute value of scattering intensity, the fluctuation magnitude of electron density can be identified. The curve shape and the peak intensity position are related to the correlations of the density fluctuations. Thus, SAXS can provide useful data about phase transitions if these processes are accompanied by changes in the fluctuation magnitude [9][10][11].

SAXS measurements were carried out on a laboratory SAXS instrument (NanoStar, Bruker) equipped with a micro focus Cu-Kα X-ray source, collimating system with motorized scatterless slits (Xenocs, France) and HiStar 2D multiwire gas detector (Siemens/Bruker). Scattering patterns were corrected for the detector's dark current, spatial distortion and flat field. They were normalized using sample thickness, exposure time, sample transmission and the detector normalization coefficient. They were integrated using the Fit2D and SASview software.

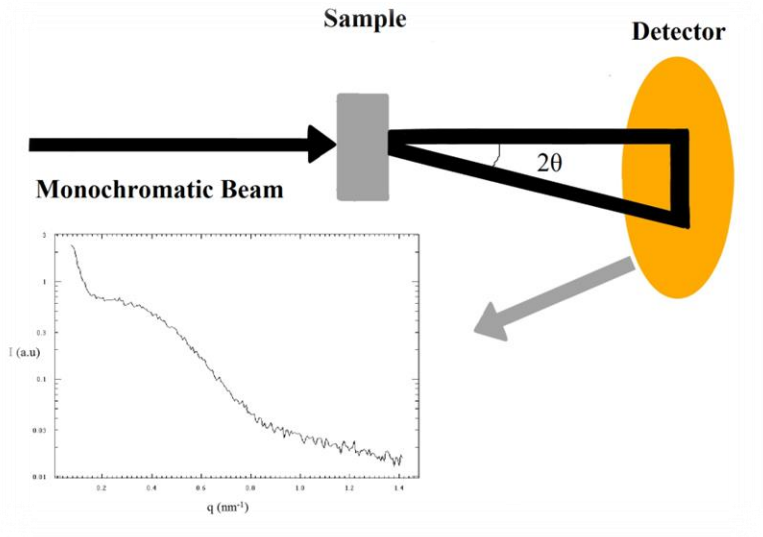

Figure 3.3. Simplified working diagram of scattering instrument.

3.4. X-ray photoelectron spectroscopy (XPS)

XPS, also known as electron spectroscopy for chemical analysis (ESCA), is sensitive technique of a surface (~10 nm) that used for define the constituent elements and the chemical composition of a materials specimen. It presents quantitative and qualitative data about the chemical structure of the materials specimen. Moreover this technique is exclusive of hydrogen and helium. In the present project, XPS analysis was used to determine the C/O ratio in the GO, rGO and G.

In general, XPS employs the photoelectric impact of emitted electrons that are released as a consequence of the substrate irradiation via high-energy X-ray photons. A monochromatic X-ray beam spurs the core electrons emission from the surface atoms of the substrate. Then the excited electrons release from the material, hitting with other atoms and losing energy on the way out. The average distance of the electrons travel (free path) is determined by the kinetic energy of the electron and the solid nature that it is travelling through. This inelastic mean free path determines that electrons emitted from anywhere below 10 nm will lose sufficient energy which will not be detected. Consequently, just the emitted electrons from the uppermost 10 nm of a substrate are available to be detected and analysed [12][13].

It is useful to electrically isolate graphene samples during the analysis to prevent differential charging. Consequently, the samples were mounted by pushing the powders into indium foil, which had itself been mounted on paper onto the XPS sample holder. Indium foil alone was also analysed.

The analyses were conducted using a Kratos Supra instrument with the monochromated aluminium source, with two analysis points per specimen. Survey scans were gathered from 1200 to 0 eV binding energy, at 160 eV pass energy (a given energy to arrive at the detector) and 1 eV intervals. High-resolution O 1s, C 1s and In 3d spectra were collected over an appropriate energy range at 20 eV pass energy and 0.1 eV intervals. The analysis area was 700 µm by 300 µm.

The samples were flooded with low energy electrons from the charge neutralisation source during the data collection. Unfortunately, this resulted in a large shift in all the data towards lower binding energy, so the data needed to be corrected. Conventionally, the C1s signal for sp^3-hybridised carbon bonded to other carbons or hydrogen, expected at 285.0 eV is used to calibrate the data. However, this was not necessarily the largest carbon peak in the data collected. Instead, the data for the indium foil was corrected to make the largest C 1s component 285.0 eV for this sample, and the peak position identified for the largest In 3d peak was then used to calibrate the graphene related samples where a indium 3d peak was seen. An indium 3d peak was seen for graphene 1, and the same correction was consequently used for graphene 2. No indium signal was detected for either reduced graphene oxide analysis point, so the same correction was made as for the graphene oxide 2 analysis points.

3.5. Fourier Transformed Infrared Spectroscopy (FTIR)

Infrared spectroscopy has been a useful material analysis method for many years. An infrared spectrum shows a clear mark of a specimen with absorption or transmission peaks, that corresponds to the vibrations frequencies which happen between the atomic bonds [14]

In FTIR, radiation of infrared wavelengths travels through a sample that may be a solid, liquid or even gas. The transmittance or absorbance of infrared light is measured as a function of wavelength. FTIR offers good information about the chemical structure of the specimen including the chemical bonds. Various bonds between components will vibrate, twist and stretch due to the absorption of infrared radiation, giving rise to various peaks in the spectrum. FTIR can be used to determining the components of the material and ways in which they are linked.

A FTIR arrangement will contain an infrared radiation emitter, an interferometer, a beam splitter, mirrors and a detector. The beam splitter and mirrors serve to separate the beam into a reference and specimen beam that is then processed into an interferogram. The Fourier transform itself is the process by which an algorithm is used to transform the constructive interference observed in the interferogram into a spectrum [15].

FTIR spectroscopy is a favoured method for infrared spectral analysis for many reasons including:

- It is a non-damaging technique;
- It offers an exact scanning technique, which does not require external calibration;
- It can increase speed, collecting a scan every second;
- It is mechanically simple process, with just one mobile part [16].

FTIR spectra were recorded using a Bruker Alpha with (single bounce Diamond) Platinum-ATR accessory. Spectra were obtained at 4 cm^{-1} resolution and averages of at least 16 scans in the standard wavenumber range 400–4000 cm^{-1} at room temperature (23 ^{o}C). The software used for analysing the FTIR curves was Origin 2017.

3.6. Ultraviolet Visible Spectroscopy (UV-Vis)

Ultraviolet–visible spectroscopy or Ultraviolet-Visible Spectrophotometry (UV-Vis) refers to the absorption or reflectance spectroscopy of the ultraviolet-visible spectral region. It is concerned with the identification and measurement of organic and inorganic compounds. UV-Visible spectrometry is favoured because it is simple, quick andaccurate.

UV/VIS is an excellent instrument for probing one of three electron orbital forms:

- Single bond (σ bonding orbitals);
- Double or triple bonds (π bonding orbitals);
- Non-bonding orbitals for lone pair electrons (n) [16].

The single (σ) bonding orbital is usually lower in energy than the double π bonding orbital, that in turn is lower than the non-bonding (n) orbital, hence the sequence $\sigma < \pi < n$. When the

electromagnetic radiation of the correct frequency is absorbed, one of these orbitals transforms into an empty orbital, generally an anti-bonding orbital such as σ^* or π^* show in Figure 3.4. Differences energy between the orbitals depends on the atoms present and the nature of bonding . Most transitions from bonding orbital include only $\pi \rightarrow \pi^*$, $n \rightarrow \sigma^*$ and $n \rightarrow \pi^*$ transitions. UV-Vis employs both ultraviolet and visible light to determine the sample absorption amount. A UV-visible spectrophotometer measures the intensity of light before and after passes through a sample and compares them intensity. The transmittance is the ratio of this original light (I_o) to the light passing through the specimen (I). The spectrophotometer can also be modified to measure absorbance instead of transmittance. The energy loss in the incident beam is measured as absorption. Usually the results of the UV-vis technique are plot of absorbance versus wavelength which known as the absorption spectrum. [17].

UV-vis was carried out on a Varian Cary 50 spectrometer at a scan speed of 300 nm/min. Specimen data was collected at 0.5 nm intervals with an average time of 0.1 seconds over the range 200 nm to 900 nm. A quartz cuvette was used for analysis. First, quartz cuvette was filled with the solvent (water) and a baseline was measured. The solvent was then replaced with the sample to be measured and a baseline subtraction was performed so that only the GO, rGO and G in each specimen were being measured. The organic molecules present in all graphenes had overlapping peaks and consequently UV-vis was conducted on graphene samples only as a method of material characterisation. UV-vis spectra are described using wavelength (nm) versus absorbance in arbitrary units (au). The software used for creating the UV-vis curves was Origin 2017.

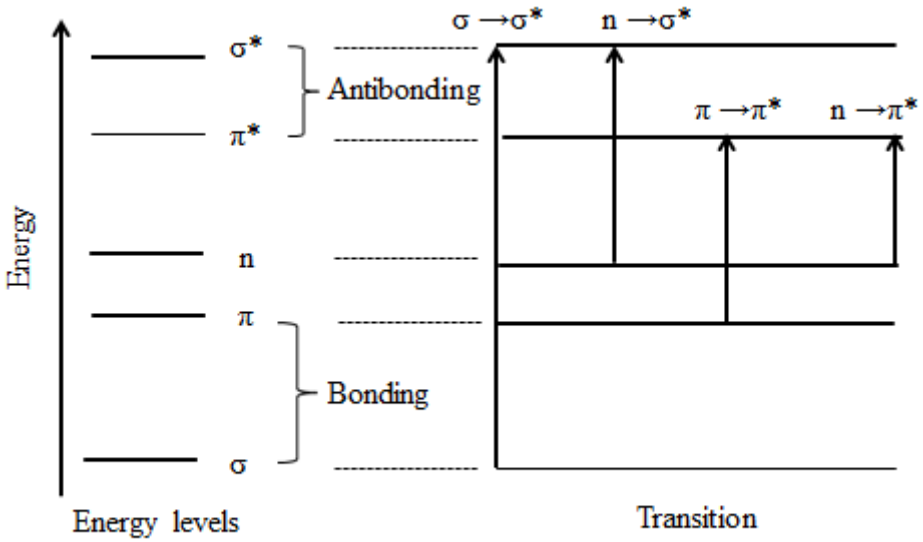

Figure 3.4. Different molecular orbital transitions [17].

3.7. Raman Spectroscopy

In 1928, the Physicist C.V. Raman observed the "Raman effect" for the first time [18]. In general, Raman spectroscopy uses monochromatic laser radiation on a surface of the material and measures the scattering that occurs as the photon frequency in the monochromatic laser light changes when it interacts with a material through adsorption and re-emission. The reemitted photon frequency can shift higher or lower than the frequency of the original monochromatic light. This effect is known as the Raman Effect. This method was used to estimate the disorder degree in G, rGO and GO nanomaterials and its nanocomposites. Furthermore Raman spectra provides information about the chemical structure and oxidation degree [19].

The Raman spectra of graphene/polymer nanocomposites were measured using a DXR Raman Microscope AIY1300736 equipped with a CCD detector. An excitation wavelength at 532nm was provided by a frequency doubled Nd/YAG laser, and the laser power at the sample position was typically 10.0 mW. Raman scattered light was collected in a 180^{o} back scattering geometry. Raman data were gathered at a spectroscopic resolution of 1.2cm^{-1}. The exposure time and number of accumulations were 2 seconds and 10 times, respectively. Raman spectra were collected from the surfaces of pellets that were obtained by cutting out the original samples and as powder for the G, rGO and GO samples. The software used for creating the Raman spectra curves was Origin 2017.

3.8. Deferential Scanning Calorimetry (DSC)

Deferential Scanning Calorimetry (DSC) is one of the most popular methods for thermal properties analysis. In general, DSC measures the variation of heat flow between a specimen and specimen reference as a function of temperature or time while the specimen and specimen reference are submitted to a controlled temperature program [20]. To complete that process, the DSC need two cells equipped with thermocouples, a programmable furnace, recorder and gas controller [20]. A DSC curve can show chemical or physical changes that occur in the specimen through the heat cycle. DSC is often used to determine thermal parameters such as the melting temperature (T_m), crystallization temperature (T_c), glass transition temperature (T_g) and heat of fusion of the sample, [21][22]. The specimen in DSC is under a nitrogen environment to prevent specimen oxidation.

The melting and crystallisation behaviour of the samples were obtained using differential scanning calorimetry (Perkin-Elmer Pyris 1 DSC system) over a temperature ranging from 25 ^{o}C to 220 ^{o}C, at heating and cooling rates of 10 ^{o}C /min under a Nitrogen atmosphere, at 30mL/min. The weight of samples was kept within 11–14 mg. The crystallinity degree of the samples was calculated according to equation 3. 2:

$$X_c(\%) = \frac{\Delta H_m}{\Delta H_o} \times 100 \qquad 3.2$$

where ΔH_m is the total heat energy per unit mass and ΔH_o is the enthalpy of fusion of a 100% crystalline sample, fixed at 293 J/g for PE and 207 J/g for PP [23][24]. Data were analysed using the software Perkin-Elmer Pyris Version 11.1.1.0492.

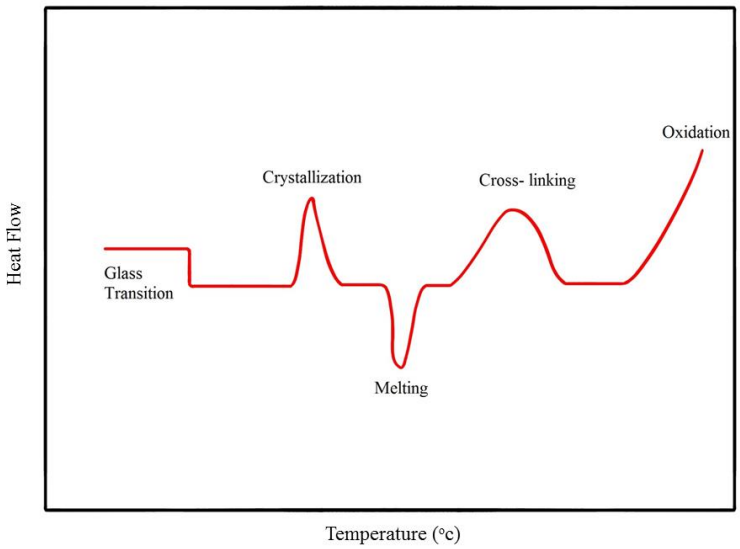

Figure 3.5. A typical DSC curve for polymer [25].

3.9. Thermal Gravimetric Analysis (TGA)

Thermal gravimetric analysis (TGA) measures the weight change in a material as a function of temperature and time under a controlled atmosphere. Materials like metals, polymers, plastics, ceramics and glasses can be analysed using TGA. It provides data about the thermal stability and decomposition patterns of a material. The main requirements for TGA instrument are an accurate balance that has a ceramic pan for loading the specimen, and a programmable furnace. The furnace can be programmed either for a constant heating rate, or for heating that acquires a constant mass loss over time. The sample is heated in different gas environments (oxygen or nitrogen). Nitrogen gas is used in this work to prevent oxidation of the samples. TGA uses a few milligrams of solid-state samples, making it a convenient method of characterisation. The work principle of the TGA is measuring and recording the weight constantly until the degradation point. TGA can consequently be used to assess the thermal stability of nanocomposites in different thermal environments. TGA is unable to present any information about the chemical changes or reactions. However, there are three ways in which material degrades: it could be random scission, systematic chain scission or a combination of both. Generally the random scission dominates in graphene/polymer nanocomposites degradation leave a sample residue known as char. [26] [27].

The samples were analysed by Thermogravimetric analysis (TGA) using a Perkin-Elmer Pyris 1TGA, with a linear heating rate of 10 ^{o}C min^{-1}, under a pure nitrogen atmosphere at 60 ml/min. The temperature ranged from ambient to 800 ^{o}C. The initial weight of samples was kept within 7–9 mg. Data were analysed using the software Perkin-Elmer Pyris Version 11.1.1.0492. The software used for creating the TGA curves was Origin 2017.

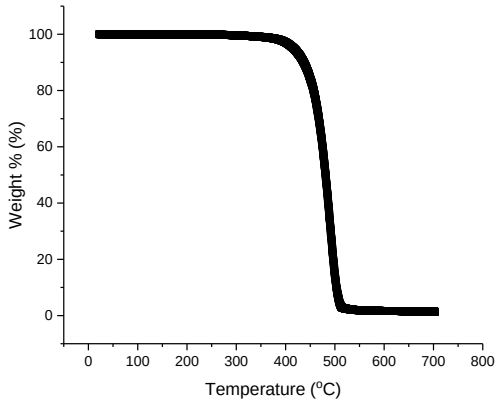

Figure 3.6. A typical thermal degradation TGA curve.

3.10. Conductivity measurement

The electrical conductivity or resistant of graphene/polymer nanocomposites are dependent on good dispersion and distribution of nanoparticle filler into the polymer layers. Another factor is the homogeneity between the filler and the host matrix material.

The dc-conductivity of the 1 mm thickness films was analysed by putting them between two stainless steel electrodes. The electrical connection is created through copper wires which using silver paste on the stainless steel electrodes. The specimen area and thickness were obtained using a screw gauge. The electrical conductivity (σ) of the specimen was measured by the two probe technique with an electrometer (Keithley, model 2400) at room temperature using equation 3. 3:

$$\sigma = \frac{1}{R} \times \frac{l}{a} \qquad 3.3$$

where R is the electrical resistance , a is the area and l is the thickness of the specimen [28]. The current–voltage ($I-V$) studies are done using the same specimen by applying voltage from $-30\ to\ +30\ V$ and the current was measured at each applied voltage.

3.11. Mechanical Properties

The mechanical behaviour of graphene /polymer nanocomposites are quite importance for engineering and industrial applications. The tensile test gives rise to stress-strain curves, where the stress is a force per area while the strain is a dimensionless quantity. Tensile strength is independent of the specimen size while it is dependent on material type and preparation method of the specimen. Typically, a dog bone shaped specimen is drawn linearly at a steady extension rate until it distorts or breaks. An analysis of the deformation profile provides elastic modulus, yield strength, ultimate tensile strength and elongation. The specimen is placed in the frame machine between the grips with the change in gauge length over the tensile test recorded automatically.

A universal test machine (HOUNSFIELD) tensile testing frame was used to perform a tensile test on the nanocomposites at a crosshead speed rate 20 mm/min at room temperature. A gauge length of 25 mm was used for the samples. Qmat software was used to calculate elastic modulus and tensile strength and other mechanical parameters. For the nanocomposites, four specimens of each category were tested and their average values were reported.

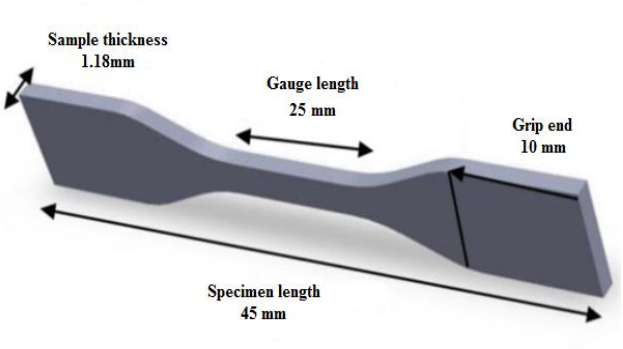

Figure 3.7. Dimensions of tensile composite specimen (mm).

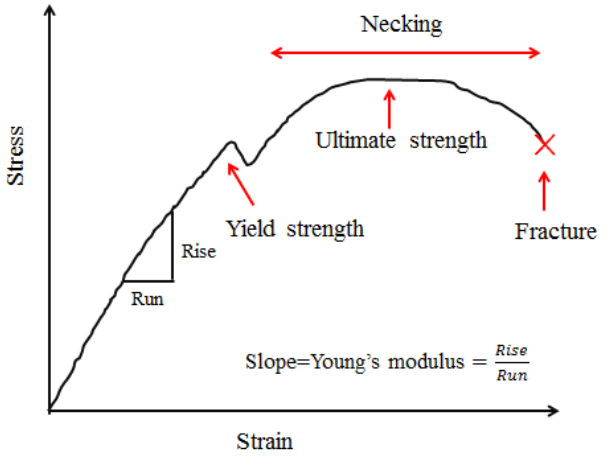

Figure 3.8. The typical Stress-Strain curve [30].

3.12. Dynamic Mechanical Analysis (DMA)

Dynamic mechanical analysis (DMA) determines the materials mechanical response through various temperatures and frequencies. A DMA applies an oscillating force to a specimen material then measures the response of the material to that force. DMA is a good method for characterizing a phase transition and the phase separation as well other mechanical characteristic modulus in the linear regime. In DMA, a sinusoidal tensile strain is applied to a specimen sheet and the stress response is separated into storage and loss components, as related by the following equation

$$E^* = E' + E'' \qquad 3.4$$

where E^* is the complex modulus, E' is the storage elastic modulus, and E'' is the loss modulus. The specimen damping coefficient, $tan\ \delta$, can be calculated from [29]:

$$tan\ \delta = \frac{E''}{E'} \qquad 3.5$$

This mechanical damping or internal friction shows the energy dissipated value as heat through the deformation process [30] [31].

The dynamic mechanical analyser (DMA) Perkin Elmer D8000 was used to test the thermo-mechanical properties of polymers. Small rectangular specimens sheet of around 25mm × 10mm × 1mm, made by hot press moulding, were tested. The three point bending mode was used in all measurements, which were taken in tension mode at 1Hz frequency at ambient temperature that in a broad temperature range from − 150 °C to 100 °C, achieved using a heating rate of 3 °C \ min. Liquid nitrogen was used to reach the lower required temperatures.

References

[1] Goldstein, J., Newbury, D.E., Joy, D.C., Lyman, C.E., Echlin, P., Lifshin, E., Sawyer, L.& Michael, J.R.(2003). Scanning Electron Microscopy and X-ray Microanalysis, 3, Springer , New York, United State .

[2] Utracki, L. A. & Wilkie, C. (2014) Polymer Blends Handbook,2, Springer Netherlands , New York, United State .

[3] Mattox, D. M.(1998) Handbook of Physical Vapor Deposition (PVD) Processing: Film Formation, Adhesion, Surface Preparation and Contamination Control. Elsevier inc Amsterdam, Netherlands.

[4] Iqbal, M. Z. (2016). Structure-Property Relationships in Graphene/Polymer Nanocomposites. PhD Thesis, Colorado School of Mines.

[5] Saw, C. K. (2005). X-ray scattering techniques for characterization of nanosystems In: Challa, S. &Kumar,R.(Eds), Nanotechnologies for Life Sciences, 3, UCRL-JRNL-211387.

[6]Beer, F.C.(2015). The Journal of The Southern African Institute of Mining and Metallurgy,115, 913– 924.

[7] Heimo, S. &Yashveer, S.(2013). The SAXS Guide,3, Anton Paar GmbH, Austria.

[8]Pauw, B. R. (2014). Corrigendum: Everything SAXS: small-angle scattering pattern collection and correction (2013 J. Phys.: Condens. Matter 25 383201). Journal of Physics: Condensed Matter, 26(23), 239501.

[9] Vonk, C.; Kortleve, G.(1967). X-ray small-angle scattering of bulk polyethylene. Kolloid-Zeitschrift und Zeitschrift für Polymere, 220 (1), 19-24.

[10] Fischer, E. (1971) .Small angle x-ray scattering studies of phase transitions in polymeric and oligomeric systems. Pure and Applied Chemistry, 26 (3-4), 385-422.

[11] Chu, B.; Hsiao, B. S. (2001) .Small-angle X-ray scattering of polymers. Chemical reviews, 101 (6), 1727-1762.

[12] Morgan, D. J. (2010). X-Ray Photoelectron Spectroscopy (XPS): An Introduction, 1–7.

[13]Dissertation, a. (2009). Processing , Morphology and Properties of Graphene Reinforced Polymer Nanocomposites. Polymer, 52(September), 1532–1538.

[14] Straughan, B. P. and Walker, S. (1976). Spectroscopy, 2, John Wiley and Sons.

[15] Stuart, B., Skoog, D. A., West, D. M., Holler, J., Crouch, S. R., Larkin, P. J., Socrates, G. (2004). Infrared Spectroscopy: Fundamentals and Applications. Vasa, 40(6), 146–208.

[16] Fawcett, A. H. (1996). Polymer spectroscopy, John Wiley and Sons.

[17] Wenzel, T., (2013) .Douglas A. Skoog, Donald M.West, F. James Holler, and Stanley R. Crouch: Fundamentals of analytical chemistry, 9th ed., international ed. Anal Bioanal Chem . 405,7903–7904

[18] Singh, R. (2002). C. V. Raman and the Discovery of the Raman Effect. Physics in Perspective, 4(4), 399–420.

[19] Bumbrah, G. S., & Sharma, R. M. (2016). Raman spectroscopy - Basic principle, instrumentation and selected applications for the characterization of drugs of abuse. Egyptian Journal of Forensic Sciences, 6(3), 209–215.

[20]Hatakeyama, T., & Quinn, F. (1999). Thermal Analysis : Fundamentals and Applications to Polymer Science. Talanta, 256, 1–411.

[21]How, L., & Networks, N. (2005). Book Re View S. Ethology, 2(6), 2005–2007.

[22] Menczel ,J.& Prime ,R.(2009) Thermal Analysis of Polymers- Fundamentals and Applications, John Wiley & Sons.

[23]Pluta, M., Alexandre, M., Blacher, S., Dubois, P., & Jérôme, R. (2001). Metallocene-catalyzed polymerization of ethylene in the presence of graphite. II. Structure and electrical properties of the composites. Polymer, 42(22), 9293–9300.

[24] Dai, J., Xu, X., Yang, J., Zhang, N., Huang, T., Wang, Y. Zhang, C. (2015). Greatly enhanced porosity of stretched polypropylene/graphene oxide composite membrane achieved by adding pore-forming agent. RSC Adv., 5(27), 20663–20673.

[25] Philosophy, D. O. F., & Patel, G. (2014). Spectroscopic Investigations on Polymer Blends / Composites, University of Baroda, India.

[26] How, L., & Networks, N. (2005). Book Re View S. Ethology, 2(6), 2005–2007.

[27] Wong, a. C.-Y., & Lam, F. (2002). Study of selected thermal characteristics of polypropylene/polyethylene binary blends using DSC and TGA. Polymer Testing, 21(6), 691–696.

[28] Layek, R. K., Samanta, S., & Nandi, A. K. (2012). The physical properties of sulfonated graphene/poly(vinyl alcohol) composites. Carbon, 50(3), 815–827.

[29] Tajvidi, M., Falk, R. H., & Hermanson, J. C. (2006). Effect of natural fibers on thermal and mechanical properties of natural fiber polypropylene composites studied by dynamic mechanical analysis. Journal of Applied Polymer Science, 101(6), 4341–4349.

[30] Ehrenstein, G. W., Riedel, G., & Trawiel, P. (2004). Chapter 6 Dynamic Mechanical Analysis. Thermal Analysis of Plastics: Theory and Practice, 236–299.

[31] Khonakdar, H. A., Wagenknecht, U., Jafari, S. H., Hässler, R., & Eslami, H. (2004). Dynamic mechanical properties and morphology of polyethylene/ethylene vinyl acetate copolymer blends. Advances in Polymer Technology, 23(4), 307–315.

Chapter 4

Understanding the Structure, Phase Transition and Properties Behaviour of the Polymer Host Matrix of Graphene Nanoparticles

In this chapter, we present a comprehensive study of the structure and properties of the single polymer host matrix (PE and PP) and the blend polymer host matrix (PB and PBC) including the phase transition, separation and miscibility of the blend. This provides a baseline from which to study the effect of graphene addition on the structure and properties of the graphene/polymer nanocomposites, as presented in later chapters. The main methods, which were used in this part of the project, including the materials, results and discussion and the summary are outlined below.

4.1. Materials

In this study, two widely used polymer materials were used, namely metallocene linear low density polyethylene (m-LLDPE, hereafter referred to as PE) and polypropylene homopolymer (PP), which were obtained from a commercial supplier (RESINEX). Key physical data for each polymer are given in Table 4.1. The weight-average molecular weight (M_w) was measured by gel permeation chromatography (GPC, PSS Polymer Standard Service, Mainz, Germany), and the melting temperature was characterized using DSC. The PE/PP compatibilizer polymer (ethylene-*co*-glycidyl methacrylate) (PE-*co*-GMA) was supplied by Sigma-Aldrich (Gillingham, United Kingdom). All polymers were received from the supplier in pellet form and were used as supplied.

Polymer	Supplier	Melt flow index (gm/10 min)	Melting temperature (°C)	Density (g/cm^3)	M_n g/mol	PDI ($= \frac{M_w}{M_n}$)
PE	The Dow chemical company	1.0	124	0.917	70700	3.33
PP homo	Saudi Basic industries corporation (SABIC)	19	165	0.905	61700	5.11
PE-co-GMA	Sigma-Aldrish	5.0	99	0.94	-	-

Table.4.1. Polymeric materials data, the melt flow index and the density from supplier, the melting temperature from DSC and molecular weight details from PSS.

4.2.GPC/SEC Analysis

Gel Permeation Chromatography (GPC), or Size Exclusion Chromatography (SEC), is extensively used to obtain the molar mass distribution (MMD) in industrial analytical laboratories. Determining the MMD for PE and PP is a challenging task and rarely possible on standard bench-top equipment due to the high temperatures required to dissolve them. Therefore, a specialist service was required.

Accuracy in the molar mass determination is very important to study the miscibility and compatibility between the polymers. The injection system used was a PolymerChr GPC-IR system equipped with a PolymerChar IR-4 (infra-red) detector, using typical analysis conditions.

Sample concentrations of approximately 2.7g\L in 1, 2, 4-trichlorobenzene were added. Dissolution time was 120 min at 160 ºC. The samples were injected twice with 200 μL and the flow-rate was 1.0 mL/ min. A calibration curve with polystyrene standards was measured within the separation range of the column set. The measured molar mass distribution was made with the slice-to-slice method based on the PS-calibration curve. Calibration was conventional. The results are reported in Table 4.2.

Polymer ID	M_n/D_a	M_w/D_a	M_z/D_a	PDI(=M_w/M_n)
PE	70700	316000	926000	5.11
PP	61700	235000	579000	3.33

Table 4.2. The GPC/SEC results of the samples with broad molar mass distribution.

4. 3. Preparation

PE and PP blends samples were prepared according to the weight percentage shown in Table 4.3; 1 gram of those granules was added to 10ml of o-xylene at 135 ºC. The compatibilizer was also added at the same time. The polymers were dissolved with the help of a magnetic stirrer for 35 minutes. The mixture was transferred to a petri dish and then dried in an oven at 80 ºC for 12 hours. The complete solvent removal was confirmed by DSC, where no solvent peak was detected. The sample was then ground with a manual grinder. 1 mm thick composite sheets were obtained by pressing the ground samples between two sheets of PTFE using a hydraulic press, MOORE LTD (Birmingham. England) at 210 ºC under 3 tons for 10 min. Then the specimen were quenched immediately into water at room temperature.

Sample ID	PE (wt%)	PP (wt%)	PE-co-GMA (wt%)
PE	100	0.0	0.0
PP	0.0	100	0.0
PB	50	50	0.0
PBC	50	50	5.0

Table 4. 3. Weight percentages of each component in the different samples.

Figure 4.1. The Preparation of polymers matrices.

4.4. Results and Discussion

Preliminary investigations indicated that o-xylene was a good solvent for PE and PP homo. The optimum ratio of solvent o-xylene is 100 mg/ml, and minimum temperature at which a homogeneous solution was obtained, was 135 ºC.

4.4.1. WAXD results

A WAXD pattern of PP, PE and PB is shown in Figures 4.2, 4.3 and 4.4. PP reflection is present at 2θ equal to 14º, 16.8º, 18.5º, 21.2º and 21.8º, representing diffraction from the 110, 040,130, 111, 131 and 041 of the monoclinic α- form crystals from lattice planes. The reflection at 21.8º is due to both the 131 and 041 of the orthorhombic crystals from lattice planes. WAXD of PE is governed by the 110 and 200 reflections at 2θº equal to 21.4º and 23.7º [1]. The diffraction pattern of the PB contained no new absorption bands or any shift in the position of diffraction line; the patterns were approximately the combined the diffraction pattern PE and PP as shown in Figure 4.5, because the PE and PP are immiscible so cannot co-crystallize.

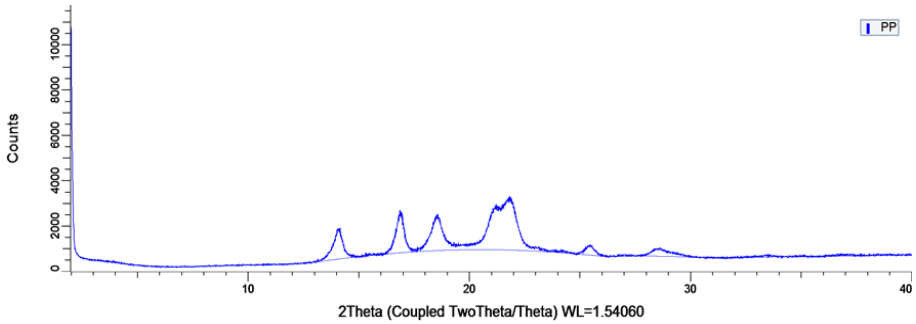

Figure 4. 2. The curves of WAXD patterns of PP.

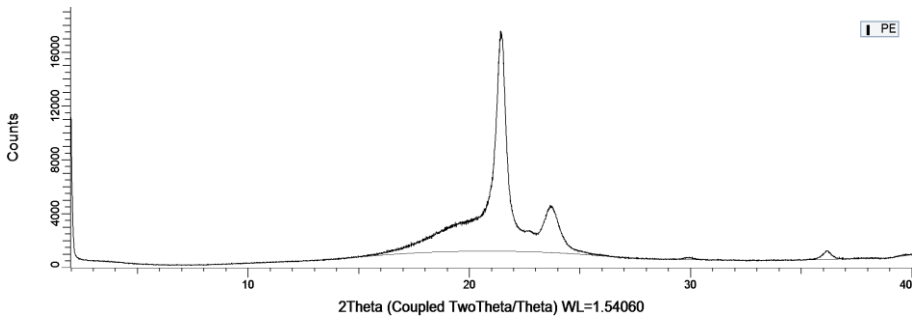

Figure 4. 3. The curves of WAXD patterns of PE.

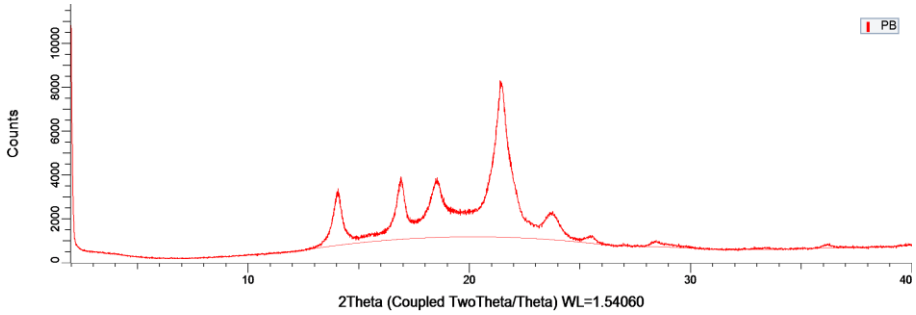

Figure 4. 4. The curves of WAXD patterns of PB.

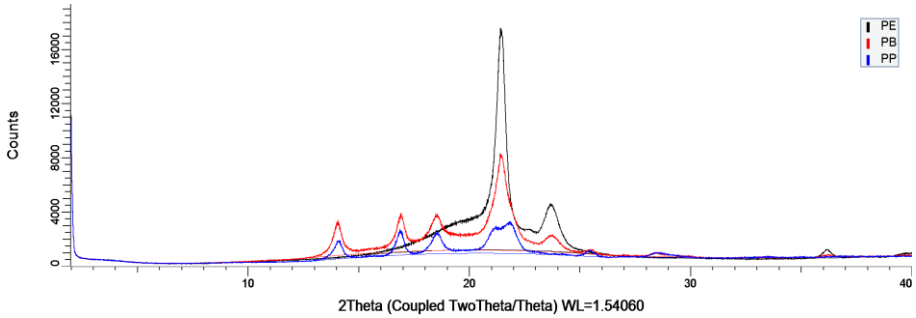

Figure 4. 5. The curves of WAXD patterns of PE, PB and PP.

The crystallite size τ, as determined by the widths of the peaks by using the Scherrer equation $\tau = K\lambda/(\beta \cos\theta)$ where K is a dimensionless shape factor, with a value close to unity, the typical value of K being around 0.9 and β is the peak width at half the maximum intensity (FWHM). The PP crystallite size is less than in the PB blend as well as in PE as shown in Table 4.4. Also, the addition of homo PP to the PE caused a slight decrease in the interlayer spacing ($d = n\lambda/2sin\theta$) of the PE sample, as shown in Table 4.5. That means that the crystallization behaviour of PE is affected by the PP [2].

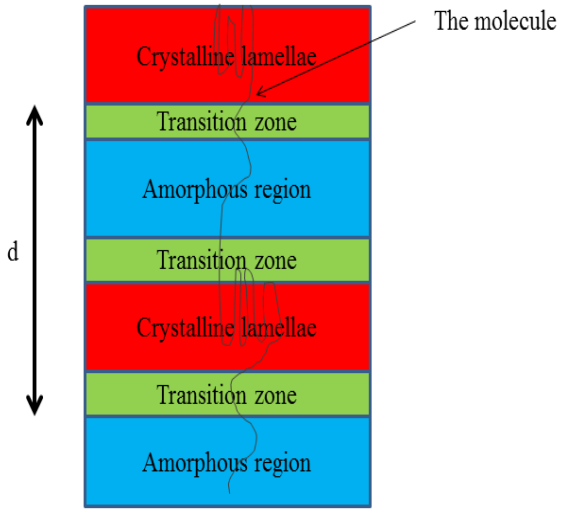

Figure 4.6. Schematic of the interlayer spacing of semi-crystalline polymers.

2θ	14°		16.8°		18.5°		21.4°		23.7°	
Sample ID	FWHM	τ (Å)	FWHM	τ (Å)	FWHM	τ (Å)	FWHM	τ (Å)	FWHM	τ (Å)
PE	-	-	-	-	-	-	0.437	205.5	0.574	157.1
PP	0.382	233.1	0.370	241.3	0.476	188.1	1.195	75.2	-	-
PB	0.351	253.7	0.329	271.5	0.404	221.2	0.570	157.6	0.489	184.3

Table 4. 4. The crystallite size values of PE, PB and PP from the reflection peaks in WAXD data.

The interlayer spacing d(Å)			
2θ	PE	PB	PP
14°	-	6.307	6.288
16.8°	-	5.246	5.239
18.5°	-	4.797	4.780
21.5°	4.14	4.129	4.070
23.7°	3.746	3.740	-

Table 4.5. The interlayer spacing of PE, PB and PP.

Figure 4.7 shows the WAXD patterns of the PBC. PB and PBC both have a broad amorphous background imposed on sharper diffraction lines due the crystalline regions. The crystallite size decreased with increasing the PE-co-GMA content, as illustrated in Table 4.6. The PBC has a similar crystallization structure to PB with no effect on the crystallization from the PE-co-GMA which is shown Table 4.7.

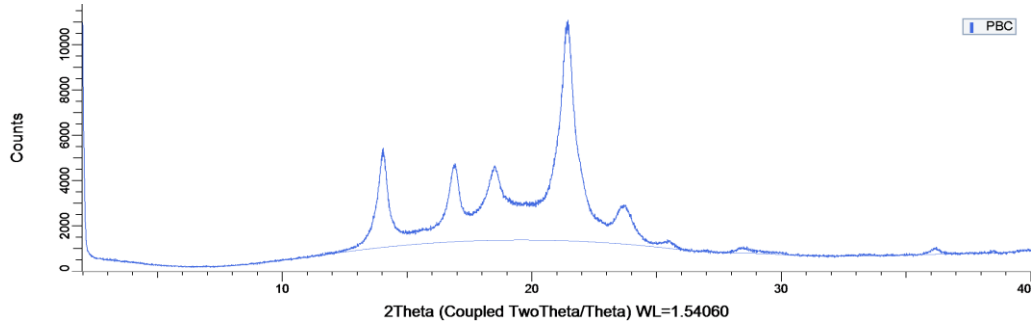

Figure 4.7. The curves of WAXD patterns of PBC.

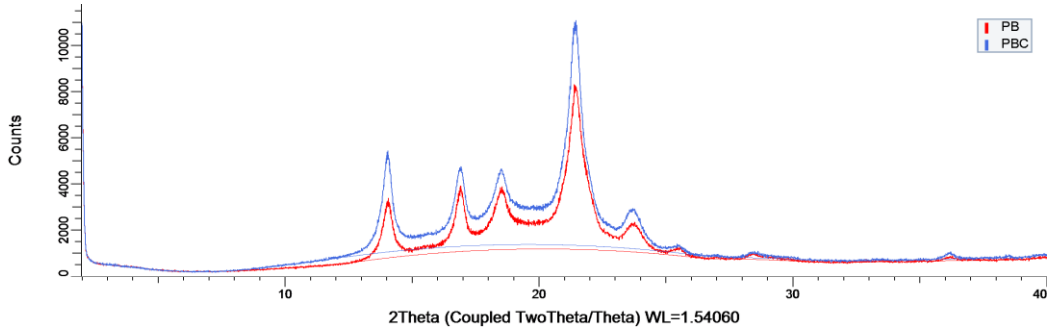

Figure 4.8. The curves of WAXD patterns of PB and PBC.

2θ	14°		16.8°		18.5°		21.4°		23.7°	
Sample ID	FWHM	τ (Å)	FWHM	τ (Å)	FWHM	τ (Å)	FWHM	τ (Å)	FWHM	τ (Å)
PB	0.351	253.7	0.329	271.5	0.404	221.2	0.584	153	0.500	180
PBC	0.369	241.1	0.370	241.3	0.438	204.4	0.516	174.1	0.465	193.8

Table 4.6. The FWHM values of PB and PBC reflection peaks in WAXD data and crystallite size.

The interlayer spacing d(Å)		
2θ	PB	PBC
14°	6.307	6.297
16.8°	5.246	5.246
18.5°	4.797	4.797
21.5°	4.129	4.157
23.7°	3.740	3.753

Table 4.7. The interlayer spacing of the PB and PBC.

4.4.2. SAXS

The properties of polymers and their blends depend on the linear degree of crystallinity χ_l and the interlamellar structure, that is the link between the crystalline and the amorphous areas. Figures 4.9, 4.10, 4.11 and 4.12 give the SAXS profiles, intensity vs scattering vector (q nm^{-1}), for the specimens of PE, PB, PP and PBC blends respectively. In order to interpret the SAXS data, the curves are Lorentz-corrected; i.e., the intensity is multiplied by q^2 [3][4]. Figure 4.13 and 4.14 show Lorentz corrected curves for (PE, PB, PP) and (PB, PBC) blends respectively. A distinct interference maximum is generally observed in SAXS profiles for semi crystalline polymers and polymer blends due to periodic lamellar stacks [5][6]. The long period distance, Figure 4.15, ($L_P = 2\pi/q_{\max}$ [7] while $q = (4\pi\, sin\theta)/\lambda$ [8]) was estimated from the position of the intensity maxima [9], as demonstrated in Figures 4.13 and 4.14. The morphology parameters of the lamellar stacks were determinate from the linear correlation function $(LCF), \gamma(r)$, calculated from the cosine transformation of the Lorentz-corrected SAXS intensity distribution:

$$\gamma(r) = \frac{\int_0^\infty q^2\, I(q)\cos(qr)dq}{\int_0^\infty q^2\, I(q)dq} \qquad 4.1$$

Using the $LCF\ \gamma(r)$ curves shown in Figures 4.16, 4.17, 4.18 and 4.19, the long period L_p was obtained directly. The linear crystallinity χ_l was determined from the $LCF\ \gamma(r)$ as well by using the following equation

$$\chi_l\left(1-\chi_l\right) = \frac{D_o}{L_p} \qquad 4.2$$

where D_o is the average core thickness [10]. The D_o is the position at the end of the linear section in the $LCF\ \gamma(r)$. The thickness of the crystalline layers l_c and amorphous l_a layers in the polymer stacks calculated by following equations

$$l_c = \chi_l L_p \qquad 4.3$$

$$l_a = (1-\chi_l)L_p \qquad 4.4$$

From those results, the linear crystallinity χ_l value is can found by following equation

$$\chi_l = \frac{l_c}{L_p} = \frac{l_c}{l_c + l_a} \qquad 4.5$$

The long period of PE, PP and PB lamellae are 145±2, 125±1, and 141±2 Å, respectively. PB has different structures in comparison with PE and PP, as indicated by the observed maxima positions at 125±1 Å [11]. Likewise, an increase in the long period distance occurred. Furthermore, PBC from Figure 4.10 is characterized by a maximum at 146.5±2Å which indicates an increase in the long period with addition the PE-co-GMA [12]. The thickness of the crystalline l_c and amorphous l_a layers and linear crystallinity χ_l of the PE, PP, PB and PBC specimens were reported in Table 4.8. The crystalline layers thickness in PP is higher than PE corresponding to the higher crystallinity degree of the PP. The crystalline layers thickness decreases upon blending the PE with PP due to different crystalline types causing a decrease in the crystallinity and an increase in the amorphous layers thickness, which is discussed later in the DSC section.

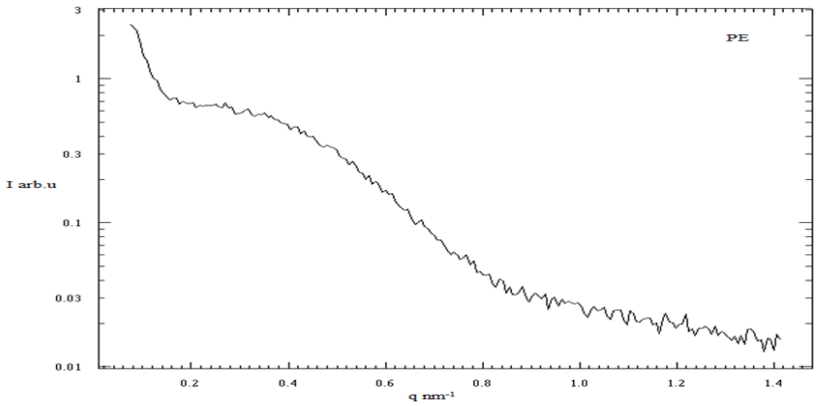

Figure 4.9. SAXS profiles for the PE sample.

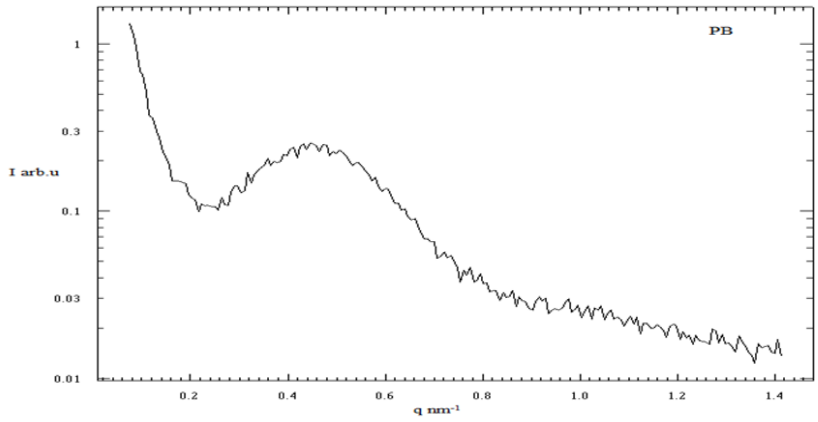

Figure 4.10. SAXS profiles for the PB sample.

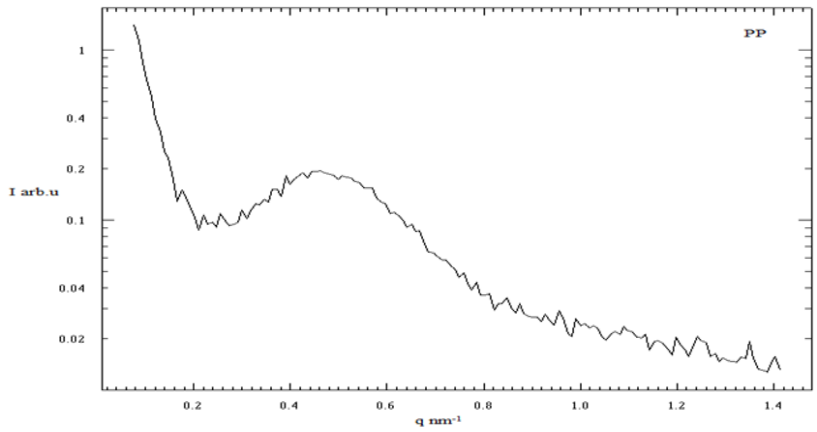

Figure 4.11. SAXS profiles for the PP sample.

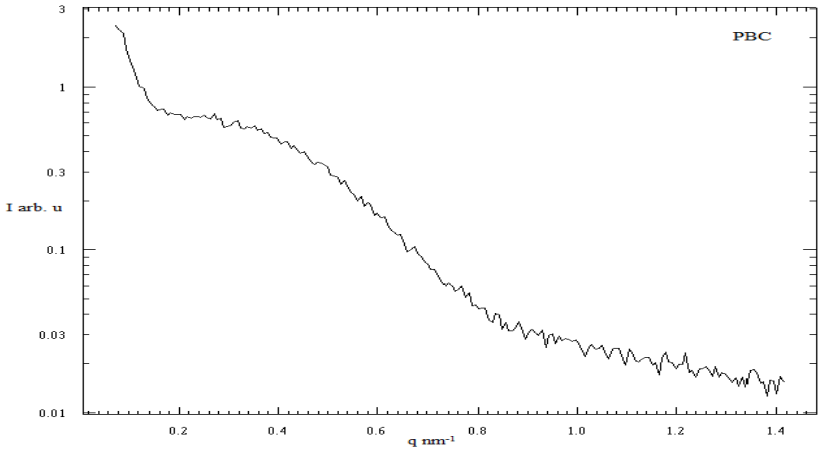

Figure 4.12. SAXS profiles for the PBC sample.

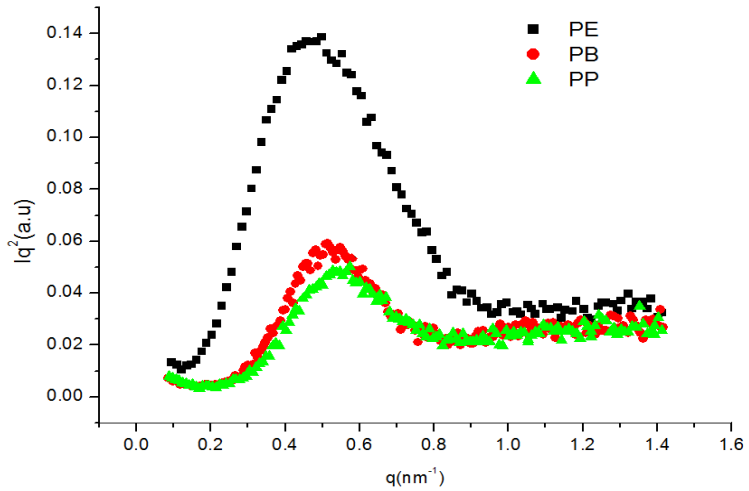

Figure 4.13. Lorentz-corrected SAXS curves for the PE, PB, and PP samples.

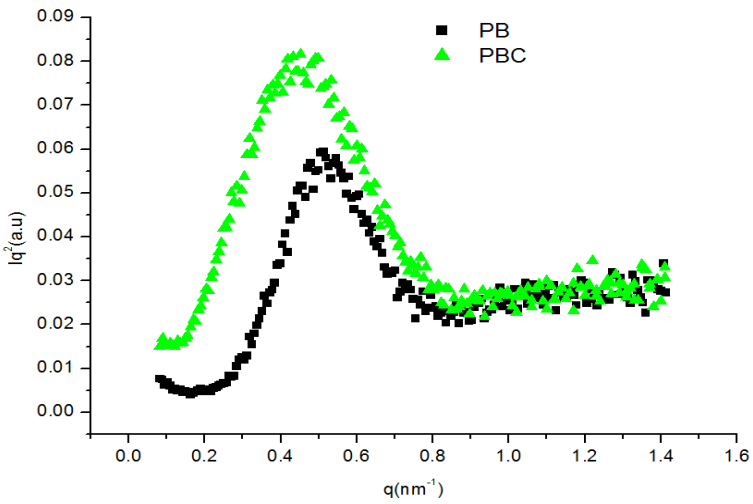

Figure 4.14. Lorentz-corrected SAXS curves for the PB and PBC samples.

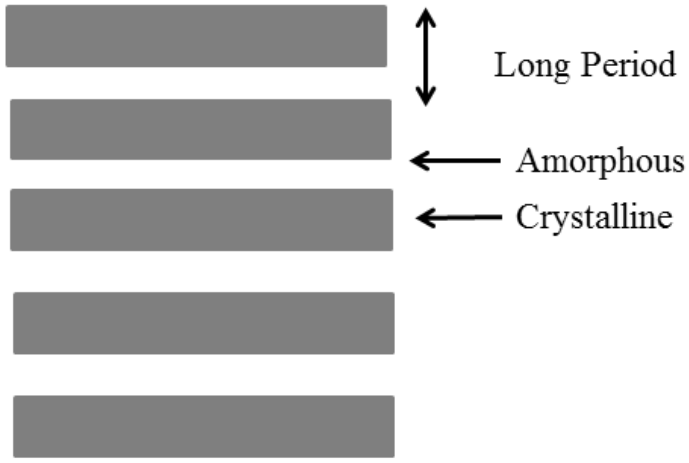

Figure 4.15. Schematic of the long period distance of lamellar.

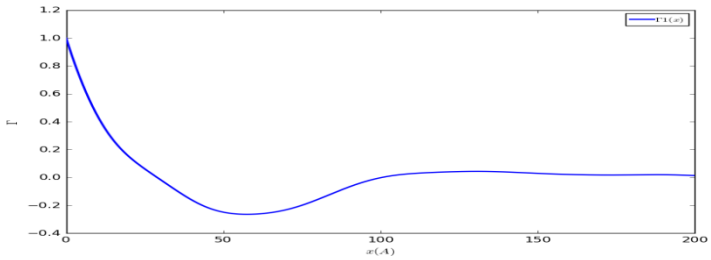

Figure 4.16. $\gamma(r)$ linear correlation function of the PE.

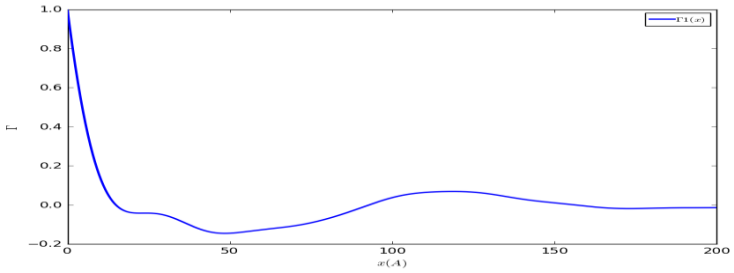

Figure 4.17. $\gamma(r)$ Function of the PP.

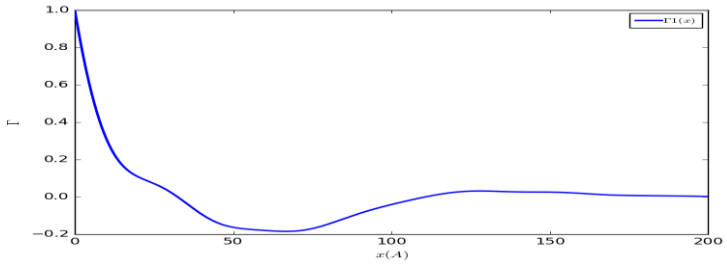

Figure 4.18. $\gamma(r)$ Function of the PB.

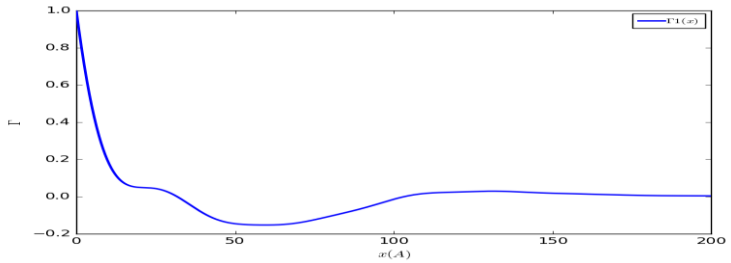

Figure 4.19. $\gamma(r)$ Function of the PBC.

Sample ID	l_c	l_a	L_p	χ_l
PE	20	125	145± 2	0.14
PP	42	83	125±1	0.34
PB	13	128	141±2	0.10
PBC	10	136	146±2	0.07

Table 4.8. The thickness of the crystalline lamellae and amorphous lamellae, long period and linear crystallinity of the PE, PB, PP , PB and PBC samples.

4.4.3. Crystallization and Melting Behaviour

The crystallization and melting behaviour as studied by DSC are shown in Figures 4.20, 4.21, 4.22 and 4.23. The crystallization temperature T_c, melting temperature T_m, melting enthalpy ΔH_m and the degree of crystallization X_c of PE, PP, PB and PBC for all the blends are reported in Table 4.9. The T_m of PE is 124±1 ºC, whilst it is 123±1 ºC and 122±1 ºC in PB and PBC respectively, so that the addition of PP is seen to lower slightly the PE melting temperature. The PP melting peak was observed in all the blends at almost 165±1 ºC, as Furukawa et. al. reported in reference [2]. These results demonstrate that blends of PP and PE are thermodynamically incompatible [13]. The melting enthalpy of the PP and PE are 98 Jg^{-1} and 99 Jg^{-1} respectively, decreasing in the blends (Table 4.9). This value is the energy required to melt the crystalline regions, and is directly proportional to the crystallinity volume, indicating that a lower crystallinity developed for the two components in the blends [14]. The crystallization peak of PP is observed at 119±1 ºC, decreasing to 115±1 ºC upon blending with PE. Furthermore, it continued to change slightly by adding changes further upon addition of the PE-co-GMA, to 114±1 ºC. The crystallization temperature of PE is lower than the PP. It is observed clearly at 103±1 ºC in PE specimen, 107±1 ºC in PB and 106±1 ºC in PBC with no clear difference between the treated (PB) and untreated (PBC) blends. This is because the PE-co-GMA role has enhanced the adhesion and miscibility between the polymers without affecting the crystallization, a finding supported by the WAXD and SAXS study. The decrease in the degree of crystallinity in the blend occurs because very fast quenching (achieved by flowing the sample under cold water) can prevent crystallization induced segregation [15][16] [17] .

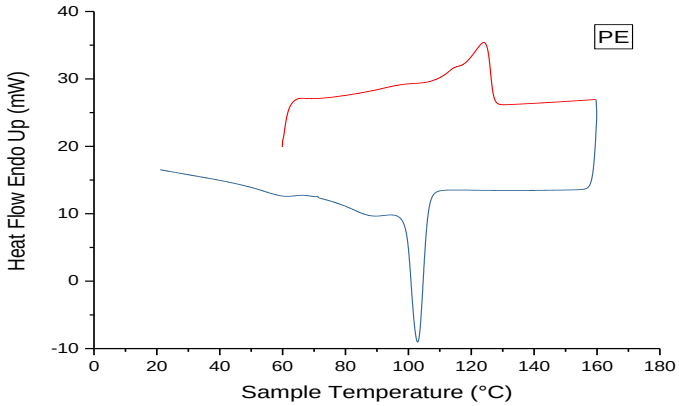

Figure 4.20. The DSC curve of a blend of PE.

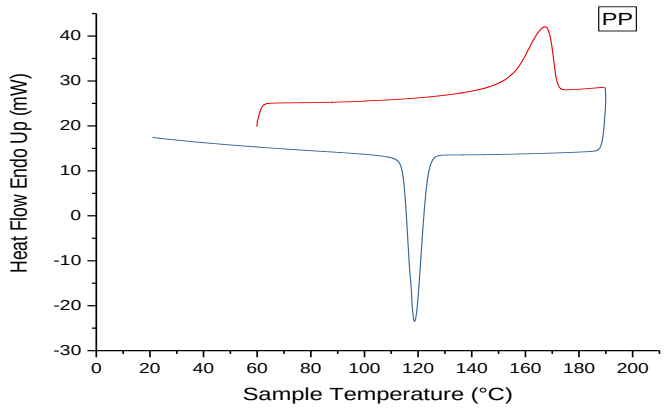

Figure 4.21. The DSC curve of a blend of PP.

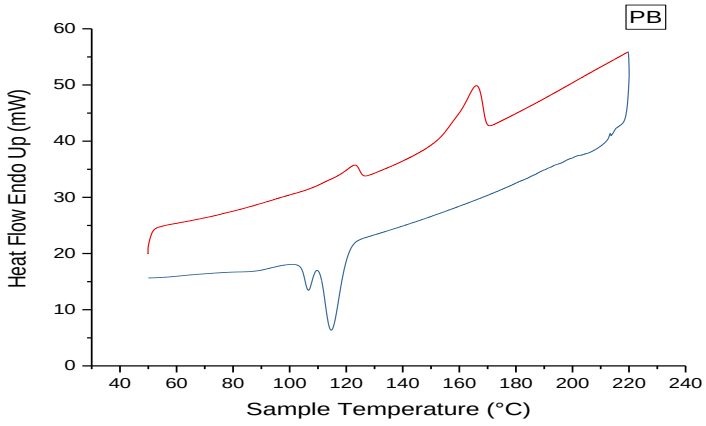

Figure 4.22. The DSC curve of a blend of PB.

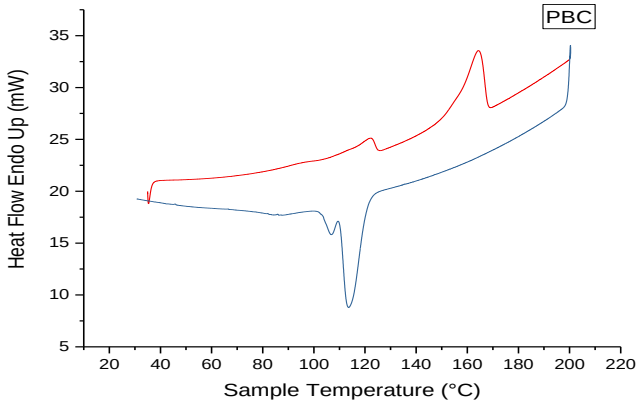

Figure 4.23. The DSC curve of a blend of PBC.

	T_c/ °C		T_m/ °C		ΔH_m/Jg^{-1}		X_c (%)		
Sample ID	PE	PP	PE	PP	PE	PP	PE	PP	total
PE	103±1	-	124±1	-	99	-	26	-	26
PP	-	119±1	-	165±1	-	98	-	48	48
PB	107±1	115±1	123±1	167±1	15	46	5	22	27
PBC	106±1	114±1	122±1	164±1	12	47	4	23	27

Table 4.9. Crystallization, melting and melting enthalpy temperature of PE and PP in the blends.

4.4.4. Thermal Behaviour

The thermogravimetric curves are shown in Figure 4.24. All the curves have a single degradation step [18]. Degradation temperatures are shown in Table 4.10. PE starts, as defined by a loss of 1wt%, to degrade at 365±3 °C and PP at 279±3 °C. The single degradation step arises from the fact that the polymers consist of carbon-carbon bonds (backbone) as main chain. A temperature increase promotes random scission, with associated thermal degradation taking place at a susceptible part of the polymer main chain [19]. The PB blends begin to degrade at 299±3 °C. The low thermal stability of the PB blend (relative to PE) is probably due to oxidizing the mixture during the blend and drying processes that will promote and cause the degradation process [20] [21]. The thermal stability of the PB is more than the single PP, so that the thermal stability of the polymers follows sequence PE > PB > PP. However, it is clear that the degradation occurs over a wider range of temperatures in the blend than in the pure components.

Adding the poly (ethylene-co-glycidyl methacrylate) (PE-co-GMA) to the blend PBC at 5wt%, increased the thermal stability of the blend. The PBC starts to degrade at 386±3 °C, an increase of 87±3 °C. This might be due to the higher thermal stability of PE-co-GMA polymer [15].

Under a nitrogen environment, all polymer samples have degraded completely without leaving any noticeable residue by 700 °C which is in agreement with values observed in the literature[22][23].

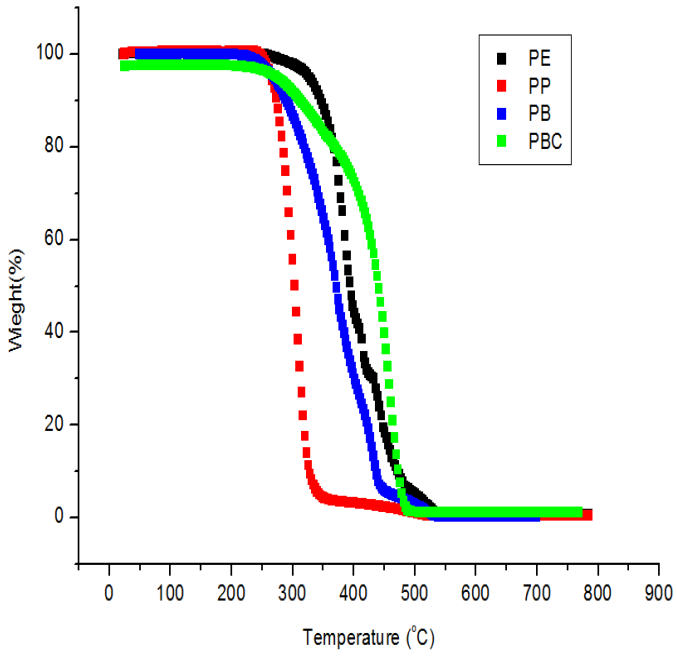

Figure 4.24. The TGA decomposition curves of the sample.

Sample ID	$T_{(99wt\%)}$ °C	$T_{(50wt\%)}$ °C	$T_{(1.0wt\%)}$ °C
PE	366±3	394±3	539±3
PP	279±3	303±3	500±3
PB	299±3	371±3	524±3
PBC	386±3	442±3	679±3

Table 4.10. Decomposition temperatures of the samples at different remaining weight percentages.

4.4.5. Mechanical Properties

The elastic modulus (MPa); yield strength (MPa); ultimate tensile strength (MPa); and elongation (mm) were measured for PP, PE, PB and PBC specimens, as shown in Table 4.11 and Figure 4.25. The homo polypropylene has the highest elastic modulus which is because PP chains are rigid due the methyl group which is attached to every second carbon atom of the PP backbone chain. These groups hinder rotation of the chain producing a stronger but less flexible material. PE exhibits elastic behaviour, with a lower elastic modulus and higher elongation compared to homo PP [24]. The elongation of the PB is lower than the parent polymers, because the blend is incompatible, as shown in the DSC data is supports the results from the DSC data. The mechanical properties increase by addition of the PE-co-GMA compatibilizer. In general, PE-co-GMA as a compatibilizer improves the

interfacial adhesion, which results in an increase in tensile properties. increase through its glycidyl group and double bond and hydrocarbon backbone respectively [15].

Sample ID	Elastic modulus (MPa)	Yield strength (MPa)	Ultimate tensile strength (MPa)	Elongation (mm)
PP	884±51	25±1	34±0.4	3 ±0.3
PE	38±31	9 ±0.0	16±2	175±24
PB	322±41	2 ±1	5 ±1	1 ±0.2
PBC	277±90	10 ±1	12 ±3	3 ±0.3

Table 4.11. The tensile properties of the polymer blends.

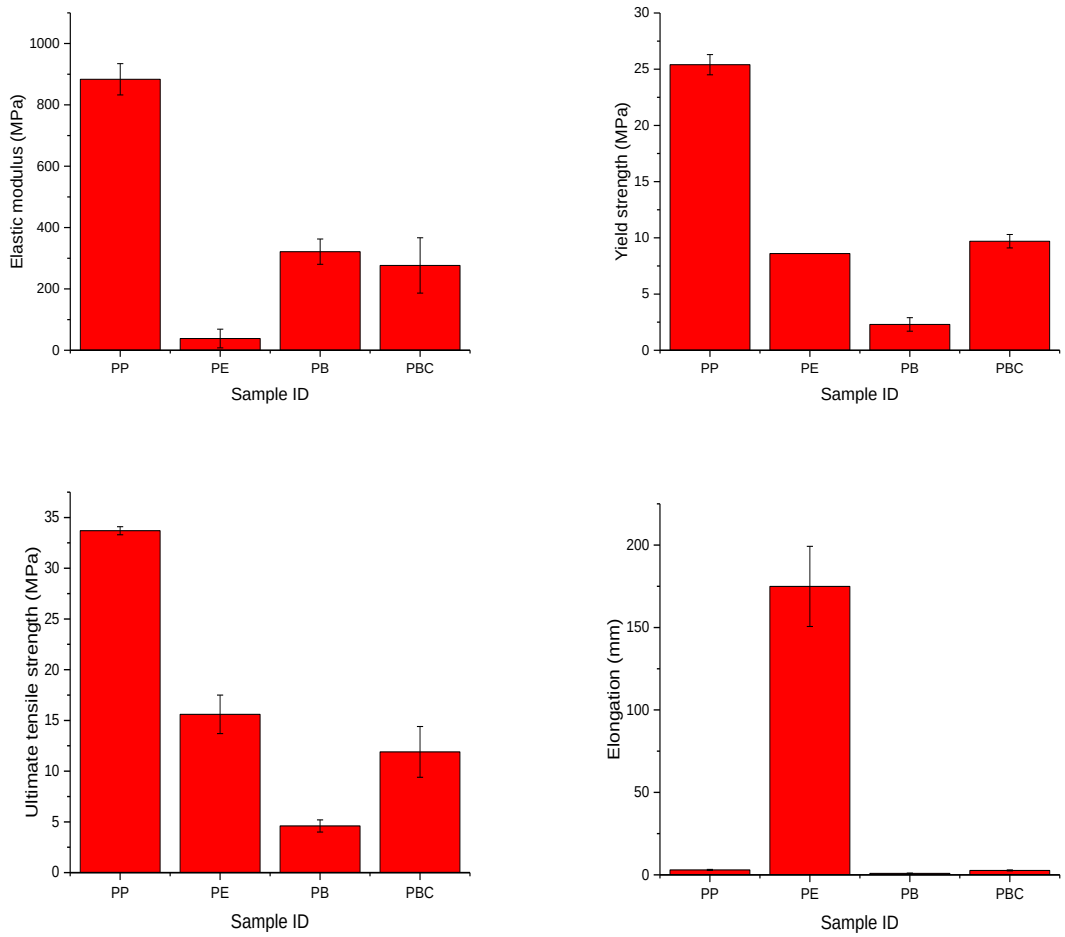

Figure 4.25. Mechanical properties of polymer blends.

4.4.6. Dynamic Mechanical Analysis (DMA)

Figure 4.26 illustrates the variation in loss tangent with temperature at 1 Hz. All the curves show the same pattern and can be divided in the three main regions indicating three separate transitions. These are referred as α-transition for the rubbery state, β-transition for the glass-rubber state and γ-transition for glassy state, in order of decreasing temperature (Figure 4.26)[25]. In PE, the α-transition was observed in the temperature range 20-100 ºC with a maximum in tan δ at 53 ºC. The β-transition was observed from 20 to −50ºC with a maximum in tan δ at -10.4 ºC. The γ-transition occurs at −117.7 ºC. The β-transition is the major transition in the polymer in general, which is when the materials are going through a glass/rubber transition. That transition is equivalent to the glass temperature T_g [26]. The β-transition of PP shown in Figure 4.26 at 5.3 ºC in agreement with that reported by Ersoy and Onder [27]. Two transitions in PB and PBC polymeric blends were observed at −2 ºC and 14.7 ºC for PB and −4.25 ºC and 21 ºC for PBC. This indicates an incompatible (immiscible) blend with two separate phase transitions, and the role of the 5% PE-co-GMA role is just to enhance the adhesion and cohesion between two polymers, and not enough to obtain a miscible blend.

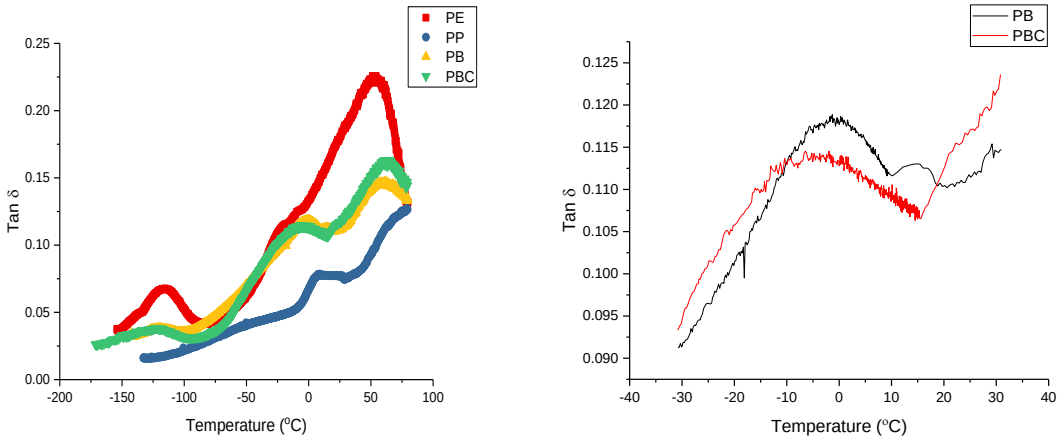

Figure 4.26. Mechanical loss factor spectra of blends polymer.

4.5. Summary and Conclusion

This present study has investigated the morphology, the phase transition, thermal and mechanical properties of PE, PP, PB and PBC, and the miscibility between two non-polar polymers (PP and PP), with and without the compatibilizer. Our results indicate the 100mg/ml ratio of the o-xylene is optimal to dissolve PB blends. Furthermore, the WAXD showed increase in the interlayer spacing and the crystallite size by addition of the PE and the PE-co-GMA to the blend. However, the 5% of PE-co-GMA dos not effect on the PB structure. Neither blend showed any co-crystallization. The long period of PB ≈141± 2 Å differs from that of PE ≈145 ±2 Å and the neat PP ≈125 ±1 Å. Moreover, it increases with the addition of the PE-co-GMA to be ≈146±2 Å. The DSC data shows that the blends have binary crystallization and melting behaviour while the crystallinity degree is lower in the PB and PBC than the PP. The thermal stability of the PE is higher than the PP and PB blend. Adding the PE-co-GMA compatibilizer causes an increase in the thermal stability. PP has superior mechanical properties, while PE provides better elastic behaviour. From that we can see the importance of blending the PP and PE. The mechanical properties increased with the addition of the PE-co-GMA. As a consequence, PBC provides the best mechanical properties. Finally, The DMA studies indicate that pure polymers (PE and PP) have three different transitions: α-transition, β-transition and γ-transition. Furthermore, PB and PBC both have two β-transitions, due to the glass transitions in the separate phases because the PE and PP are incompatible and immiscible polymers.

References

[1] Nouri, M. and Hay. J. (2006). Phase Separation in Polypropylene and Metallocene .Polymer engineering and science,889-595.

[2] Furukawa, T., Sato, H., Kita, Y., Matsukawa, K., Yamaguchi, H., Ochiai, S., Ozaki, Y. (2006). Molecular Structure, Crystallinity and Morphology of Polyethylene/Polypropylene Blends Studied by Raman Mapping, Scanning Electron Microscopy, Wide Angle X-Ray Diffraction, and Differential Scanning Calorimetry. Polymer Journal, 38(11), 1127–1136.

[3] Vonk, C. G., & Kortleve, G. (1967). X-ray small-angle scattering of bulk polyethylene - II. Analyses of the scattering curve. Kolloid-Zeitschrift & Zeitschrift F??r Polymere, 220(1), 19–24.

[4] Cser, F. (2001). About the Lorentz correction used in the interpretation of small angle X-ray scattering data of semicrystalline polymers. Journal of Applied Polymer Science, 80(12), 2300–2308.

[5]Tabatabaei, S. H., Carreau, P. J., & Ajji, A. (2008). Microporous membranes obtained from polypropylene blend films by stretching. Journal of Membrane Science, 325(2), 772–782.

[6] Sun, Y. Sen. (2006). Temperature-resolved SAXS studies of morphological changes in melt-crystallized poly(hexamethylene terephthalate) and its melting upon heating. Polymer, 47(23), 8032–8043.

[7] Thuresson, A., Segad, M., Turesson, M., & Skepö, M. (2016).Flocculated Laponite–PEG/PEO dispersions with monovalent salt, a SAXS and simulation study. J. Colloid Interf. Sci., 466, 330–342.

[8] Yang, L., Somani, R. H., Sics, I., Hsiao, B. S., Kolb, R., Fruitwala, H., & Ong, C. (2004). Shear-induced crystallization precursor studies in model polyethylene blends by in-situ rheo-SAXS and rheo-WAXD. Macromolecules, 37(13), 4845–4859.

[9] Cho, K., Li, F., & Choi, J. (1999). Crystallization and melting behavior of polypropylene and maleated polypropylene blends. Polymer, 40(7), 1719–1729.

[10]Fatnassi, M., Larbi, F. B. C., & Halary, J. L. (2010). Quantitative analysis of semicrystalline blends SAXS data: Theoretical modeling versus linear correlation function. International Journal of Polymer Science, 2010.

[11]Nedkov,T, Lendnicky. & Mihailova,M. (2008).Compatibilization of PP/PE Blends and Scraps with Royalene: Mechanical Properties, SAXS, and WAXS. Journal of Applied Polymer Science, 109, 226–233.

[12] Tajvidi, M., Falk, R. H., & Hermanson, J. C. (2006). Effect of natural fibers on thermal and mechanical properties of natural fiber polypropylene composites studied by dynamic mechanical analysis. Journal of Applied Polymer Science, 101(6), 4341–4349.

[13]Wong, a. C.-Y., & Lam, F. (2002). Study of selected thermal characteristics of polypropylene/ polyethylene binary blends using DSC and TGA. Polymer Testing, 21(6), 691–696.

[14] Chiu, F. C., Yen, H. Z., & Lee, C. E. (2010). Characterization of PP/HDPE blend-based nanocomposites using different maleated polyolefins as compatibilizers. Polymer Testing, 29(3), 397–406.
[15] Deka, B. K., & Maji, T. K. (2010). Effect of coupling agent and nanoclay on properties of HDPE, LDPE, PP, PVC blend and Phargamites karka nanocomposite. Composites Science and Technology, 70(12), 1755–1761.
[16] Sengupta, R., Chakraborty, S., Bandyopadhyay, S., Dasgupta, S., Mukhopadhyay, R., Auddy, K., & Deuri, S. (2007). A Short Review on Rubber / Clay Nanocomposites With Emphasis on Mechanical Properties. Engineering, 47, 21–25.
[17] Morgan, R. L., Hill, M. J., & Barham, P. J. (1999). Morphology, melting behaviour and co-crystallization in polyethylene blends: the effect of cooling rate on two homogeneously mixed blends. *Polymer*, *40*(2), 337–348.
[18] Zhang, J., Jiang, D. D., & Wilkie, C. A. (2006).Thermal and flame properties of polyethylene and polypropylene nanocomposites based on an oligomerically-modified clay. Polymer Degradation and Stability, 91(2), 298–304.
[19] Dikobe, D. G. (2010).Comparative study of the morphology and properties of PP/LLDPE/wood powder and MAPP/LLDPE/wood powder polymer blend composites. eXPRESS Polymer Letters, 4(11), 729–741.
[20] Chiu, F.-C., Yen, H.-Z., & Chen, C. (2010).Phase morphology and physical properties of PP/HDPE/organoclay (nano) composites with and without a maleated EPDM as a compatibilizer. Polymer Testing, 29(6), 706–716.
[21] Kim, H. S., Kim, S., Kim, H. J., & Yang, H. S. (2006).Thermal properties of bio-flour-filled polyolefin composites with different compatibilizing agent type and content. Thermochimica Acta, 451(1-2), 181–188.
[22] Wight, C. A. (2001). Kinetics of the Thermal and Thermo-Oxidative Degradation of Polystyrene , Polyethylene and Poly (propylene) Kinetics of the Thermal and Thermo-Oxidative Degradation of Polystyrene , Polyethylene and Poly (propylene), (MARCH), 775–784.
[23] Zhang, J., Jiang, D. D., & Wilkie, C. A. (2006).Thermal and flame properties of polyethylene and polypropylene nanocomposites based on an oligomerically-modified clay. Polymer Degradation and Stability, 91(2), 298–304.
[24] Salih, S. E., Hamood, A. F., & Abd Alsalam, A. H. (2013). Comparison of the characteristics of LDPE: PP and HDPE: PP polymer blends. Modern Applied Science, 7(3), 33–42.
[25] Campbell, F. Manufacturing Technology for Aerospace Structural Materials. London: Elsevier Ltd(2006).
[26] Hartmann, B., Duffy, J. V., Lee, G. F., & Balizer, E. (1988).Thermal and dynamic mechanical properties of polyurethaneureas. Journal of Applied Polymer Science, 35, 1829–1852.

[27] Ersoy, M. S., & Onder, E. (2013).Mechanical and Thermal Behaviors of Polypropylene - Multi-Walled Carbon Nanotube Nanocomposite Monofilaments. Fibres and Textiles in Eastern Europe, 98(2), 22–27.

Chapter 5

The Effect of Graphene Oxide on Structure-Property Relationships in Graphene/ Polymer nanocomposites

After understanding the structure and behavior of the host polymer matrices, in this chapter, we successfully incorporated graphene oxide nanofillers with different percentages into polyolefins in order to achieve a good dispersion and distribution by using the solution (solvent) method. Then we study the effect of the nanofiler on the structure and properties of the graphene/polymer nanocomposites.

5.1. Materials

The information and details of the polymers and compatibilizer polymer used were presented in the chapter 4. Graphene oxide (GO) was purchased (Graphene Laboratories, New York, USA) with a nominal thickness of about 1.1 ± 0.2 nm. The GO was stored and handled in a glove box in order to contain airborne particulates.

The morphology of GO studied by scanning electron microscope (SEM) and atomic force microscope (AFM) are shown in Figures 5.1 and 5.2 respectively. SEM images show exfoliation of graphite oxide to separate (single or multi layer) graphene flakes. GO sheets were exposed on the substrate. Exfoliated graphene oxide sheets scanned by AFM showed height profiles range between ~0.2 nm and ~ 0.6 nm corresponding to single layer graphene oxide sheets [1] [2].

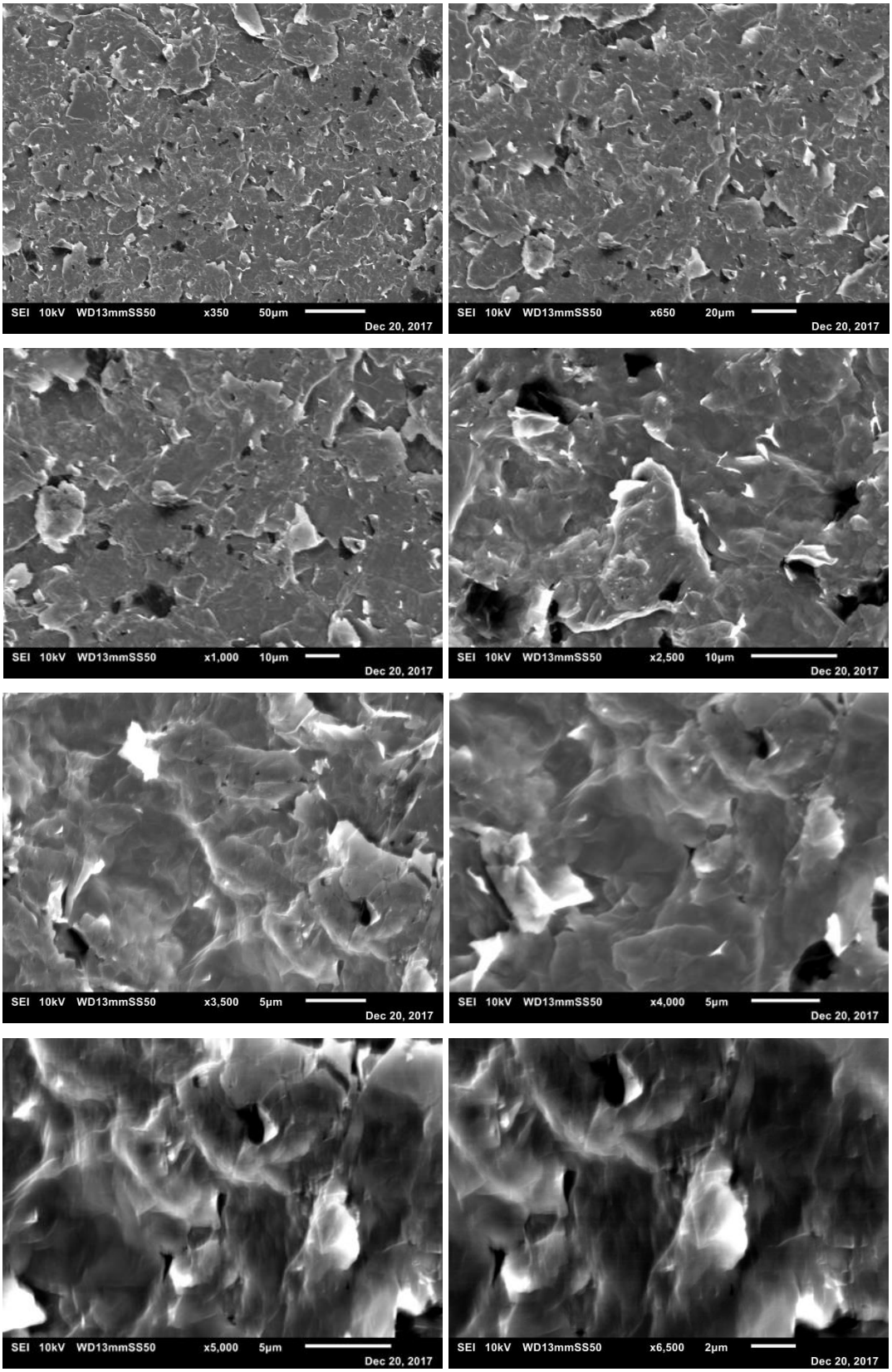

Figure 5. 1. SEM images of pure GO with different magnifications.

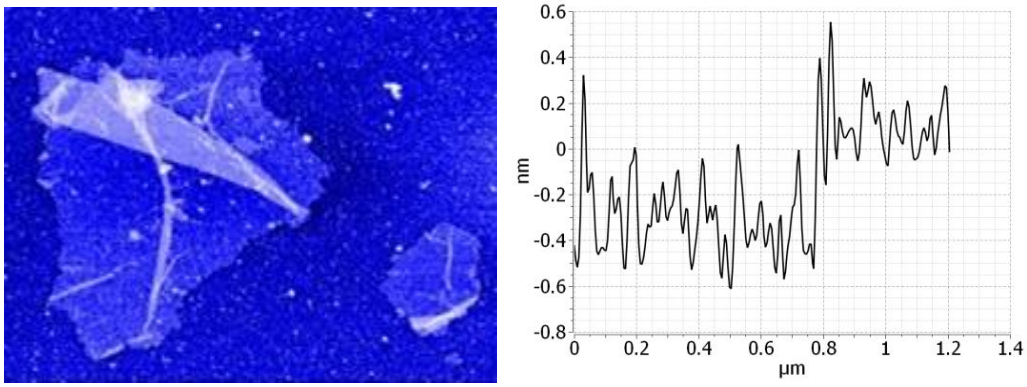

Figure 5.2. AFM image and thickness height profile of the GO deposited onto functionalized mica [3].

5.2. Solubility Tests

While most applications do not use graphene dispersions directly, many need graphene to be dispersed at appointed step during the experiment. Therefore, the stability, concentration and overall quality of the dispersion remain extremely important [4]. In order to compare the dispersion behaviour of GO in various solvents, the similar amount of GO nano particles (10 mg) was added to a given volume of solvent (5 mL), with a concentration of 2 mg/ml. The GO dispersions in water (H_2O), N,N dimethylformamide (DMF), o-xylene and tetrahydrofuran (THF) were sonicated using ultrasonic sound of frequency 40 kHz, in an ultrasound bath cleaner (Branson 2510,California, United States) for 1h to remove the large aggregates. GO forms a stable suspension in aqueous media since polar surface oxygen groups can hydrogen bond with the suspending medium. Even 4 hours after mixing, darkness of GO suspension implies good dispersibility in polar solvents, water, DMF and THF, while large precipitations were observed in the non-polar solvent o-xylene just after 1 hour; o-xylene is a good solvent for the non-polar polymers like PE and PP, "like dissolves like". GO formed fairly good dispersions in DMF and THF, but after 24 hours the GO was still suspended in water. Figure 5.3 displays the polarity index of some solvents.

In general, GO can be dispersed in many polar solvents particularly water, whereas reduce graphene oxide and pristine graphene have limited choices, such as a solvent of PE and PP. For the GO, DMF was chosen because it is compatible with o-xylene and has a higher polarity index and higher boiling point, as stated in Table 5.1.

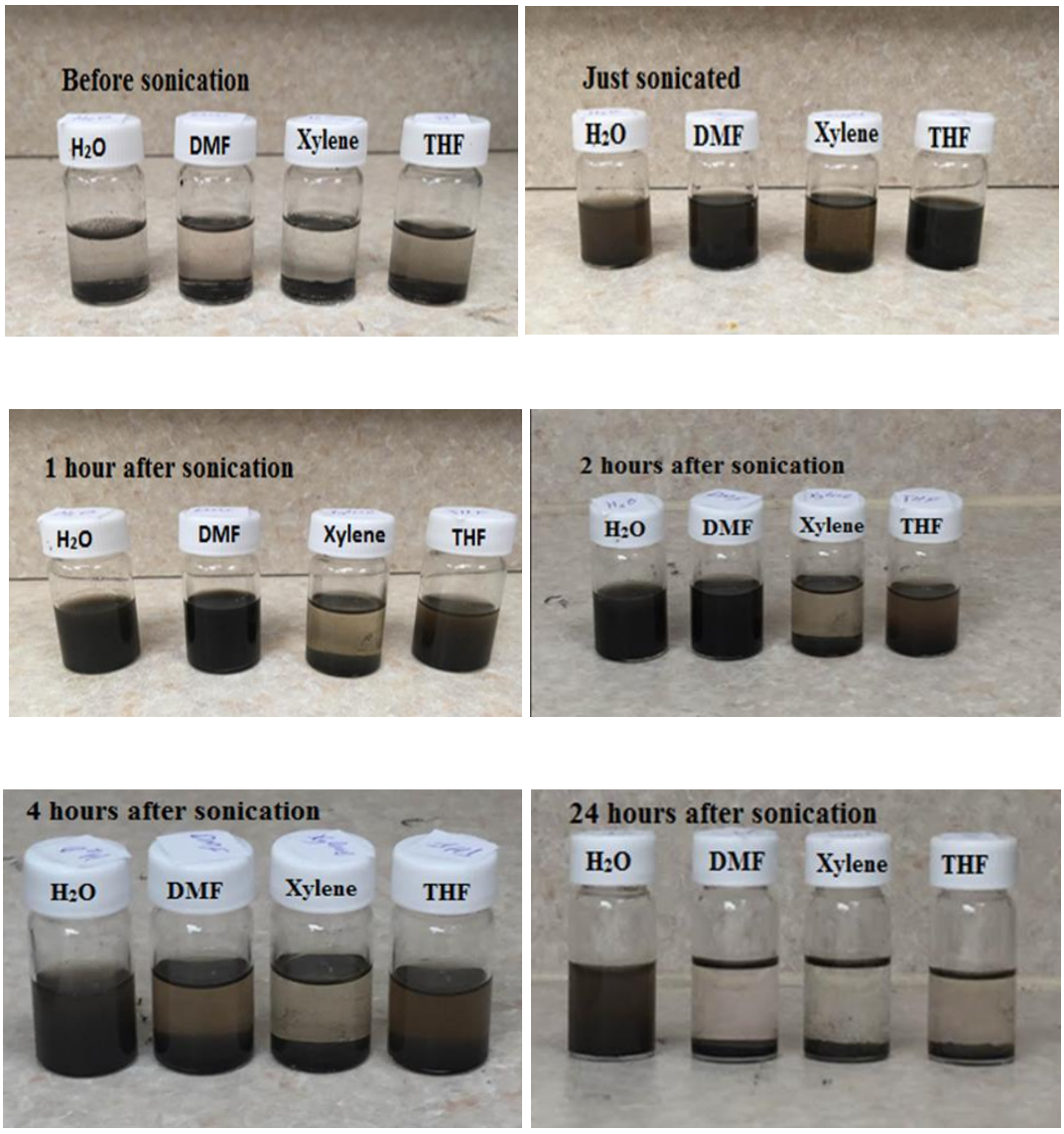

Figure 5.3. The dispersion of GO in four different polar and non-polar solvents.

Solvent	Solvent Polarity Index, *P*	Boiling point (°C)
Hexane	0.1	69
Carbon tetrachloride	1.6	77
Toluene	2.4	111
O-Xylene	2.5	144
Tetrahydrofuran	4.0	65
Ethyl Acetate	4.4	77
Methanol	5.1	65
Acetone	5.1	56
Dioxane	5.3	101
Acetonitrile	5.8	82
N,N-Dimethylformamide	6.4	153
Water	10.2	100

Table 5.1. The polarity index and the boiling point of some solvents [5].

5. 3. Graphene/Polymer Nanocomposite Processing

Graphene/polymer nanocomposites can be prepared by using a variety of preparation methods, for example the in situ polymerization method, or simply by using direct mixing such as solution method, or the melt compounding method followed by injection moulding or hot press. In this project graphene/ polymer nanocomposites are prepared using the solution method then hot press. The preparation process consists of 4 steps:

- Dissolving the polymer in solvent.
- Sonication mixing of graphene in the solvent.
- Mixing polymer with graphene in the cosolvent.
- Drying the graphene/polymer nanocomposites from solvents and moulding them.

5.3.1 Solvent method

The solvent (solution) method uses a solvent or co-solvent for dissolving the polymer and sonication for good dispersion and distribution of nanoparticles into the polymer matrix. PE and PP are non-polar polymers with high chemical resistance, and due to crystalline nature of those polymers, they do

not dissolve at room temperature. Aromatic hydrocarbons solvents such as toluene, xylene or DMF with high boiling points can dissolve PE and PP at high temperatures.

PE and PP blends were prepared based on the percentages shown in Tables 5.2 and 5.3. 2 gram of both granules were added to 20ml of o-xylene at 135 ^{o}C. Where used, the compatibilizer PE-*co*-GMA was also added at the same time. The polymers were dissolved with the help of a magnetic stirrer for 30 minutes. Strict protocols relating to the containment of solvent fumes (in a fume hood with high flow and a low sash) were therefore necessary throughout the sample preparation process.

5.3.2. Sonication mixing

The Graphene oxide was sonicated using an ultra sonication bath for 1 hour. The sonication process is done to the break-up the nanoparticles agglomerates and aggregates, inducing a regular dispersion and distribution of GO nanofiller in the solvent. The solution in the flask was exposed to ultrasonic sound of frequency 40 kHz Branson 2510 Ultrasonic (California, United State), the sound waves transmitted through the liquid promote shear stress in the solution, which overcomes the attraction force between the separate nanoparticles.

5.3.3. Mixing polymer with graphene

The Graphene solution after one hour of sonication was added to the polymer blend solution under the magnetic stirrer condition for 30 min at 135 ^{o}C.

5.3.4. Recovering and pelletizing the nanocomposites

The mixture was transferred to a petri dish, dried in an oven at 80 ^{o}C for 12 hours, leaving the GO/polymer nanocomposites. DSC confirmed complete solvent removal, where no solvent peak was observed. The resulting nanocomposite paste was then mechanically chopped to small pieces. 1 mm thick composite sheets were obtained using two sheets of teflon (PTFE) by a hydraulic hot press (Moore Ltd., Birmingham. England), at 210 ^{o}C under pressure of 5 tons for 10 minutes. Then, the specimens were quenched immediately into water at room temperature.

Number	Sample ID	PE (wt%)	PP (wt%)	GO (wt%)	PE-*co*-GMA (wt%)
1	GO	0	0	100	0.00
2	PE	100	0.0	0.00	0.00
3	PE/GO.25	100	0.0	0.25	0.00
4	PE/GO.5	100	0.0	0.50	0.00
5	PE/GO1	100	0.0	1.00	0.00
6	PE/GO2	100	0.0	2.00	0.00
7	PE/GO4	100	0.0	4.00	0.00
8	PP	0.0	100	0.00	0.00
9	PP/GO.25	0.0	100	0.25	0.00
10	PP/GO.5	0.0	100	0.50	0.00
11	PP/GO1	0.0	100	1.00	0.00
12	PP/GO2	0.0	100	2.00	0.00
13	PP/GO4	0.0	100	4.00	0.00
14	PB	50	50	0.00	0.00
15	PB/GO.25	50	50	0.25	0.00
16	PB/GO.5	50	50	0.50	0.00
17	PB/GO1	50	50	1.00	0.00
18	PB/GO2	50	50	2.00	0.00
19	PB/GO4	50	50	4.00	0.00
20	PBC	50	50	0.00	5.00
21	PBC/GO.25	50	50	0.25	5.00
22	PBC/GO. 5	50	50	0.50	5.00
23	PBC/GO1	50	50	1.00	5.00
24	PBC/GO2	50	50	2.00	5.00
25	PBC/GO4	50	50	4.00	5.00

Table 5.2. Weight percentages (wt%) of polymers pellets, graphene and compatibilizer used in the nanocomposites preparation.

Number	Sample ID	PE(g)	PP(g)	GO(g)	PE-*co*-GMA (g)
1	GO	0	0	100	0.00
2	PE	2.00	0.00	0.0	0.00
3	PE/GO.25	2.00	0.00	0.005	0.00
4	PE/GO.5	2.00	0.00	0.010	0.00
5	PE/GO1	2.00	0.00	0.020	0.00
6	PE/GO2	2.00	0.00	0.040	0.00
7	PE/GO4	2.00	0.00	0.080	0.00
8	PP	0.00	2.00	0.0	0.00
9	PP/GO.25	0.00	2.00	0.005	0.00
10	PP/GO.5	0.00	2.00	0.010	0.00
11	PP/GO1	0.00	2.00	0.020	0.00
12	PP/GO2	0.00	2.00	0.040	0.00
13	PP/GO4	0.00	2.00	0.080	0.00
14	PB	1.00	1.00	0.0	0.00
15	PB/GO.25	1.00	1.00	0.005	0.00
16	PB/GO.5	1.00	1.00	0.010	0.00
17	PB/GO1	1.00	1.00	0.020	0.00
18	PB/GO2	1.00	1.00	0.040	0.00
19	PB/GO4	1.00	1.00	0.080	0.00
20	PBC	1.00	1.00	0.0	0.10
21	PBC/GO.25	1.00	1.00	0.005	0.10
22	PBC/GO. 5	1.00	1.00	0.010	0.10
23	PBC/GO1	1.00	1.00	0.020	0.10
24	PBC/GO2	1.00	1.00	0.040	0.10
25	PBC/GO4	1.00	1.00	0.080	0.10

Table 5. 3. Weight of polymers pellets, graphene and compatibilizer used in the nanocomposites preparation.

Figure 5.4. The preparation steps of the nanocomposites.

5.4. Results and Discussion

5.4.1. WAXD results

The WAXD patterns of GO is displayed in Figures 5.5, while the patterns for PE, and PE/GO4, PP and PP/GO4 , PB, PB/GO4 and PBC and PBC/GO4 are shown in Figures 5.6 ,5.7, 5.8 and 5.9, the rest of samples of 0.25, 0.50, 1, 2 wt% present similar behaviour to 4wt% ,which is in agreement with observed in the literature [6]. With reference to the GO, the reflection peaks were assigned as the (130) and (200) plane of pure GO at 2θ≈ 10.8º and 23.8º, the second reflection at 23.8°is due to incomplete oxidation of graphite, graphite can't be oxidized 100%. The WAXD pattern around 23° is very broad, it can come from relatively amorphous (weakly ordered) regions in the GO. In PE/GO4 samples, the (110) and (200) reflections from the polymer crystallites are present at 2θ equal to 21.5° and 23.7° and do not appear to be significantly shifted in the presence of GO. In PP/GO4, reflection is present at 2θ values of 14º, 16.8º, 18.5º, 21.2º and 21.8º, representing diffraction from the (110), (040), (130), (111), (131) and (041) lattice planes of polypropylene. As might be expected for blends that are not co-crystallised, but are simple mixtures of the two component polymers, the diffraction pattern of PB/GO4 and PBC/GO4 are, broadly speaking, additive combinations of the diffraction patterns of PE/GO4 and PP/GO4. There is no detectable GO characteristic peak in the nanocomposites. The absence of a characteristic peak of GO in the composites is commonly interpreted to indicate the delamination or exfoliation of the GO within the nanocomposite samples, or rather an absence of stacked, graphitic regions, even for relatively low GO contents from 0-4wt% [7][8][9]. The broad peaks are related to the insertion of polymers chains between the stacked GO layers [10].

The X-ray peaks shows that the oxygen containing groups increase the nanocomposites interlayer spacing (Table 5.4). The larger interlayer spacing of GO is ≈ 8.17 Å (usually between about 0.6 and 0.8 nm depending on comparative humidity), which facilitates intercalation by polymers. The aromaticity of the graphene sheets is reduced as epoxide and hydroxyl groups are also formed during the oxidation process, resulting in increased an interlayer spacing (d spacing). Furthermore, the polar functional groups of GO support immediate intercalation of hydrophilic molecules with an increase of the interlayer spacing of the polymer. X-ray diffraction suggested the individual graphene oxide sheets remain stacked loosely and more exfoliated in the polymer matrix [11]. The estimated crystallite size, shown in Table 5.5, decreases while the intensity of WAXD increases in the presence of GO [12]. According to the classical Scherrer analysis, the width of the diffraction peaks gives information about the characteristic size of the scattering crystallite, with larger crystallites producing sharper diffraction peaks. It was observed that the presence of graphene oxide led to an increase in the full width at half-maximum of the diffraction peaks, indicating that the insertion of GO was producing a decrease in characteristic crystalline size within the polymer phase of the nanocomposite materials.

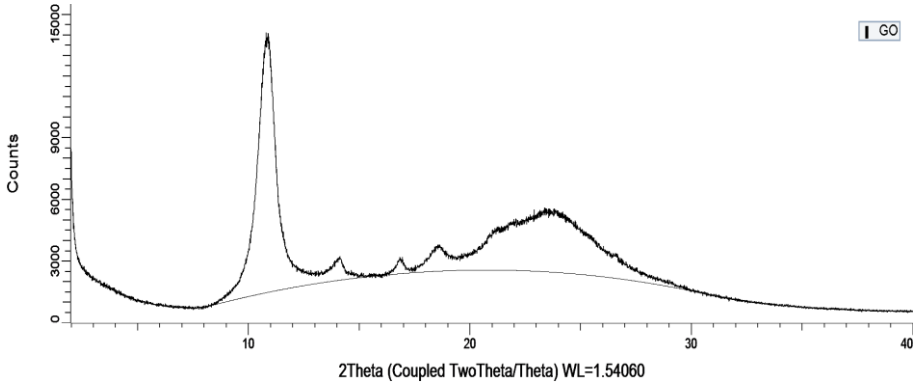

Figure 5. 5. The curves of WAXD patterns of GO pure.

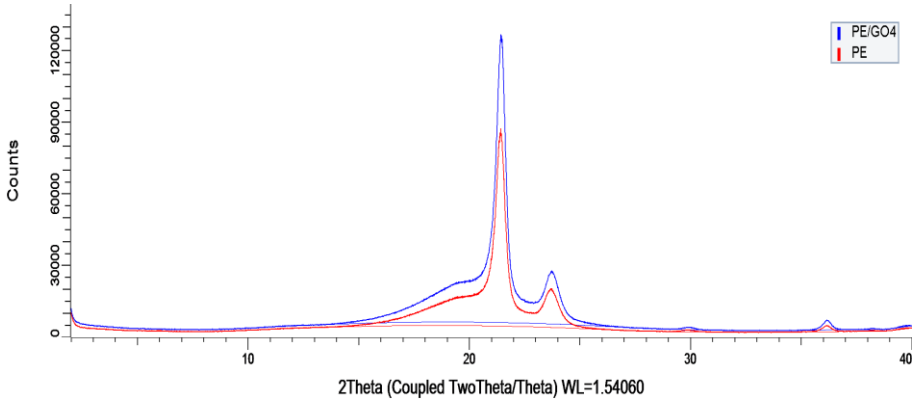

Figure 5. 6. The curves of WAXD patterns of PE and PE/ GO4.

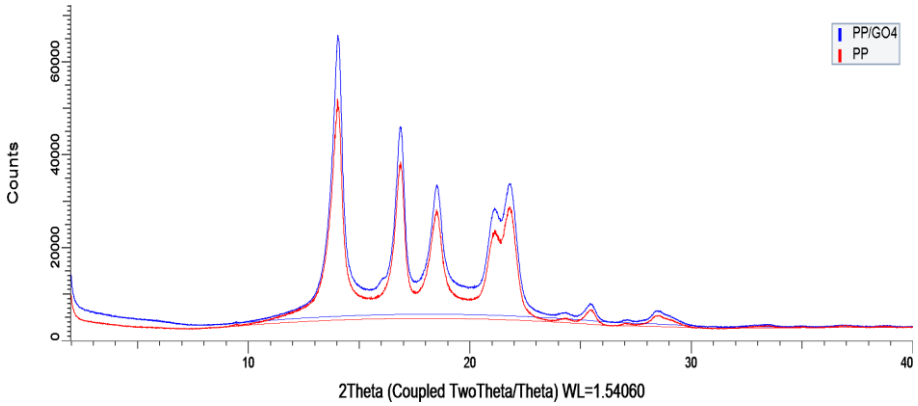

Figure 5. 7. The curves of WAXD patterns of PP and PP/ GO4.

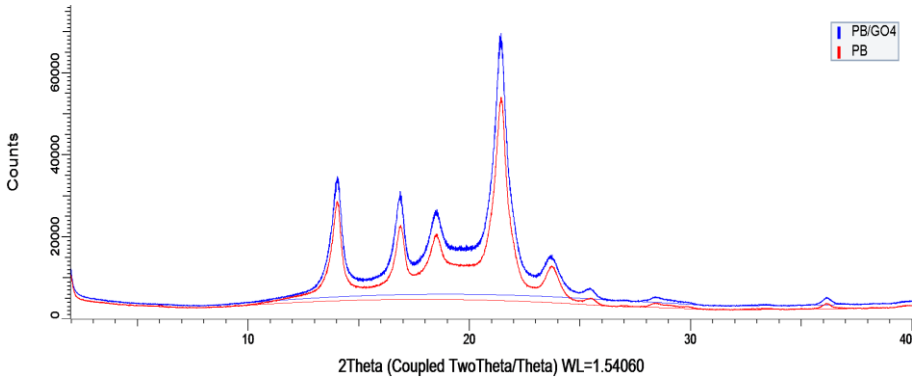

Figure 5. 8. The curves of WAXD patterns of PB and PB/ GO4.

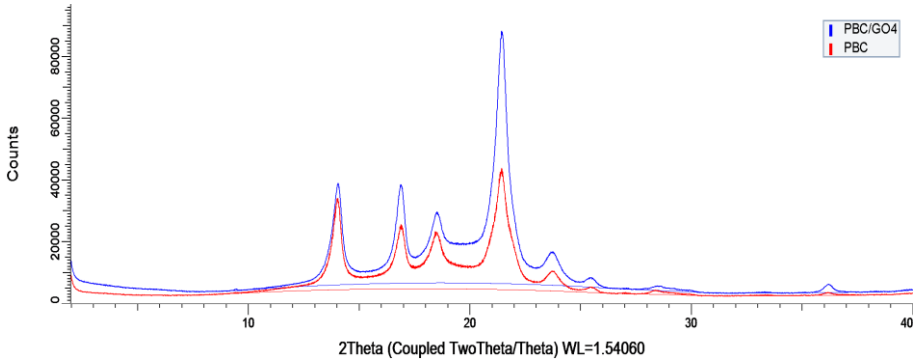

Figure 5. 9. The curves of WAXD patterns of PBC and PBC/GO4.

The interlayer spacing d(Å)								
2θ	PE	PE/GO4	PP	PP/GO4	PB	PB/GO4	PBC	PBC/GO4
14°	-		6.288	6.310	6.307	6.331	6.297	6.310
16.8°	-		5.239	5.277	5.246	5.248	5.246	5.263
18.5°	-		4.780	4.794	4.797	4.906	4.797	4.800
21.5^0	4.141	4.150	4.070	4.072	4.129	4.141	4.157	4.159
23.7°	3.746	3.766	-	-	3.740	3.759	3.753	3.795

Table 5.4. The interlayer spacing of pure PE,PP,PB , PBC and PNCs of 4wt% of GO.

2θ	14°		16.8°		18.5°		21.4°		23.7°	
Sample ID	FWHM	τ (Å)	FWHM	τ (Å)	FWHM	τ (Å)	FWHM	τ (Å)	FWHM	τ (Å)
PE	-	-	-	-	-	-	0.437	205.5	0.536	168.1
PE/GO4							0.449	200.1	0.562	160.4
PP	0.382	233.1	0.370	241.3	0.476	188.1	1.195	75.2	-	-
PP/GO4	0.479	185.6	0.417	213.9	0.515	173.6	1.219	73.7	-	-
PB	0.351	253.7	0.329	271.5	0.404	221.2	0.486	185.0	0.489	184.3
PB/GO4	0.475	187.4	0.390	229.0	0.478	187.2	0.555	161.9	0.532	169.6
PBC	0.369	241.1	0.370	241.3	0.438	209.5	0.516	174.1	0.465	193.8
PBC/GO4	0.444	200.5	0.387	230.5	0.433	206.8	0.529	169.7	0.502	179.8

Table 5.5. The FWHM values of pure PE, PP, PB, PBC and PNCs of 4wt% of GO reflection peaks in WAXD data and crystallite size.

5.4.2. SAXS study

SAXS investigates many structural features at different length scales that are relevant to polymers and polymer nanocomposites. The lamellar thickness (L_p) can be obtained from the maxima in the Kratky plots [13], likewise referred to as Lorentz-corrected plots, where $I(q)q^2$ is plotted versus the scattering vector (q). The corresponding plots in Figure 5.10 indicate the presence of the lamellar peak expected from the fact that PE, PP, PB and PBC are semicrystalline polymers or blends thereof. As a basic first level of interpretation, the maxima are translated into length scales by $L_p \sim \frac{2\pi}{q}$. The lamellar long period L_p is the sum of lengths of the crystalline and amorphous fractions in polymers ($L_p \approx l_c + l_a$ where l_c is the crystalline thickness and l_a is the amorphous thickness) [14]. In general, the long period increased systematically with the addition of GO as shown in Figure 5.11, although the degree of increase fluctuated between the different sample types tested. The long periods of PE and PP are around 145±2 Å and 125±1 Å, respectively, while the long period of PE/GO4, and PP/GO4, are 162±1 Å and 133±2 Å, respectively. This indicates an increase in amorphous or crystalline thickness, or both. It is possible to envisage the GO being present in the inter-lamellar crystalline/amorphous area causing an increase in the spacing of polymer layers. An increase in crystalline thickness of polymer could be attributed to the positioning of GO nanoparticles near the crystalline/amorphous interface causing increased irregular chain folding where an increase in thickness of the interfacial zone may appear as an increase in crystalline block thickness (Table 5.6) [8]. The situation is further complicated in the case of the polymer blend samples where two semicrystalline polymer species, and therefore two long periods are present. The increase in L_p has been stated to have a direct effect on the macroscopic mechanical properties of polymers. Specifically, the elastic modulus of polymers decreases with increasing L_p. Accordingly , the crystalline layers l_c

and amorphous l_a layers increased as well. The long period, the thickness of the crystalline and amorphous layers and the linear crystallinity were determined by using the linear correlation function $LCF\ \gamma(r)$, and are reported in Table 5.6.

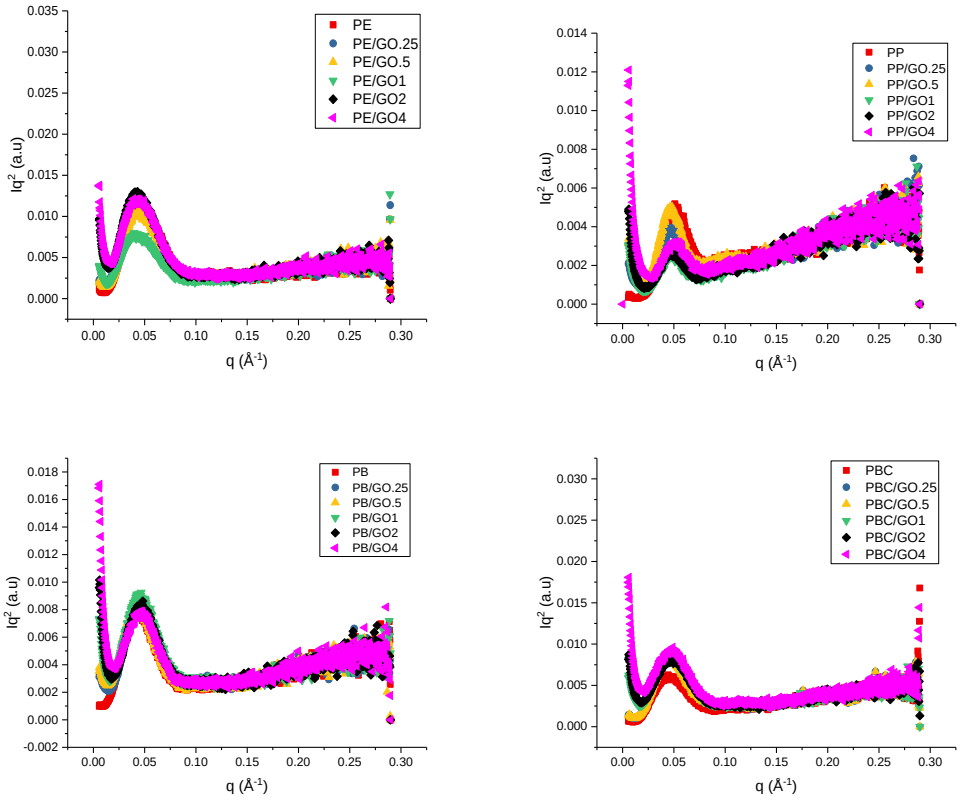

Figure 5. 10. Lorentz-corrected SAXS curves for the pure PE,PP, PB and PBC samples and their PNCs.

Specimens ID	Long period (Å)	Crystalline layers thickness(Å)	Amorphous Layers thickness(Å)	linear crystallinity
PE	145±2	20	124.7	0.14
PE/GO4	162±1	26.4	134.5	0.16
PP	125±1	42.1	83.3	0.34
PP/GO4	133±2	50.8	82.5	0.38
PB	141±2	13.5	128	0.10
PB/GO4	154±1	21.9	132	0.14
PBC	147±2	10.3	135.9	0.07
PBC/GO4	149±1	24.6	124.4	0.17

Table 5.6.The long period, the thickness of the crystalline and amorphous layers and the linear crystallinity of pure PE, PP, PB and PBC and PNCs of 4wt% of GO.

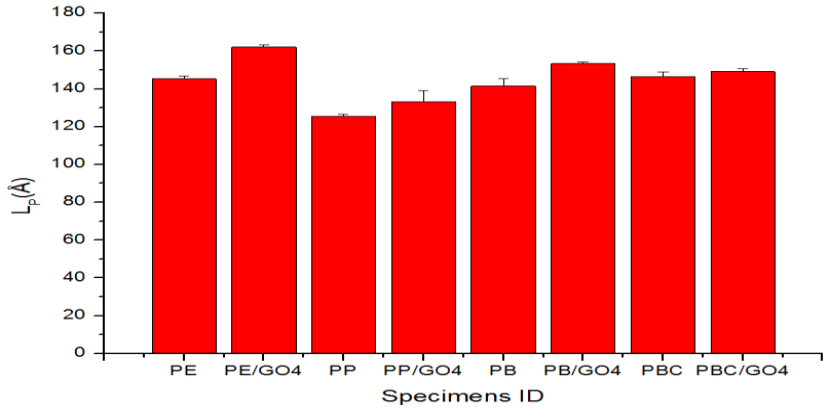

Figure 5.11. Long period of lamellar of pure PE, PP, PB and PBC and PNCs of 4wt% of GO.

5.4.3. FTIR analysis

The chemical structure of GO/polymer nanocomposites was studied by FTIR to determine the type of the chemical bonds and the functional groups present in the polymers and the nanocomposites. The GO spectra are indicative of various functional groups including single bonds, double bonds, trans groups and non-conjugated groups. In Figure 5.12 the FTIR spectrum for PE, the wavenumber 2915.04 cm^{-1} indicates a single bonded C–CH_3 functional group while 2817.35 cm^{-1} and 1615.46 are characteristic of C-H stretching bands. The wavenumber of 1468.01 cm^{-1} is CH_2 scissor and asymmetric band, and 729.38 cm^{-1} indicates the CH_2-CH_3 ethyl group attached to backbone [15][16]. The FTIR spectrum of the PP sample displays the characteristic broad and intense band that extends from 2949.28 to 2722.58 cm^{-1}, referred to the valence vibrations of the COH bonds, a band located at 1453.28 cm^{-1} is characteristic of methylene CH_2 groups, and a band at around 1375.18 cm^{-1} is attributed to the methylene CH_3 group [17]. According to the FTIR spectra, all the peaks of the PB and PBC polymer blends are in conformity with those of PP matrices. This is ascribed to PE and PP that are both polyolefins polymers are not compatible [18]. The 5wt% of PE-co-GMA in PBC is not enough to impact upon the FTIR spectra of PBC, which also shows a similar structure to PB. The FTIR spectrum of graphene it has been shown in Rattna & et al. [19]. The peaks of pure GO are: at 3340 cm^{-1} O-H stretching vibrations, at 1730 cm^{-1} stretching vibrations from C = O (carbonyl/carboxyl), at 1630 cm^{-1} skeletal vibrations from unoxidized graphitic domains (aramotic), at 1226 cm^{-1} C-OH stretching vibrations, at 1044 cm^{-1} C-O stretching vibrations (alkoxy) .The absence of graphene oxide peaks in PE/GO4, PP/GO4, PB/GO4 and PBC/GO4 is a strong indication of graphene sheets exfoliation inside the polymer [20][21].

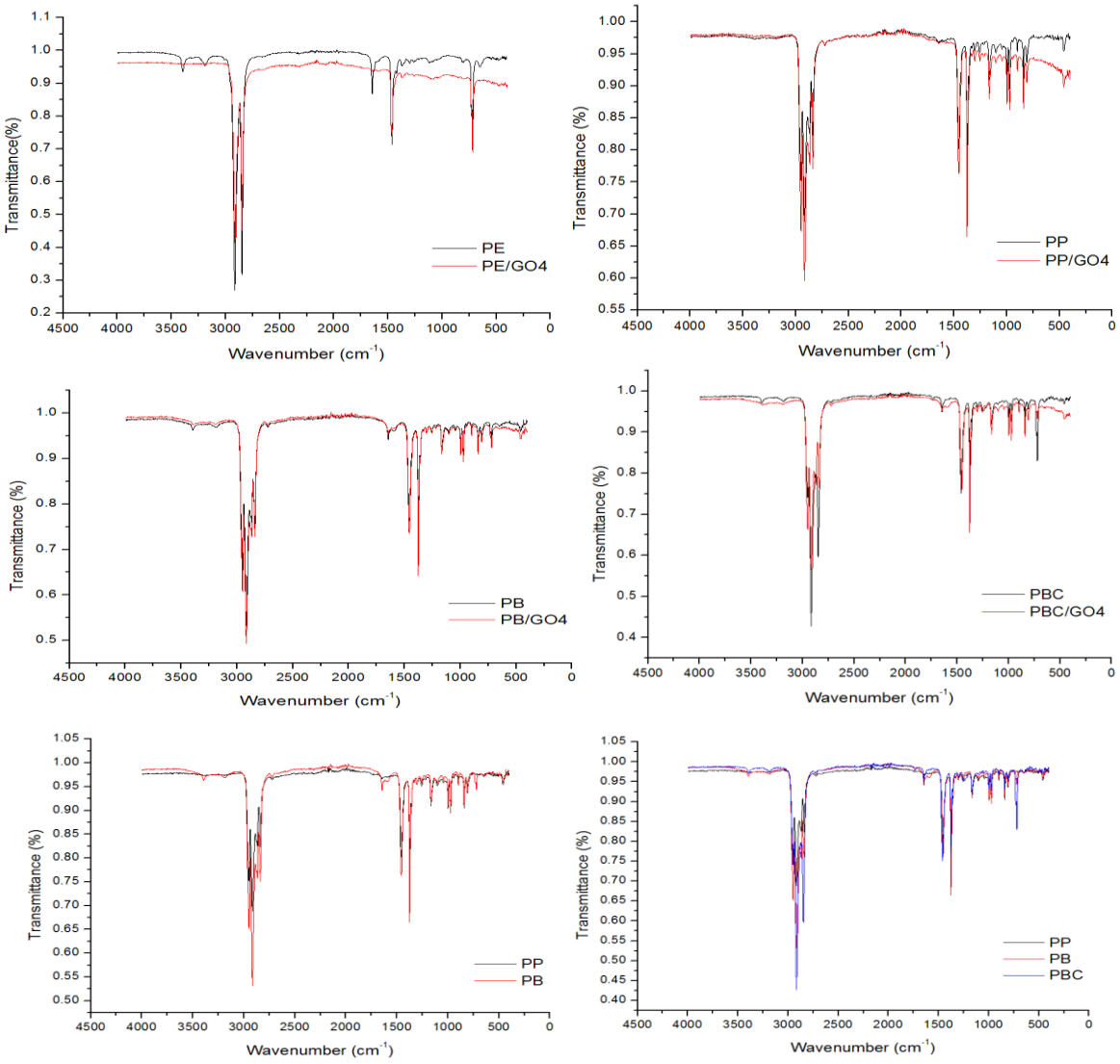

Figure 5.12. FTIR spectra of pure PE, PP, PB and PBC and PNCs of 4wt% of GO.

5.4.4 Raman Spectra

Raman spectroscopy is a sensitive light scattering technique, complementary to FTIR, and provides a spectral fingerprint for samples. Raman spectroscopy is used for analysing hybridization state in carbons. Figures 5.13, 5.14, 5.15 and 5.16 shows Raman spectra of PE, PE/GO4, PP, PP/GO4, PB, PB/GO4, PBC and /PBC/GO4 respectively. The assignment of the Raman lines in the spectra of metallocene PE and homo PP represent the range of the C–C stretching vibrations and the CH_2 and CH_3 deformation vibrations contains non-overlapping lines corresponding to the vibrations of macromolecules in various phase and conformational states [22].The peaks of PE in the low-frequency region, from 1000 to 1600 cm^{-1}, relate to vibration modes of C-C bonds, meaning that there

were distortions in this polymeric bond. In the spectrum of this polymer peaks in the region of high frequency (2500-3200 cm^{-1}) are attributed to the methylene group (-CH_2-) characteristic of polyethylene. The Raman lines at 1061, 1127, 1293, and 1437 cm^{-1} are the most important to characterise the chemical structure. For all types of the polymer blends, these lines correspond to the deformation vibrations of CH_2 groups in CH_2- chains. The Raman line at 1437 cm^{-1} is assigned to the vibrations of macromolecules localized in the orthorhombic crystalline phase of PE. The line at 1127 cm^{-1} belongs to the vibrations of CH_2-chains in trans-conformation, for example PE crystallites and CH_2-chains in trans conformation, which are localized in the amorphous phase. The feature at 1293 cm^{-1} corresponds to the vibrations of CH_2-chains with a considerable amount of gauche conformers, which are localized in the amorphous phase [23][24][25][26].

For PP, bands between 3000 and 2500 cm^{-1} are attributed to CH_2 and CH_3 stretching modes of the polymeric chains. The spectral region at lower frequencies between 1500 and 800 cm^{-1} is representative of CH_2 and CH_3 bending modes along with stretching and bending vibrations of C–C bonds. The vibrational range from 850 to 800 cm^{-1} is very interesting as they are specific signals indicating that crystalline and amorphous phases of the polymeric matrix are present. In particular, the peak at 840 cm^{-1} primarily assigned to r(CH3) modes is related to the crystalline phase of polypropylene, the band at 807 cm^{-1} is due to r (CH_3) and backbone stretching (C–C) typical of isomeric defects of PP helical chains, and the wide absorption at 830 cm^{-1} (r (CH_3)) is characteristic of the PP amorphous phase [27][28].

Similar variations were observed in the spectra of the PB and PBC blends. Table 5.7 reports all the band assignments made by referring to the combination of PE and PP Raman spectra. In the range of the stretching vibrations of the CH_2 and CH_3 groups, addition of the PE content causes an increase in the intensity of the line assigned to the symmetrical valence vibration of the CH_2 group and a simultaneous monotonic shift of the peak position of this line from 2839 cm^{-1} (neat PP) to 2846 cm^{-1} (neat PE). For the PB and PBC blends under study, the Raman bands presented a lower intensity. The feature at 1328 cm^{-1} observed only as small asymmetry of the line at 1218 cm^{-1}. Except for a double peak in the spectral region from 1400 to 1500 cm^{-1}, the Raman lines of the PE vibrations do not overlap with the Raman lines of the PP vibrations [29][30][31][32].

The Raman spectra of the PE/GO4, PP/GO4, PB/GO4 and PBC/GO4 present the G band at around 1437, 1458, 1455 and 1456 cm^{-1} respectively, and D band at around 1294, 1328, 1327 and 1327 cm^{-1}. The intensity of G band was higher than that of D band. The G band includes the vibration of sp^2-hybridized carbon and D band is related to defects due to grain boundaries and vacancies. As a consequence, Raman spectroscopy can be employed to evaluate the hybridization state in carbon.

Figure 5.17 of pure GO shows an intensive G-band at 1582 cm^{-1}, also a less intensive D-band at 1351 cm^{-1} a primary in-plane vibrational mode and a G' or (2D) band at 2658 cm^{-1} with a shoulder at 2925

cm^{-1} is visible. It is characteristic of sp^2 systems, arising from a second-order excitation process. An electron near the K point (Dirac point) at the corner of the Brillouin zone is excited to the conduction band of graphene, and the electron (or the corresponding hole) is further scattered, by the phonon vibration, as shown in Figure 5.18 (b), to the inequivalent K' point [30]. In order to conserve energy and momentum, the electron (or hole) is scattered by a second phonon vibration, back to the K point where the electron-hole recombines, emitting a photon in the process. The third band of interest for graphene-type materials is the D band which, as shown in the Raman spectrum of GO although characteristic of graphitic materials, in pristine sp^2 hybridised samples this band is Raman inactive. Like the G' Raman scattering, an electron (or hole) is excited by an incident photon, and is further scattered by the phonon breathing mode shown in Figure 5.18 (b). The D band is a one-phonon process and thus requires an atomic defect which breaks the symmetry of the sp^2 lattice to scatter the electron (or hole) back to the K point making the process Raman active [33]. As a result the D band is known as the disordered band, with the relative areas of the D and G bands being used as a measure of defect density in a graphene type structure. Although, it is worth noting that the I_D/I_G ratio of defective graphene type materials does not tend to change significantly in response to further surface functionalisation, the D/G ratio is dominated by the structural defects (holes) of a sheet rather than the level of oxidation, for example, which has comparatively little effect on the I_D/I_G ratio [34][35][36][37][38]. The I_D/I_G value was calculated as (0.285) for our pure GO sample.

Raman shift (cm^{-1})	Assignments (PE)	Assignments (PP)	Features
807		C–C stretching	Crystalline
840		CH3 rocking	Crystalline
972		CH3 rocking	Crystalline
1035	C–C stretching		All-trans -$(CH_2)_n$-
1151		C–C stretching	All-trans -$(CH2)_n$-
1218	CH_2 rocking		Crystalline
1328		CH2 twisting	Amorphous
1358		CH3 wagging	Amorphous
1458		CH2 bending	Crystalline

Table 5.7. Wavenumber(cm^{-1}) and assignments of the Raman bands of both PB and PBC.

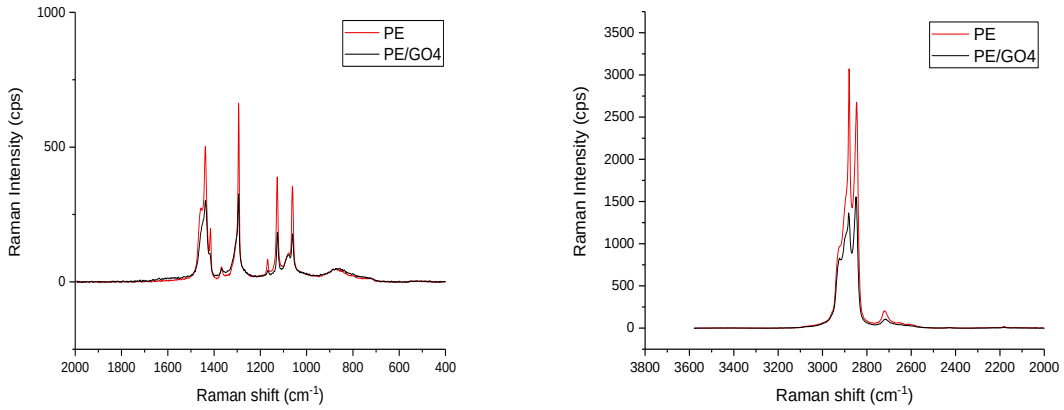

Figure 5.13. Raman spectra of PE, PE/GO4.

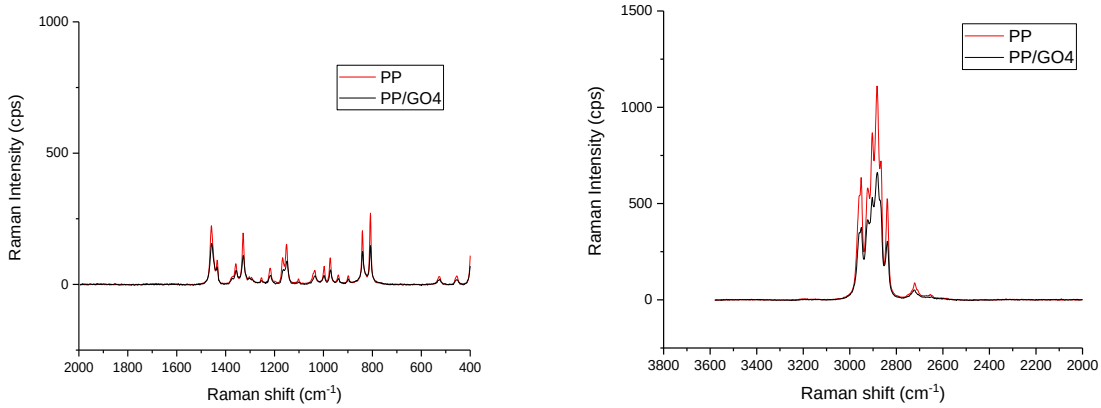

Figure 5.14. Raman spectra of PP and PP/GO4.

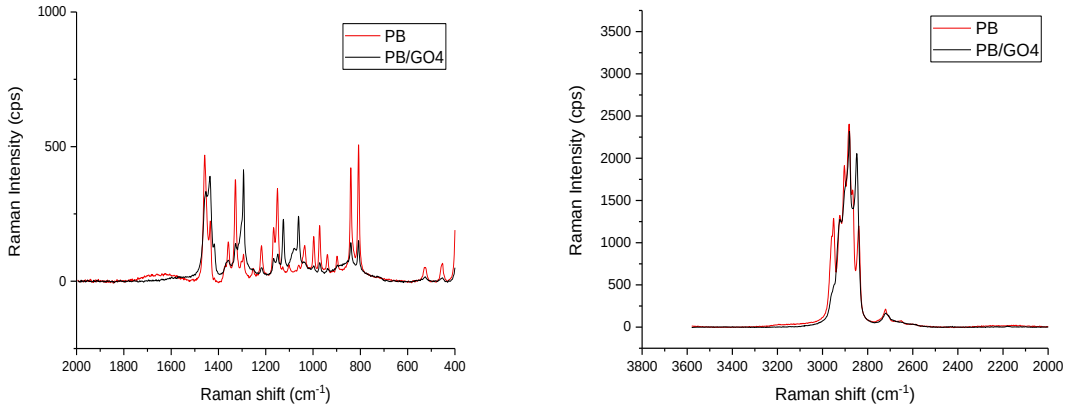

Figure 5.15. Raman spectra of PB and PB/GO4.

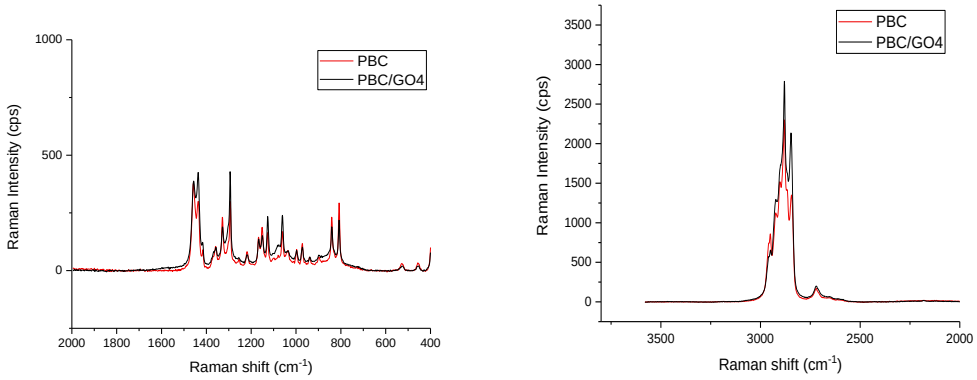

Figure 5.16. Raman spectra of PBC and PBC/GO4.

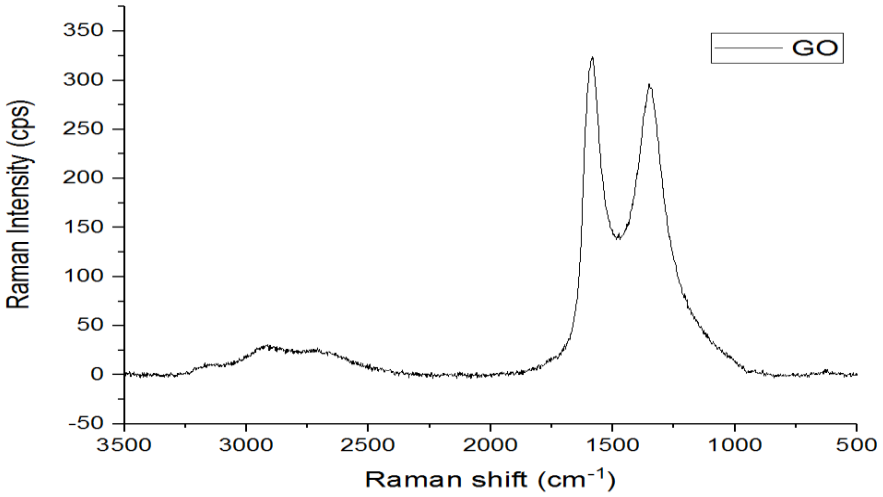

Figure 5.17. Raman spectra of pure graphene oxide GO.

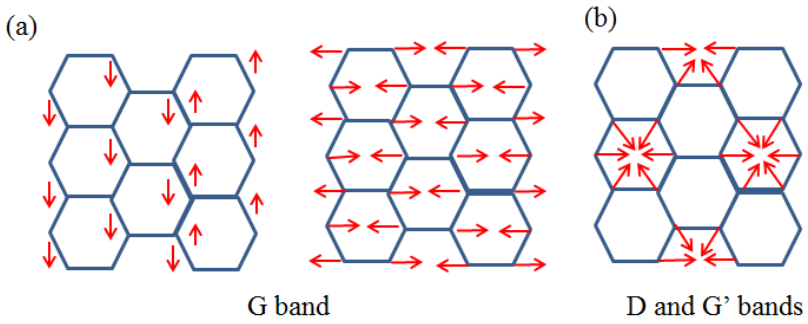

Figure 5.18. The optical phonon vibrations of graphene, with the sp^2 C-C stretching modes which correspond to (a) the G band, and (b) the D and G' bands in Raman [21].

5.4.5. Crystallization and Melting Behaviour

DSC and TGA were applied to estimate the impact of the addition of different weight percentages (wt.%) of GO on the thermal features of PE, PP, PB and PBC. The crystallization and melting temperatures obtained are reported in Tables 5.8, 5.9, 5.10 and 5.11. Compared with the single PE host matrix, melting temperatures of the nanocomposites were not significantly influenced by GO addition (Table 5.8), and the melting temperature degree was around 123±1 ºC in most of the PE/GO nanocomposites. However, the addition of GO increases the crystallization temperature in all the samples, increasing in PE from 103±1 ºC to 108±1 ºC with the addition of GO at 4 wt%. The increase in the T_c of PE (Figure 5.19), in the presence of graphene, has industrial value due to its consequences for a shorter processing cycle, thus increasing the production rate. The graphene acts as a nucleating agent for PE and PP, so that the nucleation mode is heterogeneous instead of homogeneous, considerably decreasing the nucleation free energy, allowing the molecular chain to attach and be arranged in an ordered fashion around the nucleating agent. The degree of crystallinity as measured via DSC in PE/GO.25 (with 0.25wt%) is lower than the pure PE, but the crystallinity degree increased upon further addition of GO up to 4wt%. The same thermal behaviour happened in the PP/GO nanocomposites, as displayed in Table 5.9, with the crystallization temperature increased slightly with increasing GO content. No clear effect on the melting temperature of around 167±1 ºC was observed. Further, it was observed that the degree of crystallinity is lower in the PP/GO nanocomposites (between 35-38%) than the clean PP (48 %). The supercooling degree ($\Delta T = T_m - T_c$) required for the nanocomposites crystallization [7], was higher in PP/GO nanocomposites compared with that required for pure PP, while it was lower in PE/GO nanocomposites than PE. The increase or decrease in the degree of supercooling indicates interactions between both PE and PP with GO. The thermal behaviours of the PB and PBC are reported in Tables 5.10 and 5.11. The melting and the crystallization temperatures of PB and PBC and their nanocomposites remained constant with no clear change exhibited at any of the GO weight percentage, with similar values to those for pure PB and PBC. A slight change in the crystallinity degree was detected due to the GO addition. This decrease might be interpreted as the effect of the GO nano particles hindering the chain mobility [11]. We conclude that there is no obvious effect of the GO on the thermal parameters or the crystallinity degree in the blended (PB and PBC) samples [39].

Specimens ID	T_c (ºC)	T_m (ºC)	ΔH_m J/g	ΔT (ºC)	X_c (%)
PE	103±1	124±1	77	21	26
PE/GO.25	104±1	122±1	62	18	21
PE/GO.5	105±1	123±1	61	18	21
PE/GO1	106±1	123±1	65	17	22
PE/GO2	107±1	123±1	68	16	23
PE/GO4	108±1	123±1	69	15	23

Table 5.8 .The DSC parameters of PE/GO nanocomposites.

Specimens ID	T_c (ºC)	T_m (ºC)	ΔH_m J/g	ΔT (ºC)	X_c (%)
PP	119±1	167±1	100	49	48
PP/GO.25	117±1	166±1	73	49	35
PP/GO.5	117±1	167±1	76	50	37
PP/GO1	117±1	167±1	79	50	38
PP/GO2	119±1	166±1	76	47	37
PP/GO4	120±1	168±1	74	48	36

Table 5.9 .The DSC parameters of PP/G nanocomposites

a) b)

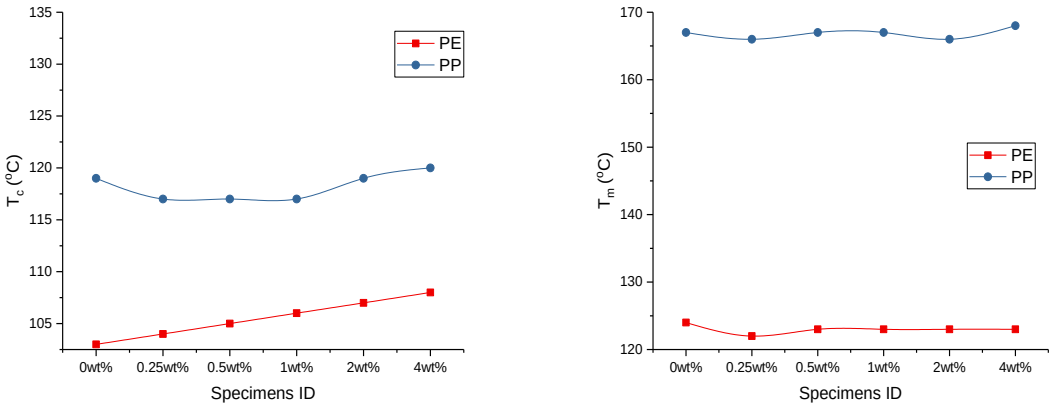

Figure 5.19.The a) crystallization temperature b) melting temperature of PE, PP and their GO nanocomposites.

Specimens ID	T_c (ºC)		T_m (ºC)		ΔH_m J/g		X_c (%)		
	PE	PP	PE	PP	PE	PP	PE	PP	PB
PB	109±1	115±1	123±1	166±1	15	46	5	22	27
PB/GO.25	106±1	116±1	123±1	166±1	23	39	8	19	27
PB/GO.5	107±1	118±1	123±1	166±1	29	36	10	14	24
PB/GO1	107±1	117±1	123±1	166±1	26	37	9	18	27
PB/GO2	107±1	118±1	123±1	166±1	27	35	9	17	26
PB/GO4	106±1	117±1	124±1	167±1	23	41	9	20	28

Table 5.10 .The DSC parameters of PB/G nanocomposites.

Specimens ID	T_c (ºC)		T_m (ºC)		ΔH_m J/g		X_c (%)		
	PE	PP	PE	PP	PE	PP	PE	PP	PBC
PBC	106±1	114±1	122±1	164±1	23	33	4	23	27
PBC/GO.25	107±1	116±1	123±1	166±1	29	43	10	21	31
PBC/GO.5	105±1	114±1	123±1	166±1	28	38	10	18	28
PBC/GO1	106±1	114±1	123±1	165±1	26	40	9	19	28
PBC/GO2	108±1	117±1	123±1	166±1	28	36	10	17	27
PBC/GO4	106±1	133±1	123±1	166±1	26	35	9	17	26

Table 5.11 .The DSC parameters of PBC/G nanocomposites.

5.4.6. Thermal Stability

TGA was used to examine the thermal stability of the nanocomposites. TGA data of nanocomposite samples with reference to the pure polymers are plotted in Figure 5.20, 5.21, 5.22 and 5.23. The onset of decomposition temperature (T_{onset}), the decomposition temperature at 50% weight loss ($T_{50\%}$) and the decomposition temperature at 95% weight loss ($T_{95\%}$) of the composites are presented in Tables 5.12, 5.13, 5.14 and 5.15. TGA revealed that the decomposition temperature increased with adding GO content. These results suggest that GO can act as effective thermal barrier which helps to hinder the degradation of PE by preventing the emission of gaseous molecules, disrupting the oxygen supply during thermal degradation, and the formation of char layers on the surface of the nanocomposite [40]. The onset degradation temperature increased by around 110±3 ºC with 0.25 wt% GO content compared to neat PE. The thermal stability of the nanocomposites continued to increase with increasing GO content at 0.25, 0.5 and 1 wt%, with no further effect at 2 wt% and 4 wt%.

The degradation of PE produces mostly α-olefins like 1-hexene. This process happens through a mechanism of cleavage of the polymeric chains [41]. This degradation becomes less effective when the polymeric chains have decreased mobility. The GO presences in the nanocomposites arguably gives rigidity to the polymeric matrices, reducing the mobility of polymer chain and consequently hindering the polymer degradation.

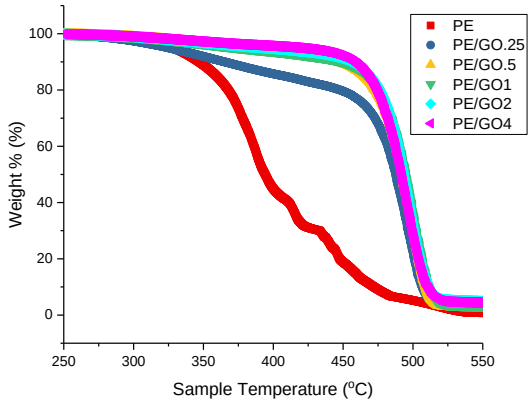

Figure 5. 20. TGA curves of PE nanocomposites.

Specimens ID	T_{onset} (°C)	$T_{50\%}$ (°C)	$T_{95\%}$(°C)
PE	365±3	394±3	502±3
PE/GO.25	475±3	488±3	513±3
PE/GO.5	475±3	493±3	514±3
PE/GO1	480±3	494±3	517±3
PE/GO2	478±3	493±3	546±3
PE/GO4	474±3	492±3	521±3

Table 5.12. Thermal degradation temperatures of the PE/GO nanocomposites.

The GO addition effect on the PP nanocomposites is similar to the PE nanocomposites, increasing T_{onset}, $T_{50\%}$ and $T_{95\%}$, as shown in Figure 5.21, compared to the temperatures for pure PP. Enhancements of around 164±3, 169±3 and 150±3 °C for T_{onset}, $T_{50\%}$ and $T_{95\%}$ are observed respectively with only 0.25 wt% GO. This is clear evidence that added GO can act as a flame retardant, by significantly increasing the thermal stability of PP. The PP nanocomposite degradation temperatures continued to rise gently until 2 wt%, while no further effects were visible by 4wt%. This may suggest that after 2 wt% the GO is well dispersed and further GO addition leads to poor dispersion [9].

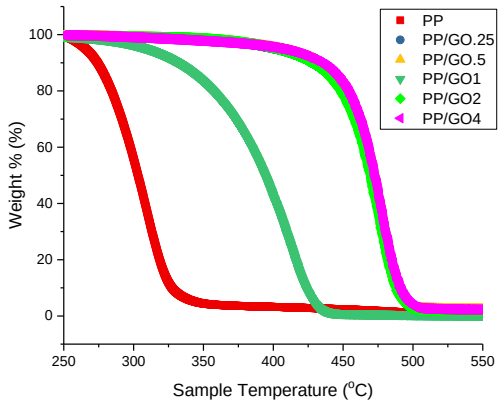

Figure 5. 21. TGA curves of PP nanocomposites.

Specimens ID	T_{onset} (°C)	$T_{50\%}$ (°C)	$T_{95\%}$(°C)
PP	276±3	303±3	344±3
PP/GO.25	440±3	472±3	494±3
PP/GO.5	452±3	473±3	496±3
PP/GO1	409±3	443±3	481±3
PP/GO2	445±3	470±3	494±3
PP/GO4	453±3	473±3	497±3

Table 5. 13. Thermal degradation temperatures of PP /GO nanocomposites.

With regard to the TGA curves for the PB and the PB/GO nanocomposites in Figure 5.22, The GO-containing sample shows enhanced thermal stability compared with PB, which is arguably due to improved adhesion and miscibility between the two incompatible polymers in the presence of GO. The surface chemistry of GO plays a key role in its compatibilizing effect for immiscible blends through favourable interactions, such as π-π stacking and hydrogen bonding [39]. The initial decomposition temperature increased significantly, by around 132±3 °C and 199±3 °C just by addition of 0.25wt% and 0.5wt% of GO respectively, with further slight increases at 1 wt% and 2 wt%. The 4 wt% nanocomposite yielded the maximum observed value of $T_{95\%}$ when compared with neat PB.

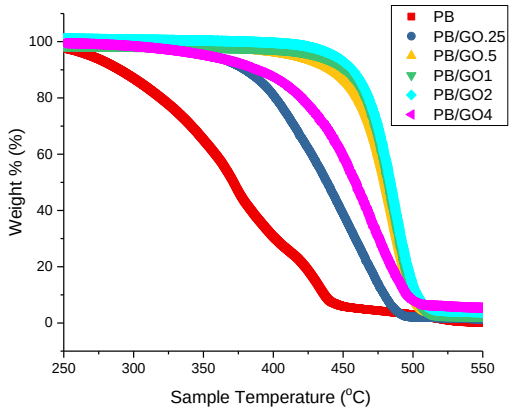

Figure 5.22. TGA curves of PB nanocomposites.

Specimens ID	T_{onset} (°C)	$T_{50\%}$ (°C)	$T_{95\%}$(°C)
PB	257±3	372±3	463±3
PB/GO.25	389±3	439±3	487±3
PB/GO.5	456±3	480±3	506±3
PB/GO1	463±3	482±3	482±3
PB/GO2	462±3	484±3	513±3
PB/GO4	418±3	459±3	583±3

Table 5.14. Thermal degradation temperatures of PB /GO nanocomposites.

The effect of GO upon blends treated with compatibilizer, shown in Figure 5.25 and Table 5.15, appears similar to the untreated blends, but the effect was less pronounced than in the PB nanocomposites group. That is clear when we compare the initial decomposition temperatures of PB (257±3°C) and PBC (407±3 °C). The addition of 0.25 wt% and 0.5 wt% of GO, enhanced T_{onset} to 447±3 °C and 455±3 °C respectively, while gently increasing as GO concentration was further increased. PBC already has increased thermal stability due to the improvements in PE/PP miscibility and adhesion resulting from the presence of PE-co-GMA, which may explain why the impact of GO is less than for blends without the compatibiliser.

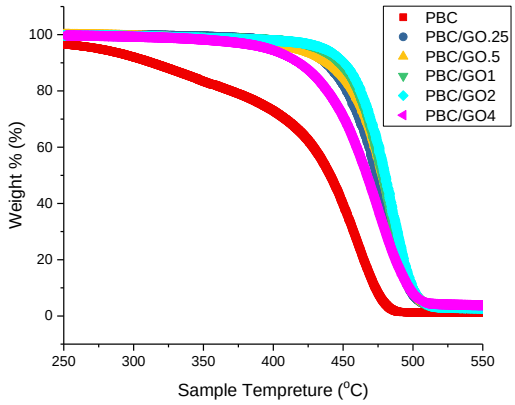

Figure 5.23. TGA curves of PBC nanocomposites.

Specimens ID	T_{onset} (°C)	$T_{50\%}$ (°C)	$T_{95\%}$(°C)
PBC	407±3	441±3	479±3
PBC /GO.25	447±3	474±3	505±3
PBC /GO.5	455±3	479±3	507±3
PBC /GO1	457±3	478±3	506±3
PBC /GO2	458±3	480±3	507±3
PBC /GO4	433±3	468±3	507±3

Table 5.15. Thermal degradation temperatures of PBC /GO nanocomposites.

5.4.7. Conductivity

Graphene has a quite high surface/mass ratio, and sp^2 bonded carbon atoms arranged in hexagonal 2D lattice give rise to one of the highest electron conductivities [8][42]. One of the unique features of graphene is high mobility of the charge carrier (20 m^2 V^{-1} s^{-1}) [39]. Graphene conductivity arises from its sp^2 aromatic structure where the π-π bonding electrons can move from one carbon atom to another (conducting electricity). However, the electrical conductivity investigation demonstrates that graphene oxide doesn't provide any electrical conductivity; it is an insulator. Figure 5.26 shows I-V characteristic curves of graphene/polymer with 2wt% (the rest of samples present similar behaviour). Graphene oxide is an insulator owing to oxidation, this is due to the reaction between the oxygenated groups with carbon atoms in the graphene structure during the oxidization of the graphite. GO contains small amounts of hydroxyl, epoxy, and carboxylic groups on its surface. By using solid state nuclear magnetic resonance (NMR) spectroscopy to probe the samples, Lerf et al.(1998)[43] were able to suggest a nonstoichiometric form, containing hydroxyl and epoxy functional groups and some

carbonyl groups (carboxyl, carbonyl, ester) along the graphite oxide sheet edge. Oxidization leads to the disruption of the sp^2 . A large fraction of the graphene atoms are converted from sp^2 to sp^3 to attach to oxygen and the aromatic structure is lost in many regions on the graphene skeleton as GO contains significant amount of oxygen to the lack of sufficient π-π conjugation. On the other hand, in the studies of the pristine graphene oxidation, it has been revealed that the insertion of functional groups and lattice defects provides advantages such as increased bonding to polymers and catalytic activity, at the same time decreases the electron mobility and can induce semiconducting behaviour [44].

Depending on the preparation technique and the resulting of the reduction degree, whole graphene materials derivatives can be fabricated with a wide range of chemical, physical and engineering properties. A single layer of GO has a carbon to oxygen ratio (C/O) x is ~3.95. Values of $x<1.5$ have been reported in a small number of studies and theoretical evidence exists that materials with such low C/O ratio are thermodynamically stable. However, large degrees of oxidation may not be possible in the Hummers' method due to kinetic limitations. After reduction GO becomes conductive through restoration of π-π bonding or sp^2 hybridization due to removal of oxygen functionalities. Punckt et al. (2013) [45] reported the smallest ratio of (C/O) to obtain electrical conductivity again is 7.3 ± 0.1, and lower that the GO is still an insulator [46].

However, conductivity of Graphene oxide depends on many factors such as degree of graphite exfoliation, number of layers, surface oxygen functional groups and especially impurity level. If there is any acidic impurity present, graphene oxide can show very unusual behaviour due to the moisture absorbing property of the trace acidic phase (remaining sulphur content or chloride counterpart) from the final rinsing of graphene oxide dispersion by hydrochloric acid (HCl).

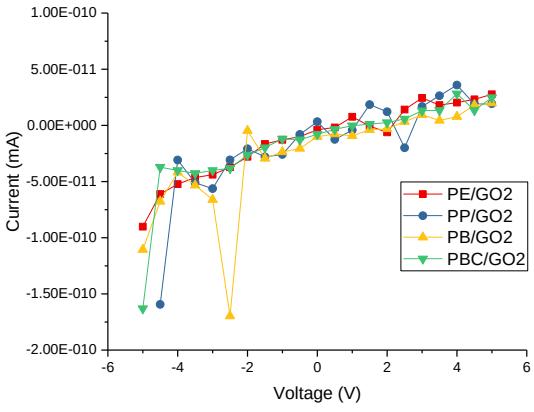

Figure 5.24. The I-V characteristic curves, defines the resistive the graphene/polymer nanocomposites.

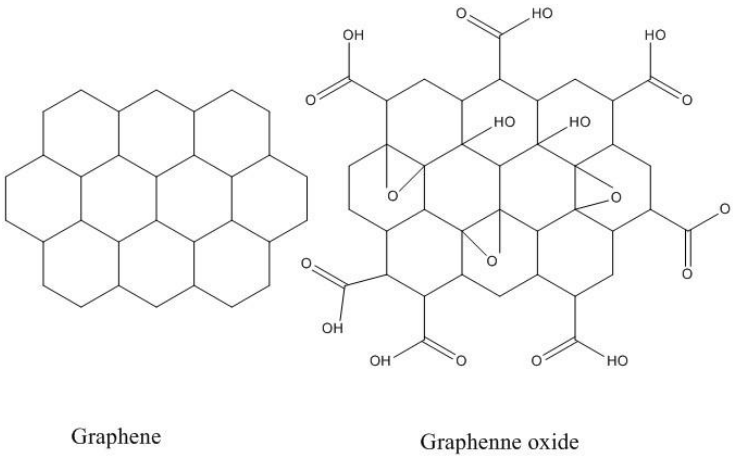

Figure 5.25. Molecular structure of graphene and graphene oxide [10].

5.4.8. Mechanical Properties

The influence of GO on the elastic modulus and ultimate tensile strength of GO/ polymer nanocomposites are shown in Figure 5.28 and Table 5.16. The data show a slight decrease in the tensile strength of the nanocomposites in comparison to the PE. A decrease in the tensile strength in PE is due a decrease in the molecular mobility meaning that the molecules are unable to dissipate energy as mechanical energy. Above 1wt% GO, the tensile strength then begins to increase with further increasing GO concentration at the higher loadings, although remains the same as the neat material within experimental error. The elastic modulus decreased with the addition of GO until 1 wt% and then increased with higher graphene content. Other groups have studied the crystallisation behaviour in order to explain non-monotonic changes in mechanical properties with GO concentration [41].

Specimens ID	Elastic modulus (MPa)	Ultimate tensile strength (MPa)
PE	38±6	17±2
PE/GO.25	32±3	8±5
PE/GO.5	26±7	9 ±6
PE/GO1	25±2	12±4
PE/GO2	34±1	14 ±7
PE/GO4	43±5	16 ±10

Table 5.16. The elastic modulus and the tensile strength at break of PE nanocomposites.

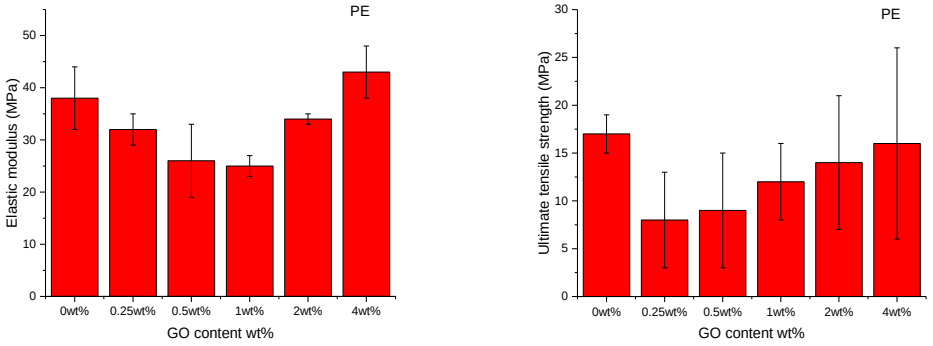

Figure 5.26. The elastic modulus and the tensile strength at break of PE nanocomposites

Table 5.17 and Figure 5.29 display the elastic modulus and the tensile strength at break of PP/GO nanocomposites. The mechanical properties of PP/GO nanocomposites are quite correlated with the material type, amount, fillers dispersion, and the exfoliation of fillers into polymer matrix layers. A strong influence of the GO addition level on the mechanical properties was observed. The tensile strength and tensile modulus of the PP/GO nanocomposite samples were much lower than the mechanical properties of pure PP [47] [48].

Specimens ID	Elastic modulus (MPa)	Ultimate tensile strength (MPa)
PP	884±51	34±1
PP/GO.25	29±1	7±1
PP/GO.5	60±27	17±6
PP/GO1	43±5	8±4
PP/GO2	52±5	12±6
PP/GO4	52±5	11±6

Table 5.17. The elastic modulus and the tensile strength at break of PP nanocomposites.

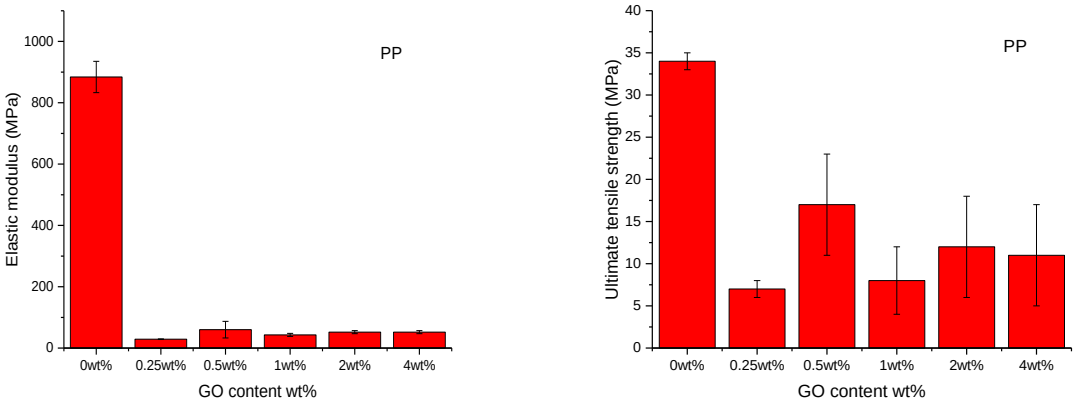

Figure 5.27. the elastic modulus and the tensile strength at break of PP nanocomposites.

The tensile tests of PB/GO nanocomposites, summarised in Table 5.18 and Figure 5.30, show that the addition of GO improved the tensile strength, with a rise from 5 MPa in neat polymer blend to 16 MPa in PB/G.25 with just 0.25wt% of graphene oxide, with the largest effect happening for a very small addition of GO. This may be because of the compatibilizing effect of graphene oxide (GO) in the immiscible polymer blend, reducing the interfacial energy between the component polymers. The interfacial interaction, which depends on the GO surface chemistry and the polymers functionality [49], determines the dispersion degree of GO into the polymer blends, interfacial adhesion strength and reinforcement efficiency. It should be noted that the oxygen functional groups on GO also prefer the employment of these carbon nanostructures in polymer blends because they can reinforce the interfacial interaction between GO and polymer [50]. Overall, the thermodynamic work of adhesion (W_a) of many polymers with GO increases with increases in the polymer polarity , suggesting a stronger interfacial interaction (F_{pg}), and as a result a higher interfacial strength forms in the more polar polymer based nanocomposites [51].

Specimens ID	Elastic modulus (MPa)	Ultimate tensile strength (MPa)
PB	322±41	5 ±1
PB/GO.25	86±15	16±7
PB/GO.5	61±15	17±7
PB/GO1	69±20	13±4
PB/GO2	58±19	13±4
PB/GO4	40±10	11±6

Table 5.18. The elastic modulus and the tensile strength at break of PB nanocomposites.

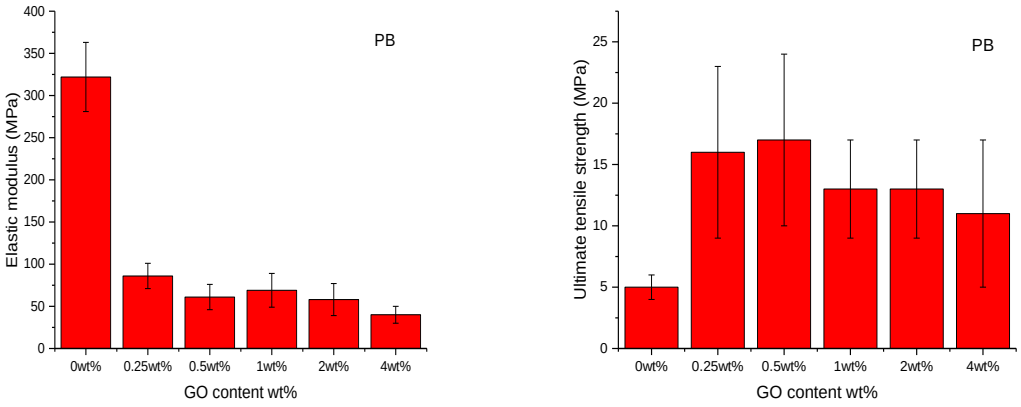

Figure 5.28. The elastic modulus and the tensile strength at break of PB nanocomposites

The PBC nanocomposites with 5wt% of PE-co-GMA, shown in Table 5.19 and Figure 5.31, show clearly improved tensile strength compared to the pure polymer blend from 5 MPa for PB to 12 MPa for PBC. The pure PBC blend exhibited greater enhancement in the mechanical properties than uncompatibilized blend (PB) [41]. However, in the PBC nanocomposites , no clear effect was seen on the tensile strength. This could indicate that the PE-co-GMA compatibilizer hinders graphene distribution and dispersion at smaller concentrations. This could result from the relatively low melt flow index of the PE-co-GMA (5.0 gm/10 min). At higher GO concentrations, this effect is overcome and the GO is able to impart an improvement on the mechanical properties [52].

Specimens ID	Elastic modulus (MPa)	Ultimate tensile strength (MPa)
PBC	277±45	12 ±3
PBC /GO.25	51±9	12±5
PBC /GO.5	66±6	12±6
PBC/GO1	52±19	13±6
PBC/GO2	70±14	15±7
PBC /GO4	74±17	14±6

Table 5.19. The elastic modulus and the tensile strength at break of PBC nanocomposites.

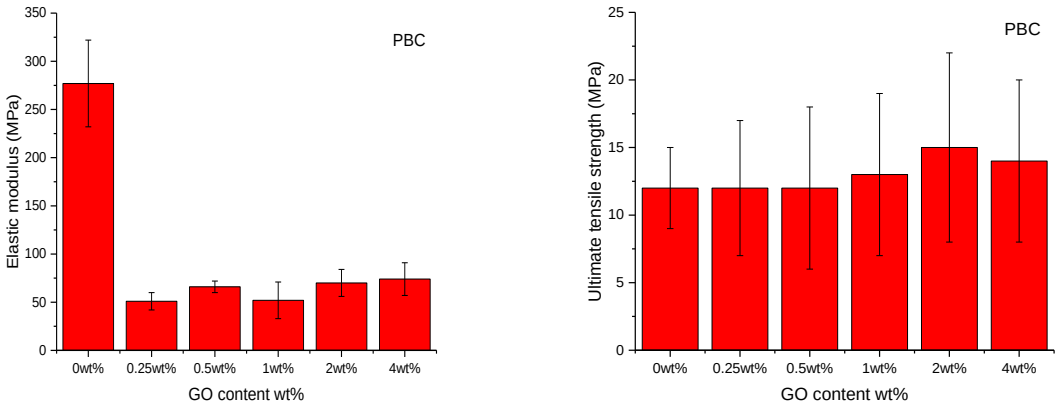

Figure 5.29. The elastic modulus and the tensile strength at break of PBC nanocomposite.

5.5. Summary and Conclusion

This study involves the preparation, characterization, properties and relation between them of the graphene oxide (GO) based on blend of metallocene linear low density polyethylene (PE) and homo polypropylene (PP). Wide- and Small angle X-ray scattering (WAXD and SAXS) have been applied to characterize the semicrystalline morphology of nanocomposites. The interlayer spacing (d spacing), and the lamellar thickness (L_p) increase by addition of the GO while the crystallite size (τ) is decreased. The Fourier transform infrared spectroscopy (FTIR) and Raman spectroscopy described chemical structure of nanocomposites and the I_D/I_G value was calculated as 0.285 in GO powder.

Electrical studies confirmed that GO, with conductivity far inferior to pristine graphene, did not improve the conductivity of the nanocomposites, and it is found that the graphene/ polymer oxide is a good insulator.

The thermal properties were investigated by Deferential Scanning Calorimetry (DSC) and Thermal Gravimetric Analysis (TGA), and showed that the addition of graphene oxide did not have a pronounced effect on the crystallization temperature of the nanocomposites, while thermal stability was significantly improved.

The GO act as compatibilizer between PE and PP and improved the tensile strength as measured by tensile test.

According to the high thermal stability and electrical isolation the graphene oxide based polyethylene/ polypropylene blend could have a potential application as a material for electrical insulation.

References

[1] Mahmood, H., Habib, A., Mujahid, M., Tanveer, M., Javed, S., & Jamil, A. (2014). Band gap reduction of titania thin films using graphene nanosheets. Materials Science in Semiconductor Processing, 24(1), 193–199.

[2] Feng, H., Cheng, R., Zhao, X., Duan, X., & Li, J. (2013). A low-temperature method to produce highly reduced graphene oxide. Nature Communications, 4, 1539.

[3] Graphene supermarket, United State, New York, 2009.

[4] Johnson, D. W., Dobson, B. P., & Coleman, K. S. (2015). A manufacturing perspective on graphene dispersions. Current Opinion in Colloid and Interface Science, 20(5-6), 367–382.

[5] Harris, D. (1998). Quantitative Chemical Analysis, 9th ed. Handbook of HPLC, Marcel Dekker, New York.

[6] Wu, J., Huang, G., Li, H., Wu, S., Liu, Y., & Zheng, J. (2013). Enhanced mechanical and gas barrier properties of rubber nanocomposites with surface functionalized graphene oxide at low content. Polymer (United Kingdom), *54*(7), 1930–1937.

[7] Kim, S., Do, I., & Drzal, L. T. (2009). Multifunctional xGnP/LLDPE nanocomposites prepared by solution compounding using various screw rotating systems. Macromolecular Materials and Engineering, 294(3), 196–205.

[8]Layek, R. K., Samanta, S., & Nandi, A. K. (2012). The physical properties of sulfonated graphene/poly(vinyl alcohol) composites. Carbon, 50(3), 815–827.

[9] Milani, M. A., Gonzalez, D., Quijada, R., Basso, N. R. S., Cerrada, M. L., Azambuja, D. S., & Galland, G. B. (2013). Polypropylene/graphene nanosheet nanocomposites by in situ polymerization: Synthesis, characterization and fundamental properties. Composites Science and Technology, 84, 1–7.

[10] Abdullah, S. I., & Ansari, M. N. M. (2015). Mechanical properties of graphene oxide (GO)/epoxy composites. HBRC Journal, 11(2), 151–156.

[11] Bhawal, P., Ganguly, S., Chaki, T. K., & Das, N. C. (2016). Synthesis and characterization of graphene oxide filled ethylene methyl acrylate hybrid nanocomposites. RSC Advances, 6(25), 20781–20790.

[12]Potts, J. R., Dreyer, D. R., Bielawski, C. W., & Ruoff, R. S. (2011). Graphene-based polymer nanocomposites. Polymer, 52(1), 5–25.

[13] Goderis, B., Reynaers, H., Koch, M. H. I., & Mathot, V. B. F. (1999). Use of SAXS and linear correlation functions for the determination of the crystallinity and morphology of semi-crystalline polymers. Application to linear polyethylene. J. Polym. Sci., Part B: Polym. Phys., 37(14), 1715–1738.

[14] Fatnassi, M., Larbi, F. B. C., & Halary, J. L. (2010). Quantitative analysis of semicrystalline blends SAXS data: Theoretical modeling versus linear correlation function. International Journal of Polymer Science, 2010.

[15]Chandra, R., & Rustgi, R. (1997). Biodegradation of maleated linear low-density polyethylene and starch blends. Polymer Degradation and Stability, 56(2), 185–202.
[16] Sarker, M., Rashid, M. M., & Molla, M. (2011). Abundant High-Density Polyethylene (HDPE-2) Turns into Fuel by Using of HZSM-5 Catalyst. Journal of Fundamentals of Renewable Energy and Applications, 1(November), 12.
[17] Rjeb, A., Tajounte, L., Chafik El Idrissi, M., Letarte, S., Adnot, A., Roy, D., & Kaloustian, J. (2000). IR spectroscopy study of polypropylene natural aging. Journal of Applied Polymer Science, 77(8), 1742–1748.
[18] Lin,J., Pan, Y., Liu,C., Huang,C., Hsieh,C., Chen,C., Lin,Z., & Lou,C.(2015). Preparation and Compatibility Evaluation of Polypropylene/High Density Polyethylene Polyblends. Materials, 8, 8850–8859.
[19]Rattana, T., Chaiyakun, S., Witit-Anun, N., Nuntawong, N., Chindaudom, P., Oaew, S., & Limsuwan, P. (2012). Preparation and characterization of graphene oxide nanosheets. Procedia Engineering, 32, 759–764.
[20] Drewniak, S., Muzyka, R., Stolarczyk, A., Pustelny, T., Kotyczka-Morańska, M., & Setkiewicz, M. (2015). Studies of Reduced Graphene Oxide and Graphite Oxide in the Aspect of Their Possible Application in Gas Sensors. Sensors (Basel, Switzerland), 16(1), 103.
[21] Khenfouch, M. (2012). Morphological, Vibrational and Thermal Properties of Confined Graphene Nanosheets in an Individual Polymeric Nanochannel by Electrospinning. Graphene, 01(02), 15–20.
[22]Zavgorodnev, Y. V, Sagitova, E. A., Nikolaeva, G. Y., Prokhorov, K. A., Pashinin, P. P., Novokshonova, L. A., Antipov, E. M. (n.d.). RAMAN STRUCTURAL STUDY OF OLEFIN BLENDS.
[23]Bulkin, B. J. (1978). Raman Spectra of. Applications of Polymer Spectroscopy, 3(c), 121–133.
[24]Liço, E., Marku, J., & Chatzhitheodoridis, E. (2014). Physico-mechanical properties changes in virgin and recycled polyethylene fibers during recycling process, 55, 373–377.
[25]Sato, H., Shimoyama, M., Kamiya, T., Amari, T., Aic, S., Ninomiya, T., Ozaki, Y. (2002). Raman spectra of high-density, low-density, and linear low-density polyethylene pellets and prediction of their physical properties by multivariate data analysis. Journal of Applied Polymer Science, 86(2), 443–448.
[26]De Castro, K. C., Sowek, A. B., Pinheiro, L. A., Pessan, L. A., & Canevarolo, S. V. (2014). Development and characterization of post-consumer rubber tire powder, high density polyethylene and ethylene-octene-1 copolymer ternary mixtures. Polimeros, 24(6), 654–660.
[27]Carniato, F., Fina, A., Tabuani, D., & Boccaleri, E. (2008). Polypropylene containing Ti- and Al-polyhedral oligomeric silsesquioxanes: crystallization process and thermal properties. Nanotechnology, 19(47), 475701.

[28]Nielsen, A. S., Batchelder, D. N., & Pyrz, R. (2002). Estimation of crystallinity of isotactic polypropylene using Raman spectroscopy. Polymer, 43(9), 2671–2676.
[29]Shemouratov, Y. V., Prokhorov, K. A., Sagitova, E. A., Nikolaeva, G. Y., Pashinin, P. P., Lebedev, Y. A., & Antipov, E. M. (2009). Raman study of polyethylene-polypropylene blends. Laser Physics, 19(12), 2179–2183.
[30]Tomba, J. P., Mana, C. D., Perez, C. J., Desimone, P. M., & Galland, G. B. (2016). Microstructural characterization of semicrystalline copolymers by Raman spectroscopy. Polymer Testing, 52(April), 71–78.
[31]Furukawa, T., Sato, H., Kita, Y., Matsukawa, K., Yamaguchi, H., Ochiai, S., Ozaki, Y. (2006). Molecular Structure, Crystallinity and Morphology of Polyethylene/Polypropylene Blends Studied by Raman Mapping, Scanning Electron Microscopy, Wide Angle X-Ray Diffraction, and Differential Scanning Calorimetry. Polymer Journal, 38(11), 1127–1136.
[32]Liebscher, M., Blais, M. O., Pötschke, P., & Heinrich, G. (2013). A morphological study on the dispersion and selective localization behavior of graphene nanoplatelets in immiscible polymer blends of PC and SAN. Polymer (United Kingdom), 54(21), 5875–5882.
[33]Eigler, S., Dotzer, C., & Hirsch, A. (2012). Visualization of defect densities in reduced graphene oxide. Carbon, 50(10), 3666–3673.
[34]Zhou, S., & Bongiorno, A. (2013). Origin of the chemical and kinetic stability of graphene oxide. Scientific Reports, 3, 2484.
[35]Song, P., Cao, Z., Cai, Y., Zhao, L., Fang, Z., & Fu, S. (2011). Fabrication of exfoliated graphene-based polypropylene nanocomposites with enhanced mechanical and thermal properties. Polymer, 52(18), 4001–4010.
[36]Huang, G., Ni, Z., Chen, G., Pang, W., & Zhao, Y. (2016). Effects of gamma irradiation and accelerated aging on GO/UHMWPE nanocomposites. International Journal of Polymer Analysis and Characterization, 5341(April), 1–11.
[37]Ye, S., Cao, Y., Feng, J., & Wu, P. (2013). Temperature-dependent compatibilizing effect of graphene oxide as a compatibilizer for immiscible polymer blends. RSC Advances, 3(21), 7987.
[38] Thomas, H. R. (2015). The structure and reactivity of graphene oxide.
[39] Suñer, S., Joffe, R., Tipper, J. L., & Emami, N. (2015). Ultra high molecular weight polyethylene/graphene oxide nanocomposites: Thermal, mechanical and wettability characterisation. Composites Part B: Engineering, 78, 185–191.
[40]Noorunnisa Khanam, P., AlMaadeed, M. A., Ouederni, M., Mayoral, B., Hamilton, A., & Sun, D. (2016). Effect of two types of graphene nanoplatelets on the physico–mechanical properties of linear low–density polyethylene composites. Advanced Manufacturing: Polymer & Composites Science, 2(2), 67–73.

[41] De C. Fim, F., Basso, N. R. S., Graebin, A. P., Azambuja, D. S., & Galland, G. B. (2013). Thermal, electrical, and mechanical properties of polyethylene-graphene nanocomposites obtained by in situ polymerization. Journal of Applied Polymer Science, 128(5), 2630–2637.
[42] Kucinskis, G., Bajars, G., & Kleperis, J. (2013). Graphene in lithium ion battery cathode materials: A review. Journal of Power Sources, 240, 66–79.
[43] Lerf, A., He, H., Forster, M., & Klinowski, J. (1998). Structure of Graphite Oxide Revisited. Journal of Physical Chemistry B, 102(23), 4477–4482.
[44]Aref, A. H., Entezami, A. A., Erfan-Niya, H., & Zaminpayma, E. (2017). Thermophysical properties of paraffin-based electrically insulating nanofluids containing modified graphene oxide. Journal of Materials Science, 52(5), 2642–2660.
[45]Punckt, C., Muckel, F., Wolff, S., Aksay, I. A., Chavarin, C. A., Bacher, G., & Mertin, W. (2013). The effect of degree of reduction on the electrical properties of functionalized graphene sheets. Applied Physics Letters, 102(2), 1–6.
[46] Eda, G., Mattevi, C., Yamaguchi, H., Kim, H., & Chhowalla, M. (2009). Insulator to semimetal transition in graphene oxide. Journal of Physical Chemistry C, 113(35), 15768–15771.
[47]Huang, C.-L., Lou, C.-W., Liu, C.-F., Huang, C.-H., Song, X.-M., & Lin, J.-H. (2015). Polypropylene/Graphene and Polypropylene/Carbon Fiber Conductive Composites: Mechanical, Crystallization and Electromagnetic Properties. Applied Sciences, 5(4), 1196–1210.
[48] Chammingkwan, P., Matsushita, K., Taniike, T., & Terano, M. (2016). Enhancement in mechanical and electrical properties of polypropylene using graphene oxide grafted with end-functionalized polypropylene. Materials, 9(4).
[49]Wan, C., & Chen, B. (2012). Reinforcement and interphase of polymer/graphene oxide nanocomposites. Journal of Materials Chemistry, 22(8), 3637.
[50]Cao, Y., Feng, J., & Wu, P. (2012). Polypropylene-grafted graphene oxide sheets as multifunctional compatibilizers for polyolefin-based polymer blends. Journal of Materials Chemistry, 22(30), 14997.
[51]K. L. Johnson, K. Kendall and A. D. Roberts (1971) . Proceedings of the Royal Society of London. 324, 301–313.
[52] Chammingkwan, P., Matsushita, K., Taniike, T., & Terano, M. (2016). Enhancement in mechanical and electrical properties of polypropylene using graphene oxide grafted with end-functionalized polypropylene. Materials, 9(4).

Chapter 6

The Effect of Carbon/Oxygen Ratio upon Structure-Property Relationships in Graphene/ Polymer Nanocomposites

We noted some limitation of GO performance due to the oxygen functional group in previous chapter. To address that, in this chapter we reduced the oxygen functional group by using the reduced graphene oxide and the pristine graphene. Three different source of graphene were used and all show improved properties of the polyolefins after incorporation of graphene nanofillers. The effect of increase the C/O ratio study of GO, rGO and G blend with PE and PP prepared by solution blending is reported. The main methods, which were used in this part of the project, including the materials, results and discussion and the summary are outlined below.

6.1. Materials

The details of the polymer used are presented in chapter 4. The GO, rGO and G details are surmised in Table 6.1. The surface morphology was studied by SEM which is shown in Figures 6.1, 6.2 and 6.3. The SEM images reveals freestanding GO nanosheets, the edges of the GO sheets become crumpled, folded, and restacked, and the surface of GO display a soft carpet-like morphology, perhaps because of the presence of residual H_2O molecules and hydroxyl or carboxyl groups, a consequence of deformation through the process of exfoliation of graphite oxide into graphene oxide and restacking. Moreover, many various layers of aggregate, agglomerate and smashed graphene sheets connected with each other to form a continuous conducting network are seen. Figures 6.2 and 6.3 shown the SEM images of rGO and G respectively. In contrast to GO, the rGO and G displays clear rippled silk-like waves or a flaky, scale-like, layered structure, which are entangled with each other.

Graphene type	Graphene symbols	Colour	Flake size (microns)	Thickness (nm)	(C/O) ratio	Specific surface area m^2/g
Single layer graphene oxide	GO	Brown	0.5-5	1.1 ± 0.2	~3.95	~833
High Surface Area Reduced Graphene Oxide	rGO	Black	~3-5	~1	~10.5	~833
Graphene Nanopowder	G	Black	~10	~1.6	~38	~400 – 800

Table 6.1. Graphene materials details from supplier.

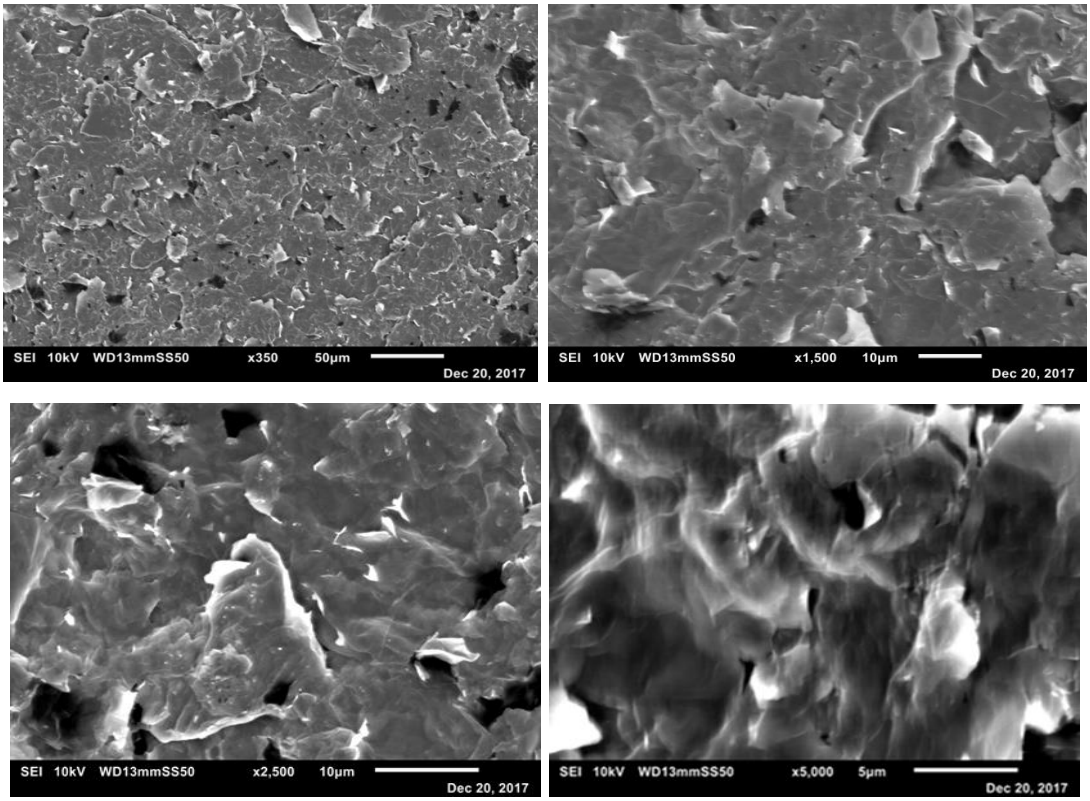

Figure 6.1. SEM image of GO at various level of magnification.

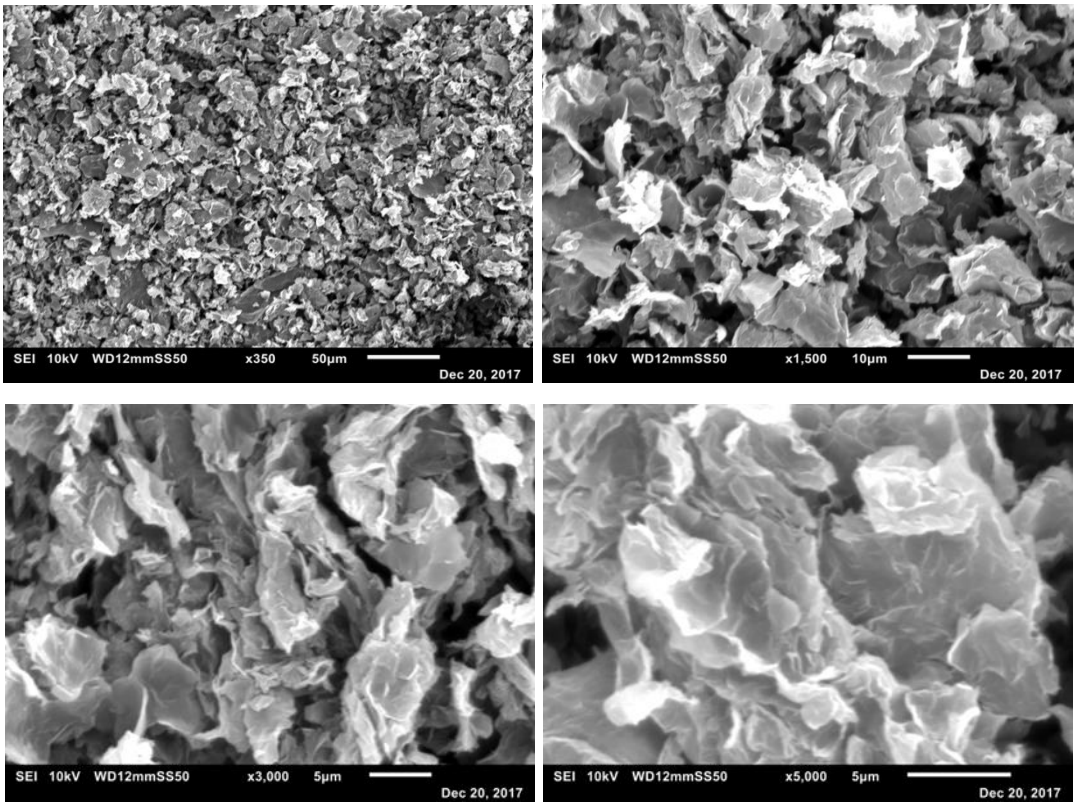

Figure 6.2. SEM image of rGO at various level of magnification.

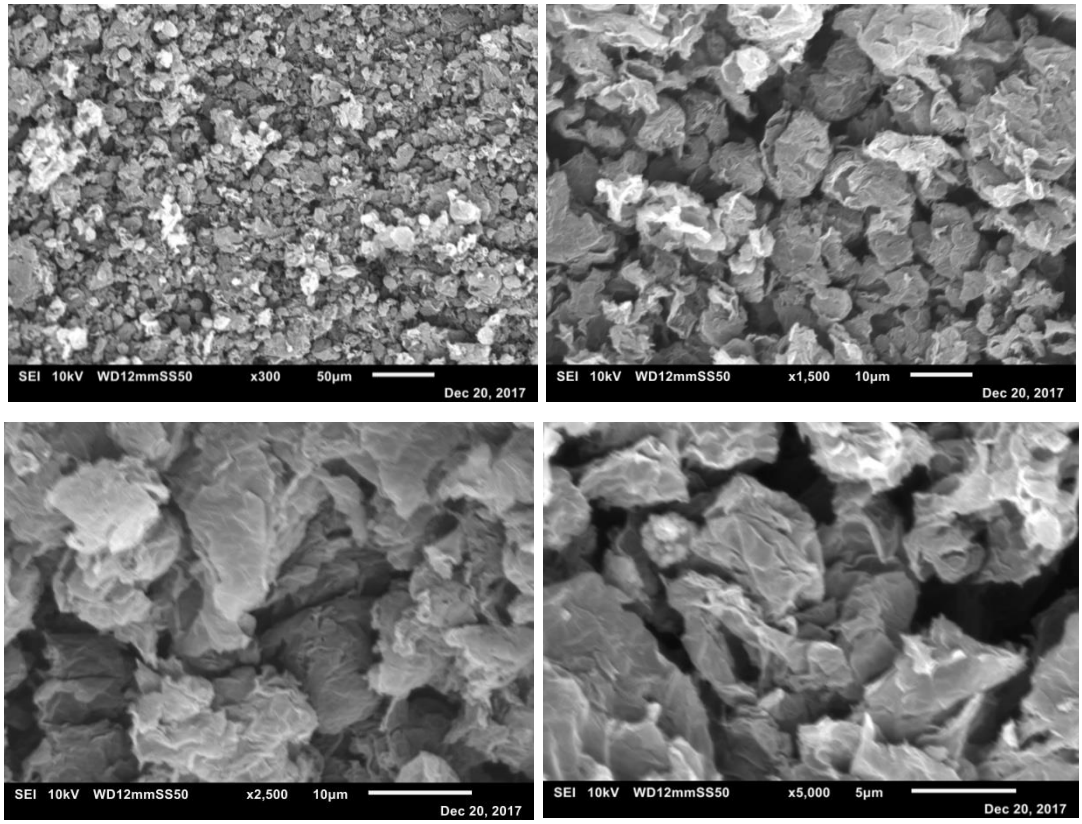

Figure 6.3. SEM image of G at various level of magnification.

6. 2. Polymer nanocomposite preparation

Figure 6.4 shows the volume difference of 10 mg of the three used types of graphene. The preparation of graphene (GO, rGO and G)/polymer nanosheets (Figure 6.5) were described in the previous chapter, with the weight percent and the absolute weight as indicated in Tables 6.2 and 6.3.

Figure 6.4. 10 mg of the GO, rGO and G.

Figure 6.5. The preparation steps of polymer/graphene nanocomposites.

Number	Sample ID	PE (wt%)	PP(wt%)	GO(wt%)	rGO(wt%)	G(wt%)	PE-co-GMA (wt%)
1	GO	0	0	100	0	0	0
2	rGO	0	0	0	100	0	0
3	G	0	0	0	0	100	0
4	PE/GO	100	0	2	0	0	0
5	PE/rGO	100	0	0	2	0	0
6	PE/G	100	0	0	0	2	0
7	PP/GO	0	100	2	0	0	0
8	PP/rGO	0	100	0	2	0	0
9	PP/G	0	100	0	0	2	0
10	PB/GO	50	50	2	0	0	0
11	PB/rGO	50	50	0	2	0	0
12	PB/G	50	50	0	0	2	0
13	PBC/GO	50	50	2	0	0	5
14	PBC/rGO	50	50	0	2	0	5
15	PBC/G	50	50	0	0	2	5

Table 6.2. Weight percent of polymers pellets, graphene and compatibilizer used in preparation of polymer /graphene nanocomposites.

Number	Sample ID	PE (g)	PP(g)	GO(g)	rGO (g)	G(g)	PE-co-GMA (g)
1	GO	0	0	0.02	0	0	0
2	rGO	0	0	0	0.02	0	0
3	G	0	0	0	0	0.02	0
4	PE/GO	2.0	0.0	0.040	0.00	0.00	0.0
5	PE/rGO	2.0	0.0	0.00	0.040	0.00	0.0
6	PE/G	2.0	0.0	0.00	0.00	0.040	0.0
7	PP/GO	0.0	2.0	0.040	0.00	0.00	0.0
8	PP/rGO	0.0	2.0	0.00	0.040	0.00	0.0
9	PP/G	0.0	2.0	0.00	0.00	0.040	0.0
10	PB/GO	1.0	1.0	0.040	0.00	0.00	0.0
11	PB/rGO	1.0	1.0	0.00	0.040	0.00	0.0
12	PB/G	1.0	1.0	0.00	0.00	0.040	0.0
13	PBC/GO	1.0	1.0	0.040	0.00	0.00	0.1
14	PBC/rG	1.0	1.0	0.00	0.040	0.00	0.1
15	PBC/G	1.0	1.0	0.00	0.00	0.040	0.1

Table 6.3. Weight of polymers pellets, graphene and compatibilizer used in preparation of polymer/graphene nanocomposites.

6.3. Results and Discussion

6. 3. 1. XPS results

X-ray photoelectron spectroscopy (XPS) was used to determine the carbon hybridization on the graphene surface. The full scan spectra of the pristine graphene, graphene oxide and reduced graphene oxide are shown in Figures 6.6, 6.7 and 6.8. The peaks at binding energy of 280 eV and 528 eV are ascribed to C1s and O1s. The O1s is ascribed to the adsorbed molecular oxygen on the surface of pristine graphene [1]. The O1s peak is negligible implying very low content, which in turn gives a very low O/C ratio. The C1s and O1s binding energies are approximately 283 eV to and 529 eV in GO and 281 eV and 529 eV in rGO respectively. The C/O ratio of G, rGO and GO are calculated and summarised in Table 6.4.

Figures 6.6, 6.7 and 6.8 show the de-convoluted XPS spectra for the C1s orbital of the G, GO and rGO. The binding energies of four components, such as 284 eV (C=C) , 285 eV (C-C), 286 eV (C–O) and 288 eV (C=O), provide evidence for the formation of sp^2 carbon, sp^3 carbon , hydroxyl and epoxy, and carbonyl functional groups respectively [2][3]. As shown in Figure 6.9, 6.10 and 6.11 only an obvious asymmetric sp^2 C1s peak at 283.49 eV can be detected in the XPS spectra of exfoliated graphene, indicating the high purity of all three graphene samples [4]. The core level high resolution O1s of G, rGO and GO are shown in Figures 6.12, 6.13 and 6.14. As would be expected, the graphene oxide shows a considerable increase in oxygen concentration. The oxygen high resolution spectra are consistent with predominantly (C-O) or (C-OH) type oxygens at approximately 533 eV and some(C=O) type oxygens at approximately 531 eV, while (C-O-C) at ~ 532 eV and (C-O-H) at ~ 531 eV in rGO. The core level high resolution O1s spectral peaks are significantly less intense compared to O1s spectral peaks of GO. This confirms that GO has been converted to rGO [5][6]. Just one single peak was observed to O1s in graphene (C=O) at ~ 531.52 eV, for the lack of that functional group.

Sample ID	C (at %)	O (at %)	C/O ratio
G	98.65±0.2	1.1±0.1	≈ 89.7
rGO	82.8±0.4	16.65±0.2	≈ 4.9
GO	67.35±2.1	30.65±1.2	≈2.2

Table 6.4. Atomic composition of carbon and oxygen, as well as the C/O ratios obtained from XPS analysis of G, rGO and GO.

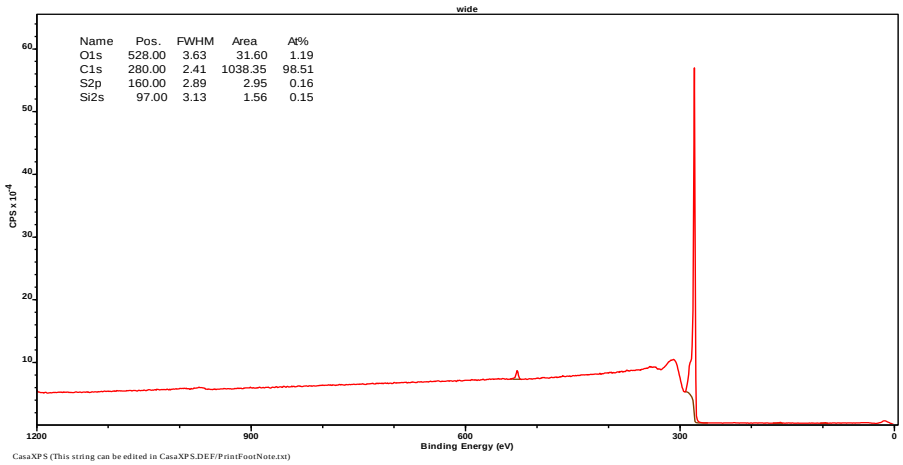

Figure 6.6. XPS survey scan of graphene.

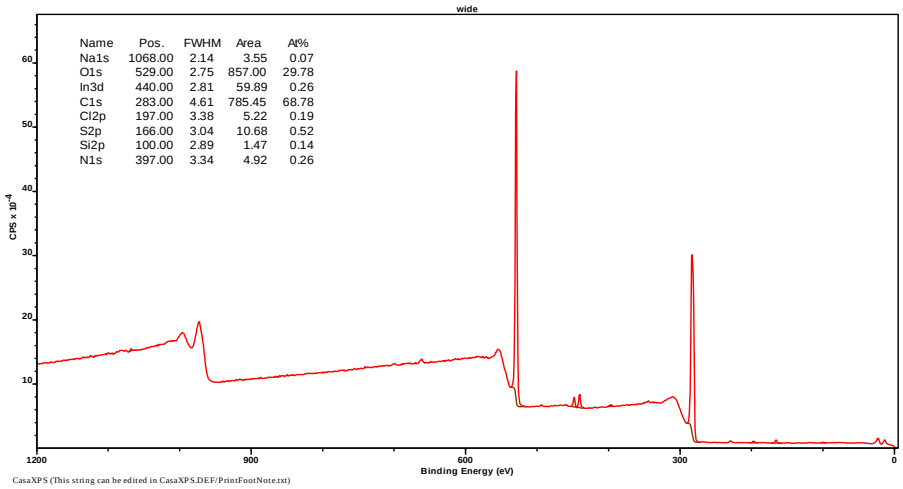

Figure 6.7. XPS survey scan of graphene oxide.

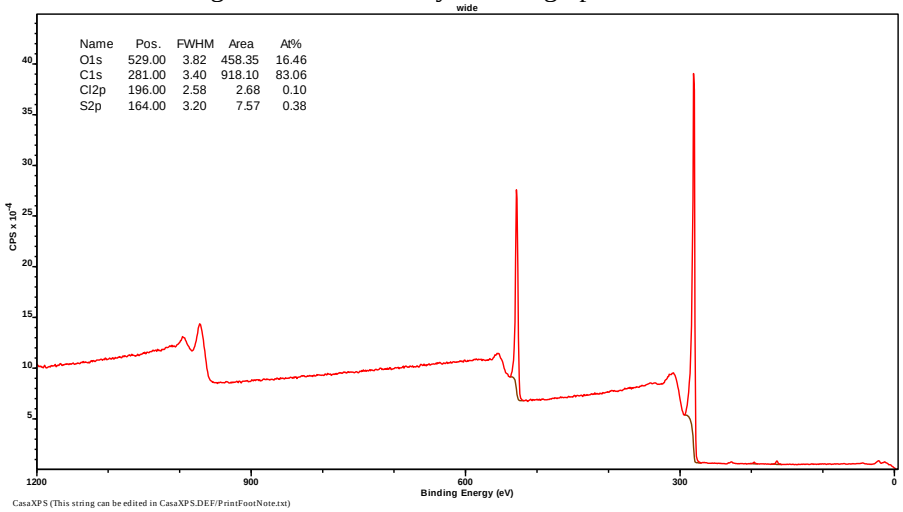

Figure 6.8. XPS Survey scan of reduced graphene oxide.

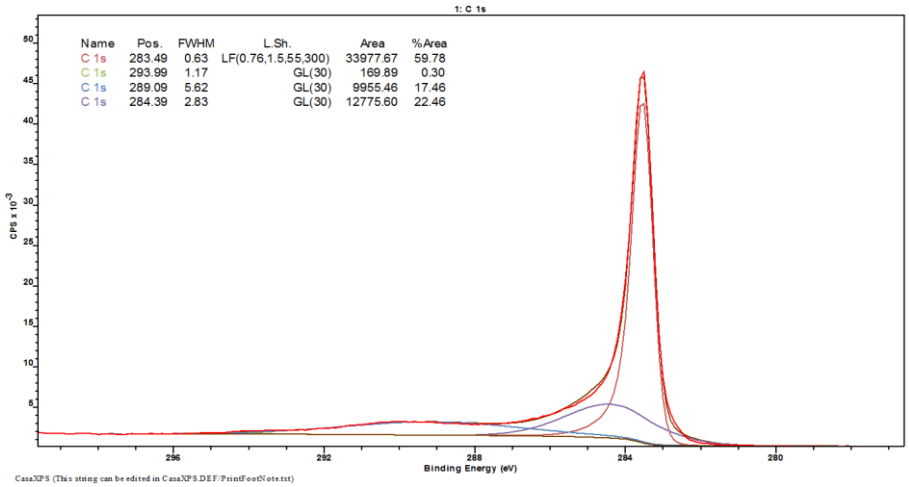

Figure 6.9. Deconvolution of C 1s scan core-level XPS spectra of the Graphene.

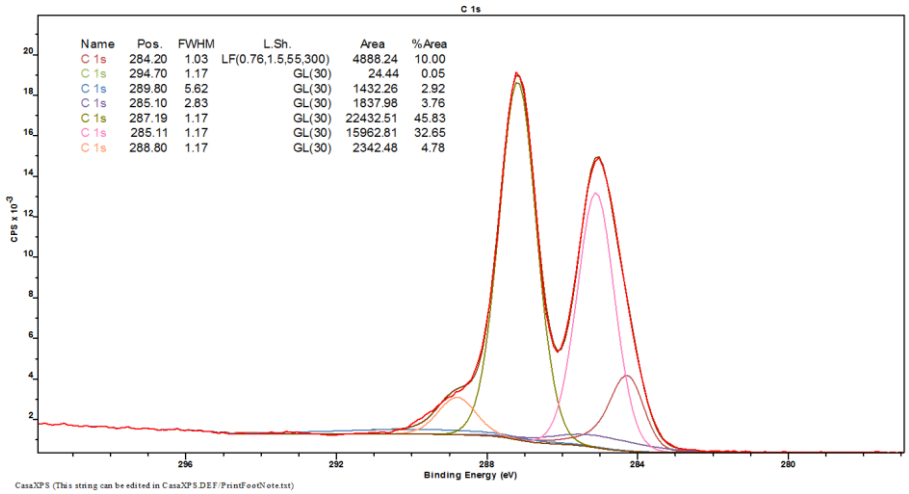

Figure 6.10. Deconvolution of C 1s scan core-level XPS spectra of the graphene oxide.

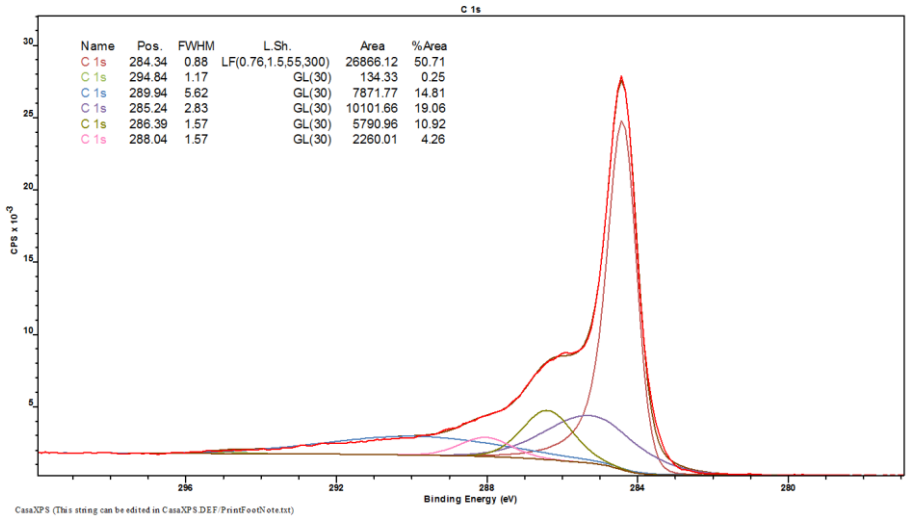

Figure 6.11. Deconvolution of C 1s scan core-level XPS spectra of the reduced graphene oxide.

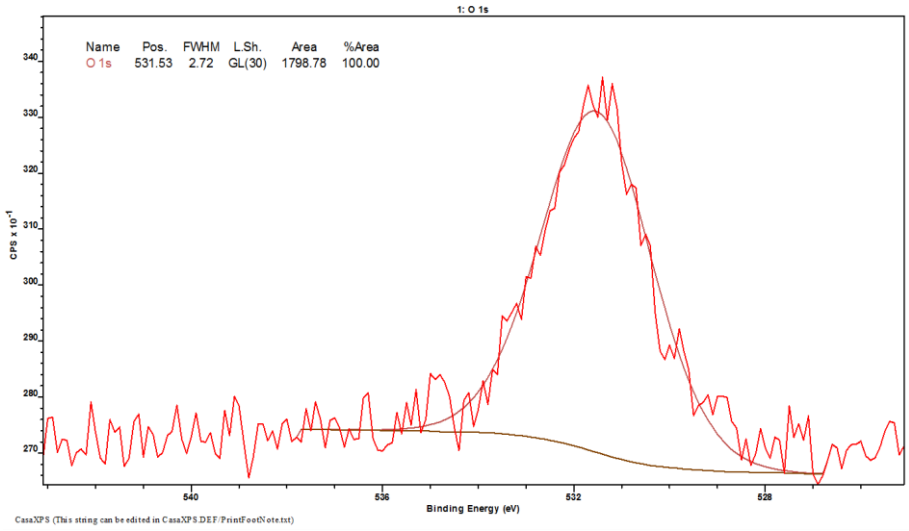

Figure 6.12. Deconvolution of O1s scan core-level XPS spectra of the graphene.

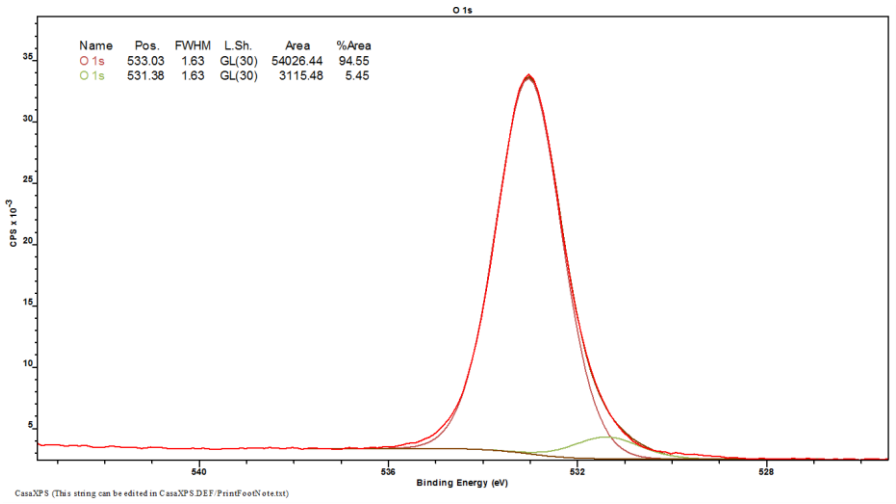

Figure 6.13. Deconvolution of O1s scan core-level XPS spectra of the graphene oxide.

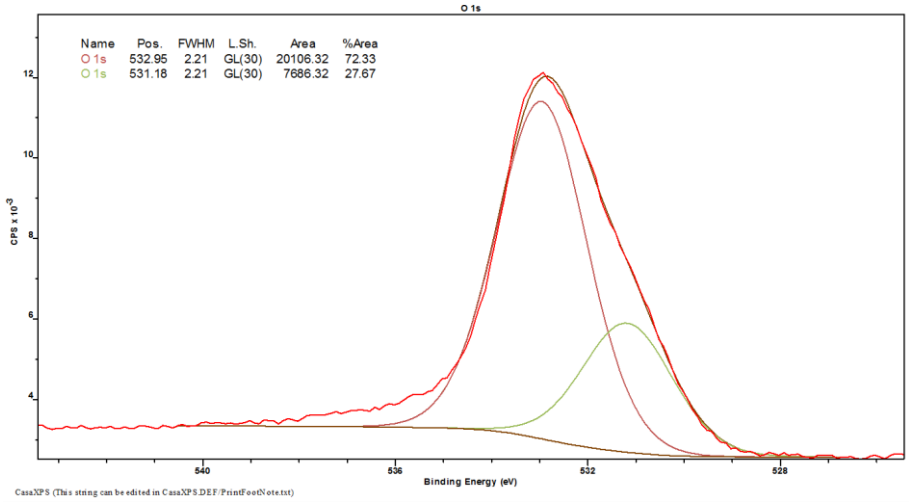

Figure 6.14. Deconvolution of O1s scan core-level XPS spectra of the reduced graphene oxide.

6.3.2. WAXD study

The effect of GO, rGO and G on the crystalline structure of the PE, PP, PB and PBC composite was determined using wide angle X-ray diffraction (WAXD), to determine the exfoliation of the GO, rGO and G platelets in the polymer host matrix. WAXD patterns, shown in Figure 6.15, present the diffraction peaks of the pure GO, rGO and G. The diffraction peak (2θ) around 10.8° corresponds to the reflection of GO, and the interlayer spacing of GO (8.17 Å) and rGO (8.09 Å) is much larger than that of pristine graphene (d≈3.48 Å) due to the presence of oxygen-containing functional groups such as hydroxyl, epoxy, and carboxyl groups on the surface of graphene sheet [7]. The peak at 23.7° is due to incomplete oxidation of graphene. The WAXD pattern of rGO exhibits peaks at 2θ≈10.9° and at 2θ≈ 24°, corresponding to reflection from (200) lattice planes, and 2θ ≈ 10.8° and 23.7° of GO reflection according (130) and (200) plane. The G sample, synthesized through thermal exfoliation and reduction of GO, does not show any sharp clear peaks, highlighting disorder and exfoliation. However, the broad and weak peak at 25.6°, relating to an interlayer spacing of d≈3.48 Å, is associated with graphitic (002) plane. The broadening of G peak, compared to the GO and rGO, points to a decrease in the crystalline size and/or a less ordered structure, the crystalline size calculated as 113.8, 66.3 and 42.6 Å for GO, rGO and G respectively . The d-spacing of GO, rGO and G were calculated as 8.17, 8.04 and 3.48 nm, respectively. The loss of the peak at 25.6° and the increase of the d-spacing from the original G suggests that the Van der Waals interaction between layers become weaker due to the insertion of oxygen-containing functional groups [8]. The disappearance of the GO, rGO and G peaks in all the polymer /GO, rGO and G (Figures 6.16, 6.17, 6.18 and 6.19) indicates the presence of exfoliated graphitic layers of GO, rGO or G. This indicates complete exfoliation of the graphene nanoparticle in the nanocomposites with low graphene contents (2wt%). For the higher graphene contents, the graphene peak indicates incomplete exfoliation [9] [4]. The effect of GO, rGO and G are similar, and all decrease the crystallite size of the polymer nanocomposites with similar ratio (Tables 6.5, 6.7, 6.9 and 6.11). Tables 6.6, 6.8, 6.10 and 6.12 shown the intensity and the internal spacing of the polymer / GO and polymer / rGO nanocomposites are higher than the G/polymer nanocomposites which is higher than the pure polymer.

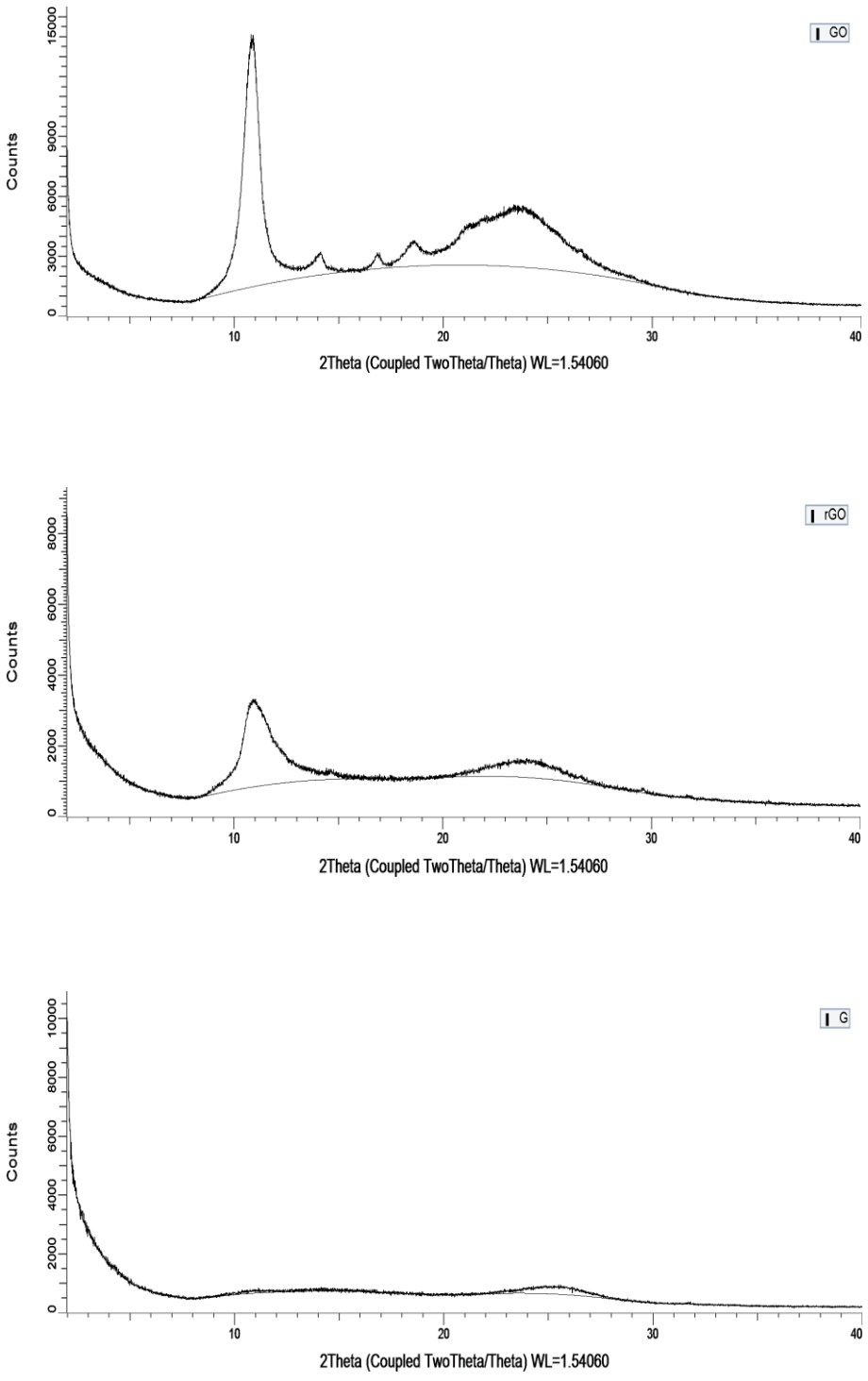

Figure 6.15.the WAXD pattern of the pure GO, rGO and G.

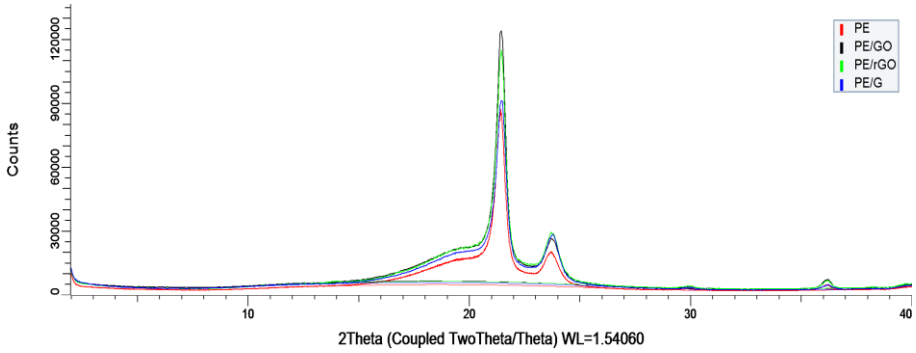

Figure 6.16. The WAXD curves patterns of the PE/graphene nanocomposites.

2θ	21.4°		23.7°		36.2°	
Sample ID	FWHM	τ (Å)	FWHM	τ (Å)	FWHM	τ (Å)
PE	0.437	205.5	0.536	168.1	0.390	238.1
PE/GO	0.453	198.5	0.552	163.5	0.418	222.3
PE/rGO	0.449	200.2	0.542	166.5	0.381	243.9
PE/G	0.481	187.0	0.572	157.6	0.477	194.5

Table 6.5. The FWHM values of the PE /graphene of reflection peaks in WAXD data and crystallite size.

The interlayer spacing d(Å)				
2θ	PE	PE/GO	PE/rGO	PE/G
21.4°	4.14	4.15	4.15	4.15
23.7°	3.74	3.75	3.75	3.75
36.2°	2.48	2.49	2.49	2.49

Table 6.6. The interlayer spacing of the PE /graphene nanocomposites.

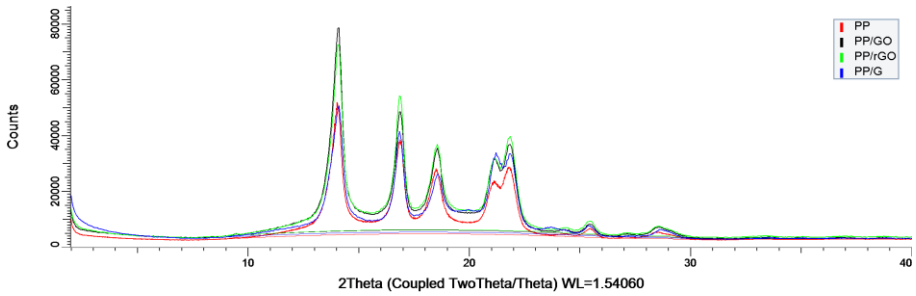

Figure 6.17. The WAXD curves patterns of the PP/graphene nanocomposites.

2θ	14°		16.8°		18.5°		21.1°	
Sample ID	FWHM	τ (Å)	FWHM	τ (Å)	FWHM	τ (Å)	FWHM	τ (Å)
PP	0.397	224.0	0.370	241.5	0.456	196.2	1.195	75.2
PP/GO	0.506	175.8	0.415	215.2	0.471	189.8	1.197	75.1
PP/rGO	0.493	233.1	0.370	241.3	0.486	184.1	1.166	77.1
PP/G	0.539	165.1	0.399	223.7	0.461	194.0	1.173	76.7

Table 6.7. The FWHM values of the PP /graphene of reflection peaks in WAXD data and crystallite size.

The interlayer spacing d(Å)				
2θ	PP	PP/GO	PP/rGO	PP/G
14°	6.28	6.29	6.29	6.29
16.9°	5.24	5.25	5.25	5.25
18.6°	4.78	4.79	4.79	4.79
21.9°	4.05	4.07	4.07	4.06

Table 6.8. The interlayer spacing of the PP /graphene nanocomposites.

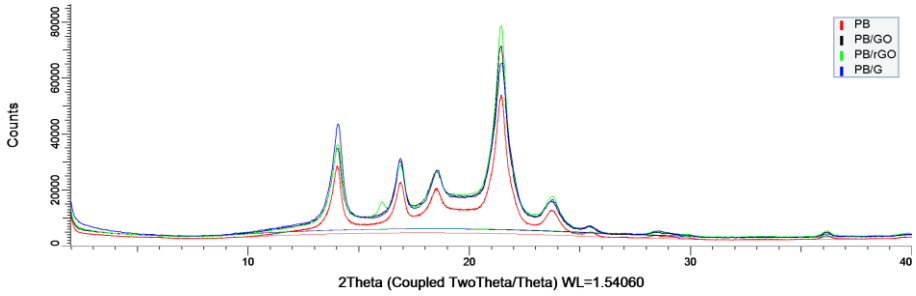

Figure 6.18. The WAXD curves patterns of the PB/graphene nanocomposites.

2θ	14°		16.8°		18.5°		21.4°		23.7°	
Sample ID	FWHM	τ (Å)	FWHM	τ (Å)	FWHM	τ (Å)	FWHM	τ (Å)	FWHM	τ (Å)
PB	0.351	253.7	0.329	271.5	0.404	221.2	0.486	185.0	0.489	184.3
PB/GO	0.469	189.5	0.412	216.6	0.506	176.9	0.557	161.2	0.556	162.2
PB/rGO	0.477	186.6	0.413	241.3	0.455	196.6	0.541	166.1	0.518	174.2
PB/G	0.494	165.1	0.413	216.1	0.461	194.0	1.173	76.7	0.553	163.2

Table 6.9. The FWHM values of the PB /graphene of reflection peaks in WAXD data and crystallite size.

The interlayer spacing d (Å)				
2θ	PB	PB/GO	PB/rGO	PB/G
14°	6.29	6.30	6.30	6.30
16.8°	5.24	5.25	5.25	5.25
18.5°	4.78	5.25	4.79	4.79
21.4°	4.13	4.14	4.14	4.14
23.7°	3.74	3.75	3.75	3.75

Table 6.10. The interlayer spacing of the PB /graphene nanocomposites.

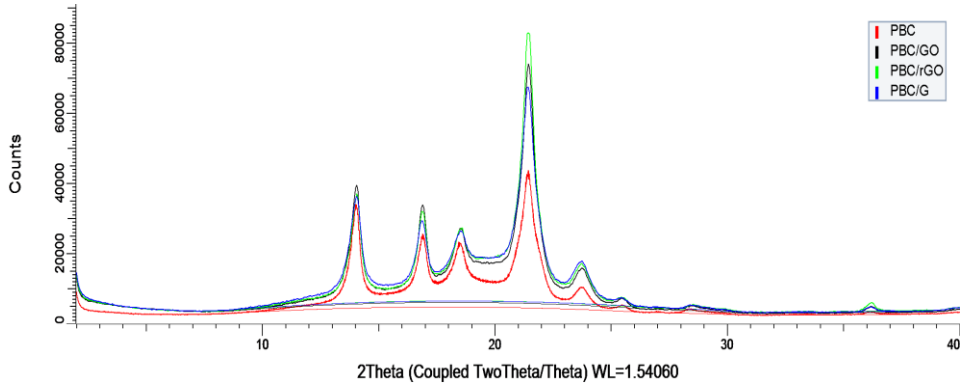

Figure 6.19. The WAXD curves patterns of the PBC/graphene nanocomposites.

2θ	14°		16.8°		18.5°		21.4°		23.7°	
Sample ID	FWHM	τ (Å)	FWHM	τ (Å)	FWHM	τ (Å)	FWHM	τ (Å)	FWHM	τ (Å)
PBC	0.369	241.1	0.370	241.3	0.438	209.5	0.516	174.1	0.465	193.8
PBC/GO	0.443	200.6	0.395	225.8	0.464	192.8	0.551	162.9	0.511	176.6
PBC/rGO	0.458	194.3	0.397	224.6	0.436	205.0	0.539	166.7	0.527	171.1
PBC/G	0.494	165.1	0.413	216.1	0.461	194.0	1.173	76.7	0.553	163.2

Table 6.11. The FWHM values of the PBC /graphene of reflection peaks in WAXD data and crystallite size.

The interlayer spacing d(Å)				
2θ	PBC	PBC/GO	PBC/rGO	PBC/G
14°	6.29	6.30	6.30	6.30
16.8°	5.23	5.24	5.25	5.26
18.5°	4.78	4.79	4.79	4.79
21.4°	4.14	4.15	4.15	4.15
23.7°	3.74	3.75	3.75	3.75

Table 6.12. The interlayer spacing of the PBC /graphene nanocomposites.

6.3.3. Raman spectroscopy

The most prominent and most important of the GO Raman spectra are the D, G, 2D and D + D' peaks shown in Figure 6.20. The D peak at about 1351.33 cm^{-1} originates from the breathing modes of six-membered rings that are activated by defects, and the G peak at ~ 1582cm^{-1} arises from the first-order scattering of the E_{2g} mode (see Figure 6.21)[10]. The 2D peak at ~2658 cm^{-1} is the second order of the D peak and the D + D' peak at ~ 2925cm^{-1} is due to the defect activated combination of phonons. The D/G ratio is the measure of the disorder in graphene, which is influenced by edges, charge puddles, ripples, or many other defects. The I_D/I_G ratio in Raman spectroscopy can be used to evaluate the distance between defects in graphene and GO, and increases with increasing mean distance between two defects (L_D) [11][12]. We used this relation to characterize GO, rGO and G. After reduction reaction, the D/G intensity ratio (I_D/I_G) of graphene rises from 0.285 to 1.137 to 1.726 respectively as shown in Table 6.13. This increase is a consequence of forming of new graphitic regions that are numerous in number and smaller in size with respect to the ones present in graphene oxide. [13]. The D + D' peak is higher in intensity than the 2D peak, in both the spectra of GO and rGO shown in Figures 6. 22 and 6. 23. That change is due to the removal of functional groups and formation of defects. This observation is consistent with the literature [11]. The Raman spectra of rGO nanosheets contain a strong band at ~1585 cm^{-1} (G band) and a weak band at ~1354 cm^{-1} (D

band). The G and D bands are attributed to the first-order scattering from the E_{2g} phonon of sp^2 carbon bonding and structural defects (disorder-induced modes), respectively [14]. The 2D band in rGO is substantially lower and wider than G band, suggesting the presence of multi-layered graphene derivatives. For the GO sample one can notice that the relative intensity ratio between D and G peaks is smaller than for rGO and G, suggesting lower disorder GO. However, it should be mentioned, that C–C stretching vibration region (1300 to 1650 cm^{-1}), and C–H bending in-plane vibration region (1000 to 1500 cm^{-1}) for rGO is overlapping with graphene modes [15]. Apparently in Figure 6.23, the Raman spectrum of the pristine graphene shows an intensive G-band at ~1584 cm^{-1}. Also an intensive D-band at ~1336 cm^{-1} and a 2D- band at 2658 cm^{-1} wile D+D' at ~ 2925 cm^{-1} is visible. These values are typical graphite structures and an indication for many stacked layers [16]. These results indicate that the graphene oxide has been successfully exfoliated to graphene sheets [17]. However, a high I_D/I_G ratio of the pristine graphene about ~1.7 indicates the presence of localized sp^3 defects within the sp^2 carbon network [18].

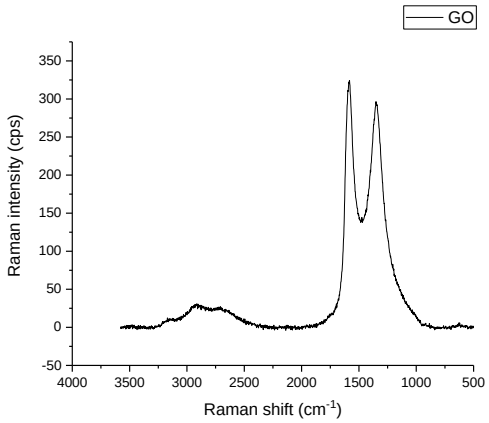

Figure 6.20. The Raman spectra of graphene oxide.

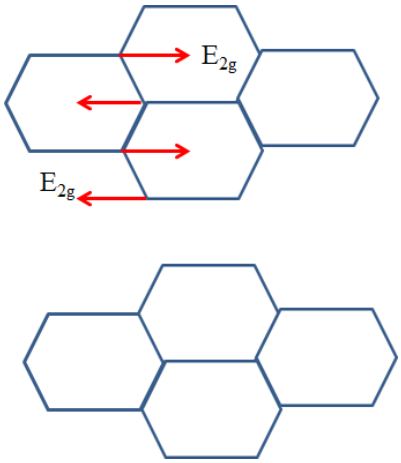

Figure 6.21. E_{2g} vibrational mode of carbon atoms in one graphite layer [11].

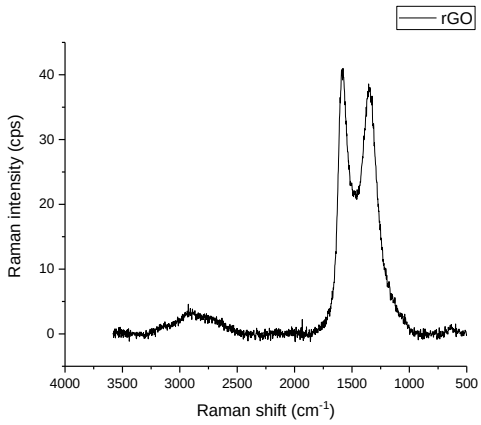

Figure 6.22. The Raman spectra of reduced graphene oxide.

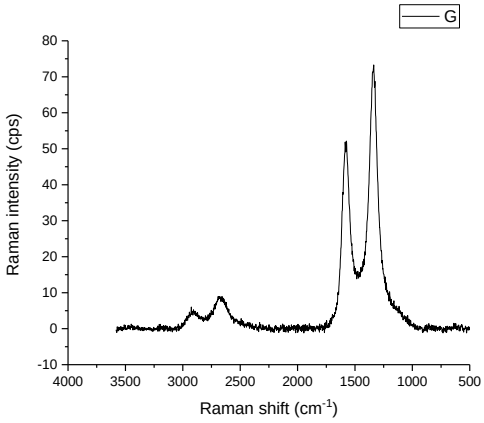

Figure 6.23. The Raman spectra of pristine graphene.

Graphene ID	I_D	I_G	I_D/I_G
GO	150.57	527.96	0.29
rGO	1311.65	1153.97	1.14
G	4167.08	2414.83	1.73

Table 6.13. The I_D/I_G ratio of GO, rGO and G.

6.3.4. FTIR analysis

The nature of the molecular interaction between chemical groups on G, GO and rGO surfaces and the matrix PE and PP blends, and the presence of functional groups on the G, GO and rGO surfaces can be investigated by measuring the extent of shift in the Fourier transform infrared (FTIR) spectrum for the main groups on the graphene and the matrix polymer after addition the graphene. The FTIR spectrum of the G and GO, GO and rGO have previously been presented by Wang, X. & et, al. [19] and Konios, D. & et, al. [20].

In contrast to the G, the GO shows many various absorption peaks of oxygen functional groups, such as: O-H stretching vibration at 3428 cm^{-1}, carbonyl C =O stretching vibration at 1730 cm^{-1}, C=C vibration in aromatic (phenol) ring at 1621 cm^{-1}, C –OH bending vibration at 1400 $cm^{-1}$and C – OH stretching vibration of alcohol at1231 cm^{-1}, as well as C– O stretching vibrations or epoxy C –O –C vibrations at 1050 cm^{-1}. After the reduction of the oxygen function group to convert GO to rGO, the absorption peaks of the C =O and C−OH in rGO decreased or disappear depending on the rate of the oxygen reduction. Furthermore, two peaks in rGO related to the C–O–C stretching vibrations appeared at 1167 and 1120 cm^{-1}. The formation of additional C–O–C bonds can be explained by the removal of water (H−OH) from the GO sheets [11] [12] [13] [21] [22].

The interfacial interactions among polyethylene polymer with GO, rGO and G nanoplatelets were characterized by FTIR, as displayed in Figures 6.24, 6.25, 6.26 and 6.27 and summarized in Tables 6.14, 6.15, 6.16 and 6.17. It should be noted that the distinctive peaks of pure polymer were still present upon addition of both GO, rGO and G. The polymer graphene nanocomposite shows almost the same absorption peaks as pure polymer. The absence of rGO and GO and graphene oxide peaks is a strong indication of the exfoliation of graphene sheets inside the nanocomposites. This means that there is no new bond formed or strong chemical interaction occurring in the blend and nanocomposites upon addition of G, rGO or GO. This is expected due to G and rGO not having any functional groups available to form strong interface with a polymer matrix and no chemical interaction between the polar (GO) and non-polar compounds (PE or PP). This indicates that any change on the structure or the properties of the nanocomposites is the result of the physical interaction only between the graphenes and the PE, PP blends host matrices [23].

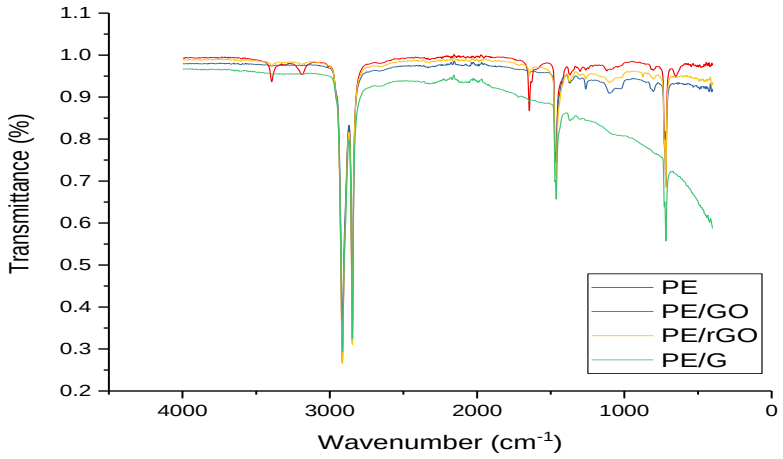

Figure 6.24. FTIR spectra of pure PE and PEs graphenen nanocomposites

Wavenumber (cm^{-1})	Compound group name in the nanocomposites			
	PE	PE/GO	PE/rGO	PE/G
2915.04	C-CH_3	C-CH_3	C-CH_3	C-CH_3
2847.35	CH_2	CH_2	CH_2	CH_2
1645.64	Non-Conjugated	-	-	-
1462.96		CH_3	CH_3	CH_3
1368.62	CH_3	-		CH_3
1098.56	-	-CH= CH_2		
729.10	-	-CH=CH-(Cis)	-	-
719	-CH=CH-(Cis)	-	-CH=CH-(Cis)	-
652.24	-CH=CH-(Cis)	-CH=CH-(Cis)	-	-

Table 6.14. Characteristic infrared transmission of PE nanocomposites [24] [25].

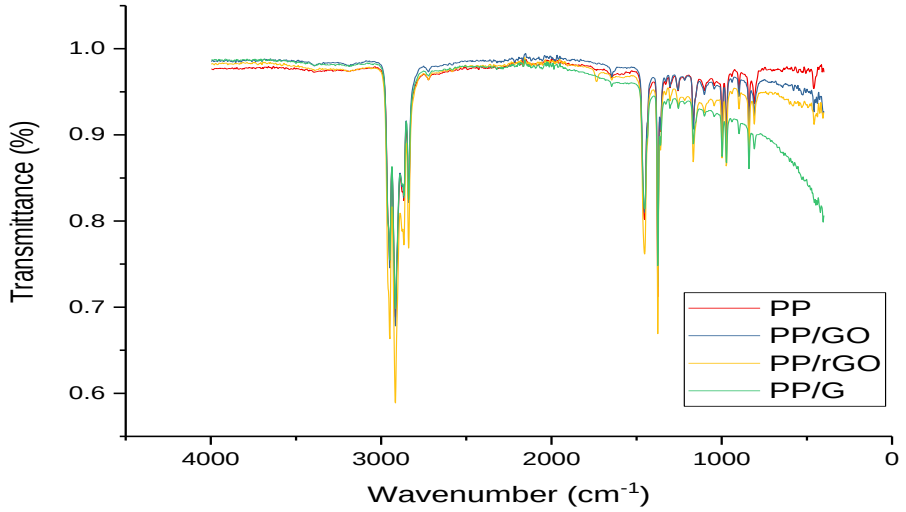

Figure 6.25. FTIR spectra of pure PP and PPs graphene nanocomposites.

Wavenumber (cm^{-1})	Compound group name in the nanocomposites			
	PP	PP/GO	PPrGO	PPG
2949.49	C-CH_3	C-CH_3	C-CH_3	C-CH_3
2916.51	C-CH_3	C-CH_3	C-CH_3	C-CH_3
2837.99	C-CH_3	C-CH_3	C-CH_3	C-CH_3
2721.27	C-CH_3	C-CH_3	C-CH_3	C-CH_3
1734.44	-	-	Amides	-
1645.33	Amides	Amides	-	Amides
1452.13	CH_2	CH_2	CH_2	
1375.02	CH_3	CH_3	CH_3	CH_3
997.12	-CH=CH- (Trans)	-CH=CH- (Trans)	-CH=CH- (Trans)	-CH=CH- (Trans)
840.37	C=CH_2	C=CH_2	C=CH_2	C=CH_2
457.5	-CH=CH-(Cis)	-CH=CH-(Cis)	-CH=CH-(Cis)	-CH=CH- (Cis)

Table 6.15. Characteristic infrared transmission of PP nanocomposites [26].

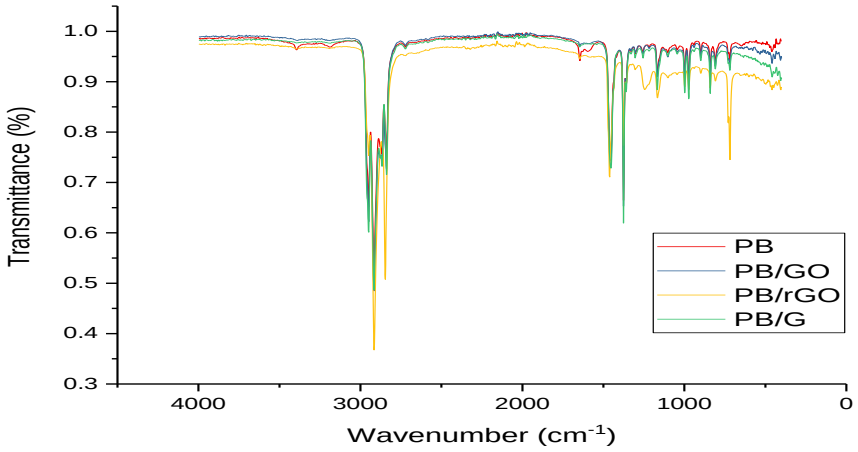

Figure 6.26. FTIR spectra of pure PB and PBs graphene nanocomposites.

Wavenumber (cm^{-1})	Compound group name in the nanocomposites			
	PB	PB/GO	PB/rGO	PB/G
2949.09	C-CH_3	C-CH_3	C-CH_3	C-CH_3
2916.60	C-CH_3	C-CH_3	C-CH_3	C-CH_3
2838.41	C-CH_3	C-CH_3	C-CH_3	C-CH_3
2722.20	C-CH_3	C-CH_3	-	C-CH_3
1645.40	Amides	Amides	-	-
1455.39	CH_2	CH_2	CH_2	CH_2
1375.41	CH_3	CH_3	CH_3	CH_3
1166.93	-CH= CH_2	-CH= CH_2	-CH= CH_2	-CH= CH_2
997.56	-CH=CH- (Trans)	-CH=CH- (Trans)	-CH=CH- (Trans)	-CH=CH- (Trans)
840.79	-CH= CH_2	-CH= CH_2	-CH= CH_2	-CH= CH_2
808.62	C=CH_2	C=CH_2	C=CH_2	C=CH_2
719.48	-CH=CH-(Cis)	-CH=CH-(Cis)	-CH=CH-(Cis)	-CH=CH-(Cis)

Table 6.16 . Characteristic infrared transmission of PB nanocomposites [27].

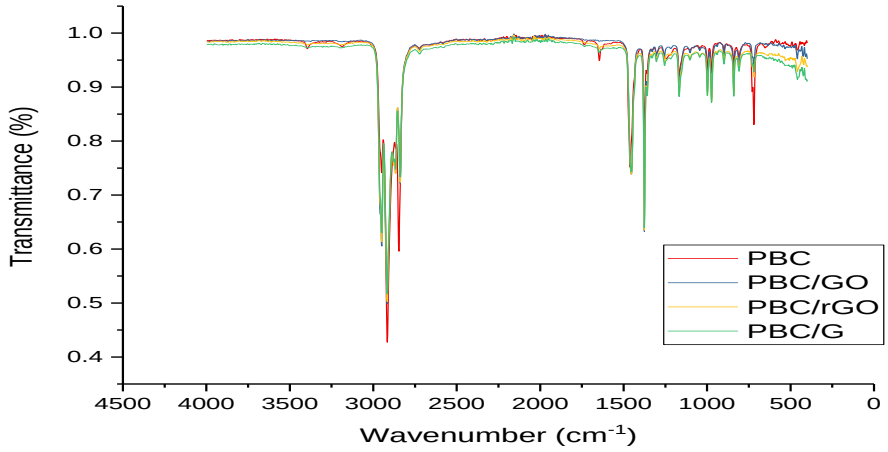

Figure 6.27. FTIR spectra of pure PBC and PBCs graphene nanocomposites.

Wavenumber (cm^{-1})	Compound group name in the nanocomposites			
	PBC	PBC/GO	PBC/rGO	PBC/G
2949.52	C-CH_3	C-CH_3	C-CH_3	C-CH_3
2916.04	C-CH_3	C-CH_3	C-CH_3	C-CH_3
2847.44	C-CH_3	C-CH_3	C-CH_3	C-CH_3
2721.32	-	C-CH_3	C-CH_3	C-CH_3
1645.44	Amides	-	-	-
1461.74	CH_2	CH_2	CH_2	CH_2
1375.70	CH_3	CH_3	CH_3	CH_3
972.72	-CH=CH- (Trans)	-CH=CH- (Trans)	-CH=CH- (Trans)	-CH=CH- (Trans)
840.89	-CH= CH_2	-CH= CH_2	-CH= CH_2	-CH= CH_2
719.48	-CH=CH-(Cis)	-CH=CH-(Cis)	-CH=CH-(Cis)	-CH=CH-(Cis)

Table 6.17. Characteristic infrared transmission of PBC nanocomposites [27].

6.3.5. UV–vis spectroscopy

The UV-visible spectra of GO and rGO are shown in Figure 6.28. There are two distinctive absorption bands in the UV-visible spectra of GO. The absorption band centered at ~255 nm is attributed to $\pi \rightarrow \pi^*$ transitions of aromatic C-C bonds. The shoulder centered at ~ 335 nm corresponds to $n \rightarrow \pi^*$ transitions of C=O bonds. After the reduction reaction with hydrazine hydrate, the absorbance in the whole spectra increases, also the absorption peak at ~255 redshifts to ~265 nm in rGO and at ~284 nm in graphene and the other absorption band at ~ 335 is completely removed (Figure 6.29). The UV-

visible spectra results demonstrate that the oxygen containing functional groups on the surface of GO are mostly removed and electronic conjugation within graphene nanosheets is restored via reduction reaction. Similar results were also obtained by Yu et al. [28] and Xu et al. [29] [30].

Figure 6.29 shows that the absorbance of GO is higher than that of rGO and G. This stems from the recuperation of sp^2 carbons after reduction and the restoration of the electronic network of rGO and G. The UV-vis study highlighted the fact that GO is easily dispersed in water whereas rGO and G required to be dispersed in ethanol or DMF. This has negative implications for the dispersion characteristics of rGO and G in organic compounds of ε-caprolactam [31].

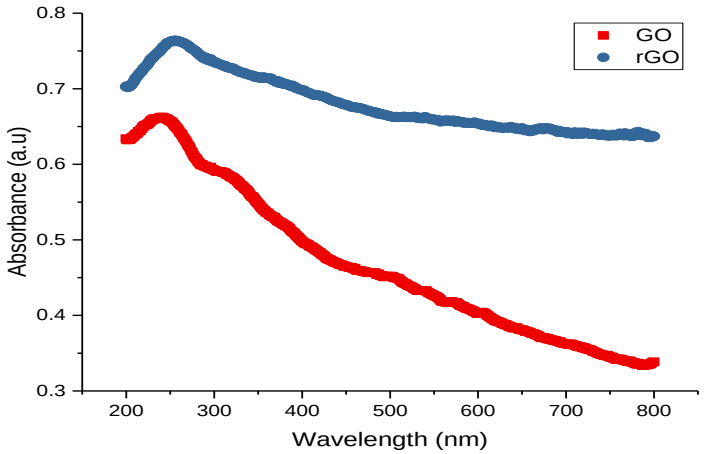

Figure 6.28. UV-visible spectra of GO and rGO.

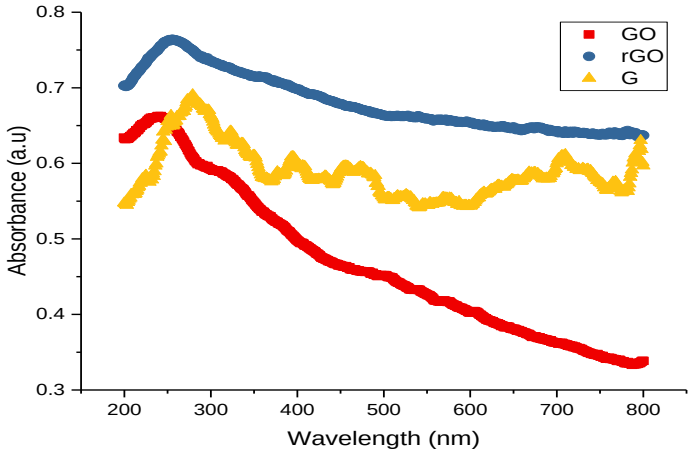

Figure 6.29. UV-visible spectra of GO, rGO and G.

6.3.6. Crystallization and Melting Behaviour

Differential scanning calorimetry (DSC) was used to assess the effect of the addition of GO, rGO and G at 2wt% on the melting temperature (T_m), crystallization temperature (T_c) and degree of crystallinity (X_c) of the polymer blends (PE, PP, PB and PBC). The DSC data are summarised in Table 6.20. The melting temperature of the PEs, PPs PBs and PBCs nanocomposites do not change with addition of the different three types of graphene (see Table 6.18, Figure 6.30). There is also no clear effect on the crystallization temperature of the PBs and PBCs nanocomposites, whereas the crystallization temperature of the PEs and PPs nanocomposites increase by addition of the GO, rGO and G (see Figure 6.31). It was observed that the graphene addition caused a considerable change in the crystallization temperature (T_c) of PE and PP, with T_c noticeably increasing through the addition of all graphene types. An increase in the crystallization temperature of PE and PP, in the presence of graphene, has industrial value due to a shorter processing cycle, which results in a higher production rate [32]. As discussed in the previous chapter, the graphene acts as the nucleating agent for crystallisation of PE and PP, which makes the nucleation mode heterogeneous instead of homogeneous, significantly decreasing the nucleation free energy, and allow the molecular chain to attach to and be arranged orderly on the nucleating agent [33]. Graphene demonstrate important influence over the T_c of PE and PP. Such a result is ascribed to the nanometer size effect of graphene. With the same content, graphene contribute to a greater surface area and at the same time greater nucleation sites, thereby having a greater effect on the T_c of PE and PP. The presence of graphene in polyolefins matrix affects the crystallization process of that polyolefins as evidenced by changes the crystallization temperature. The degree of crystallinity fluctuated, but the general trend is decreasing with increase the GO wt%, due to the fast cooling the sample by quenched directly into water at room temperature. This decrease could be explained as well by the effect of the graphene layers on the degree of crystallization by hindering the chain mobility [38].

Specimens ID	T_c (°C)		T_m (°C)		ΔH_m J/g		ΔT (°C)	X_c (%)		
	PE	PP	PE		PE	PP		PE	PP	PB
PE	103±1	-	124±1	-	77	-	21	26	-	-
PE/GO	107±1	-	123±1	-	68	-	16	23	-	-
PE/rGO	107±1	-	123±1	-	74	-	17	25	-	-
PE/G	107±1	-	123±1	-	77	-	17	26	-	-
PP	-	119±1	-	167±1	-	100	49	-	48	-
PP/GO	-	119±1	-	166±1	-	76	47	-	37	-
PP/rGO	-	121±1	-	165±1	-	78	44	-	38	-
PP/G	-	123±1	-	163±1	-	80	40	-	39	-
PB	109±1	115±1	123±1	166±1	15	46	-	5	22	27
PB/GO	107±1	118±1	123±1	166±1	27	35	-	9	17	26
PB/rGO	106±1	117±1	123±1	165±1	29	37	-	10	18	28
PB/G	n.d	115±1	121±1	165±1	22	40	-	8	19	27
PBC	106±1	114±1	122±1	164±1	23	33	-	4	23	27
PBC/GO	108±1	117±1	123±1	166±1	28	36	-	10	17	27
PBC/rGO	106±1	113±1	122±1	164±1	28	32	-	10	16	26
PBC/G	n.d	114±1	121±1	165±1	32	23	-	11	11	22

Table 6.18 .The DSC parameters of the polymer/ GO, rGO and G nanocomposites.

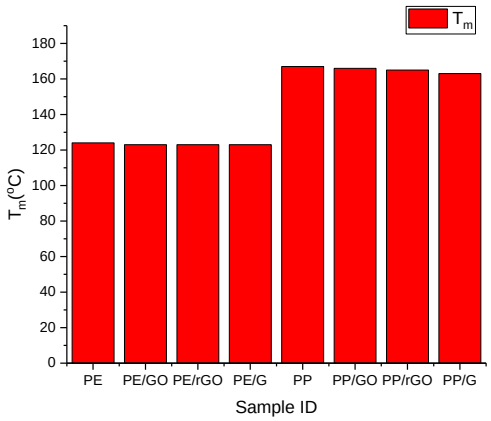

Figure 6.31. The melting temperature (T_m) of PE and PP graphene nanocomposites.

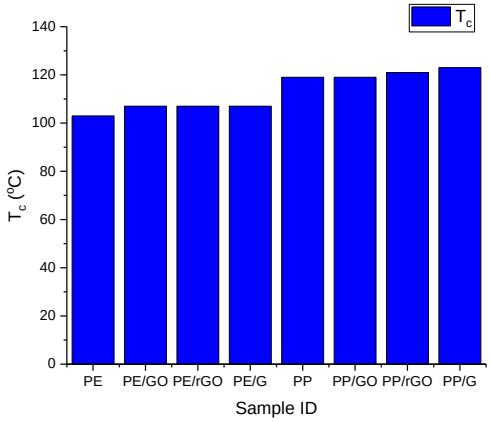

Figure 6.31. The crystallization temperature (T_c) of PE and PP graphene nanocomposites.

6.3.7. Thermal stability

The pristine graphene powder displays just a very slow mass loss up to 400 ºC, indicating almost complete removal of the functional groups. GO has a 12% mass loss around 100 °C, resulting from removal of oxygen functionalities as adsorbed water evaporates and a further 46% mass loss from 300 °C to 400 °C because the heating continues to remove the oxygen-containing functional groups. The mass loss of rGO is clearly lower than that of GO, specifically the mass loss from 100 ºC to 200 °C, which reveals a noticeable decrease in the quantity of oxygen-containing functional groups and a deep reduction of GO. Meanwhile, a higher mass loss of 26% is found around 700 °C in rGO (Table 6.19 and Figure 6.32).

Graphene ID	100 ºC	200 ºC	300 ºC	400 ºC	500 ºC	600 ºC	700 ºC
G	0	0	0	1	2	3	4
rGO	3	8	13	15	17	20	26
GO	12	20	43	46	49	51	55

Table 6.19. The lost weight percent (wt%) of G, rGO and GO at different temperatures.

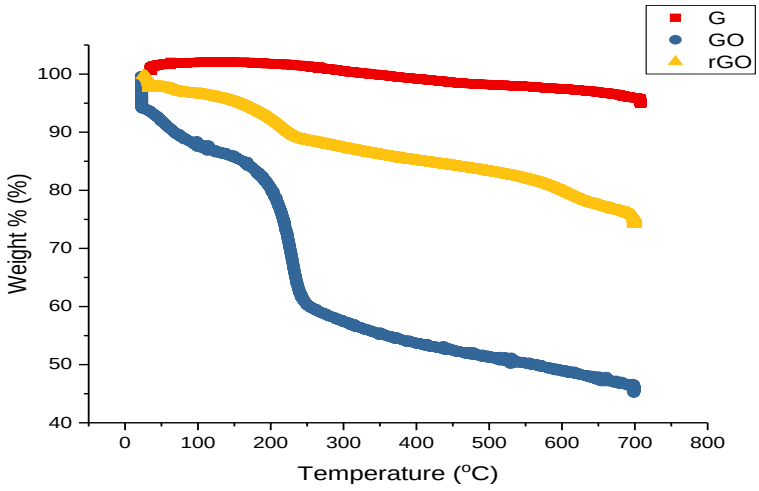

Figure 6.32. The TGA curves of the G, rGO, GO from room temperature to 700 °C.

The thermal stability of the PE/(G, rGO, GO) nanocomposites were investigated by TGA. The thermogravimetric data are summarised in Figure 6.33 and Table 6.20. This figure shows the TGA curves for the pure PE and the PE/ (G, rGO, GO), nanocomposites while the table displays the temperature at the remaining weight percent of 99%, 50% and 5%. At 99wt% of the sample the degradation temperature of the PE/GO increased by 113±3 °C from the pure PE. The increase is 98±3 °C and 120±3 °C in the PE/rGO and PE/G respectively from the pure PE. The fact that there is an increase in stability in the presence of graphene suggests that G, rGO, GO are well exfoliated in the polymeric matrix by using the solution mixing method [35].

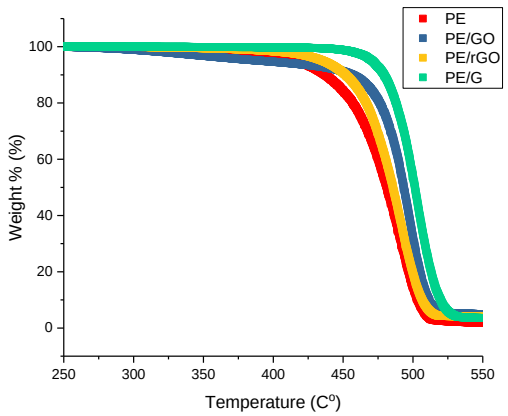

Figure 6.33. The TGA decomposition curves of the PE nanocomposites.

Specimens ID	$T_{99\%}$ (°C)	$T_{50\%}$ (°C)	$T_{5\%}$ (°C)
PE	365±3	394±3	502±3
PE/GO	478±3	493±3	546±3
PE/rGO	463±3	486±3	515±3
PE/G	485±3	501±3	528±3

Table 6.20. Thermal degradation temperatures of the PE nanocomposites.

Figure 6.34 and Table 6.21 show the thermal properties of PP and its nanocomposites, demonstrating a great improvement in the thermal resistance for the degradation with an increase of 173±3 °C from the neat PP in the temperature at which 99% weight of sample remains by addition of 2wt% of GO, and 187±3 °C by addition of the rGO and G. Moreover, the graphene still continues to provide clear improvement at higher temperatures by increasing the temperature at which 50% weight of sample remains to 167±3, 176±3 and 179±3 °C from the pure PP. Furthermore, at 5 remaining weight percent the temperature rise up to 150±3, 154±3 and 165±3 °C from PP by presence GO, rGO and G. These features are strong indications that graphite products can function as a flame retardant, significantly improving the thermal stability of polypropylene [3].

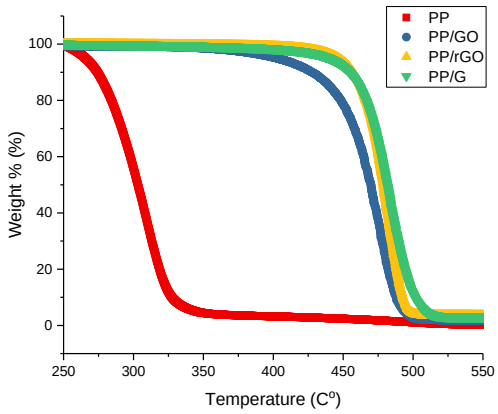

Figure 6.34. The TGA decomposition curves of the PP nanocomposites.

Specimens ID	$T_{99\%}$ (°C)	$T_{50\%}$ (°C)	$T_{5\%}$ (°C)
PP	276±3	303±3	344±3
PP/GO	449±3	470±3	494±3
PP/rGO	463±3	479±3	498±3
PP/G	463±3	482±3	509±3

Table 6.21. Thermal degradation temperatures of the PP nanocomposites.

The PB/(GO, rGO and G) and PBC/(GO, rGO and G) nanocomposites provided similar improvement to PE and PP as seen in Figures 6.35 and 6.36 and Tables 6.22 and 6.23, but with different ratio of improvement depending on the dispersion and distribution of these graphene products inside the polymer matrix of PB and PBC.

The presence of G, rGO, GO which are highly stable material and stiffer than both PE and PP grant stiffness to the polymeric matrices, reducing the chain mobility and consequently retarding the degradation of the polymer. The fact that polyolefins (PE and PP) increased the stability in the presence of graphene suggested that the G, rGO, GO disperse to some extent in the polymeric matrix. Reduce the oxygen functional group improve the thermal stability as the data in Figure 6.32 illustrates . In addition to the dispersion of the filler and the C/O ratio effect, its concentration also had a key role in the thermal properties of the nanocomposites [36].

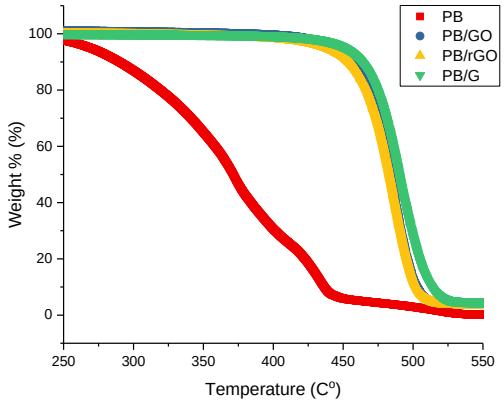

Figure 6.35. The TGA decomposition curves of the PB nanocomposites.

Specimens ID	$T_{99\%}$ (°C)	$T_{50\%}$ (°C)	$T_{5\%}$ (°C)
PB	299±3	371±3	463±3
PB/GO	462±3	484±3	513±3
PB/rGO	462±3	484±3	513±3
PB/G	470±3	490±3	532±3

Table 6.22. Thermal degradation temperatures of the PB nanocomposites.

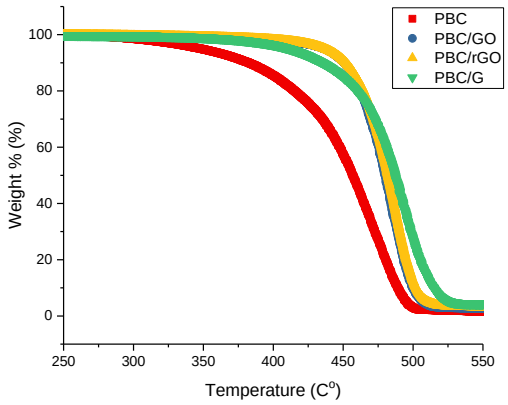

Figure 6.36. The TGA decomposition curves of the PBC nanocomposites.

Specimens ID	$T_{99\%}$ (°C)	$T_{50\%}$ (°C)	$T_{5\%}$ (°C)
PBC	407±3	442±3	496±3
PBC/GO	458±3	480±3	507±3
PBC/rGO	461±3	482±3	511±3
PBC/G	472±3	487±3	527±3

Table 6.23 Thermal degradation temperatures of the PBC nanocomposites.

6.4. Summary and Conclusion

This study investigates the effect of the change the carbon to oxygen ratio (C/O) by using three different types of graphene on the structure-properties relation in PE, PP, and blends of them. These nanocomposites were prepared by solution method, where GO, rGO and G powder was dispersed by sonication in DMF solvent while o-xylene was used for dissolving the polymers. Scanning Electron Microscope (SEM) and Wide Angle X-ray Diffraction (WAXD) have been used to analyse the polymers' semi-crystalline morphology. The interlayer spacing (d-spacing) and the intensity increased by addition of all types of the graphene while the crystallite size decrees. The chemical structure characterized by X-ray Photoelectron Microscopy (XPS), Fourier Transform Infrared Spectroscopy (FTIR) Raman Spectroscopy (RS) and UV–vis spectroscopy. The C/O ratio was calculated as≈ 89.7, 4.9 and 2.2 for the G, rGO and GO respectively. While the I_D/I_G ratios increased with increasing the C/O ratio, the I_D/I_G values were calculated as 0.285, 1.137 and 1.726 for pure GO, rGO and G sample.

The thermal properties were investigated by Deferential Scanning Calorimetry (DSC) and Thermal Gravimetric Analysis (TGA), and revealed that the addition of GO, rGO and G did not have a pronounced effect on the melting temperatures (T_m) of the nanocomposites, while the crystallisation temperature increased with addition all of the three graphene types with similar percent for different C/O ratio. The thermal stability was clearly improved and increased with decreasing the oxygen function group content in the graphene.

These studies form the basis of a wider study of various forms of graphene in nanocomposites with industrially relevant polymers. These findings underline the importance of considering graphene/polymer interactions in the thermal stability (fire retardants) of polymers for an appropriate design of composite materials for aerospace industry.

References

[1] Dai, J., Xu, X., Yang, J., Zhang, N., Huang, T., Wang, Y., Zhang, C. (2015). Greatly enhanced porosity of stretched polypropylene/graphene oxide composite membrane achieved by adding pore-forming agent. RSC Adv., 5(27), 20663–20673.

[2] Lilloja, J., Kibena-Põldsepp, E., Merisalu, M., Rauwel, P., Matisen, L., Niilisk, A., Tammeveski, K. (2016). An Oxygen Reduction Study of Graphene-Based Nanomaterials of Different Origin. Catalysts, 6(8), 108.

[3] Ye, S., Cao, Y., Feng, J., & Wu, P. (2013). Temperature-dependent compatibilizing effect of graphene oxide as a compatibilizer for immiscible polymer blends. RSC Advances, 3(21), 7987.

[4]Guo, C., Zhou, L., & Lv, J. (2013). Effects of expandable graphite and modified ammonium polyphosphate on the flame-retardant and mechanical properties of wood flour-polypropylene composites. Polymers and Polymer Composites, 21(7), 449–456.

[5] Yu, Y.-H., Lin, Y.-Y., Lin, C.-H., Chan, C.-C., & Huang, Y.-C. (2014). High-performance polystyrene/graphene-based nanocomposites with excellent anti-corrosion properties. Polym. Chem., 5(2), 535–550.

[6] Muralikrishna, S., Sureshkumar, K., Varley, T. S., Nagaraju, D. H., & Ramakrishnappa, T. (2014). In situ reduction and functionalization of graphene oxide with l-cysteine for simultaneous electrochemical determination of cadmium(II), lead(II), copper(II), and mercury(II) ions. Analytical Methods, 6(21), 8698–8705.

[7] Wang, D., Niu, W., Tan, M., Wu, M., Zheng, X., Li, Y., & Tsubaki, N. (2014). Pt nanocatalysts supported on reduced graphene oxide for selective conversion of cellulose or cellobiose to sorbitol. ChemSusChem, 7(5), 1398–1406.

[8] Chammingkwan, P., Matsushita, K., Taniike, T., & Terano, M. (2016). Enhancement in mechanical and electrical properties of polypropylene using graphene oxide grafted with end-functionalized polypropylene. Materials, 9(4).

[9] Milani, M. A., Gonzlez, D., Quijada, R., Basso, N. R. S., Cerrada, M. L., Azambuja, D. S., & Galland, G. B. (2013). Polypropylene/graphene nanosheet nanocomposites by in situ polymerization: Synthesis, characterization and fundamental properties. Composites Science and Technology, 84, 1–7.

[10]Wang, Y., Alsmeyer, D. C., & McCreery, R. L. (1990). Raman Spectroscopy of Carbon Materials: Structural Basis of Observed Spectra. Chemistry of Materials, 2(5), 557–563

[11] Eigler, S., Dotzer, C., & Hirsch, A. (2012). Visualization of defect densities in reduced graphene oxide. Carbon, 50(10), 3666–3673.

[12]Bhawal, P., Ganguly, S., Chaki, T. K., & Das, N. C. (2016). Synthesis and characterization of graphene oxide filled ethylene methyl acrylate hybrid nanocomposites. RSC Advances, 6(25), 20781–20790.

[13]Çiplak, Z., Yildiz, N., & Çalimli, A. (2015). Investigation of Graphene/Ag Nanocomposites Synthesis Parameters for Two Different Synthesis Methods. Fullerenes, Nanotubes and Carbon Nanostructures, 23(4), 361–370.

[14] Rattana, T., Chaiyakun, S., Witit-Anun, N., Nuntawong, N., Chindaudom, P., Oaew, S., Limsuwan, P. (2012). Preparation and characterization of graphene oxide nanosheets. Procedia Engineering, 32, 759–764.

[15]Kondratowicz, I., Żelechowska, K., Majdecka, D., & Bilewicz, R. (2015). Synthesis and modification of reduced graphene oxide aerogels for biofuel cell applications. Materials Science-Poland, 33(2).

[16] Liebscher, M., Blais, M. O., Pötschke, P., & Heinrich, G. (2013). A morphological study on the dispersion and selective localization behavior of graphene nanoplatelets in immiscible polymer blends of PC and SAN. Polymer (United Kingdom), 54(21), 5875–5882.

[17] Khenfouch, M. (2012). Morphological, Vibrational and Thermal Properties of Confined Graphene Nanosheets in an Individual Polymeric Nanochannel by Electrospinning. Graphene, 01(02), 15–20.

[18] Kuilla, T., Bhadra, S., Yao, D., Kim, N. H., Bose, S., & Lee, J. H. (2010). Recent advances in graphene based polymer composites. Progress in Polymer Science Volume, 35(11), 1350–1375.

[19]Wang, X., Xing, W., Song, L., Yang, H., Hu, Y., & Yeoh, G. H. (2012). Fabrication and characterization of graphene-reinforced waterborne polyurethane nanocomposite coatings by the sol-gel method. Surface and Coatings Technology, 206(23), 4778–4784.

[20]Konios, D., Stylianakis, M. M., Stratakis, E., & Kymakis, E. (2014). Dispersion behaviour of graphene oxide and reduced graphene oxide. Journal of Colloid and Interface Science, 430, 108–112.

[21] Trapalis, A., Todorova, N., Giannakopoulou, T., Boukos, N., Speliotis, T., Dimotikali, D., & Yu, J. (2016). TiO2/graphene composite photocatalysts for NOx removal: Acomparison of surfactant-stabilized graphene and reduced grapheneoxide. Applied Catalysis B: Environmental, 180(January), 637–647.

[22] Naebe, M., Wang, J., Amini, A., Khayyam, H., Hameed, N., Li, L. H., Fox, B. (2014). Mechanical property and structure of covalent functionalised graphene/epoxy nanocomposites. Scientific Reports, 4, 4375.

[23] Chieng, B. W., Ibrahim, N. A., Yunus, W. M. Z. W., Hussein, M. Z., Then, Y. Y., & Loo, Y. Y. (2014). Effects of graphene nanoplatelets and reduced graphene oxide on poly(lactic acid) and plasticized poly(lactic acid): A comparative study. Polymers, 6(8), 2232–2246.

[24]Chandra, R., & Rustgi, R. (1997). Biodegradation of maleated linear low-density polyethylene and starch blends. Polymer Degradation and Stability, 56(2), 185–202.

[25] Sarker, M., Rashid, M. M., & Molla, M. (2011). Abundant High-Density Polyethylene (HDPE-2) Turns into Fuel by Using of HZSM-5 Catalyst. Journal of Fundamentals of Renewable Energy and Applications, 1(November), 12.

[26] Rjeb, A., Tajounte, L., Chafik El Idrissi, M., Letarte, S., Adnot, A., Roy, D., & Kaloustian, J. (2000). IR spectroscopy study of polypropylene natural aging. Journal of Applied Polymer Science, 77(8), 1742–1748.

[27] Lin,J., Pan, Y., Liu,C., Huang,C., Hsieh,C., Chen,C., Lin,Z., & Lou,C.(2015). Preparation and Compatibility Evaluation of Polypropylene/High Density Polyethylene Polyblends. Materials, 8, 8850–8859.

[28]Yu, S., Yin, Y., and Liu, J. (2013) Silver nanoparticles in the environment.
Environ. Sci.: Process. Impacts., 15: 78–92.
[29] Xu, Z., Gao, H., and Guoxin, H. (2011) Solution-based synthesis
and characterization of a silver nanoparticle-graphene hybrid film.
Carbon, 49: 4731–4738.

[30] Çiplak, Z., Yildiz, N., & Çalimli, A. (2015). Investigation of Graphene/Ag Nanocomposites Synthesis Parameters for Two Different Synthesis Methods. Fullerenes, Nanotubes and Carbon Nanostructures, 23(4), 361–370.

[31] Parades, J. I., Villar-Rodil, S., Martínez-Alonso, A., & Tascón, J. M. D. (2008). Graphene oxide dispersions in organic solvents. Langmuir, 24(19), 10560–10564.

[32] Gopakumar, T. G., & Pagé, D. J. Y. S. (2004). Polypropylene/graphite nanocomposites by thermo-kinetic mixing. Polymer Engineering & Science, 44(6), 1162–1169.

[33] Huang, C.-L., Lou, C.-W., Liu, C.-F., Huang, C.-H., Song, X.-M., & Lin, J.-H. (2015). Polypropylene/Graphene and Polypropylene/Carbon Fiber Conductive Composites: Mechanical, Crystallization and Electromagnetic Properties. Applied Sciences, 5(4), 1196–1210.

[34]Kim, S., Do, I., & Drzal, L. T. (2009). Multifunctional xGnP/LLDPE nanocomposites prepared by solution compounding using various screw rotating systems. Macromolecular Materials and Engineering, 294(3), 196–205.

[35] De C. Fim, F., Basso, N. R. S., Graebin, A. P., Azambuja, D. S., & Galland, G. B. (2013). Thermal, electrical, and mechanical properties of polyethylene-graphene nanocomposites obtained by in situ polymerization. Journal of Applied Polymer Science, 128(5), 2630–2637.

[36] Sengupta, R., Chakraborty, S., Bandyopadhyay, S., Dasgupta, S., Mukhopadhyay, R., Auddy, K., & Deuri, a S. (2007). A Short Review on Rubber / Clay Nanocomposites with Emphasis on Mechanical Properties. Engineering, 47, 21–25.

Chapter 7

Conclusion and Future Work

7.1. Summary and Conclusions

Graphene and its derivatives have potential applications in many fields including polymer composites. In this work fundamental studies of graphene and related materials along with various graphene/polymer nanocomposite preparation methods and properties are reported. The work placed an emphasis on the material characteristics and the properties of the graphene, polymer and graphene/polymer nanocomposite. Overall, the thesis shows a collection of experimental work that focussed on three major objectives with regard to graphene/polymer nanocomposites:

I. Understanding the structure, phase transition and properties of the polymer host matrix of graphene nanoparticles;
II. Studying the effect of different percentages of graphene oxide on the structure-property relationships in graphene/polymer nanocomposites;
III. Discussing the influence of carbon/oxygen ratio upon structure-property relationships in graphene/polymer nanocomposites, by using three different types of graphene.

The first objective was achieved by determining the preparation method of the four polymer host matrices, metallocene linear low density polyethylene (PE), polypropylene homopolymer (PP), blend of PE and PP (PB) and blend of PE , PP and 5wt% of compatibilizer polymer (ethylene-*co*-glycidyl methacrylate) (PE-*co*-GMA) referred to as PBC. The polymers were processed using a solution method with o-xylene as the solvent. The results indicated that the 100mg/ml ratio of o-xylene is optimal to dissolve the PE, PP and their blends. The crystallinity was characterized by using wide angle x-ray diffraction (WAXD) and small angle x-ray scattering Measurements (SAXS). Information about the polymer host matrix structure has been obtained, like the crystallite size, interlayer spacing, lamella thickness and linear crystallinity, and the combination of the two crystallization structures indicates an immiscible blend between those two polymers. Furthermore, the molecular weight was measured for both pure polymers, which will enable future studies on different molecular weight polymers to be well compared to the current study. The thermal and crystallization behaviour have been obtained by deferential scanning calorimetry (DSC) and the thermal gravimetric analysis (TGA), with the data showing that the blends have binary crystallization and melting behaviour while the crystallinity degree is lower in the PB and PBC than the PP. Moreover, the thermal stability of the PE is higher than the PP and the PB blend. Adding the PE-co-GMA compatibilizer (sample PBC) causes an increase in the thermal stability. Also, PP provides superior mechanical properties, while PE provides better elastic behaviour. From this, we can see the importance of blending PP and PE, while adding the PE-co-GMA improved the mechanical properties. The final step of studying the polymer

host matrix was the dynamic mechanical analysis (DMA) study applied to the four sample types. The results of the DMA indicate that the pure polymers (PE and PP) have three different transitions: an α-transition, a β-transition and a γ-transition. The transition zone, in PB and PBC blend has two β-transitions, which appear as separate phase transitions because the PE and PP are thermodynamic incompatible and immiscible polymers.

Based on the previous results from the host polymer matrices, graphene oxide (GO) was added with 6 different weight fractions (0.0, 0.25, 0.5, 1, 2, 4 wt. %) into the four host polymer matrices (PE, PP, PB and PBC). That happened after applying a solubility test and obtaining the best pair of compatible solvents for the GO and the polymers. The effective dispersion of GO by using the solution method was confirmed by the absence of the distinctive peak from stacked (graphitic) GO in the WAXD scan in all the GO/polymer nanocomposites. The study of the effect of GO on the crystal structure was investigated by calculating a linear correlation function from the SAXS data. Mixing GO with the polyolefins had a measurable effect upon the polymers' crystal structure. However, no chemical reaction between the polymer and GO was observed for samples prepared by the solution method. This was realized in Fourier transformed infrared spectroscopy (FTIR) scans which showed an absence of GO peaks in the polymer nanocomposites that is also an indication of graphene sheets exfoliation into the polymer layers, at the highest concentration of 4wt%. The characteristic D/G ratio is dominated by the structural defects (holes) of a sheet rather than the level of oxidation, and the I_D/I_G intensity ratio value was calculated as 0.285 for our pure GO sample by Raman spectroscopy. To evaluate the effect of the addition of GO on the thermal and crystallization behaviour, DSC and TGA were used. While the melting temperatures of the nanocomposites were not significantly influenced by GO addition, the crystallization temperature was increased by increasing the GO weight fraction. This property presents technological importance because it results in a shorter processing cycle, thereby increasing the production rate. The degree of supercooling increases in PP/GO nanocomposites while it decreases in PE/GO nanocomposites. The increase or decrease in the degree of supercooling indicates to physical reaction between the Polyolefins (POs) and GO. The thermal stability improved by adding GO up to and including a fraction of 2wt%, demonstrating an optimal fraction of graphene in the polymer nanocomposites (PNCs) above which further addition has no benefit. The high carbon/oxygen ratio in the GO causes high electrical resistance. Due to its improved thermal stability and electrical insulation the graphene oxide based PE and PP blend could have a possible application as a material for electrical insulation. However, the addition of GO decreased the mechanical properties as investigated by the tensile strength.

The previous results derived from one type of graphene with uniform carbon/oxygen (C/O) ratio. Therefore, the C/O ratio was varied in order to study the effect of graphene materials with different ratios of C/O on the structure-property relations of resulting nanocomposites. Three different source of graphene which are GO, reduce graphene oxide (rGO) and pristine graphene (G) were used for that

purpose, and all showed improvements in some properties of the polyolefins after incorporation of graphene nanofillers. First the C/O ratio of G, rGO and GO were calculated from X-ray photoelectron spectroscopy *(*XPS) survey scans, which quantitatively determined the surface compositions of deposits of the materials. The surface morphology of the G, rGO and GO was described by scanning electron microscope (SEM). Then the impact of C/O ratio on the crystalline structure was measured using WAXD. The interlayer spacing in GO and rGO are larger than that of pristine graphene owing to the introduction of oxygen-containing functional groups. Furthermore, the disappearance of G peak at 25.6^{o} in GO and rGO and increase of the d-spacing from the original G suggest that the van der Waals interaction between layers became weaker due to the intercalation of oxygen-containing functional groups. The nature of defects which are present in carbon nanomaterials structure can be estimated by calculating the ratio of D/G peaks intensity. A high I_D/I_G ratio of the pristine graphene indicates the presence of localized sp^3 defects within the sp^2 carbon network. Furthermore, the chemical structure of the PNCs was observed to be similar to the POs, and the increase the C/O ratio by reduction of the oxygen containing function did not appear to affect the chemical structure. Accordingly, UV-visible spectra of GO, rGO and G showed that the absorbance of GO is higher than that of rGO and G. This stems from the recuperation of sp^2 carbons after reduction and the restoration of the electronic network of rGO and G. However, there was no clear effect of changing the C/O ratio upon the crystallization and melting behaviour. The rGO and G presented similar effects to that of GO, even with different ratios of C/O. However, reducing the oxygen-containing functionality yielded an improvement in the thermal stability, across different weight fractions of nanofiller and within different polymer host matrices. That is arguably a consequence of the relatively high thermal stability of the pristine graphene, which decreases respectively for rGO and then GO. These studies form the basis of a wider study of various forms of graphene in nanocomposites with industrially relevant polymers. These findings underline the importance of considering graphene/polymer interactions in improving the thermal stability (fire retardants) of polymers for an appropriate design of composite materials for aerospace industry.

7.2. Future Research Directions

Polymer nanocomposites are used in a variety of applications ranging from high-tech and high-performance materials to household daily appliances. Nanocomposites are a very rapidly growing field, and there are many opportunities to pursue this field in the future. During the course of this thesis, a number of new alterations and ideas were identified to improve the main goals delineated in the beginning. In order to keep within the original scope of the project, and due to the time constraints and instrument limitations at the time, not all the ideas could be pursued to completion. However, there are still many challenges and issues to overcome in order to realize the full potential of these

materials in these applications. In the following sections, a few strategies to improve the current research are discussed, and platforms the applications of this research are suggested.

Dispersion and distribution of graphene into polyolefins is very important to develop and improve the electrical and thermal conductivity, mechanical properties and gas barriers of the polymers. To attain most of these characteristics it is necessary to have exfoliation, an interconnected graphene network. However, dispersions and distribution of graphene in polymers is challenging. Good dispersion can be partially obtained by either sonication of the graphene into a co-solvent with the polymer, before co-precipitation, or drying to a film, or by dispersing graphene in a monomer and polymerising in situ to produce a composite. In a suitable situation solvent processed composites lock the graphene into its well-dispersed form in the solvent; however, it is usually necessary to modify the graphene to improve its dispersibility and its interaction with the polymer matrix. In situ polymerisation can give better results that may be due to the graphene participating in the polymerisation, grafting polymer chains on to graphene sheets

Melt compounding provides the most a simple way of dispersing nanofillers in a polymer matrix and it has been used to exfoliate the graphene fillers into many of polymers. Fair levels of dispersion and distribution the fillers can be obtained in these systems but the addition of the nanoparticles increases the viscosity of the polymer melt significantly and clearly makes processing more difficult. The twin-screw extruder, as an effective method to produce nanocomposites of graphene/ polymer, applies solid state shear stress. However, compared to in situ polymerisation and solution method, melt blending using resins and traditional instruments such as extruders and blenders is more attractive since this processes relaxes the requirement for solvent selection and temperature ,e.g. the elevated temperatures required to dissolve polyolefins. This gives a wider range of choices with regards to the selection of polymer grades and choice of graphene type. Moreover, melt mixing is economical and appropriate for mass production more than solution and in situ polymerization methods.

On the materials side, a potential route would be to use thermosetting polymers such as epoxy resin instead of thermoplastic polymers, then to study the effects of graphene on structure and properties of epoxy resin. Epoxy resin as a polymer matrix has high stiffness, dimensional stability and chemical resistance, which make it the most important thermosetting resin in the industry for structural and functional composites. Epoxy resins are used in many applications such as adhesives, in electronics for encapsulation and in the aerospace manufactures as matrices for composites.

Appendix

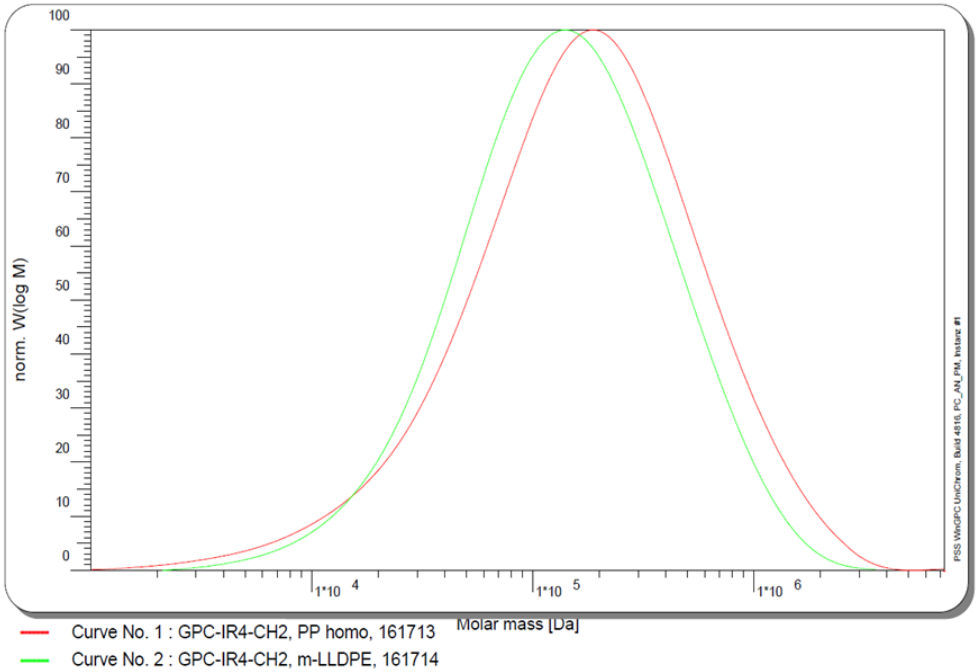

Figure A.1. The molar mass distribution curves of PE and PP.

Samples ID	Na	O	In	N	C	Cl	S	Si
Graphene 1	<0.1	1.0	0.1	<0.1	98.8	<0.1	0.1	<0.1
Graphene 2	<0.1	1.2	<0.1	<0.1	98.5	<0.1	0.2	0.2
Graphene Oxide 1	0.3	31.5	0.3	0.2	65.9	0.2	1.0	0.7
Graphene Oxide 2	0.1	29.8	0.3	0.3	68.8	0.2	0.5	0.1
Reduced Graphene Oxide 1	<0.1	16.8	<0.1	<0.1	82.5	0.1	0.5	0.1
Reduced Graphene Oxide 2	<0.1	16.5	<0.1	<0.1	83.1	0.1	0.4	<0.1

Table A.1. Surface compositions (atomic %) determined by quantifying XPS survey scans.

Bibliography

Abdullah, S. I., & Ansari, M. N. M. (2015). Mechanical properties of graphene oxide (GO)/epoxy composites. HBRC Journal, 11(2), 151–156.

Amani, M., Sharif, M., Kashkooli, A., Rahnama, N., & Fazli, A. (2015). Effect of mixing conditions on the selective localization of graphite oxide and the properties of polyethylene/high-impact polystyrene/graphite oxide nanocomposite blends. RSC Advances, 5(95), 77723–77.

Aref, A. H., Entezami, A. A., Erfan-Niya, H., & Zaminpayma, E. (2017). Thermophysical properties of paraffin-based electrically insulating nanofluids containing modified graphene oxide. Journal of Materials Science, 52(5), 2642–2660.

Avouris, P.(2010) Graphene: Electronic and photonic properties and devices. Nano Letters, 10(11):4285–4294.

Aziz, A. A., Akil, H. M., Jamaludin, S. M. S., & Ramli, N. A. M. (2011). The effect of multiple compatibilizers on the impact properties of polypropylene/polystyrene (PP/PS) blend. Polymer - Plastics Technology and Engineering, 50(8), 768–775.

Barkoula, N. M., Alcock, B., Cabrera, N. O., & Peijs, T. (2008). Fatigue properties of highly oriented polypropylene tapes and all-polypropylene composites. Polymers and Polymer Composites, 16(2), 101–113.

Beer, F.C.(2015). The Journal of The Southern African Institute of Mining and Metallurgy,115, 913–924.

Bhawal, P., Ganguly, S., Chaki, T. K., & Das, N. C. (2016). Synthesis and characterization of graphene oxide filled ethylene methyl acrylate hybrid nanocomposites. RSC Advances, 6(25), 20781–20790.

Borm P J A, Robbins D, Haubold S, Kuhlbusch T, Fissan H, Donaldson K, Schins R P F, Stone V, Kreyling W, Lademann J, Krutmann J, Warheit D, Oberdorster E (2006) The potential risks of nanomaterials: a review carried out for ECETOC (review) Part. Fibre Toxicol, 3–11.

Braun, D., Cherdron, H., Rehahn, M., Ritter, H. & Voit, B. (2005) Polymer synthesis: Theory and Practice, 4th edition, Springer-Verlag Berlin Heidelberg, 12.

Bulkin, B. J. (1978). Raman Spectra of. Applications of Polymer Spectroscopy, 3(c), 121–133.

Bumbrah, G. S., & Sharma, R. M. (2016). Raman spectroscopy - Basic principle, instrumentation and selected applications for the characterization of drugs of abuse. Egyptian Journal of Forensic Sciences, 6(3), 209–215.

Campbell, F. Manufacturing Technology for Aerospace Structural Materials. London: Elsevier Ltd(2006).

Cao, Y., Feng, J., & Wu, P. (2012). Polypropylene-grafted graphene oxide sheets as multifunctional compatibilizers for polyolefin-based polymer blends. Journal of Materials Chemistry, 22(30), 14997.

Cao, Y., Zhang, J., Feng, J., & Wu, P. (2011). Compatibilization of immiscible polymer blends using graphene oxide sheets. ACS Nano, 5(7), 5920–7.

Carniato, F., Fina, A., Tabuani, D., & Boccaleri, E. (2008). Polypropylene containing Ti- and Al-polyhedral oligomeric silsesquioxanes: crystallization process and thermal properties. Nanotechnology, 19(47), 475701.

Chandra, R., & Rustgi, R. (1997). Biodegradation of maleated linear low-density polyethylene and starch blends. Polymer Degradation and Stability, 56(2), 185–202.

Chee, W. K., Lim, H. N., Huang, N. M., & Harrison, I. (2015). Nanocomposites of graphene/polymers: a review. RSC Adv., 5(83), 68014–68051

Chen, C., & White, J. (1993). Compatibilizing Agents in Polymer Blends: Interfacial Tension, Phase Morphology, and Mechanical Properties. Polymer Science and Engineering, 33(14), 923-930.

Chieng, B. W., Ibrahim, N. A., Yunus, W. M. Z. W., Hussein, M. Z., Then, Y. Y., & Loo, Y. Y. (2014). Effects of graphene nanoplatelets and reduced graphene oxide on poly(lactic acid) and plasticized poly(lactic acid): A comparative study. Polymers, 6(8), 2232–2246.

Chiu, F. C., Yen, H. Z., & Lee, C. E. (2010). Characterization of PP/HDPE blend-based nanocomposites using different maleated polyolefins as compatibilizers. Polymer Testing, 29(3), 397–406 .

Chiu, F.-C., Yen, H.-Z., & Chen, C. (2010). Phase morphology and physical properties of PP/HDPE/organoclay (nano) composites with and without a maleated EPDM as a compatibilizer. Polymer Testing, 29(6), 706–716 .

Cho, K., Li, F., & Choi, J. (1999). Crystallization and melting behavior of polypropylene and maleated polypropylene blends. Polymer, 40(7), 1719–1729 .

Choi, W., Lahiri, I., Seelaboyina, R., & Kang, Y. S. (2010). Synthesis of graphene and its applications: A review. Critical Reviews in Solid State and Materials Sciences, 35(1), 52–71.

Chu, B.; Hsiao, B. S. (2001) .Small-angle X-ray scattering of polymers. Chemical reviews, 101 (6), 1727-1762.

Churg, A. (2003). Interactions of exogeneous or evoked agents and particles: the role of reactive oxygen species Free Radical Biol. & Med, 34, 1230–1235

Çiplak, Z., Yildiz, N., & Çalimli, A. (2015). Investigation of Graphene/Ag Nanocomposites Synthesis Parameters for Two Different Synthesis Methods. Fullerenes, Nanotubes and Carbon Nanostructures, 23(4), 361–370.

Cristina, B. , Ivan. I., Pacheco, B. & Kevin, R.(2007). Nanomaterials and nanoparticles: Sources and toxicity. Biointerphases , 2(4), 17 –172.

Cromer, B. M., Scheel, S., Luinstra, G. A., Coughlin, E. B., & Lesser, A. J. (2015). In-situ polymerization of isotactic polypropylene-nanographite nanocomposites. Polymer (United Kingdom), 80, 275–281.

Cser, F. (2001). About the Lorentz correction used in the interpretation of small angle X-ray scattering data of semicrystalline polymers. Journal of Applied Polymer Science, 80(12), 2300–2308.

D. Harris.(1998). Quantitative Chemical Analysis, 9th ed. Handbook of HPLC, Marcel Dekker, New York.

Dai, J., Xu, X., Yang, J., Zhang, N., Huang, T., Wang, Y., Zhang, C. (2015). Greatly enhanced porosity of stretched polypropylene/graphene oxide composite membrane achieved by adding pore-forming agent. RSC Adv., 5(27), 20663–20673.

De C. Fim, F., Basso, N. R. S., Graebin, A. P., Azambuja, D. S., & Galland, G. B. (2013). Thermal, electrical, and mechanical properties of polyethylene-graphene nanocomposites obtained by in situ polymerization. Journal of Applied Polymer Science, 128(5), 2630–2637.

De Castro, K. C., Sowek, A. B., Pinheiro, L. A., Pessan, L. A., & Canevarolo, S. V. (2014). Development and characterization of post-consumer rubber tire powder, high density polyethylene and ethylene-octene-1 copolymer ternary mixtures. Polimeros, 24(6), 654–660.

Deka, B. K., & Maji, T. K. (2010). Effect of coupling agent and nanoclay on properties of HDPE, LDPE, PP, PVC blend and Phargamites karka nanocomposite. Composites Science and Technology, 70(12), 1755–1761.

Deka, B. K., & Maji, T. K. (2011). Study on the properties of nanocomposite based on high density polyethylene, polypropylene, polyvinyl chloride and wood. Composites Part A: Applied Science and Manufacturing, 42(6), 686–693.

Deng, H., Lin, L., Ji, M., Zhang, S., Yang, M., & Fu, Q. (2014). Progress on the morphological control of conductive network in conductive polymer composites and the use as electroactive multifunctional materials. Progress in Polymer Science, 39(4), 627–655.

Dikobe, D. G. (2010). Comparative study of the morphology and properties of PP/LLDPE/wood powder and MAPP/LLDPE/wood powder polymer blend composites. eXPRESS Polymer Letters, 4(11), 729–741

Dissertation, a. (2009). Processing , Morphology and Properties of Graphene Reinforced Polymer Nanocomposites. Polymer, 52(September), 1532–1538.

Donaldson, K., Stone, V., Borm, A., Jimenez, A., Gilmour, S., Schins, F., Knaapen, M., Rahman, I., Faux, P., Brown, M., MacNee, W. (2003). Oxidative stress and calcium signaling in the adverse effects of environmental particles PM10 Free Radical Biol. & Med, 34, 1369-1382.

Dowling, a, Clift, R., Grobert, N., Hutton, D., Oliver, R., & O'neill, O. (2004). Nanoscience and nanotechnologies : opportunities and uncertainties. London The Royal Society The Royal Academy of Engineering Report, 46(July), 618–618.

Drewniak, S., Muzyka, R., Stolarczyk, A., Pustelny, T., Kotyczka-Morańska, M., & Setkiewicz, M. (2015). Studies of Reduced Graphene Oxide and Graphite Oxide in the Aspect of Their Possible Application in Gas Sensors. Sensors (Basel, Switzerland), 16(1), 103.

Dreyer, D., Park, S., Bielawski, C. & Ruoff, R.(2010). The chemistry of graphene oxide, Chem.Soc.Rev., 39, 228–240.

Eda, G., Mattevi, C., Yamaguchi, H., Kim, H., & Chhowalla, M. (2009). Insulator to semimetal transition in graphene oxide. Journal of Physical Chemistry C, 113(35), 15768–15771.

Ehrenstein, G. W., Riedel, G., & Trawiel, P. (2004). Chapter 6 Dynamic Mechanical Analysis. Thermal Analysis of Plastics: Theory and Practice, 236–299.

Eigler, S., Dotzer, C., & Hirsch, A. (2012). Visualization of defect densities in reduced graphene oxide. Carbon, 50(10), 3666–3673.

Ersoy, M. S., & Onder, E.(2013). Mechanical and Thermal Behaviors of Polypropylene - Multi-Walled Carbon Nanotube Nanocomposite Monofilaments. Fibres and Textiles in Eastern Europe, 98(2), 22–27.

Fairclough,P. Correlation function. Unpublished manuscript, The University of Sheffield Sheffield.UK (2014).

Fatnassi, M., Larbi, F. B. C., & Halary, J. L. (2010). Quantitative analysis of semicrystalline blends SAXS data: Theoretical modeling versus linear correlation function. International Journal of Polymer Science, 2010.

Fawcett, A. H. (1996). Polymer spectroscopy, John Wiley and Sons.

Fekete, E., Foldes, E., Damsits, F., & Pukanszky, B. (2000). Interaction-structure-property relationships in amorphous polymer blends. Polymer Bulletin, 44(4), 363–370.

Feng, H., Cheng, R., Zhao, X., Duan, X., & Li, J. (2013). A low-temperature method to produce highly reduced graphene oxide. Nature Communications, 4, 1539.

Feng, J., Winnik, M. A., Shivers, R. R., & Clubb, B. (1995). Polymer Blend Latex Films: Morphology and Transparency. Macromolecules, 28(23), 7671–7682.

Fischer, E. (1971) .Small angle x-ray scattering studies of phase transitions in polymeric and oligomeric systems. Pure and Applied Chemistry, 26 (3-4), 385-422.

Flory,P. (1941). Thermodynamics of High Polymer Solutions.Journal of chemical physics, 9(21), 440-440.

Fouad, H., Mourad, a.-H. I., & Barton, D. C. (2005). Effect of pre-heat treatment on the static and dynamic thermo-mechanical properties of ultra-high molecular weight polyethylene. Polymer Testing, 24(5), 549–556.

Freudenberg K (1932) The relation of cellulose to lignin in wood. J Chem Edu 9(Part II) 1171–1180.

Fu, C., Zhao, G., Zhang, H., & Li, S. (2013). Evaluation and Characterization of Reduced Graphene Oxide Nanosheets as Anode Materials for Lithium-Ion Batteries. *Int. J. Electrochem. Sci*, *8*, 6269 – 6280.

Furukawa, T., Sato, H., Kita, Y., Matsukawa, K., Yamaguchi, H., Ochiai, S., Ozaki, Y. (2006). Molecular Structure, Crystallinity and Morphology of Polyethylene/Polypropylene Blends Studied by Raman Mapping, Scanning Electron Microscopy, Wide Angle X-Ray Diffraction, and Differential Scanning Calorimetry. Polymer Journal, 38(11), 1127–1136.

Gao, W. (2015). The chemistry of graphene oxide. Graphene Oxide: Reduction Recipes, Spectroscopy, and Applications, 61–95.

Geim, A.K. (2011). Nobel Lecture: Random walk to graphene. Reviews of Modern Physics, 83(3),851–862.

Geim, A.K., Novoselov K.S.(2007). The rise of graphene. Nature Materials, 6(3),183–191.

Goderis, B., Reynaers, H., Koch, M. H. I., & Mathot, V. B. F. (1999). Use of SAXS and linear correlation functions for the determination of the crystallinity and morphology of semi-crystalline polymers. Application to linear polyethylene. J. Polym. Sci., Part B: Polym. Phys., 37(14), 1715–1738.

Goldstein, J., Newbury, D.E., Joy, D.C., Lyman, C.E., Echlin, P., Lifshin, E., Sawyer, L.& Michael, J.R.(2003). Scanning Electron Microscopy and X-ray Microanalysis, 3, Springer , New York, United State .

Gopakumar, T. G., & Pagé, D. J. Y. S. (2004). Polypropylene/graphite nanocomposites by thermo-kinetic mixing. Polymer Engineering & Science, 44(6), 1162–1169.

Graphene supermarket, United State, New York, 2009.

Guo, C., Zhou, L., & Lv, J. (2013). Effects of expandable graphite and modified ammonium polyphosphate on the flame-retardant and mechanical properties of wood flour-polypropylene composites. Polymers and Polymer Composites, 21(7), 449–456.

Guo, Y., Bao, C., Song, L., Yuan, B., & Hu, Y. (2011). In situ polymerization of graphene, graphite oxide, and functionalized graphite oxide into epoxy resin and comparison study of on-the-flame behavior. Industrial and Engineering Chemistry Research, 50(13), 7772–7783.

Gurunathan, S., Han, J., Park, J., Kim, E., Choi ,Y., Kwon,N.& Kim, J.(2015). Reduced graphene oxide–silver nanoparticle nanocomposite: a potential anticancer nanotherapy. International Journal of Nanomedicine. 10, 6257–6276.

Hartmann, B., Duffy, J. V., Lee, G. F., & Balizer, E. (1988).Thermal and dynamic mechanical properties of polyurethaneureas. Journal of Applied Polymer Science, 35, 1829–1852.

Hatakeyama, T., & Quinn, F. (1999). Thermal Analysis : Fundamentals and Applications to Polymer Science. Talanta, 256, 1–411.

Heimo, S. &Yashveer, S.(2013). The SAXS Guide,3, Anton Paar GmbH, Austria.

Henrique, P., Camargo, C., Satyanarayana, K. G., & Wypych, F. (2009). Nanocomposites : Synthesis , Structure , Properties and New Application Opportunities. Materials Research, 12(1), 1–39.

How, L., & Networks, N. (2005). Book Re View S. Ethology, 2(6), 2005–2007.

How, L., & Networks, N. (2005). Book Re View S. Ethology, 2(6), 2005–2007.

Huang, C.-L., Lou, C.-W., Liu, C.-F., Huang, C.-H., Song, X.-M., & Lin, J.-H. (2015). Polypropylene/Graphene and Polypropylene/Carbon Fiber Conductive Composites: Mechanical, Crystallization and Electromagnetic Properties. Applied Sciences, 5(4), 1196–1210.

Huang, C.-L., Lou, C.-W., Liu, C.-F., Huang, C.-H., Song, X.-M., & Lin, J.-H. (2015). Polypropylene/Graphene and Polypropylene/Carbon Fiber Conductive Composites: Mechanical, Crystallization and Electromagnetic Properties. Applied Sciences, 5(4), 1196–1210.

Huang, G., Ni, Z., Chen, G., Pang, W., & Zhao, Y. (2016). Effects of gamma irradiation and accelerated aging on GO/UHMWPE nanocomposites. International Journal of Polymer Analysis and Characterization, 5341(April), 1–11.

Huang, J. C. (2002). Carbon black filled conducting polymers and polymer blends. Advances in Polymer Technology, 21(4), 299–313.

In-Yup, J.,& Jong-Beom, B.(2010). Nanocomposites Derived from Polymers and Inorganic Nanoparticles. Materials. 3, 3654–3674.

Iqbal, M. Z. (2016). Structure-Property Relationships in Graphene/Polymer Nanocomposites. PhD Thesis, Colorado School of Mines.

Jaemyung, K., Laura, J., Cote, F., Wa, Y., Kenneth, R., Shull, A., & Huang, J. (2010). Graphene Oxide Sheets at Interfaces. J. Am. Chem. Soc., 132(23), 8180–8186.

Johnson, D. W., Dobson, B. P., & Coleman, K. S. (2015). A manufacturing perspective on graphene dispersions. Current Opinion in Colloid and Interface Science, 20(5-6), 367–382.

Jump up to: a b Tan, N. (1994). Reactive Compatibilization in Immiscible Polymer Blends. Doctor of Philosophy Thesis, University of Maryland.

K. L. Johnson, K. Kendall and A. D. Roberts (1971) . Proceedings of the Royal Society of London. 324, 301–313.

Kalaitzidou, K., Fukushima, H., Drzal, L.T., (2007). A new compounding method for exfoliated graphite-polypropylene nanocomposites with enhanced flexural properties and lower percolation threshold. Compos. Sci. Technol. 67, 2045-2051.

Kar, G. P., Biswas, S., & Bose, S. (2015). Tailoring the interface of an immiscible polymer blend by a mutually miscible homopolymer grafted onto graphene oxide: outstanding mechanical properties. Phys. Chem. Chem. Phys., 17(3), 1811–1821.

Kasaliwal, G. , Goldel, A. and Potschke, P. (2009).Influence of processing conditions in small-scale melt mixing and compression molding on the resistivity and morphology of polycarbonate- MWNT composites. Journal of Applied Polymer Science, 112(6), 3494–3509.

Kerstin, M., Elodie B., Marcos L., Maria J., Yolanda, E., José, L., Oliver, M., Alvise ,B., Steve, H., Uwe, B., Germán, P., Marius, J., Martina, L., Zuzana, S., Sara ,C.& Markus, S.(2017). Review on the Processing and Properties of Polymer Nanocomposites and Nanocoatings and Their Applications in the Packaging, Automotive and Solar Energy Fields. nanomaterials Review.7–47.

Khan, M., Al-Marri, A. H., Khan, M., Mohri, N., Adil, S. F., Al-Warthan, A., Tahir, M. N. (2014). Pulicaria glutinosa plant extract: a green and eco-friendly reducing agent for the preparation of highly reduced graphene oxide. RSC Advances, *4*(46), 24119.

Khenfouch, M. (2012). Morphological, Vibrational and Thermal Properties of Confined Graphene Nanosheets in an Individual Polymeric Nanochannel by Electrospinning. Graphene, 01(02), 15–20.

Khonakdar, H. A., Wagenknecht, U., Jafari, S. H., Hässler, R., & Eslami, H. (2004). Dynamic mechanical properties and morphology of polyethylene/ethylene vinyl acetate copolymer blends. Advances in Polymer Technology, 23(4), 307–315.

Kim, H. S., Kim, S., Kim, H. J., & Yang, H. S. (2006). Thermal properties of bio-flour-filled polyolefin composites with different compatibilizing agent type and content. Thermochimica Acta, 451(1-2), 181–188 .

Kim, H., Abdala, A.A.& Macosko, C.W.(2010) Graphene/polymer nanocomposites. Macromolecules, 43 (16):6515–6530.

Kim, K., Regan, W., Geng, B., Alemán, B., Kessler, B. M., Wang, F., Zettl, A. (2010). High-temperature stability of suspended single-layer graphene. Physica Status Solidi - Rapid Research Letters, 4(11), 302–304.

Kim, S., Do, I., & Drzal, L. T. (2009). Multifunctional xGnP/LLDPE nanocomposites prepared by solution compounding using various screw rotating systems. Macromolecular Materials and Engineering, 294(3), 196–205.

Kittelson D B (2001) Recent measurements of nanoparticle emission from engines Current Research on Diesel Exhaust Particles, Japan Association of Aerosol Science and Technology, 9 January ,Tokyo,Japan.

Koch, C. C. (2003). Top-Down Synthesis of Nanostructured Materials: Mechanical and Thermal Processing Methods. Rev.Adv.Mater.Sci, 5, 91–99.

Kondratowicz, I., Żelechowska, K., Majdecka, D., & Bilewicz, R. (2015). Synthesis and modification of reduced graphene oxide aerogels for biofuel cell applications. Materials Science-Poland, 33(2).

Konios, D., Stylianakis, M. M., Stratakis, E., & Kymakis, E. (2014). Dispersion behaviour of graphene oxide and reduced graphene oxide. Journal of Colloid and Interface Science, 430, 108–112.

Kucinskis, G., Bajars, G., & Kleperis, J. (2013). Graphene in lithium ion battery cathode materials: A review. Journal of Power Sources, 240, 66–79.

Kuilla, T., Bhadra, S., Yao, D., Kim, N. H., Bose, S., & Lee, J. H. (2010). Recent advances in graphene based polymer composites. Progress in Polymer Science Volume, 35(11), 1350–1375.

Layek, R. K., Samanta, S., & Nandi, A. K. (2012). The physical properties of sulfonated graphene/poly(vinyl alcohol) composites. Carbon, 50(3), 815–827.

Layek, R. K., Samanta, S., & Nandi, A. K. (2012). The physical properties of sulfonated graphene/poly(vinyl alcohol) composites. Carbon, 50(3), 815–827.

Lee K et al (2014) On the use of nanocellulose as reinforcement in polymer matrix. Compos Sci Technol 105:15–27

Lee, C., Wei, X., Kysar, J. W., & Hone, J. (2008). Measurement of the Elastic Properties and Intrinsic Strength of Monolayer Graphene. Science, 321(July), 385–388.

Lerf, A., He, H., Forster, M., & Klinowski, J. (1998). Structure of Graphite Oxide Revisited. Journal of Physical Chemistry B, 102(23), 4477–4482.

Li, B., Wan, C., Zhang, Y.& Ji, J.(2010). Blends of Poly(2,6-dimethyl-1,4-phenylene oxide)/ Polyamide 6 Toughened by Maleated Polystyrene-based Copolymers: Mechanical Properties, Morphology, and Rheology. Journal of Applied Polymer Science, 115,3385–3392.

Liço, E., Marku, J., & Chatzhitheodoridis, E. (2014). Physico-mechanical properties changes in virgin and recycled polyethylene fibers during recycling process, 55, 373–377.

Liebscher, M., Blais, M. O., Pötschke, P., & Heinrich, G. (2013). A morphological study on the dispersion and selective localization behavior of graphene nanoplatelets in immiscible polymer blends of PC and SAN. Polymer (United Kingdom), 54(21), 5875–5882.

Lilloja, J., Kibena-Põldsepp, E., Merisalu, M., Rauwel, P., Matisen, L., Niilisk, A., Tammeveski, K. (2016). An Oxygen Reduction Study of Graphene-Based Nanomaterials of Different Origin. Catalysts, 6(8), 108.

Lin,J., Pan, Y., Liu,C., Huang,C., Hsieh,C., Chen,C., Lin,Z., & Lou,C.(2015). Preparation and Compatibility Evaluation of Polypropylene/High Density Polyethylene Polyblends. Materials, 8, 8850–8859.

Liu, J., Tang, J., & Gooding, J. J. (2012). Strategies for chemical modification of graphene and applications of chemically modified graphene. Journal of Materials Chemistry, 22(25), 12435.

Liu, J., Yang, W.& Tao, L. (2010) Thermosensitive graphene nanocomposites formed using pyrene-terminal polymers made by RAFT polymerization. J Polym Sci Part A: Polym Chem;48,425–33.

Liu, X., Zheng, M., Xiao, K., Xiao, Y., He, C., Dong, H., Liu, Y. (2014). Simple, green and high-yield production of single- or few-layer graphene by hydrothermal exfoliation of graphite. Nanoscale, 6(9), 4598.

Mahmood, H., Habib, A., Mujahid, M., Tanveer, M., Javed, S., & Jamil, A. (2014). Band gap reduction of titania thin films using graphene nanosheets. Materials Science in Semiconductor Processing, 24(1), 193–199.

Mattevi, C., Eda, G., Agnoli, S., Miller, S., Mkhoyan, K. A., Celik, O., Chhowalla, M. (2009). Evolution of electrical, chemical, and structural properties of transparent and conducting chemically derived graphene thin films. Advanced Functional Materials, 19(16), 2577–2583.

Mattox, D. M.(1998) Handbook of Physical Vapor Deposition (PVD) Processing: Film Formation, Adhesion, Surface Preparation and Contamination Control. Elsevier inc Amsterdam, Netherlands.

Menczel ,J.& Prime ,R.(2009) Thermal Analysis of Polymers- Fundamentals and Applications, John Wiley & Sons.

Milani, M. A., Gonzalez, D., Quijada, R., Basso, N. R. S., Cerrada, M. L., Azambuja, D. S., & Galland, G. B. (2013). Polypropylene/graphene nanosheet nanocomposites by in situ polymerization: Synthesis, characterization and fundamental properties. Composites Science and Technology,84, 1–7.

Mishra, S. K., Tripathi, S. N., Choudhary, V., & Gupta, B. D. (2014). SPR based fibre optic ammonia gas sensor utilizing nanocomposite film of PMMA/reduced graphene oxide prepared by in situ polymerization. Sensors and Actuators, B: Chemical, 199, 190–200.

Moniruzzaman, M., & Winey, K. I. (2006). Polymer nanocomposites containing carbon nanotubes. Macromolecules, 39(16), 5194–5205.

Moon, I. K., Lee, J., Ruoff, R. S., & Lee, H. (2010). Reduced graphene oxide by chemical graphitization. Nature Communications, 1(6), 1–6.

Morgan, D. J. (2010). X-Ray Photoelectron Spectroscopy (XPS): An Introduction, 1–7.

Müller, M. (2004). Phase Behavior and Chain Conformations in Polymer Blends: Monte Carlo Simulation vs Mean Field Theory. Computational Soft Matter: From Synthetic Polymers to Proteins, Lecture Notes (Vol. 23).

Muralikrishna, S., Sureshkumar, K., Varley, T. S., Nagaraju, D. H., & Ramakrishnappa, T. (2014). In situ reduction and functionalization of graphene oxide with l-cysteine for simultaneous electrochemical determination of cadmium(II), lead(II), copper(II), and mercury(II) ions. Analytical Methods, 6(21), 8698–8705.

Naebe, M., Wang, J., Amini, A., Khayyam, H., Hameed, N., Li, L. H., Fox, B. (2014). Mechanical property and structure of covalent functionalised graphene/epoxy nanocomposites. Scientific Reports, 4, 4375.

Natta, G.; Pino, P.; Mazzanti, P.(1973) Regular linear head-to-tail polymerizates of certain unsaturated hydrocarbons and filaments comprising said polymerizates. U.S. Patent 3,715,344.

Nedkov,T, Lendnicky. & Mihailova,M. (2008).Compatibilization of PP/PE Blends and Scraps with Royalene: Mechanical Properties, SAXS, and WAXS. Journal of Applied Polymer Science, 109, 226–233 .

Nguyen, Q.T., Baird, D.G., (2006). Preparation of polymer–clay nanocomposites and their properties. Adv. Polymer. Tech. 25, 270-285.

Nielsen, A. S., Batchelder, D. N., & Pyrz, R. (2002). Estimation of crystallinity of isotactic polypropylene using Raman spectroscopy. Polymer, 43(9), 2671–2676.

Noorunnisa Khanam, P., AlMaadeed, M. A., Ouederni, M., Mayoral, B., Hamilton, A., & Sun, D. (2016). Effect of two types of graphene nanoplatelets on the physico–mechanical properties of linear low–density polyethylene composites. Advanced Manufacturing: Polymer & Composites Science, 2(2), 67–73.

Nouri, M. and Hay. J. (2006). Phase Separation in Polypropylene and Metallocene .Polymer engineering and science,889-595 .

Novoselov, K.S.(2011) Nobel lecture: Graphene: Materials in the flatland. Reviews of Modern Physics, 83(3):837–849

Ogawa, T. (1997.). Poly (silmethylene) -Based Polymer Blends . L In Situ Polymerization in Silicon-Based Polymers, 399–405.

Pandikumar, A., Soon How, G. T. & See, T. P. (2014) .Graphene and its nanocomposite material based electrochemical sensor platform for dopamine, RSC Advances, 4(108), 63296–63323,.

Pandikumar, A., Soon How, G. T., See, T. P., Omar, F. S., Jayabal, S., Kamali, K. Z., Huang, N. M. (2014). Graphene and its nanocomposite material based electrochemical sensor platform for dopamine. RSC Adv., 4(108), 63296–63323.

Parades, J. I., Villar-Rodil, S., Martínez-Alonso, A., & Tascón, J. M. D. (2008). Graphene oxide dispersions in organic solvents. Langmuir, 24(19), 10560–10564.

Park, S. & Ruoff, R.(2009). Chemical methods for the production of graphenes. Naturenanotechnology,4, 217–224.

Park, S., An, J., Potts, J. R., Velamakanni, A., Murali, S., & Ruoff, R. S. (2011). Hydrazine-reduction of graphite- and graphene oxide. Carbon, 49(9), 3019–3023.

Paudel, A., Worku, Z. A., Meeus, J., Guns, S., & Van Den Mooter, G. (2013). Manufacturing of solid dispersions of poorly water soluble drugs by spray drying: Formulation and process considerations. International Journal of Pharmaceutics, 453(1), 253–284.

Pauw, B. R. (2014). Corrigendum: Everything SAXS: small-angle scattering pattern collection and correction (2013 J. Phys.: Condens. Matter 25 383201). Journal of Physics: Condensed Matter, 26(23), 239501.

Pedro ,C., Kestur, S. & Fernando, W.(2009) Nanocomposites: Synthesis, Structure, Properties and New Application Opportunities. Materials Research, 12(1), 1-39.

Philosophy, D. O. F., & Patel, G. (2014). Spectroscopic Investigations on Polymer Blends / Composites, University of Baroda, India.

Pluta, M., Alexandre, M., Blacher, S., Dubois, P., & Jérôme, R. (2001). Metallocene-catalyzed polymerization of ethylene in the presence of graphite. II. Structure and electrical properties of the composites. Polymer, 42(22), 9293–9300.

Potts, J. R., Dreyer, D. R., Bielawski, C. W., & Ruoff, R. S. (2011). Graphene-based polymer nanocomposites. Polymer, 52(1), 5–25.

Punckt, C., Muckel, F., Wolff, S., Aksay, I. A., Chavarin, C. A., Bacher, G., & Mertin, W. (2013). The effect of degree of reduction on the electrical properties of functionalized graphene sheets. Applied Physics Letters, 102(2), 1–6.

Rattana, T., Chaiyakun, S., Witit-Anun, N., Nuntawong, N., Chindaudom, P., Oaew, S., Limsuwan, P. (2012). Preparation and characterization of graphene oxide nanosheets. Procedia Engineering, 32, 759–764.

Rjeb, A., Tajounte, L., Chafik El Idrissi, M., Letarte, S., Adnot, A., Roy, D., & Kaloustian, J. (2000). IR spectroscopy study of polypropylene natural aging. Journal of Applied Polymer Science, 77(8), 1742–1748.

Robeson, L. (2014). Historical perspective of advances in the science and technology of polymer blends. Polymers, 6(5), 1251–1265.

Robeson, L. M., Ed.(2007). Polymer Blends : a Comprehensive Review; Hanser: Munich ; Cincinnati.

Roe, R.J. (1993). Use of Block Copolymer as Polymer Blend Compatibilizer. U.S. Army Research Office. Rudin, A. & Phillip, C. (2013). The Elements of Polymer Science and Engineering. 3rd. Oxford: Academic Press.

Sadasivuni, K. K., Ponnamma, D., Kim, J., & Thomas, S. (2015). Graphene-based polymer nanocomposites in electronics. Graphene-Based Polymer Nanocomposites in Electronics, 1–382.

Saldivar-Guerra,E. & Vivaldo-Lima. E. (2013). Handbook of Polymer Synthesis, Characterization, and Processing. 3rd edition. New York: John Wiley & Sons, 11–12.

Salih, S. E., Hamood, A. F., & Abd Alsalam, A. H. (2013). Comparison of the characteristics of LDPE: PP and HDPE: PP polymer blends. Modern Applied Science, 7(3), 33–42.

Samperi, F., Battiato, S., Recca, G., Puglisi, C., & Mendichi, R. (2015). Reactive melt mixing of PC/PEN blend. Structural characterization of reaction products. Polymer, 74, 108–123.

Sarker, M., Rashid, M. M., & Molla, M. (2011). Abundant High-Density Polyethylene (HDPE-2) Turns into Fuel by Using of HZSM-5 Catalyst. Journal of Fundamentals of Renewable Energy and Applications, 1(November), 12.

Sato, H., Shimoyama, M., Kamiya, T., Amari, T., Aic, S., Ninomiya, T., Ozaki, Y. (2002). Raman spectra of high-density, low-density, and linear low-density polyethylene pellets and prediction of their physical properties by multivariate data analysis. Journal of Applied Polymer Science, 86(2), 443–448.

Saw, C. K. (2005). X-ray scattering techniques for characterization of nanosystems In: Challa, S. &Kumar,R.(Eds), Nanotechnologies for Life Sciences, 3, UCRL-JRNL-211387.

Schwierz, F.(2010) Graphene transistors. Nature Nanotechnology, 5(7):487–496.

Scobbo, J.J, Jr and Goettler, L.A. (2003)Applications of polymer alloys and blends, in Polymer Blends Handbook (ed. L.A. Utracki), Kluwer Academic Publishers, pp. 951–976.

Sengupta, R., Chakraborty, S., Bandyopadhyay, S., Dasgupta, S., Mukhopadhyay, R., Auddy, K., & Deuri, a S. (2007). A Short Review on Rubber / Clay Nanocomposites With Emphasis on Mechanical Properties. Engineering, 47, 21–25

Seuring, J., & Agarwal, S. (2012). Polymers with upper critical solution temperature in aqueous solution. Macromol. Rapid Commun., 33(22), 1898–1920.

Shamiri, A., Chakrabarti, M. H., Jahan, S., Hussain, M. A., Kaminsky, W., Aravind, P. V., & Yehye, W. A. (2014). The influence of Ziegler-Natta and metallocene catalysts on polyolefin structure, properties, and processing ability. Materials, 7(7), 5069–5108.

Shanks, R. A., Li, J., and Yu, L. (2000). Polypropylene – polyethylene blend morphology controlled by time – temperature – miscibility. Materials Science, 41, 2133–2139.

Shemouratov, Y. V., Prokhorov, K. A., Sagitova, E. A., Nikolaeva, G. Y., Pashinin, P. P., Lebedev, Y. A., & Antipov, E. M. (2009). Raman study of polyethylene-polypropylene blends. Laser Physics, 19(12), 2179–2183.

Si, M., Araki, T., Ade, H., Kilcoyne, a. L. D., Sokolov, J. C., Rafailovich, M. H., & Fisher, R. (2006). Compatibilizing Bulk Polymer Blends by Using Organoclays Compatibilizing Bulk Polymer Blends by Using Organoclays. Macromolecules, 39(14), 4793–4801.

Singh ,A. K., Rajiv, P. and Dhananjai, P.(2013). A comparative thermal, optical, morphological and mechanical properties studies of pristine and C15A nanoclay-modified PC/PMMA blends: a critical evaluation of the role of nanoclay particles as compatibilizers. The Royal Society of Chemistry, 3, 15411–15420.

Singh V., Joung D., Zhai L., Das S., Khondaker S.I.& Seal S.(2011) Graphene based materials: Past, present and future. Progress in Materials Science,56(8):1178–1271.

Singh, R. (2002). C. V. Raman and the Discovery of the Raman Effect. Physics in Perspective, 4(4), 399–420.

Singh, R. K., Kumar, R., & Singh, D. P. (2016). Graphene oxide: strategies for synthesis, reduction and frontier applications. RSC Adv., 6(69), 64993–65011.

Snook, G. A., Kao, P., & Best, A. S. (2011). Conducting-polymer-based supercapacitor devices and electrodes. Journal of Power Sources, 196(1), 1–12.

Song, P., Cao, Z., Cai, Y., Zhao, L., Fang, Z., & Fu, S. (2011). Fabrication of exfoliated graphene-based polypropylene nanocomposites with enhanced mechanical and thermal properties. Polymer, 52(18), 4001–4010.

Sonnier, R., Massardier, V., & Cassagnau, P. (2008). Compatibilization of hiPP / HDPE blends by a metallocene copolymer. Journal of Materials, 1–4.

Stankovich, S., Dikin, D. A., Dommett, G. H. B., Kohlhaas, K. M., Zimney, E. J., Stach, E. A., Ruoff, R. S. (2006). Graphene-based composite materials. Nature, 442(7100), 282–286.

Straughan, B. P. and Walker, S. (1976). Spectroscopy, 2, John Wiley and Sons. Stuart, B., Skoog, D. A., West, D. M., Holler, J., Crouch, S. R., Larkin, P. J., Socrates, G. (2004). Infrared Spectroscopy: Fundamentals and Applications. Vasa, 40(6), 146–208.

Suk, J. W., Piner, R. D., An, J., & Ruoff, R. S. (2010). Mechanical Properties of Monolayer Graphene Oxide, 4(11), 6557–6564.

Sun, Y. Sen. (2006).Temperature-resolved SAXS studies of morphological changes in melt-crystallized poly(hexamethylene terephthalate) and its melting upon heating. Polymer, 47(23), 8032–8043 .

Sundararaj, U.& Macosko, C. W.(1995). Drop Breakup and Coalescence in Polymer Blends: The Effects of Concentration and Compatibilization. Macromolecules, 28, 2647–2657.

Suñer, S., Joffe, R., Tipper, J. L., & Emami, N. (2015). Ultra high molecular weight polyethylene/graphene oxide nanocomposites: Thermal, mechanical and wettability characterisation. Composites Part B: Engineering, 78, 185–191.

Tabatabaei, S. H., Carreau, P. J., & Ajji, A. (2008). Microporous membranes obtained from polypropylene blend films by stretching. Journal of Membrane Science, 325(2), 772–782 .

Tajvidi, M., Falk, R. H., & Hermanson, J. C. (2006).Effect of natural fibers on thermal and mechanical properties of natural fiber polypropylene composites studied by dynamic mechanical analysis. Journal of Applied Polymer Science, 101(6), 4341–4349 .

Taniike, T., Goto, K., & Terano, M. (2015). Active site nature of magnesium dichloride-supported titanocene catalysts in olefin polymerization, 2(1), 57–63.

Teo, B. K., & Sun, X. H. (2007). Classification and representations of low-dimensional nanomaterials: Terms and symbols. Journal of Cluster Science, 18(2), 346–357.

Thomas, H. R. (2015). The structure and reactivity of graphene oxide.

Thuresson, A., Segad, M., Turesson, M., & Skepö, M. (2016). Flocculated Laponite–PEG/PEO dispersions with monovalent salt, a SAXS and simulation study. J. Colloid Interf. Sci., 466, 330–342 .

Tiwari, R., Srivastava, B., Tiwari, G., & Rai, A. (2009). Extended release promethazine HCl using acrylic polymers by freeze-drying and spray-drying techniques: Formulation considerations. Brazilian Journal of Pharmaceutical Sciences, 45(4), 829–840.

Tomba, J. P., Mana, C. D., Perez, C. J., Desimone, P. M., & Galland, G. B. (2016). Microstructural characterization of semicrystalline copolymers by Raman spectroscopy. Polymer Testing, 52(April), 71–78.

Tong, J., Huang, H.-X., & Wu, M. (2017). Promoting compatibilization effect of graphene oxide on immiscible PS/PVDF blend via water-assisted mixing extrusion. Composites Science and Technology, 149, 286–293.

Topham, P. D., Howse, J. R., Fernyhough, C. M., & Ryan, A. J. (2007). The performance of poly(styrene)-block-poly(2-vinyl pyridine)-block-poly(styrene) triblock copolymers as pH-driven actuators. Soft Matter, 3(12), 1506–1512.

Trapalis, A., Todorova, N., Giannakopoulou, T., Boukos, N., Speliotis, T., Dimotikali, D., & Yu, J. (2016). TiO2/graphene composite photocatalysts for NOx removal: Acomparison of surfactant-stabilized graphene and reduced grapheneoxide. Applied Catalysis B: Environmental, 180(January), 637–647.

Tripathi, S. N., Rao, G. S. S., Mathur, A. B., & Jasra, R. (2017). Polyolefin/graphene nanocomposites: a review. RSC Adv., 7(38), 23615–23632.

Upadhyay, R. , Soin, N. and Roy, S.(2014) .Role of graphene/metaloxide composites as photocatalysts, adsorbents and disinfectants in water treatment: a review," RSC Advances,. 4(8) 3823–3851.

Utracki, L. A. & Wilkie, C. (2014) Polymer Blends Handbook,2, Springer Netherlands , New York, United State .

Utracki, L.(2002). Compatibilization of Polymer Blends.The Canadian Journal of Chemical Engineering, 80, 1008–1016.

Verdejo R., Bernal M.M., Romasanta L.J., Lopez-Manchado M.A.(2011) Graphene filled polymer nanocomposites. Journal of Materials Chemistry, 21(10):3301–3310.

Vonk, C. G., & Kortleve, G. (1967). X-ray small-angle scattering of bulk polyethylene - II. Analyses of the scattering curve. Kolloid-Zeitschrift & Zeitschrift für Polymere, 220(1), 19–24.

Walsh, D. J. & Rostami, S.(1984). The miscibility of high polymers: The role of specific interactions. Advances in Polymer Science,120–163.

Wan, C., & Chen, B. (2012). Reinforcement and interphase of polymer/graphene oxide nanocomposites. Journal of Materials Chemistry, 22(8), 3637.

Wang, C., Frogley, M.D. , Cinque, G., Liu, L.-Q. &Barber, A.H. (2013). Deformation and failure mechanisms in graphene oxide paper using in situ nanomechanical tensile testing .Carbon, 63 , 471-477.

Wang, D., Niu, W., Tan, M., Wu, M., Zheng, X., Li, Y., & Tsubaki, N. (2014). Pt nanocatalysts supported on reduced graphene oxide for selective conversion of cellulose or cellobiose to sorbitol. ChemSusChem, 7(5), 1398–1406.

Wang, S. J., Geng, Y., Zheng, Q., & Kim, J. K. (2010). Fabrication of highly conducting and transparent graphene films. Carbon, 48(6), 1815–1823.

Wang, X., Xing, W., Song, L., Yang, H., Hu, Y., & Yeoh, G. H. (2012). Fabrication and characterization of graphene-reinforced waterborne polyurethane nanocomposite coatings by the sol-gel method. Surface and Coatings Technology, 206(23), 4778–4784.

Wang, Y., Alsmeyer, D. C., & McCreery, R. L. (1990). Raman Spectroscopy of Carbon Materials: Structural Basis of Observed Spectra. Chemistry of Materials, 2(5), 557–563

Weeks, N. E., Karasz, F. E. & MacKnight, W. J.(1977). Enthalpy of mixing of poly(2,6-dimethyl phenylene oxide) and polystyrene. Journal of Applied Physics, 48, 4068–4071.

Wenzel, T., (2013) .Douglas A. Skoog, Donald M.West, F. James Holler, and Stanley R. Crouch: Fundamentals of analytical chemistry, 9th ed., international ed. Anal Bioanal Chem . 405,7903–7904

Wight, C. A. (2001).Kinetics of the Thermal and Thermo-Oxidative Degradation of Polystyrene , Polyethylene and Poly (propylene) Kinetics of the Thermal and Thermo-Oxidative Degradation of Polystyrene , Polyethylene and Poly (propylene), (MARCH), 775–784.

Wildes, G., Keskkula, H., & Paul, D. R. (1999). Coalescence in PC/SAN blends: Effect of reactive compatibilization and matrix phase viscosity. Polymer, 40(20), 5609–5621.

Won, J., Richard, S., Piner, D., An, J. & Ruoff. R.(2010) American Chemical Society , 4 (11), 6557–6564 .

Wong, a. C.-Y., & Lam, F. (2002). Study of selected thermal characteristics of polypropylene/polyethylene binary blends using DSC and TGA. Polymer Testing, 21(6), 691–696.

Wu, J., Huang, G., Li, H., Wu, S., Liu, Y., & Zheng, J. (2013). Enhanced mechanical and gas barrier properties of rubber nanocomposites with surface functionalized graphene oxide at low content. *Polymer (United Kingdom)*, *54*(7), 1930–1937.

Wu, T., Wang, X., Qiu, H., Gao, J., Wang, W., & Liu, Y. (2012). Graphene oxide reduced and modified by soft nanoparticles and its catalysis of the Knoevenagel condensation. Journal of Materials Chemistry, 22(11), 4772.

Xu, Z., Gao, H., and Guoxin, H. (2011) Solution-based synthesis and characterization of a silver nanoparticle-graphene hybrid film.Carbon, 49: 4731–4738.

Yang, J., Feng, C., Dai, J., Zhang, N., Huang, T., Wang, Y. (2013) . Compatibilization of immiscible nylon 6/poly(vinylidene fluoride) blends using graphene oxides .Polymer International, 62 (7), 1085-1093.

Yang, L., Somani, R. H., Sics, I., Hsiao, B. S., Kolb, R., Fruitwala, H., & Ong, C. (2004). Shear-induced crystallization precursor studies in model polyethylene blends by in-situ rheo-SAXS and rheo-WAXD. Macromolecules, 37(13), 4845–4859 .

Yavari, F., & Koratkar, N. (2012). Graphene-based chemical sensors. Journal of Physical Chemistry Letters, 3(13), 1746–1753.

Ye, S., Cao, Y., Feng, J., & Wu, P. (2013). Temperature-dependent compatibilizing effect of graphene oxide as a compatibilizer for immiscible polymer blends. RSC Advances, 3(21), 7987.

Yin, Z. Y., Sun, S. Y., Salim, T., Wu, S. X., Huang, X. A., He, Q. Y., … Zhang, H. (2010). Organic Photovoltaic Devices Using Highly Flexible Reduced Graphene Oxide Films as Transparent Electrodes. Acs Nano, 4(9), 5263–5268.

Yin, Z., Wu, S., Zhou, X., Huang, X., Zhang, Q., Boey, F., & Zhang, H. (2010). Electrochemical deposition of ZnO nanorods on transparent reduced graphene oxide electrodes for hybrid solar cells. Small, 6(2), 307–312.

Yokouchi, M., Seto, S.& Kobayashi, Y.(1983). Comparison of polystyrene, poly (styrene/acrylonitrile), high-impact polystyrene, and poly(acrylonitrile/butadiene/styrene) with respect to tensile and impact properties. Journal of applied polymer, 28(7), 2209–2216.

Young, R. J., Kinloch, I. a., Gong, L., & Novoselov, K. S. (2012). The mechanics of graphene nanocomposites: A review. Composites Science and Technology, 72(12), 1459–1476.

Young, R.J &Lovell, P.A (2011).Introduction to polymers ,3 edition ,CRC press,London,United Kingdoom.

Yu, L., Dean, K., & Li, L. (2006). Polymer blends and composites from renewable resources. Progress in Polymer Science (Oxford), 31(6), 576–602.

Yu, S., Yin, Y., and Liu, J. (2013) Silver nanoparticles in the environment. Environ. Sci.: Process. Impacts., 15: 78–92.

Yu, Y.-H., Lin, Y.-Y., Lin, C.-H., Chan, C.-C., & Huang, Y.-C. (2014). High-performance polystyrene/graphene-based nanocomposites with excellent anti-corrosion properties. Polym. Chem., 5(2), 535–550.

Zavgorodnev, Y. V, Sagitova, E. A., Nikolaeva, G. Y., Prokhorov, K. A., Pashinin, P. P., Novokshonova, L. A., Antipov, E. M. (n.d.). RAMAN STRUCTURAL STUDY OF OLEFIN BLENDS.

Zhang, J., Jiang, D. D., & Wilkie, C. A. (2005). Polyethylene and polypropylene nanocomposites based upon an oligomerically modified clay. Thermochimica Acta, 430(1–2), 107–113.

Zhang, J., Jiang, D. D., & Wilkie, C. A. (2006). Thermal and flame properties of polyethylene and polypropylene nanocomposites based on an oligomerically-modified clay. Polymer Degradation and Stability, 91(2), 298–304 .

Zhang, Q. & Hoogenboom, R (2015). Polymers with upper critical solution temperature behavior in alcohol/water solvent mixtures. Progress in Polymer Science, 48 ,122–142 .

Zhanga, H., Zhenga, W., Yana, Q., Yanga, Y., Wang, J., Lu, Z., Ji, G.& Yu, Z.(2010) Electrically conductive polyethylene terephthalate/graphene nanocomposites prepared by melt compounding. Polymer ,51 , 1191–1196.

Zheng,Q., Li,Z., Jialin,Y. & Kim,J. (2010). Molecular Dynamics Study of the Effect of Chemical Functionalization on the Elastic Properties of Graphene Sheets. Journal of Nanoscience and Nanotechnology ,10(11),7070-7074.

Zhou, S., & Bongiorno, A. (2013). Origin of the chemical and kinetic stability of graphene oxide. Scientific Reports, 3, 2484.